Miniaturised bandpass filters for wireless communications.

Lakshman Athukorala

School of Electronics and Computer Science

MINIATURISED BANDPASS FILTERS FOR WIRELESS COMMUNICATIONS

LAKSHMAN ATHUKORALA

A thesis submitted in partial fulfilment of the

requirements of the University of Westminster

for the degree of Doctor of Philosophy

February 2012

ABSTRACT

The wireless industry has seen exceptional development over the past few decades due to years of sustained military and commercial enterprise. While the electromagnetic spectrum is becoming increasingly congested, there is a growing tendency to strive for higher bandwidths, faster throughputs, greater versatility, compatibility and interoperability in current and emerging wireless technologies. Consequently, an increasingly stringent specification is imposed upon the frequency utilization of wireless devices.

New challenges are constantly being discovered in the development and realization of RF and microwave filters, which have not only sustained but fuelled microwave filter research over the many years. These developments have encouraged new solutions and techniques for the realization of compact, low loss, highly selective RF and microwave bandpass filters.

The theme of this dissertation is the realization of planar compact performance microwave and RF bandpass filters for wireless communication systems. The work may be broadly categorised into three sections as follows.

The first section presents a novel compact planar dual-mode resonator with several interesting and attractive features. Generally, planar microwave dual-mode resonators are known to half the filter footprint. However, it is found that the proposed resonator is capable of achieving further size reductions. In addition the resonator inherently possesses a relatively wide stopband as the lowest spurious harmonic resonance is observed at thrice the fundamental frequency. Properties of this resonator, such as these and more are explored in depth to arrive at an accurate electrical equivalent circuit, which is used as the basis for high order filter design.

The application of these resonators in the design of bandpass filters is the subject of the second section. A general filter design procedure based on the equivalent circuit is presented to assist the design of all-pole filters. Alternatively, it is shown that generalised Chebyshev filters with enhanced selectivity may be developed with cross coupled resonator topologies. The discussions are supplemented with detailed design examples which are accompanied by theoretical, simulated and experimental results in order to illustrate the filter development process and showcase practical filter performance.

The third section explores the possibility of employing these resonators in the development of frequency tunable bandpass filters. Preference is given to varactor diodes as the tuning element due to the numerous qualities of this device in contrast to other schemes. In particular, interest is paid to center frequency tuned filters with constant bandwidth. Tunable filters constructed with the dual-mode resonator are shown to have a relatively wide tuning range as well as significantly higher linearity in comparison to similar published works. In line with the previous section, experimental verification is presented to support and supplement the discussions.

Table of Contents

List of Figures and Tables

Chapter 2

Chapter 3

Chapter 4

Chapter 5

Chapter 4

ACKNOWLEDGEMENTS

Appreciation and heartfelt gratefulness is what I hold towards my director of studies, Dr. Djuradj Budimir. In addition to offering me a research opportunity at the university, he has kept me motivated throughout my doctoral work. I greatly value his encouragement, advice, support and understanding during my studies especially during the early stages when the objectives seemed farfetched and the learning curve was steep. He was always able to find time, even when he was busy, for discussions and advice for which I am truly thankful.

Very closely to my supervisor, I would also like to express my deepest gratitude to my second supervisor, Dr. Andrzej Tarczynski, who has been a sheer source of inspiration throughout my many years at the university. I am truly thankful for his support and encouragement and continue to admire him for his remarkable character and personality.

Next, I am deeply indebted to Professor R.C.S Morling and Dr. Cheng Lee for offering me part time employment at the university, which had greatly alleviated financial difficulties. I have learnt such a lot while working with them and I am sincerely grateful for this.

Especially, thanks are due to the internal thesis examiner Dr. Mohammed Al-Janabi for his valuable time spent reading this report as well as for all his support and advice in the preparation of this text. I sincerely appreciate and value his firm belief in me from the start of my course. External examiner Professor Dariush Mirshekar is gratefully acknowledged for his valuable time, kind advice and useful suggestions.

Extremely grateful to my university for providing me the full tuition fee waiver scholarship.

Thanks are also due to friends and family. I would like to thank my brother and my best friend, Thant Sin, for their support and encouragement throughout my studies. Finally and most importantly, I am extremely grateful to my parents, for their faith, guidance, support, encouragement and motivation without which I would have never reached this far...

LAKSHMAN ATHUKORALA

21, JUNE, 2011

AUTHOR'S DECLARATION

I declare that all the material contained in this thesis is my own work.

List of Acronyms

dB	Decibel
GHz	Gigahertz
mm	Millimetre
FBW	Fractional bandwidth
MEMS	Micro-electro-mechanical systems
RF	Radio frequency
DC	Direct current
SIR	Stepped impedance resonator
TEM	Transverse electromagnetic propagation mode
GSM	Global system for mobile communications
GPS	Global positioning system
WiMAX	Worldwide Interoperability for Microwave Access
WLAN	Wireless local area network
EM	Electromagnetic
ABCD	Transfer matrix
IM3	Third order intermodulation power
IIP3	Input referred third order intercept point
OIP3	Output referred third order intercept point
BST	Barium strontium titan ate
PET	Piezoelectric transducer

List of Publications

Journals

L. Athukorala and D.Budimir, “Open-loop tunable resonators and filters with constant bandwidth”, *IET Transactions of Microwave*, Antennas and Propagation, Accepted,2011.

L. Athukorala and D.Budimir, “Compact filter configurations using concentric microstrip open-loop resonators”, *IEEE Microwave and Wireless Component Letters*, Accepted,2011.

L. Athukorala and D.Budimir, “Compact second-order highly linear varactor tuned dual-mode filters with constant bandwidth”, *IEEE Transactions on Microwave Theory and Techniques*, Vol. 59, No.9, pp. 2214-2220, September 2011.

L. Athukorala and D.Budimir, “Design of Compact Dual-Mode Microstrip Filters”, *IEEE Transactions on Microwave Theory and Techniques*, Vol. 58, No.11, pp. 2888-2895, 2010.

L. Athukorala, and D. Budimir, "Miniaturized Bandpass Filters using Closed-loop Microstrip Ring Resonator with Parallel-Coupled Feed for Wireless Communications”, Microwave and Optical Technology Letters, Vol. 52, No. 6, pp. 1277-1280, June 2010.

L. Athukorala and D.Budimir, “Compact dual-mode open-loop microstrip resonators and filters”, *IEEE Microwave and Wireless Component Letters*, Vol. 19, No. 11, pp. 698-700, November 2009.

Conferences

L. Athukorala and D.Budimir, “Compact High Linearity Tunable Dual Mode Microstrip Filters”, European Microwave Conference, pp. 834-837, 2010.

L. Athukorala, K.Rabbi, D.Budimir, C. Panagamuwa, J. Vardaxoglou, M. Philippakis “Optically reconfigurable microstrip UWB bandpass filters”, *Loughborough Antennas and Propagation Conference*, pp.617-620, 2010.

L. Athukorala and D.Budimir, “Frequency tunable microstrip resonators and filters”, European Microwave Conference, pp. 1239-1242, 2009.

L. Athukorala and D.Budimir, “Dual-mode closed-loop microstrip filters for wireless applications”, TELSIKS, pp. 151-153, Oct 2009.

1.0 INTRODUCTION

Applications for RF and microwave bandpass filters have grown tremendously over the past few decades. Although usually associated with communications systems such as satellites, base stations and mobile phones, bandpass filters find vast ranging applications from scientific instrumentation to medical applications and even navigation. In fact, filters have evolved to become both vital and indispensible components in modern electronic systems. Regardless of their application, filters generally shape signals in amplitude and phase with respect to the signal frequency in a prescribed manner to produce an output which is more compliant.

More commonly, a microwave filter performs a frequency band limiting operation, where signals outside a particular band of interest are severely attenuated. Therefore, filters enable the finite electromagnetic spectrum to be shared allowing a multitude of radio and wireless services to coexist. It is quite common for passive filters to be categorized according to their specific band limiting function and further classified according to the nature of its response.

Over the past few decades, with the substantial growth in the number of wireless services, there is a growing trend towards systems with higher bandwidths, faster data rates and increased reliability. This continues to place an increasingly stringent requirement on modern filters and have triggered designers to seek new solutions to address crucial issues such as loss minimization, selectivity and stopband enhancement and even cost saving.

While system complexity is on the rise, system size has continued to shrink thanks to breakthroughs such as on chip integration. This approach however proves less effective with filters operating especially in the RF or microwave frequencies mainly due to two reasons.

Firstly, it is incredibly difficult to realise lumped elements with sufficient accuracy especially at microwave frequencies due to parasitic effects. Integrating planar distributed filters into an IC may seem to be a solution. However, since the size of a distributed filter is directly proportional its operating wavelength, this approach may only work on a small minority of filters, where the operating frequencies allow filters to physically fit into an IC. Secondly, the quality factor of a distributed resonator is proportional to its physical size. Therefore, distributed IC filters suffer from severe losses which may easily impair system performance.

Due to the reasons above, planar transmission line technologies such as stripline and microstrip have become immensely popular in the design of distributed filters. In addition, planar distributed filters are significantly more compact in contrast to the relatively bulky filters constructed in waveguide and coaxial media. Nevertheless, even with planar technologies, developers welcome compact filters due to cost and size saving.

Yet another important trend over the years is the increase in the number of services a wireless system is able to offer. The shift towards systems armed with multiple functionalities may require such systems to operate on multiple frequency bands. For example, a cellular phone with internet connectivity must operate on both the GSM and WiFi bands. Multiband systems traditionally use a number of fixed filters, one for each band. However, multiband filters or even tunable or reconfigurable filters may be better suited to such applications primarily due to the potentially drastic size and cost saving that may be reaped. However, multiband and tunable filters are still the subjects of intense research due to limitations such as the number of passbands achievable, center frequency tuning range, bandwidth tuning range, and linearity in addition to the issues pertaining to fixed filters.

This dissertation addresses some of the fundamental challenges facing microwave filters. As such, concerns including filter size, loss, selectivity and tunability are central to the theme of the thesis. The rest of this chapter details the aims and objectives of this investigation. This is followed by an overview of some significant contributions and developments from past research work particularly in the area of planar microwave filters not only to give a survey of the type of solutions available but also to serve as a basis for comparison. For better accessibility, an outline of the thesis is provided next with a summary of each chapter.

1.1 Research Objectives

The central aim of the research effort is the development of enhanced planar microwave and RF bandpass filters for wireless communications. In particular, the investigation addresses some of the key challenges surrounding bandpass filters such as compactness, harmonic suppression and tunability. These research objectives are tackled in the following stages.

A crucial objective of the project is the development of a novel compact planar resonator, which has the potential for harmonic suppression, tunability and dual-band performance. In this regard, several resonator structures must be investigated including open loop, quarter or half wave length resonators, circular or square ring based configurations, and disk or patch based resonators. Special preference is given to dual-mode resonator topologies since a single unit behaves as a pair of coupled resonators immediately allowing filter size to be halved. Additionally, miniaturization methods such as the slow wave approach and in particular the use of stepped impedances is given consideration in order to further reduce the resonator footprint.

Once a suitable compact resonator is developed, an electrical equivalent circuit of the resonator, that is most compatible with standard bandpass filter prototypes, must be constructed and refined not only to be able to quantify principal resonator parameters of the structure accurately but also to later facilitate the development of a filter design procedure. This may be accomplished by a two pronged approach. Firstly, the basic equivalent circuit, which accounts for the dominant electromagnetic phenomena within the resonator, may be extracted from modal analysis of the unit. The model may, depending on the degree of parasitic effects, be refined with the aid of a full wave electromagnetic simulator. The model must also be able to account for any transmission zeros in the stopband of the resonator response, which may prove crucial in the effort to improve selectivity or stopband response of filters designed at a later stage.

The application of these resonators in the design of compact bandpass filters is the next objective of the investigation. The resonator equivalent circuit may be used as a basis for developing a filter design procedure to enable high order filters to be realized with relative ease. A goal of the research effort is to establish a design procedure for realizing all-pole Butterworth and Chebyshev filters from a direct coupled resonator topology. The option of obtaining a generalised Chebyshev filtering characteristic must also be investigated possibly by employing a cross coupled resonator approach. This may enable lower order filters to achieve potentially higher skirt selectivity and in some applications substitute higher order filters which may have unacceptable passband loss. The filter design method in this case will likely be based on a coupling matrix synthesis scheme. Also to be investigated is the potential for filter stopband improvement either in extending the stopband or in sharpening the selectivity by employing any transmission zeros inherent to the resonator response.

The investigation then focuses on the application of these resonators in the development of constant bandwidth center frequency tunable bandpass filters. Growing research interest in this area has not only highlighted the importance of tunable filters but has also triggered the exploration of some very novel tunable elements. On the other hand, application of these elements in maximizing centre frequency tuning range, bandwidth tunability and filter linearity arguably sees more research interest. The aim of this investigation with regard to tunable filters would therefore be very much aligned with mainstream research interests. Filter tuning range and linearity would therefore be key parameters that must be addressed. In addition, the majority of tunable elements suffer from significant parasitic resistances which may cause undue passband loss and a noticeable degradation to filter selectivity. Methods of mitigating this effect can also be considered given the availability of sufficient resources.

1.2 Overview of Past Research

A concise overview of some of the recent advancements to distributed planar filter theory, relevant to the set objectives of this investigation is presented in this section. The first sub section presents a survey of filter miniaturization methods and compact filter structures.

1.2.1 Compact Bandpass Filters

A bandpass filter consists of a number of coupled resonators. The size of the distributed resonator and the number of resonators employed ultimately determines the overall filter footprint. Accordingly, most of the filter miniaturization techniques take measures to reduce either of these two quantities in order to reduce the overall physical size of the filter.

The slow wave effect is a rather well established approach for resonator miniaturization [1-1]. Essentially, the principle, as the name suggests, revolves around the reduction of phase velocity of the fundamental mode of a resonator. Doing so will allow the dimensions of the resonator to shrink in proportion to the reduced guided resonant wavelength. Retarding the phase velocity on a transmission line may be accomplished by either increasing the series inductance, *L*, or the shunt capacitance, *C*, since the phase velocity, V_p, is defined as (1.1).

$$V_p = \frac{1}{\sqrt{LC}} \tag{1.1}$$

However, in most slow wave resonators, the general preference is to augment the shunt capacitance since signals on higher inductive lines tend to incur more loss. On the other hand, stepped impedance resonators (SIRs), a concept largely derived from the slow wave effect, combines an enhancement of both series inductance and shunt capacitance to achieve a slower phase velocity [1-2]. In either case, in addition to compactness, slow wave resonators in general suffer less from spurious harmonics. Furthermore, the versatility of this method enables its application to a vast range of planar resonator structures.

The second, promising approach employs a special kind of resonator known as a dual-mode resonator. A dual-mode resonator behaves in theory as a pair of coupled resonators, so a single unit can substitute for two regular (single-mode) resonators. Therefore, the degree of success with this approach largely depends on the relative size of the dual-mode resonator. For example, a size reduction of 50 % may be achieved if the dual-mode resonator is identical in size to the single-mode resonator being replaced. As a consequence, the search for a miniaturized dual-mode resonator has always been at the heart of compact filter research, which has spawned several types of interesting structures. Some compact dual-mode resonators found in the research literature include the open-loop resonator [1-3], circular ring [1-4], square loop[1-5] and patch based resonators [1-6]-[1-8]. One deterrent in employing these resonators is that it may not always be physically possible to establish the required inter-resonator coupling within a dual-mode resonator due to fabrication limitations for example. Another concern is the difficulty in adjusting various coupling coefficients independently, especially between the two resonators within the dual-mode unit. Consequently, many dual-mode filter designs rely on a so called non-resonating node to be added between every dual-mode resonator in order to help establish the exact coupling coefficients [1-3]. However, such a method greatly compromises the compactness of a filter.

Yet another alternative in miniaturizing planar filters is to use multiple layers on a printed circuit board [1-9], [1-10]. Resonators that comprise the filter can be spread over the layers in order to save a significant amount of space. Since the multilayer approach can be applied to all kinds of resonators, a greater emphasis is on the resonator footprint. Therefore, this approach is usually combined with the selection of either slow wave or dual-mode resonators in order to gain maximum effect. In contrast to the single layer approach however, there is obviously additional complexity in the fabrication process as well as greater sensitivity to various tolerances.

Other possible methods of filter miniaturization include the use of high dielectric constant substrates [1-11] or the use of lumped elements [1-12]. However, there are several drawbacks to these methods, including excessive loss, which make them less widely used.

Combline bandpass filters are by far the most structurally compact owing to the short circuited distributed resonators loaded with lumped capacitances [1-13]. The larger the lumped loading capacitance, the more compact the structure and resonators as short as $\lambda_g/8$ have been employed in filter development. Another significant advantage of this resonator is that spurious harmonics occur at frequencies greater than thrice the fundamental resonant frequency, which improves further with the size of the lumped capacitance. To avoid excessive loss and to minimize tolerances, designers usually opt for distributed loading capacitances instead of lumped elements, but this elongates the resonators to slightly less than $\lambda_g/4$. This trade off becomes necessary especially at higher operating frequencies where lumped elements become increasingly unusable.

Another ubiquitous planar resonator topology is the open-loop resonator which comes in various forms ranging from square loop, circular loop, to hairpin layouts [1-14]-[1-15]. This type of resonator is very much renowned for its versatility in filter design, making it possible to achieve Butterworth, Chebyshev, and generalised Chebyshev filtering characteristics quite readily by selecting an appropriate coupling scheme. These resonators also benefit greatly when combined with SIR techniques as well as inter-digital capacitors in achieving a highly compact footprint [1-16], [1-17]. More recently, there has even been a report of a highly compact dual-mode open loop resonator [1-3]. Although these resonators are generally $\lambda_g/2$ in length, the folded form enables the lengthwise dimensions to be reduced beyond $\lambda_g/4$. Unlike the combline counterparts, these resonators have the added advantage in that there are no short circuits. Open loop filters do however suffer more from spurious harmonics which appear at around twice the fundamental resonant frequency. However, several reported methods are available in somewhat alleviating this issue. Nevertheless, the incredible versatility and compactness of this kind of resonator rationalises its widespread use in countless planar bandpass filter applications.

1.2.2 Tunable Bandpass Filters

Although research on tunable microwave filters was ongoing for some time, interest in this area has been rekindled as a result of recent technological advancements as well as the sharp rise in tunable filter applications especially in multi-band systems. In contrast to a fixed filter bank, a tunable filter has the advantage of greater functionality, significant compactness and higher selectivity [1-18]. While early research unravelled much of the theoretical aspects of tunable filter design, there have been significantly fewer efforts in implementation and realization of distributed tunable filters in transmission line media.

Generally, center frequency tunability may be achieved by incorporating a controllable reactive element in each resonator comprising a bandpass filter. In theory, a center frequency shift may be obtained when these reactive elements are varied usually in a uniform fashion.

The most widespread controllable tuning element is of course the semiconductor varactor diode, which operates as a voltage controlled capacitance when under a reverse biased voltage. Compared to most other tuning elements, the varactor diodes have superior tuning rates, compact size and operating in reverse bias allows the device to be highly power efficient. The relatively low device tolerances coupled with mass manufacturing capability had made the varactor diode a highly popular choice for tunable filter applications over the past two decades. Despite their widespread use, these devices suffer from relatively poor quality factors and tunable filters based on varactors have relatively high signal distortion (IIP3 around 6 dBm ~ 25 dBm) [1-19].

A second, but less accessible method of tuning a filter is to employ RF micro-electro-mechanical-systems (MEMS) [1-20], [1-21]. Essentially, a MEMS device is a voltage controlled actuator, and they may be used either as switches or variable capacitors. In contrast to varactor diodes, RF MEMS devices have much higher quality factors and significantly better linearity (> 40 dBm). Even through these devices have relatively slow switching speeds (order of microseconds), the largest deterrent to its widespread use is perhaps the significant reliability issues that lies with this premature technology.

Yet another emerging alternative is the use of ferroelectric materials. Ferroelectric devices such as Barium Strontium Titanate (BST) varactors behave as voltage controlled capacitances. Unlike the semiconductor varactor however, the capacitance is varied through control of the device permittivity. Although the loss, switching speeds and linearity may be comparable to their semiconductor counterparts, the tuning range of these devices is severely limited and the bias voltages required can easily reach hundreds of volts [1-22].

The tunability of combline filters has been extensively researched [1-23]-[1-25]. Tunable combline filters were first presented in [1-23] where a relatively high tuning range has been quoted (53%), with mid-band insertion loss in excess of 5 dB. The bandwidth change across the tuning range was restricted to around 12 %. Very similar results have been quoted in [1-24] where a center frequency tuning range of 40 % had been achieved with the best mid-band insertion loss of around 5 dB. A constant bandwidth, center frequency tuned, semiconductor varactor based combline filter has been reported in [1-25] with approximately 12 % tuning range where the bandwidth variation was restricted to around 3.2 %. Active tunable combline filters have also been investigated with the tuning range in the region of 45 % where the active device is used primarily to compensate for filter losses hence to improve the quality factor [1-26]. However, linearity of varactor tuned combline bandpass filters is relatively poor where the IIP3 point is generally less than 20 dBm [1-26].

The subject of tunable open-loop filters has not attracted as much research interest. Nevertheless, there has been new interest in this area recently. Out of the published research literature, there are only a handful of significant publications on the topic. In particular, a 40 % tuning range filter has been quoted with a reasonably low passband insertion loss (1.5 dB – 2.5 dB) and an impressive linearity (IIP3 > 28 dBm) [1-27]. A BST varactor based open-loop four pole quasi-elliptic tunable filter has been reported in [1-28] with a 6 % tuning range and passband insertion loss ranging between 3 to 5 dB. A highly compact open-loop dual-mode resonator based tunable filter has been reported in [1-29] with a tuning range of 41 %, a bandwidth variation of 13 % and a mid-band insertion loss of around 2.2 dB. Although there has not been so much attention paid to filter linearity, an IIP3 of around 20 dB may be anticipated given that varactor diodes are used in the majority of these experiments.

Research into the tunability of planar filters has spawned various other novel resonator configurations. An analytic design technique for the design of microstrip tunable filters has been presented in [1-30], where a second order tunable filter with a 25 % tuning range and around 8 % bandwidth variation has been demonstrated experimentally. However, this filter not only suffers from high mid-band insertion loss (around 7 dB) but also a noticeably poor selectivity due to inadequate unloaded quality factor. A highly linear second order tunable filter is presented in [1-31] with a tuning range of 35 %. The improvement to linearity was reportedly attained by employing a back to back varactor configuration and an IIP3 between 22 dBm and 41 dBm had been experimentally verified. However, there is around 15 % variation in the 3 dB bandwidth across the filter tuning range. This was later improved in a subsequent publication by the same authors where the bandwidth variation has been narrowed to around 8 % [1-32].

1.2.3 Dual-Band Bandpass Filters

With the continuous introduction of new wireless services and standards such as GSM, WiMax, WLAN and GPS to name a few, there has been a tremendous demand for multifunctional wireless systems arising especially from the commercial sector. The shift in trend has far reaching implications for bandpass filters in wireless systems. Although the obvious and trivial solution is to employ filter banks, there are considerable practical difficulties with this approach especially with size. While a tunable filter may be an excellent substitution in an application where the system requires access to only one band at any given time, they are inappropriate in applications where simultaneous access to more than one band is required. This requirement can be met elegantly by multi-band bandpass filters. The simplest of such a filter is the dual-band bandpass filter, and recent developments on this topic are outlined below.

The first and the most obvious method of realising a dual-band bandpass filter is the analytical approach. The starting point of the procedure is the low-pass prototype network, which is then transformed into a dual-band filter by application of the dual-band frequency transformation. Two dual-passband filter design techniques have been proposed based on this approach for the design of symmetric and asymmetric dual-band bandpass filters [1-33]. With the proposed methods, it was possible to obtain N/2 unique transmission zeros across the inner stopband for symmetric passbands while the same number of zeros appears at a single frequency for filters with asymmetric passbands. To prove the concept, dual-band filters have been constructed and verified in coaxial line technology.

The second technique is to exploit the first and second resonant modes of a distributed resonator in realising a dual-passband filter. One way this may be achieved is to employ stepped impedances, which according to the impedance and length ratios, allows the second resonant frequency to be shifted up or down. The control of the second mode enables the technique to be especially effective in the design of dual-band filters where the second passband occurs in the vicinity of the original second resonance. The possibility of employing SIR methods to obtain a dual-passband filter response has been thoroughly investigated [1-34], [1-35]. Despite its success, the placement of the second passband is relatively restricted since the required impedance ratios may not always be physically realizable. A second

drawback of this technique is the lack of transmission zeros in the inner stopband. A more effective approach is to load a point offset from the symmetry plane of an open-loop resonator, with an open circuited stub [1-36]. The length of the added stub and the degree of offset effectively controls the first spurious response of the resonator, which is used to set the second passband. This technique is not as restricted as the SIR method in that there is greater freedom over the choice of the second passband. In any case, when the second resonant mode is used in this manner to obtain a dual-band response, it may not always be possible to set passband bandwidths as required due to generally limited degrees of freedom of this approach.

A third and more simplistic strategy is to cascade a wideband bandpass filter with a bandstop filter to produce a dual-passband response [1-37]. Theoretically, this method permits the realization of almost any dual-band filtering characteristic. However, when the passbands are widely separated, the bandpass and bandstop filters must have wide bandwidths and therefore suffer from poor selectivity. In addition, the cascading of bandpass and bandstop structures increases the overall loss as well as circuit size.

Yet another method is to use open and short circuited stubs along the length of a transmission line [1-38]. Each stub produces a transmission zero, and the zeros may be placed in such a way to achieve a dual-passband with the desired centre frequency and bandwidth. The extension of this technique in obtaining multiband bandpass filters has been reported [1-39].

The fifth strategy is to use a pair of resonators tuned to the upper and lower passbands of the dual-passband filter. By carefully coupling these resonators in a suitable manner, it is possible to realise a dual-passband response [1-40]. This method is quite flexible. The use of two different resonators allows the external quality factors and coupling coefficients to be set almost independently [1-41] so to allow the two bandwidths and center frequencies to be readily defined according to specifications. There is also the option to split the two kinds of resonators between two layers of a printed circuit board to conserve space [1-42].

1.3 Organization of Thesis

This section summarizes the contents of the subsequent chapters to provide the reader with a quick glance at the material covered, where the conclusions are presented in chapter six.

Chapter two of the report presents background theory relevant to the research work undertaken. The characterization of microstrip lines and their properties that directly impact filter design such as attenuation and unloaded quality factor are discussed. Coupled line theory is also presented here as coupled lines are employed later in achieving inter-resonator coupling. A highlight of inverter coupled filters is presented since these prototypes are more suitable for microwave filter implementation.

Chapter three of the dissertation presents a highly compact dual-mode resonator configuration for the design of planar RF and microwave bandpass filters. The resonator is analysed and the existence of two unique modes of resonance is proved. Several variants of the dual-mode resonator, which may be suitable for different applications, are also presented. Equivalent electrical circuits are established for each configuration.

Chapter four of the report firstly explores the application of these resonators in the development of all-pole Butterworth and Chebyshev filters. A filter design technique is proposed in order to greatly facilitate and expedite the filter design process. Several filter design examples are also presented not only to supplement the discussions but to also to provide further guidelines and highlight the key stages of the process. The second half of the chapter investigates the application of these resonators in cross-coupled filters. Comparisons of simulated and measured results of the designed filters are presented to validate the arguments and to showcase performance.

Chapter five investigates the application of these resonators in fixed bandwidth, center frequency tunable bandpass filters. Varactor diodes are used as the tuning element. Measures of controlling the external quality factor and the coupling coefficients are proposed in order to significantly restrict the variation of filter bandwidth with center frequency. Additionally, these filters were shown to have significantly low distortion.

1.4 References

[1-1] J.-S. Hong and M.J. Lancaster, “Theory and experiment of novel microstrip slow-wave open-loop resonator filters”, *IEEE Transactions on Microwave Theory and Techniques*, vol. 45, no. 12, pp. 2358-2365, Dec. 1997.

[1-2] M. Sagawa, M. Makimoto and S. Yamashita, “Geometrical structures and fundamental characteristics of microwave stepped-impedance resonators”, *IEEE Transactions on Microwave Theory and Techniques*, vol. 45, no. 7, pp. 1078-1085, Jul. 1997.

[1-3] J.-S. Hong, H. Shaman and Y.-H. Chun, “Dual-mode microstrip open-loop resonators and filters”, *IEEE Transactions on Microwave Theory and Techniques*, vol. 55, no. 8, pp. 1764-1770, Aug. 2007.

[1-4] A. C. Kundu and I. Awai, “Control of attenuation pole frequency of a dual-mode microstrip ring resonator bandpass filter”, *IEEE Transactions on Microwave Theory and Techniques*, vol. 49, no. 6, pp. 1113-1117, Jun. 2001.

[1-5] J.-S. Hong and M.J. Lancaster, “Realisation of quasielliptic function filter using dual-mode microstrip square loop resonators”, *Electronic Letters*, vol. 31, no. 24, pp. 2085-2086, Nov. 1995.

[1-6] J.-S. Hong and S. Li, “Theory and experiment of dual-mode microstrip triangular patch resonators and filters”, *IEEE Transactions on Microwave Theory and Techniques*, vol. 52, no. 4, pp. 1237-1243, Apr. 2004.

[1-7] B. T. Tan, S. T. Chew, M. S. Leong and B. L. Ooi, “A modified microstrip circular patch resonator filter”, *IEEE Microwave and Wireless Component Letters*, vol. 12, no. 7, pp. 252-254, Jul. 2002.

[1-8] W.-H. Tu and K. Chang, “Miniaturized dual-mode bandpass filter with harmonic control”, *IEEE Microwave and Wireless Component Letters*, vol. 15, no. 12, pp. 838-840, Dec. 2005.

[1-9] G.-S. Huang, Y.-S. Lin, C.-H. Wang and C. H. Chen, "A novel transition-included multilayer filter", *IEEE Transactions on Microwave Theory and Techniques*, vol. 57, no. 4, pp. 807-814, Apr. 2009.

[1-10] C. Lugo and J. Papapolymerou, "Planar realization of a triple-mode bandpass filter using a multilayer configuration", *IEEE Transactions on Microwave Theory and Techniques*, vol. 55, no. 2, pp. 296-301, Feb. 2007.

[1-11] F. Winter, J. Taub and M. Marcelli, "High-dielectric constant stripline band-pass filters", *IEEE MTT-S Symposium Digest*, vol. 2, pp. 555-556, 1991.

[1-12] A.F. Sheta, K. Hettak, J.P Coupez, S. Toutain and J. P. Blot, "A new semi-lumped filter structure", *IEEE MTT-S Symposium Digest*, vol. 2, pp. 383-386, 1995.

[1-13] S. Caspi and J. Adelman, "Design of combline and interdigital filters with tapped-line input", *IEEE Transactions on Microwave Theory and Techniques*, vol. 36, no. 4, pp. 759-763, 1988.

[1-14] J.-S. Hong and M.J. Lancaster, "Couplings of microstrip square open-loop resonators for cross-coupled planar microwave filters", *IEEE Transactions on Microwave Theory and Techniques*, vol. 44, no. 12, pp. 2099-2109, Dec. 1996.

[1-15] J. Bonache, I. Gil, J. G. García and F. Martín, "Novel microstrip bandpass filters based on complementary split-ring resonators", *IEEE Transactions on Microwave Theory and Techniques*, vol. 54, no. 1, pp. 265-271, Jan. 2006.

[1-16] J.-S. Hong and M.J. Lancaster, "Theory and experiment of novel microstrip slow-wave open-loop resonator filters", *IEEE Transactions on Microwave Theory and Techniques*, vol. 45, no. 12, pp. 2358-2365, Dec. 1997.

[1-17] M. Nosrati and Z. Atlasbaf, “A compressed planar band-pass filter using microstrip square resonators with interdigital capacitor”, *International Symposium on Antennas and Propagation*, pp. 1-5, Dec. 2006.

[1-18] J. Uher, and W. J. R. Hoefer, “Tunable microwave and millimeter-wave band-pass filters”, *IEEE Transactions on Microwave Theory and Techniques*, vol. 39, no. 4, pp. 643-653, Apr. 1991.

[1-19] B. E. Carey-Smith and P. A. Warr, “Distortion mechanisms in varactor diode-tuned microwave filters”, *IEEE Transactions on Microwave Theory and Techniques*, vol. 54, no. 9, pp. 3492-3500, Sep. 2006.

[1-20] L. Dussopt and G. M. Rebeiz, “Intermodulation distortion and power handling in RF MEMS switches, varactors and tunable filters”, *IEEE Transactions on Microwave Theory and Techniques*, vol. 51, no. 4, pp. 1247-1256, Apr. 2003.

[1-21] H.-T. Kim, J.-H. Park,Y.-K. Kim and Y. Kwon, “Low-loss and compact V-band MEMS-based analog tunable bandpass filters”, *IEEE Microwave and Wireless Component Letters*, vol. 12, no. 11, pp. 432-434, Nov. 2002.

[1-22] J. Nath, D. Ghosh, J. Maria, A. I. Kingon, W. Fathelbab, P. D. Franzon and M. B. Steer, “An electronically tunable microstrip bandpass filter using thin-film barium–strontium–titanate (BST) varactors”, *IEEE Transactions on Microwave Theory and Techniques*, vol. 53, no. 9, pp. 2707-2712, Sep. 2005.

[1-23] I.C. Hunter and J.D Rhodes, “Electronically tunable microwave bandpass filters”, *IEEE Transactions on Microwave Theory and Techniques*, vol. 30, no. 9, pp. 1354-1360, Sep. 1982.

[1-24] G. Torregrosa-Penalvaand, G. López-Risueño and J. Alonso, “A simple method to design wide-band electronically tunable combline filters”, *IEEE Transactions on Microwave Theory and Techniques*, vol. 50, no. 1, pp. 172-177, Jan. 2002.

[1-25] B. Kim, S. Yun, "Varactor-tuned combline bandpass filter using step-impedance microstrip lines", *IEEE Transactions on Microwave Theory and Techniques*, vol. 52, no. 4, pp. 1279-1283, Apr. 2004.

[1-26] S. Chandler, I. Hunter, J. Gardiner, "Active varactor tunable bandpass filter", *IEEE Microwave and Guided Wave Letters*, vol. 3, no. 3, pp. 70-71, Mar. 1993.

[1-27] S. Park,M. El-Tanani,I. Reines and G. Rebeiz, S. Yun, "Low-loss 4–6-GHz tunable filter with 3-bit high-orthogonal bias RF-MEMS capacitance network", *IEEE Transactions on Microwave Theory and Techniques*, vol. 56, no. 10, pp. 2348-2355, Oct. 2008.

[1-28] S. Courrèges, Y. Li, Z. Zhaoand, K. Choi, A. Hunt and J. Papapolymerou, "A low loss X-band quasi-elliptic ferroelectric tunable filter", *IEEE Microwave and Wireless Component Letters*, vol. 19, no. 4, pp. 203-205, Apr. 2009.

[1-29] W. Tang and J.-S. Hong , "Varactor-tuned dual-mode bandpass filters", *IEEE Transactions on Microwave Theory and Techniques*, vol. 58, no. 8, pp. 2213-2219, Aug. 2010.

[1-30] J. Lee and K. Sarabandi, "An analytic design method for microstrip tunable filters", *IEEE Transactions on Microwave Theory and Techniques*, vol. 56, no. 7, pp. 1699-1706, Jul. 2008.

[1-31] M. El-Tanani and G. Rebeiz, "A two-pole two-zero tunable filter with improved linearity", *IEEE Transactions on Microwave Theory and Techniques*, vol. 57, no. 4, pp. 830-839, Apr. 2009.

[1-32] M. El-Tanani and G. Rebeiz, "Corrugated microstrip coupled lines for constant absolute bandwidth tunable filters", *IEEE Transactions on Microwave Theory and Techniques*, vol. 58, no. 4, pp. 956-963, Apr. 2010.

[1-33] G. Macchiarella and S. Tamiazzo, "Design techniques for dual-passband filters", *IEEE Transactions on Microwave Theory and Techniques*, vol. 53, no. 11, pp. 3265-3271, Nov. 2005.

[1-34] W. S. Chang and C. Y. Chang, "Analytical design of microstrip short-circuit terminated stepped-impedance resonator dual-band filters", *IEEE Transactions on Microwave Theory and Techniques*, vol. 59, no. 7, pp. 1730-1739, Jul. 2011.

[1-35] Y. Ping and M. Sun, "Dual-band microstrip bandpass filter using stepped-impedance resonators with new coupling schemes", *IEEE Transactions on Microwave Theory and Techniques*, vol. 54, no. 10, pp. 3779-3785, Oct. 2006.

[1-36] P. Mondal and M. K. Mandal, "Design of dual-band bandpass filters using stub-loaded open-loop resonators", *IEEE Transactions on Microwave Theory and Techniques*, vol. 56, no. 1, pp. 150-155, Jan. 2008.

[1-37] L. C. Tsai and C. W. Hsue, "Dual-band bandpass filters using equal-length coupled-serial-shunted lines and z-Transform technique", *IEEE Transactions on Microwave Theory and Techniques*, vol. 52, no. 4, pp. 1111-1117, Apr. 2004.

[1-38] H. M. Lee and C. M. Tsai, "Dual-band filter design with flexible passband frequency and bandwidth selections", *IEEE Transactions on Microwave Theory and Techniques*, vol. 55, no. 5, pp. 1002-1009, May 2007.

[1-39] C. Quendo, A. Manchec, Y. Clavet, E. Rius, J.F. Favennec and C. Person, "General synthesis of N-band resonator based on N-order dual behavior resonator", *IEEE Microwave Wireless Component Letters*, vol. 17, no. 5, pp. 337-339, May 2007.

[1-40] C.-Y. Chen and C.-Y Hsu, "A simple and effective method for microstrip dual-band filters design", *IEEE Microwave Wireless Component Letters*, vol. 16, no. 5, pp. 246-248, May 2006.

[1-41] X. Y. Zhang, J. Shi, J.-X. Chen and Q. Xue, “Dual-band bandpass filter design using a novel feed scheme”, *IEEE Microwave Wireless Component Letters*, vol. 19, no. 6, pp. 350-352, Jun. 2009.

[1-42] X. Y. Zhang, J.-X. Chen and Q. Xue, “Novel dual-band filter using slotline and microstrip resonators”, *Microwave Optical Technology Letters*, vol. 49, no. 5, pp. 1080-1082, May 2007.

2.0 BACKGROUND

Various background materials surrounding the lines of investigation of this dissertation are concisely covered in this section. Firstly, microstrip lines and their properties are described to highlight their effectiveness and limitations pertaining distributed planar filter realization. The significance of the unloaded quality factor of a resonator in filter design is described with a discussion on the same of microstrip resonators. Microstrip coupled lines, ubiquitously employed in a variety of bandpass filter topologies particularly for coupling resonators, is described. Lastly, a brief overview of inverter coupled filter prototypes is presented and is extended to highlight the theory of cross-coupled filters.

2.1 The Microstrip Line

The microstrip transmission line essentially consists of two conductors separated by some form of dielectric material as illustrated in Fig. 2-1. The top conductor is designated as the signal line while the bottom plate, which is usually several times wider, serves as the ground plane. The properties of these two conductors together with the dielectric filling determine the signal transmission characteristics of the line.

Due to the exposed nature of the microstrip line, the electromagnetic fields exist not only within the dielectric but some also extend into the air above. As the relative permittivity of the material ε_r is almost always greater than unity, the resulting inhomogeneous interface cannot support a pure TEM wave between the air-dielectric interface since the fields in air will invariably propagate faster than the fields within the dielectric.

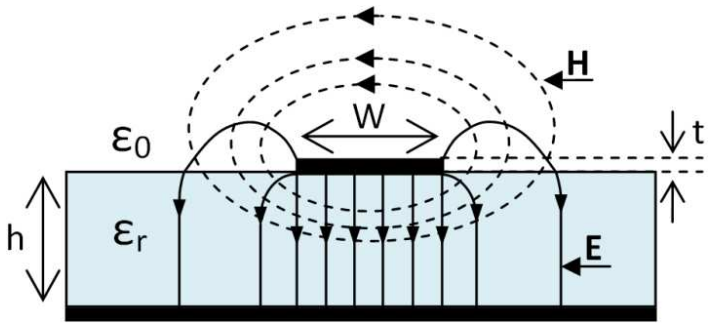

Fig. 2-1: Side on view of excited microstrip line with corresponding electric (solid lines) and magnetic (dashed lines) fields.

The relatively weak longitudinal field components however enable a quasi-static approximation to be employed in characterizing the line up to a few giga hertz [2-1]. This approach assumes the propagation of a pure TEM mode which greatly simplifies the related calculations. Once the capacitance per unit length with and without the dielectric, C_d and C_0 respectively are determined, the effective relative dielectric constant, ε_{eff}, the characteristic impedance, Z_0, phase constant, β, and phase velocity, V_p, may be computed using (2.1) - (2.4) respectively, where *c* is the speed of light in free space.

$$\varepsilon_{eff} = \frac{C_d}{C_0} \tag{2.1}$$

$$Z_0 = \frac{1}{c\sqrt{C_0 C_d}} \tag{2.2}$$

$$\beta = \frac{\omega}{c}\left(\frac{C_d}{C_0}\right) \tag{2.3}$$

$$V_p = c\sqrt{\frac{C_0}{C_d}} \tag{2.4}$$

At higher frequencies however, the above approximations lose accuracy as conductor thickness, t, substrate height, h, and line width, W, begin to have a noticeable effect on the line parameters. Curve fitting techniques have been employed to develop more accurate formulations to somewhat mitigate these higher frequency effects [2-2]. Nevertheless, this approach is useful for hand calculations in determining line parameters approximately.

Full wave electromagnetic analysis methods have become the standard nowadays due to the widespread availability of powerful computers as well as full wave electromagnetic software packages. These techniques solve Maxwell's equations, using advanced numerical methods, for the corresponding line parameters by applying the given boundary conditions. While taking into consideration all longitudinal field components as well, these calculations are usually performed over a number of frequencies and therefore are able to account for dispersive effects of the line. All in all, the full wave analysis techniques are able to provide significantly more accurate results by exploiting modern computing power.

Microstrip lines have relatively high loss arising from conductor loss, dielectric loss and radiation loss. Out of these three loss mechanisms, the conductor and dielectric loss are the most significant.

Conductors dissipate power as heat due to the finite conductance of the metal trace. Conductor loss is exacerbated at high frequencies due to the skin effect [2-3]. At RF and microwave frequencies, current is no longer uniformly distributed across the cross section of the signal trace. Due to eddy currents induced within the trace, signal current vanishes in the centre of the conductor and concentrates near the trace edges. This effectively reduces the cross-sectional area of the trace at high frequencies, increases the trace resistance and therefore also the attenuation constant of the line.

Dielectric loss is due to two factors. Firstly, real dielectrics have non-zero conductivity. Therefore, the movement of charge between the two conductors via the dielectric is one source of energy loss. Atomic and molecular resonances and the heating effect brought on as a consequence is the second source of dielectric loss. Dielectric loss grows at a much greater rate with frequency than conductor loss and becomes a major concern at higher frequencies.

Radiation loss on the other hand is caused by radiating fields inducing currents on other conducting bodies in the vicinity of the line.

Although the attenuation constant may be determined with accuracy given the exact knowledge of the trace geometry as well as the field distribution [2-4], the computation is complicated. On the other hand, methods such as the perturbation method [2-1] and Wheel's incremental inductance formula [2-5], given by (2.5), may be used to determine conductor attenuation constant, α_c, approximately, where x is the distance into the conductor trace, W is the trace width and the surface resistance, R_s, is given by (2.6).

$$\alpha_c = \frac{R_s}{2Z_0\sqrt{\mu_0/\varepsilon}}\frac{dZ_0}{dx} \tag{2.5}$$

$$R_s = \sqrt{\frac{\omega\mu_0}{2\sigma}} \tag{2.6}$$

With the widespread availability of full wave electromagnetic software, it is possible to extract the attenuation constants from a matched line, one at a time, from simulations using equation (2.7b), which may be arrived at by the simple manipulation of (2.7a), where in both equations, the magnitude of S_{21} is used rather than its decibel equivalent.

$$|S_{21}| = e^{-(\alpha_{c/d})z} \tag{2.7a}$$

$$\alpha_{c/d} = \frac{-\ln|S_{21}|}{z} \tag{2.7b}$$

For example, when the conductor attenuation constant is to be determined, the condition that tan δ = 0 is imposed and to determine the dielectric attenuation constant, the metal conductivity, σ, is assumed to be infinite. The overall attenuation constant may be found by the summation of these different attenuation constants. The net attenuation is required to determine the unloaded quality factors of distributed resonators as described in the next section.

2.2 Unloaded Quality Factor

The unloaded quality factor of a resonator is a crucial parameter which determines the feasibility of that resonator for filter implementation. Power dissipation within a resonator is inversely proportional to its unloaded quality factor. An ideal resonator having an infinitely large quality factor will not dissipate any power. In contrast, power dissipation, and therefore filter passband insertion loss increases as the unloaded quality factor lowers [2.6]. Moreover, finite quality factors cause the rounding of passband edges leading to an overall reduction in filter selectivity. Limitations in quality factor are especially a concern in high order filters since the amount of loss incurred as well as the reduction in selectivity are proportional to the number of dissipative resonators employed.

A relatively accurate formula (2.8) for estimating the mid-band insertion loss, L_i, from the unloaded quality factor of the i^{th} resonator, Q_{ui}, and fractional bandwidth, *FBW*, and filter order, *N*, is described in [2.7], where g_i are the lowpass prototype element values.

$$L_i = 4.343 \sum_{i=1}^{N} \frac{g_i}{FBW Q_{ui}} \tag{2.8}$$

Consequently, for the same unloaded quality factor, the mid-band insertion loss will increase for smaller fractional bandwidths as illustrated in Fig. 2-2 (a). Likewise, from Fig. 2-2 (b), for the same fractional bandwidth, it is seen that the mid-band insertion loss increases with lowering unloaded quality factor. It is also evident from Fig. 2-2 (c) that there is greater mid band loss for higher filter orders due to the use of more dissipative resonators.

In passive lumped element filters, finite quality factors arise mainly due to the winding resistance of the inductors. However, in distributed filters, finite resonator quality factors result largely from the loss a signal incurs as it propagates along the transmission medium.

In the case of a microstrip medium, conductor and dielectric loss may be considered the most significant contributors towards loss. Although these losses may be controlled to a certain extent by employing low loss substrates [2-8], better conducting traces [2-9]-[2-11] and resonator topologies less prone to loss [2-12], [2-13], the maximum realistically achievable unloaded resonator quality factors are generally under 300 for copper based microstrip lines [2-14].

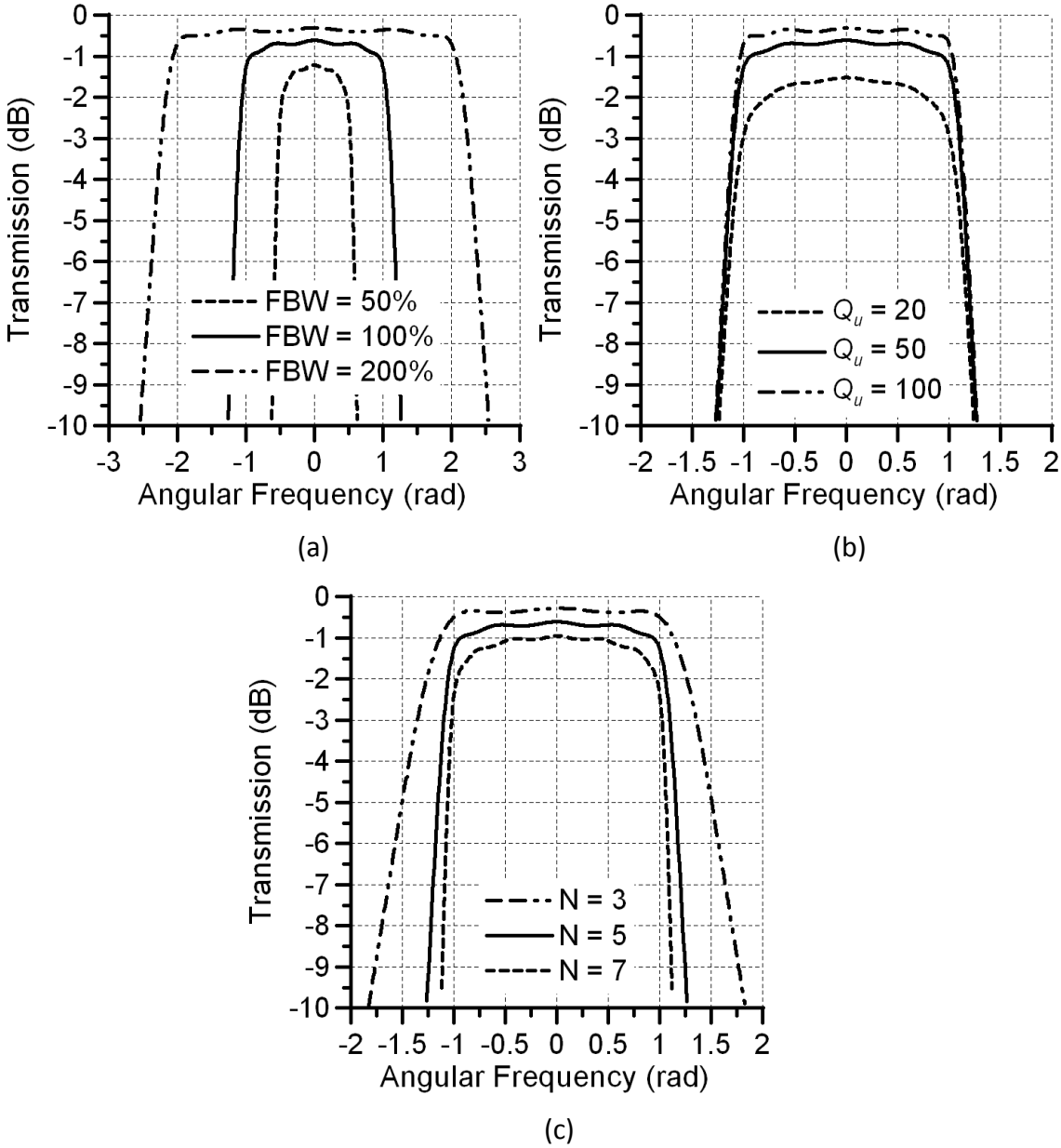

Fig. 2-2: Transmission of normalized Chebyshev bandpass filter. Filter transmission against (a) *FBW*, where Q_u = 50 and N = 5 (b) Q_u, where *FBW* = 100 % and N = 5 (c) N, where Q_u = 50 and *FBW* = 100 %

The attenuation constant is required to estimate the unloaded quality factor of a microstrip resonator. To gain insight, Fig. 2-3 plots the unloaded resonator quality factor of half wavelength microstrip resonators with a resonant frequency of 5 GHz, constructed on typical a high frequency material, against various strip impedances. The attenuation constants extracted from (2.7b) were used to calculate the unloaded quality factors of the resonators. Reducing the strip thickness not only increases the characteristic impedance of the resonator but also increases losses due to the skin resistance. Therefore, the resonator unloaded quality factor degrades with rising strip impedance. The significance of this effect can be seen in Fig. 2-3, where a dramatic reduction of the quality factor can be observed.

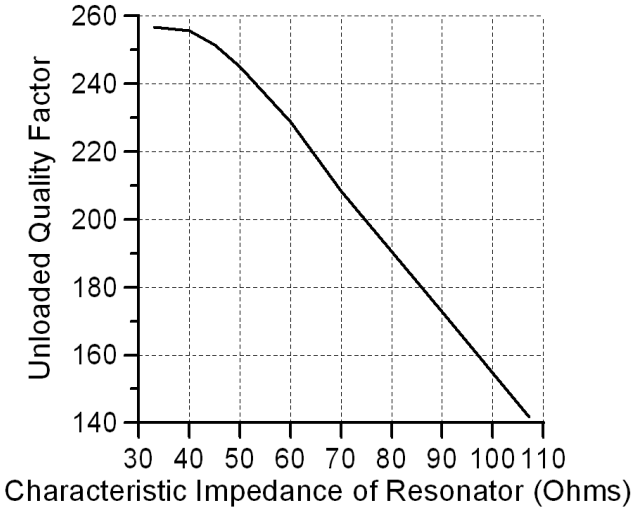

Fig. 2-3: Unloaded Q factor of microstrip λ/2 resonator for various characteristic impedances ,where substrate = Rogers 6010LM with ε_r = 10.2, h = 1.27 mm with copper conductors.

Since all practical resonators have some degree of internal loss, the resulting filters always exhibit non-zero mid-band insertion loss as well as reduced selectivity. An obvious solution to both these effects is to somehow achieve infinite unloaded quality factor. Intuitively, this implies having resonators with zero loss, which is practically impossible for passive resonators. In effect, if a negative resistance, which exactly cancels that of the resonator, is introduced, zero loss can be achieved. An active device incorporated into a resonator to compensate for its losses is able to do just this and an infinite unloaded quality factor may indeed be attained [2-15]-[2-17]. However, as with most solutions, there are tradeoffs. Active devices increase power consumption, introduce distortion components, degrade signal to noise ratio and greatly increases circuit complexity and size.

From Fig. 2-2 (b), it is evident that a slight increase in the mid-band insertion loss of a lossy filter can not only produce a flatter passband but also improve the filter selectivity. A solution derived from this principle, widely known as lossy filter synthesis [2-18]-[2-20], avoids the use of active devices altogether. Lossy elements cause the poles and zeros of a filter to shift slightly to the left in the S-domain. If all resonators have uniform unloaded quality factor, then the shift is by an amount $\alpha = \omega_0/Q_u$ [2-6]. The principle behind lossy synthesis is to predistort the original filter poles and zeros so as to compensate for these shifts. For an all-pole filter, while this involves translating the poles to the right, care must be taken to ensure that the these are strictly confined to the left half of the S-plane. Fig. 2-4 below illustrates the effect of loss on an ideal filter response and how predistortion to some degree mitigates the reduction in bandwidth and flattens the passband. Although predistorted filters are unable to compensate for the losses as in active filters, a purely passive implementation guarantees that there is no added design complexity.

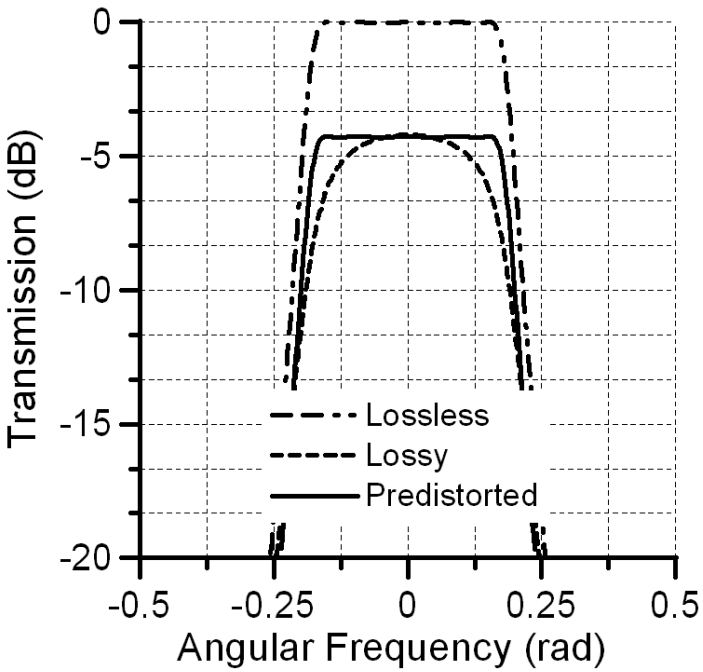

Fig. 2-4 Comparison of 5th order Chebyshev filter transmission response for lossless, lossy and predistorted cases (where Q_u = 10 for lossy and predistorted responses).

2.3 Microstrip Coupled Lines

A pair of parallel microstrip lines, in close proximity, allows a microwave signal to couple from one line to another. As such, these so called coupled microstrip lines serve as basic building blocks of microstrip filters, where they are employed in coupling resonators. The cross section of a coupled microstrip line with the corresponding electromagnetic fields in the even and odd mode is illustrated in Fig. 2-5.

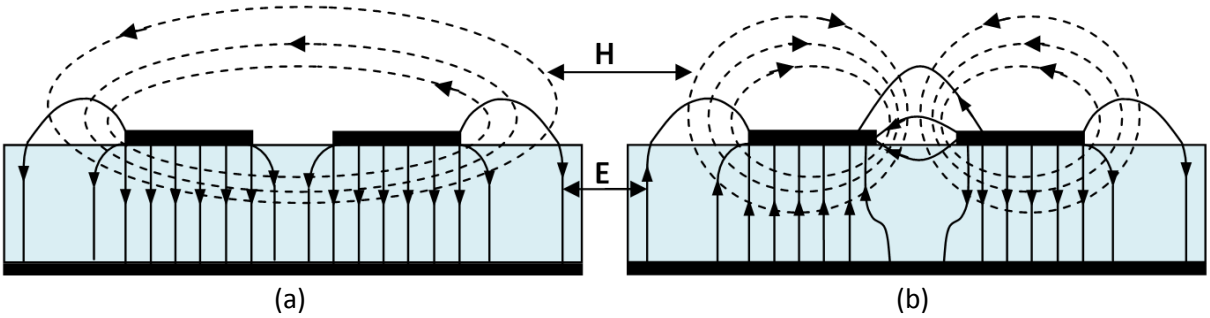

Fig. 2-5: Side on view of field distribution of microstrip coupled lines of (a) even mode (b) odd mode excitation.

Generally, any voltage or current excitation on the lines may be decomposed into even and odd components. In the even mode, signal coupling occurs via the magnetic field and in the odd mode this occurs via the electric field. Although in the general case, both types of field contribute towards coupling, they may interact in either a constructive or destructive manner depending on how the lines are excited [2-2]. Therefore, the coupling strength observed is in fact due to an interaction of these two effects. In microstrip coupled lines, due to the different field distributions, the even and odd mode propagate at slightly different phase velocities.

A lumped element model for a differential element of a pair of coupled transmission lines is illustrated in Fig. 2-6, where L_1, C_1, L_2 and C_2 are the self inductance and shunt capacitance per unit length of line 1 and line 2 respectively and L_m and C_m are the mutual inductance and capacitance per unit length between the two lines. The terminal voltages and currents in general are described by the differential equations (2.9)-(2.12).

$$\frac{dV_1}{dz} = L_1 \frac{dI_1}{dt} + L_m \frac{dI_2}{dt} \tag{2.9}$$

$$\frac{dV_2}{dz} = L_m \frac{dI_1}{dt} + L_2 \frac{dI_2}{dt} \tag{2.10}$$

$$\frac{dI_1}{dz} = C_{1g} \frac{dV_1}{dt} + C_m \frac{d(V_1 - V_2)}{dt} \tag{2.11}$$

$$\frac{dI_2}{dz} = C_m \frac{d(V_2 - V_1)}{dt} + C_{2g} \frac{dV_2}{dt} \tag{2.12}$$

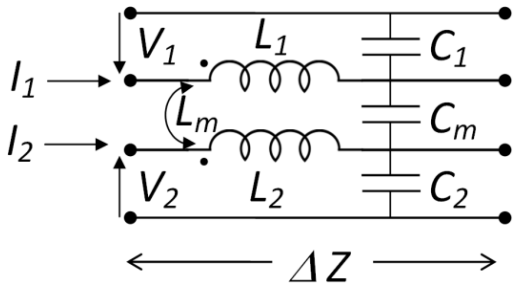

Fig. 2-6: Lumped element circuit model of coupled transmission lines

For an even mode excitation, the terminal voltages $V_1 = V_2 = V$ and currents $I_1 = I_2 = I$ are assumed. Applying these conditions to the above equations give (2.13)-(2.16), where $C_1 = C_{1g} + C_m$ and $C_2 = C_{2g} + C_m$ are the self capacitances per unit length of the lines 1 and 2 respectively.

$$\frac{dV}{dz} = L_1 \frac{dI}{dt} + L_m \frac{dI}{dt} = (L_1 + L_m) \frac{dI}{dt} \tag{2.13}$$

$$\frac{dV}{dz} = L_m \frac{dI}{dt} + L_2 \frac{dI}{dt} = (L_2 + L_m) \frac{dI}{dt} \tag{2.14}$$

$$\frac{dI}{dz} = C_{1g} \frac{dV}{dt} = (C_1 - C_m) \frac{dV}{dt} \tag{2.15}$$

$$\frac{dI}{dz} = C_{2g} \frac{dV}{dt} = (C_2 - C_m) \frac{dV}{dt} \tag{2.16}$$

The equations below indicate that the even mode equivalent inductance is L_1+L_m and L_2+L_m while the corresponding capacitance is C_1-C_m and C_2-C_m for line 1 and 2 respectively. Therefore, the even mode characteristic impedance of line 1 may be defined by (2.17) and the corresponding impedance of line 2 may be similarly defined.

$$Z_{even} = \sqrt{\frac{L_1 + L_m}{C_1 - C_m}} \tag{2.17}$$

A similar argument for the odd mode where the applied conditions are V_1 = - V_2 and currents I_1 = - I_2 yields the odd mode equivalent inductance as L_1-L_m and L_2-L_m and corresponding capacitance as C_1+C_m and C_2+C_m for line 1 and 2 respectively. Therefore, the odd mode characteristic impedance of line 1 may be defined by (2.18) and the corresponding impedance of line 2 may be defined likewise.

$$Z_{odd} = \sqrt{\frac{L_1 - L_m}{C_1 + C_m}} \tag{2.18}$$

Another key parameter especially for filter design is the coupling coefficient, defined as the ratio of the coupled energy to the stored energy. The normalized electric and magnetic coupling coefficients K_E and K_M are given by (2.19) and (2.20) respectively.

$$K_E = \frac{C_m}{\sqrt{C_1 C_2}} \tag{2.19}$$

$$K_M = \frac{L_m}{\sqrt{L_1 L_2}} \tag{2.20}$$

2.4 Inverter Coupled Filters

As lumped elements become no longer practical at high frequencies, RF and microwave filter realization relies on distributed elements based on transmission lines segments. The use of transmission line elements however has a number of drawbacks. One in particular is that depending on the type of line, it may only be practically convenient to use either series or shunt type elements. In microstrip media for example, shunt elements are usually avoided since they require the use of vias on printed circuit boards.

All-pole ladder filter prototype networks usually consist of an array of series and shunt reactive elements. For microwave filters however, due to implementation difficulties of either series or shunt elements, a different kind of lowpass filter prototype network is employed for convenience. The so called inverter coupled filter prototypes that consist exclusively of either series or shunt reactive elements are better suited for the design of distributed RF and microwave filters.

Despite only employing series or shunt reactive elements, the inverter coupled prototypes must essentially match their lowpass ladder counterparts. Immittance inverters are used in inverter coupled circuits to achieve this equivalence [2-1]. The immittance inverters effectively allow series connected elements to behave as a shunt connect elements and vice versa [2-2]. Therefore, while a series connected inverter coupled network employs inverters to realize shunt elements, a shunt connected network uses inverters to realize series elements.

In addition to the implementation of all-pole ladder filters, inverter coupled filter models can be more conveniently extended to filters where they may be non-zero coupling between non-adjacent reactive elements. These so called cross-coupled filters have the unique property of producing finite frequency transmission zeros in the filter stopband and are therefore widely employed in the development of filters with enhanced selectivity.

2.4.1 Inverter Coupled All-Pole Canonical Filter Prototypes

Lumped element all-pole ladder prototype networks consist of series connected inductive and shunt connected capacitive elements as illustrated in Fig. 2-7, where g_i are the low pass element values. Immittance inverters may be employed in order to avoid the use of either shunt or series type elements and therefore allow the same prototype to be realized with purely series or shunt elements as shown in Fig. 2-8 [2-2].

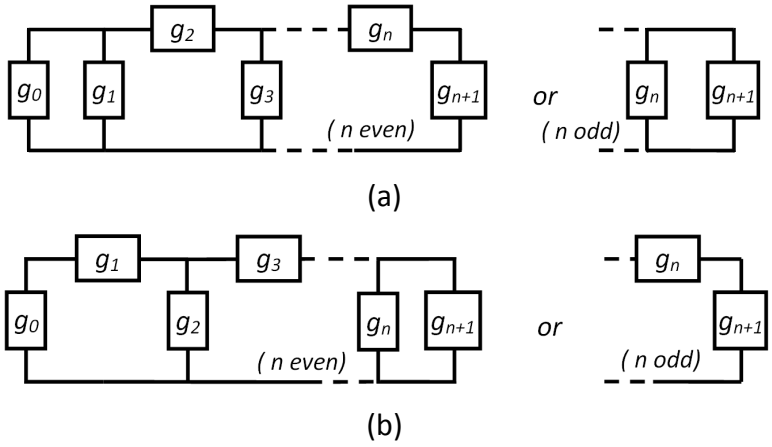

Fig. 2-7 Lowpass prototype networks for all-pole filters with (a) ladder network structure and (b) its dual.

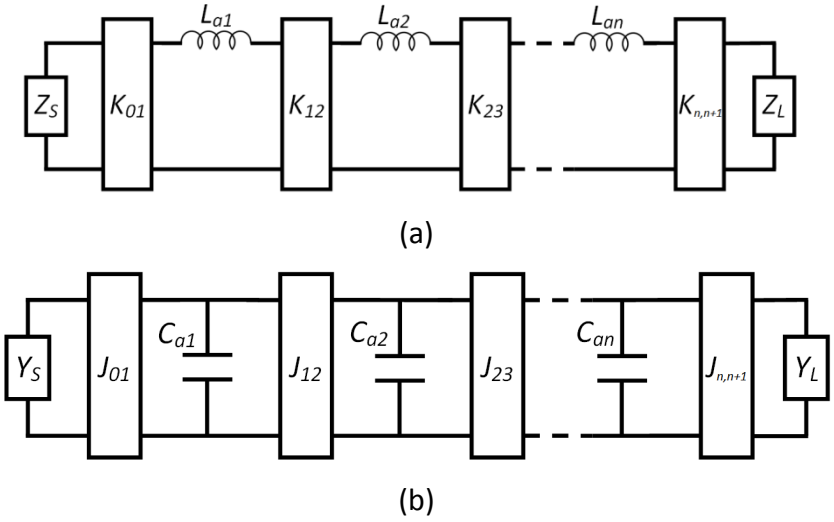

Fig. 2-8 Inverter coupled lowpass prototype networks for all-pole filters with (a) impedance and (b) admittance inverters.

In order for the lowpass ladder and inverter coupled prototypes to be equivalent, the input immittance looking into each circuit must be identical except for a constant scale factor. The input impedance of the circuits in Fig. 2-7(a) and Fig. 2-8(a), may be written as (2.21) where α is the impedance scaling factor and Z_{res1} and Z_{res2} are the residues.

$$Z_{in} = \alpha\left[g_0 + \cfrac{1}{sg_1 + \cfrac{1}{sg_2 + \cfrac{1}{sg_3 + Z_{res1}}}}\right] = \left[Z_S + \cfrac{K_{01}^2}{sL_{a1} + \cfrac{K_{12}^2}{sL_{a2} + \cfrac{K_{23}^2}{sL_{a3} + Z_{res2}}}}\right] \qquad (2.21)$$

Equating these two impedances allows the inverter impedances K_{xy} to be calculated as (2.22a)-(2.24a), in order for equivalence to be achieved. Admittance inverter parameters J_{xy} may be calculated similarly by equating the input admittance of circuits of Fig. 2-7 (b) and Fig. 2-8 (b).

$$K_{01} = \sqrt{\frac{Z_S L_{a1}}{g_0 g_1}} \qquad (2.22a)$$

$$K_{i,i+1} = \sqrt{\frac{L_{ai} L_{ai+1}}{g_i g_{i+1}}} \qquad (2.23a)$$

$$K_{n,n+1} = \sqrt{\frac{L_{an} Z_L}{g_n g_{n+1}}} \qquad (2.24a)$$

The bandpass filter transformations may be applied directly to the inverter coupled prototypes in order to obtain filters that comprise exclusively of either series or shunt resonators as shown in Fig. 2-9. The impedances of the inverters are invariant under this transform and may be calculated by (2.22b)-(2.24b) given the bandpass element values, L_{si}, the filter angular center frequency, ω_0, and the fractional bandwidth, *FBW* [2-2].

$$K_{01} = \sqrt{\frac{Z_S FBW\, \omega_0 L_{s1}}{g_0 g_1}} \qquad (2.22b)$$

$$K_{i,i+1} = FBW\, \omega_0 \sqrt{\frac{L_{si} L_{si+1}}{g_i g_{i+1}}} \qquad (2.23b)$$

$$K_{n,n+1} = \sqrt{\frac{FBW\, \omega_0 L_{sn} Z_L}{g_n g_{n+1}}} \qquad (2.24b)$$

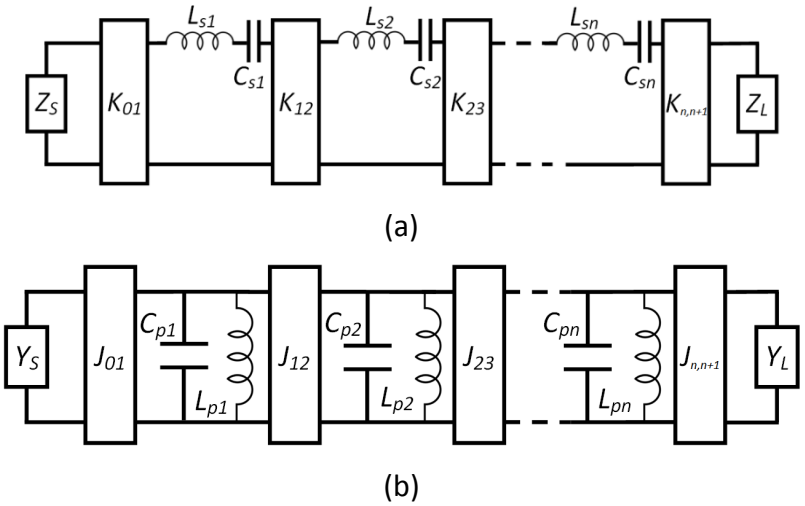

Fig. 2-9 Inverter coupled bandpass filter networks with (a) series and (b) parallel resonators.

2.4.2 Cross-Coupled Filters

The previous section described inverter coupled lowpass prototype filters and their relationship with all-pole prototype ladder networks. The resulting inverter coupled all-pole filter consisted of reactive elements that are only coupled to adjacent elements via immittance inverters. A wider class of filtering functions are generally available if there exists non-zero coupling between non-adjacent reactive elements.

Cross-coupled filter configurations are commonly employed in realizing filters with finite frequency transmission zeros [2-2]. The zeros of such a filter result in better skirt selectivity for the same filter order compared to an all-pole filter. The maximum number of zeros produced is equal to the total number of bypassed reactive elements [2-21]. However, these zeros distort the phase response especially when placed in the vicinity of the filter passband.

A widely adopted method of designing cross-coupled filters is to use computer based optimization in order to extract the filter parameters [2-2]. The general impedance matrix, $[Z]$, of a lowpass cross-coupled n^{th} order filter consisting of series inductances, $L_a = 1/\omega_C$, coupled through impedance inverters is given by (2.25), where ω_c is the angular cut-off frequency, Q_{eS} and Q_{eL} are the source and load external quality factors, m_{xy} are the normalized coupling coefficients and p is the complex lowpass frequency variable. In order for the structure to be physically realizable, this matrix must be symmetric.

$$[Z] = \begin{bmatrix} Z_s & -jK_{01} & \dots & -jK_{0n} & -jK_{0L} \\ -jK_{01} & j\omega L_a & \dots & \dots & -jK_{1L} \\ \vdots & \dots & j\omega L_a & \dots & \vdots \\ -jK_{0n} & \dots & \dots & j\omega L_a & -jK_{nL} \\ -jK_{0L} & -jK_{1L} & \dots & -jK_{nL} & Z_L \end{bmatrix}$$

$$= L_a \begin{bmatrix} \frac{1}{Q_{eS}} & -jm_{01} & \dots & -jm_{0n} & -jm_{0L} \\ -jm_{01} & p & \dots & \dots & -jm_{1L} \\ \vdots & \dots & p & \dots & \vdots \\ -jm_{0n} & \dots & \dots & p & -jm_{nL} \\ -jm_{0L} & -jm_{1L} & \dots & -jm_{nL} & \frac{1}{Q_{eL}} \end{bmatrix} \quad (2.25)$$

It is also possible define a normalized impedance matrix, $[\bar{Z}]$ as (2.26), consisting of three separate component matrices, where all matrices are of size (n+2) by (n+2), where [*U*] is an identity matrix but with the first and the last elements of the diagonal equal to zero, [*Q*] is matrix with all entries zero except for $Q_{11} = 1/Q_{eS}$ and $Q_{n+2,n+2} = 1/Q_{eL}$, and [*m*] is the normalized coupling coefficient matrix.

$$[\bar{Z}] = \frac{[Z]}{L_a} = [Q] + p[U] - j[m] \quad (2.26)$$

The scattering parameters of the filter may then be computed from the inverse of the normalized impedance matrix from (2.27) and (2.28).

$$S_{21} = 2\frac{1}{\sqrt{Q_{eS}Q_{eL}}}[\bar{Z}]^{-1}_{(n+2,1)} \quad (2.27)$$

$$S_{11} = 1 - \frac{2}{Q_{eS}}[\bar{Z}]^{-1}_{(1,1)} \quad (2.28)$$

Computer based optimization methods use the normalized impedance matrix in the form of (2.26) together with (2.27) and (2.28) in order to iteratively optimize the coupling coefficient matrix [*m*] to produce a desired filtering characteristic. Once the optimum coupling coefficients are determined, the inverter coupled bandpass filter network may be obtained by applying the bandpass frequency transformation to the series inductances, L_a, which may be used directly for microwave filter implementation.

Generally, a cross-coupled bandpass filter may have non-zero coupling between all resonators. Practically, coupling between all resonators is difficult to realize simultaneously. It may not be possible in most cases for example to place all the resonators within sufficient proximity in order to realize all the required coupling exactly.

One approach in circumventing such problems is to use conventional cross-coupled resonator configurations such as the quadruplet or the trisection filters [2-2] as illustrated in Fig. 2-10. While quadruplet section produces a pair of transmission zeros since the cross coupling bypasses two resonators, each trisection produces a single zero since only one resonator is bypassed. More transmission zeros may be produced for higher order filters that are realized by cascading these sections. For example, an eighth order filter comprising of two cascaded quadruplet sections may produce up to 4 transmission zeros.

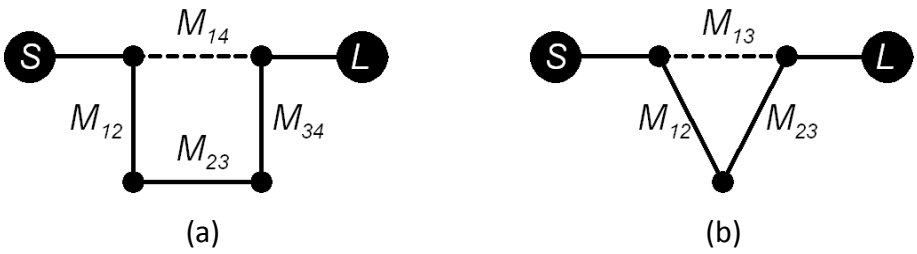

Fig. 2-10 Cross-coupled filter configurations with (a) quadruplet and (b) trisection filters, where solid and dashed lines denote direct and cross coupling respectively and dark circles represent reactive elements.

A filter example is now presented in order to evaluate and compare the performance of a standard Chebyshev and generalized Chebyshev filter of the same order. The filter specifications are: Filter order = 4, angular equi-ripple cut-off frequency = 1 rad, passband ripple = 0.01 dB, terminating impedance = 1 Ω.

The optimized coupling matrix for the Chebyshev and generalized Chebyshev filters are given by (2.29a) and (2.29b) respectively and the corresponding S-parameter response is illustrated in Fig. 2-11. The 4th order generalized Chebyshev filter is of the quadruplet filter type, with non-zero cross-coupling coefficient of - 0.275 between the 1st and the 4th reactive elements. It can be seen that for the same filter order, the generalized Chebyshev filter offers better selectivity

$$[m] = \begin{bmatrix} 0 & 1.1844 & 0 & 0 & 0 & 0 \\ 1.1844 & 0 & 1.081 & 0 & 0 & 0 \\ 0 & 1.081 & 0 & .794 & 0 & 0 \\ 0 & 0 & .794 & 0 & 1.081 & 0 \\ 0 & 0 & 0 & 1.081 & 0 & 1.1844 \\ 0 & 0 & 0 & 0 & 1.1844 & 0 \end{bmatrix} \quad (2.29a)$$

$$[m] = \begin{bmatrix} 0 & 1.1844 & 0 & 0 & 0 & 0 \\ 1.1844 & 0 & 1.081 & 0 & -0.275 & 0 \\ 0 & 1.081 & 0 & .958 & 0 & 0 \\ 0 & 0 & .958 & 0 & 1.081 & 0 \\ 0 & -0.275 & 0 & 1.081 & 0 & 1.1844 \\ 0 & 0 & 0 & 0 & 1.1844 & 0 \end{bmatrix} \quad (2.29b)$$

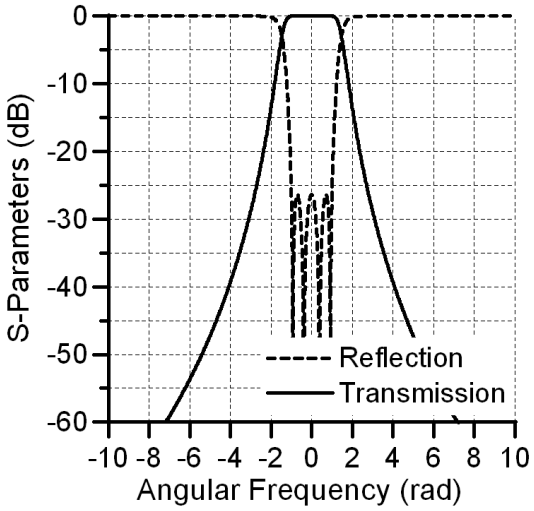

(a)

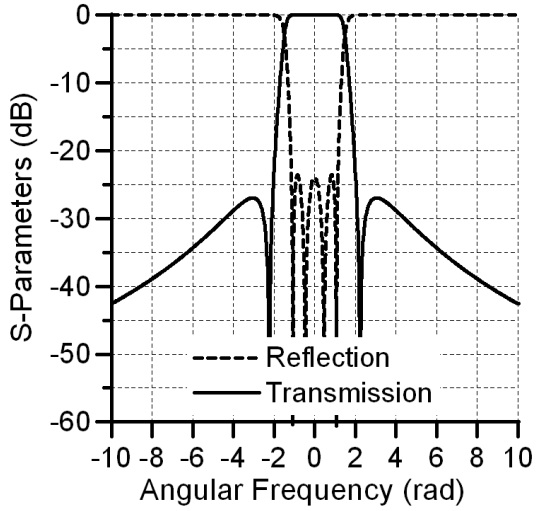

(b)

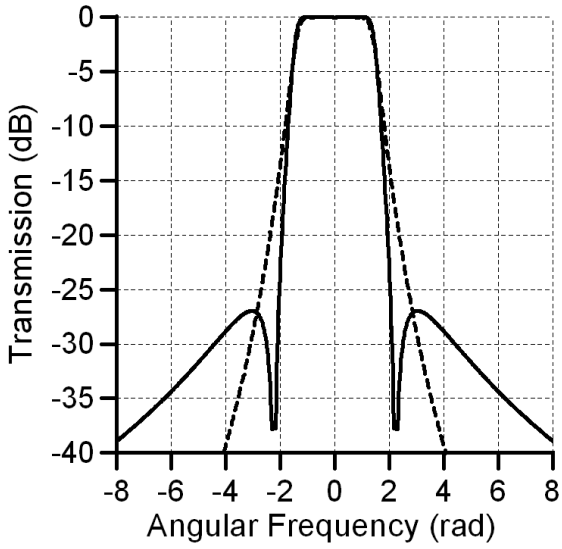

(c)

Fig. 2-11 S-parameter response of (a) Chebyshev and (b) generalized Chebyshev filters. (c) Comparison of the transmission response, where dotted line denotes the Chebyshev response.

2.5 References

[2-1] D. M. Pozar, *Microwave engineering*, 3rd edition, New York: John Wiley & Sons, 2004.

[2-2] J.-S Hong and M. J. Lancaster, *Microstrip filters for RF/microwave applications*, New York: John Wiley & Sons, 2001.

[2-3] R.A. Pucel, D.J. Masse and C. P. Hartwig, "Losses in Microstrip", *IEEE Transactions on Microwave Theory and Techniques*, vol. 16, no. 6, pp. 342 - 350, Jun. 1968.

[2-4] D. Mirshekar-Syahkal and J.B. Davies, "Accurate solution of microstrip and coplanar structures for dispersion and for dielectric and conductor losses", *IEEE Transactions on Microwave Theory and Techniques*, vol. 27, no. 7, pp. 694 - 699, Jul. 1979.

[2-5] S. B. Cohn, "Dissipation Loss in Multiple-Coupled-Resonator Filters", *Proceedings of the IRE*, vol. 47, no. 8, pp. 1342 - 1348, Aug. 1959.

[2-6] I. C. Hunter, *Theory and design of microwave filters*, London: Institute of Electrical Engineers, 2001.

[2-7] P. W. Wong and I. C. Hunter, "Electronically reconfigurable microwave bandpass filter", *IEEE Transactions on Microwave Theory and Techniques*, vol. 57, no. 12, pp. 3070 - 3079, Dec. 2009.

[2-8] Rogers Corporation, "RT/duroid 5870 /5880 High Frequency Laminates," [Online], Available: http://www.rogerscorp.com/documents/606/acm/RT-duroid-5870-5880-Data-Sheet.aspx

[2-9] S.-N. Lee, J.-I. Lee, Y.-J. Kim and J.-G. Yook, "Low-loss thin film microstrip lines and filters based on magnetorheological finishing", *IEEE Transactions on Components and Packaging Technologies*, vol. 30, no. 4, pp. 849-854, Dec. 2007.

[2-10] J. S. Hong, M. Lancaster, D. Jedamzik, and R. B. Greed, “On the development of superconducting microstrip filters for mobile communications applications”, *IEEE Transactions on Microwave Theory and Techniques*, vol. 47, no. 9, pp. 1656–1663, Sept. 1999

[2-11] F.-R. Yang, Y. Qian, R. Coccioli,and T. Itoh, “A novel low-loss slow-wave microstrip structure”, *IEEE Microwave and Guided Wave Letters*, vol. 8, no. 11, pp. 372-374, Nov. 1998.

[2-12] B. T. Tan, S. T. Chew, M. S. Leong and B. L. Ooi, “A modified microstrip circular patch resonator filter”, *IEEE Microwave and Wireless Component Letters*, vol. 12, no. 7, pp. 252-254, Jul. 2002.

[2-13] J.-S. Hong and S. Li, “Theory and experiment of dual-mode microstrip triangular patch resonators and filters”, *IEEE Transactions on Microwave Theory and Techniques*, vol. 52, no. 4, pp. 1237-1243, Apr. 2004.

[2-14] A. Gopinath, “Maximum Q-factor of microstrip resonators”, *IEEE Transactions on Microwave Theory and Techniques*, vol. 29, no. 2, pp. 128-131, Feb. 1981.

[2-15] U. Karacaoglu and I. D. Robertson, “MMIC active bandpass filters using varactor-tuned negative resistance elements”, *IEEE Transactions on Microwave Theory and Techniques*, vol. 43, no. 12, pp. 2926-2932, Dec. 1995.

[2-16] K.-K. M. Cheng and H.-Y. Chan, “Noise performance of negative-resistance compensated microwave bandpass filters—theory and experiments”, *IEEE Transactions on Microwave Theory and Techniques*, vol. 49, no. 5, pp. 924-927, May 2001.

[2-17] C.-Y Chang and T.Itoh, “Microwave active filters based on coupled negative resistance method”, *IEEE Transactions on Microwave Theory and Techniques*, vol. 38, no. 12, pp. 924-927, Dec. 1990.

[2-18] A. E. Williams, W G. Bush and R. R. Bonetti, “Predistortion techniques for multicoupled resonator filters”, *IEEE Transactions on Microwave Theory and Techniques*, vol. 33, no. 5, pp. 402-407, May 1985.

[2-19] M. Yu, R. Cameron, D. Smith, V. Dokas and Y. Wang, “Predistortion technique for cross-coupled filters and its application to satellite communication systems”, *Microwave Symposium Digest*, no. 12, pp. 245-248, Jun. 2005.

[2-20] Y. Ming, W.-C. Tang, A. Malarky, V. Dokas, R. Cameron and Y. Wang, “Predistortion technique for cross-coupled filters and its application to satellite communication systems”, *IEEE Transactions on Microwave Theory and Techniques*, vol. 51, no. 12, pp. 2505-2515, Dec. 2003.

[2-21] R. J. Cameron, “Advanced coupling matrix synthesis techniques for microwave filters”, *IEEE Transactions on Microwave Theory and Techniques*, vol. 51, no. 1, pp. 1-10, Jan. 2003.

3.0 DUAL-MODE RESONATOR

Network synthesis techniques allow the efficient design of a bandpass filter given the specification. The resulting electrical network typically consists of ideal lumped element resonators, which are not practical at RF and microwave frequencies. Therefore an additional step in the development of microwave bandpass filters is the realization of ideal resonators in distributed transmission line media. Distributed resonators however do not behave as their ideal lumped element counterparts since they suffer from limited unloaded quality factor and spurious harmonic resonances. Although virtually all microwave filters are designed around the fundamental resonance of the comprising resonators, spurious passbands are almost always present at integer multiples of the first passband.

While a multitude of bandpass filtering functions may be realised by various coupling schemes [3-1], the particular frequency behaviour of the resonator may also be exploited to realize enhanced filters such as those with wider stopbands or multiple passbands. This is especially applicable to distributed resonators since there is usually some degree of control over their frequency behaviour. The frequency response of planar resonators may be readily altered by introducing various structural changes for example to shift spurious harmonics outwards [3-2], introduce additional transmission zeros in the stopband [3-3]-[3-5] or to generate a controllable second passband [3-6] and [3-7].

A dual-mode resonator is one that essentially supports two modes of resonance that are non-harmonically related. For planar structures, resonances may occur across both dimensions, namely, the length and width of the transmission lines. For higher frequencies, there may even be resonances across the thickness of the conductor trace. However, not all of these resonances may be readily accessible and tuned. For example, the resonance across

the thickness of the conductor can only be varied by altering the thickness of the trace, which is impractical. The term dual-mode in this thesis strictly refers to structures with two modes of resonances that are not only fundamental but are also readily accessible.

While N coupled single-mode resonators are required to realize an N^{th} order bandpass filter, only $N/2$ dual-mode resonators are necessary for the same filter since each dual-mode section behaves as a pair of coupled resonators. In addition to potential side reduction, dual-mode resonators offer a possibility to reduce overall losses. Although compact dual-mode resonators such as the open-loop [3-8], circular ring [3-9], square loop [3-10] and patch based resonators [3-11]-[3-13] have already been proposed, there is still much research interest concerning the development of even more compact structures for filter realization.

This section proposes a novel, extremely compact, dual-mode resonator configuration for planar, low footprint filter realization [3-14]. Moreover, significantly greater size reductions may be achieved since stepped impedance methods are also applicable to this resonator. A rigorous analysis of the structure and its various derivatives are presented to comprehensively describe the operation of the unit in its various forms and to validate the second order nature of the configuration. Although it is shown that the resonator is particularly suited for the design of Butterworth and Chebyshev all-pole bandpass filters, it is also possible to realize filters with finite frequency transmission zeros with improved selectivity. While the dual-mode resonator is shown to have a wide stop-band, with the first spurious response at $3f_0$, methods of further improving the stop-band are proposed.

Insertion loss based filter design techniques, after the selection of a suitable filter order, generally proceed from a lumped element lowpass prototype. The procedure terminates with the application of impedance and frequency transformations to yield the required filter in lumped element form. The conversion of such a network to a distributed filter is an additional stage necessary in microwave filter realization, and this step is largely dependent on the particular transmission line and resonator structure employed. To facilitate filter design with the proposed dual-mode resonator, an accurate lumped element model connecting the various physical features to electrical parameters is presented. The model may be used to expedite the conversion of a lumped ladder network to a distributed filter.

3.1 Analysis of Dual-Mode Resonator

The proposed dual-mode resonator in its most simple form is depicted in Fig. 3-1, where Z_1 and Z_2 denote characteristic impedances, W_1 and W_2 denote line widths and θ_1 and θ_2 are the electrical lengths of the lines. In the absence of the short circuited center stub, the resonator is identical to the single-mode open-loop $\lambda_g/2$ resonator [3-15]. It will be proved that the inclusion of a short circuited stub along the symmetry plane effectively converts the single-mode resonator to a dual-mode resonator. The grounded stub is relatively short and therefore variations of this resonator may be obtained by folding the longer lines of length θ_1. Although not illustrated in Fig. 3-1, the resonator may be coupled to the input and output ports via a direct connection, by parallel coupling or through capacitive coupling.

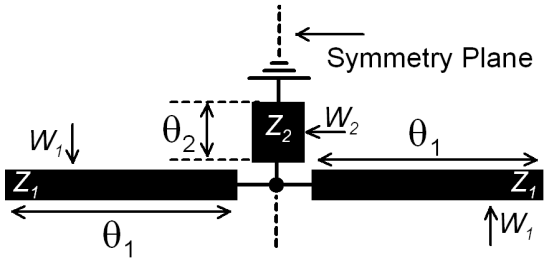

Fig. 3-1 Basic layout of proposed dual-mode resonator

Every excitation driving an electrical network can be separated into even and odd mode components and the overall response is obtained from the superposition of the two. The independence of the two modes permits circuit analysis to be carried out independently for each mode. The analysis of symmetrical networks in particular, such as that in Fig. 3-1, is greatly simplified from this method since complex circuits may be decomposed in to simpler structures. Therefore, a detailed analysis of the dual-mode resonator performed by even and odd mode decomposition can be found in the following sub sections.

3.1.1 Analysis of Odd Mode

The odd mode assumes an asymmetric excitation at the input and output ports and consequently enforces a virtual short circuit in the symmetry plane of the resonator. The short circuited stub, with characteristic impedance Z_2, is bypassed by the virtual short circuit as it appears in parallel to it. Therefore, the odd mode equivalent resonator circuit configuration takes the form of that in Fig. 3-2.

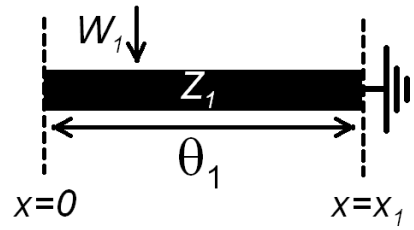

Fig. 3-2 Odd mode resonator configuration

To determine the natural modes of resonance, the following analysis is performed under sinusoidal steady state conditions assuming a loss less line. At any time along a planar transmission line, there may exist a forward and reverse travelling voltage wave and their corresponding current components. The superposition of the forward and reverse components of each type of wave yields the voltage, *V(x)*, and current distribution, *I(x)*, along the transmission line as given by equations (3.1) and (3.2), where V^+ and V^- are terms to be determined from the boundary conditions, Z_1 is the characteristic impedance and β is the propagation constant of the line.

$$V(x) = V^+ e^{-j\beta x} + V^- e^{j\beta x} \tag{3.1}$$

$$I(x) = I^+ e^{-j\beta x} - I^- e^{j\beta x} = \frac{V^+}{Z_1} e^{-j\beta x} + \frac{V^-}{Z_1} e^{j\beta x} \tag{3.2}$$

Applying the boundary conditions of the circuit in Fig. 3-2, which can be summarized as $V(x_1)$ = 0 and *I(0)* = 0, to the above equations and solving for the voltage and current distributions gives (3.3) and (3.4).

$$V(x) = 2V^+ \cos(\beta x) \tag{3.3}$$

$$I(x) = -j\frac{2V^+}{Z_1} \sin(\beta x) \tag{3.4}$$

In order to obtain the modes that may exist on the line, the boundary conditions are enforced on these equations to eliminate V^+ and this leads to the conclusion that any mode which satisfies (3.5) is a natural mode of the odd mode equivalent circuit.

$$\cos(\beta x_1) = \cos(\theta_1) = 0 \tag{3.5}$$

Solving (3.5) for the natural modes gives infinitely many solutions as given by (3.6), where λ_g is the guided wavelength.

$$\lambda_g = \frac{4x_1}{n}, \quad where\ n = 1, 3, 5 \ldots \tag{3.6}$$

For filter design, only the first resonance mode (n = 1) is considered, in which case the electrical length of the transmission line is 90^0. The remaining harmonic modes damage the response of a filter as they ultimately produce spurious responses in the stopband.

Fig. 3-3 (a) plots the magnitude of the voltage and current, for the fundamental odd mode (n = 1) along the odd mode resonator with normalized length and Z_1 = 1. The voltage and current distributions along the dual-mode resonator for an odd mode excitation can also be visualized through Fig. 3-3 (b) and (c) respectively. It is immediately evident from Fig. 3-3 (b) and (c) that the odd mode experiences a virtual ground in the symmetry plane and is therefore not affected by the short circuited stub. While the voltage standing wave reaches a maximum at both open ends, the current reaches its maximum at the symmetry plane.

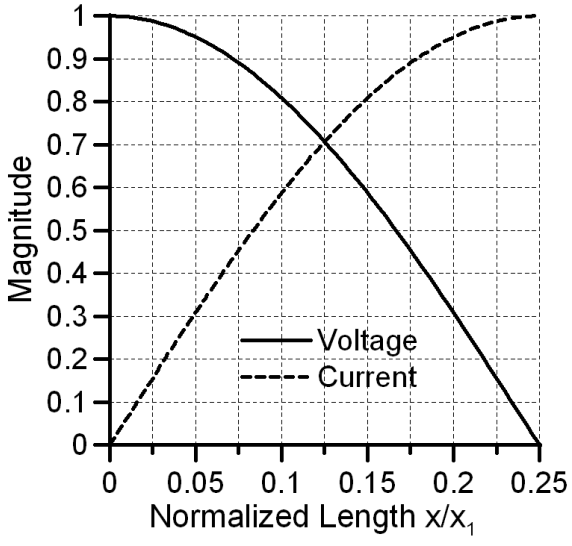

(a)

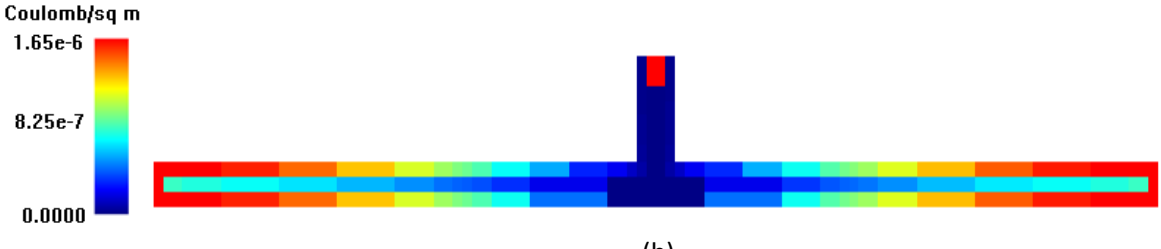

(b)

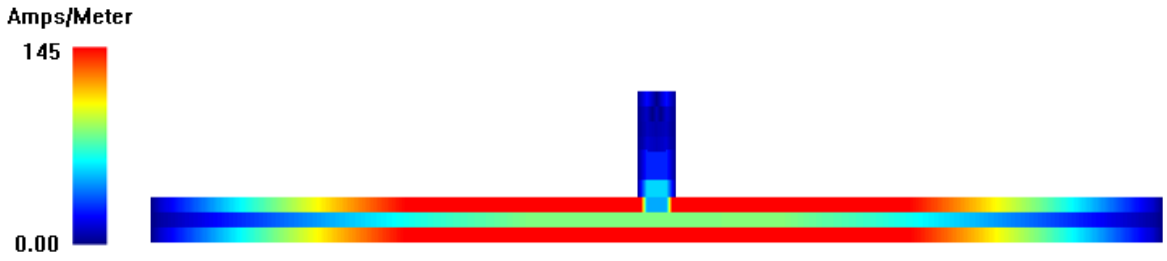

(c)

Fig. 3-3 (a) Voltage and current distribution along odd mode resonator normalised to the resonator length, where $Z_1 = 1$ (b) Full wave EM simulated charge distribution along dual-mode resonator (c) Full wave EM simulated current distribution along dual-mode resonator.

3.1.2 Analysis of Even Mode

The even mode assumes the symmetrical excitation at the input and output ports and consequently enforces a virtual open circuit in the symmetry plane of the resonator in Fig. 3-1. While this effectively bisects the dual-mode resonator along the symmetry plane, the short circuited stub is split along this plane resulting in an effective characteristic impedance in the even mode to be different to Z_2 and is therefore denoted by Z_{2e}. The even mode equivalent resonator circuit configuration takes the form of that in Fig. 3-4.

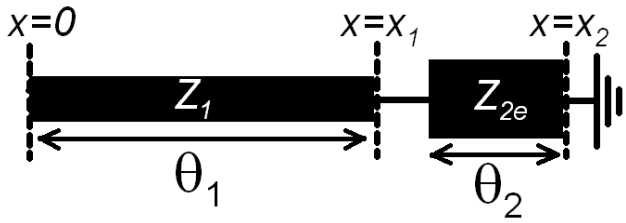

Fig. 3-4 Even mode resonator configuration

Similar to the odd mode, the even mode resonances may be determined from analysing the even mode equivalent resonator under sinusoidal steady state conditions. The even mode resonator is elongated by the short circuited stub. Lower resonant frequencies may therefore be expected for this mode. In order to obtain the voltage and current distributions as well as to quantify the natural modes, the voltage and current for each line will be solved separately and these will be matched at the boundary to obtain the complete solution.

The voltage and current along line 1 can still be expressed by (3.1) and (3.2), and applying the boundary condition *I(0)* = 0 leads to the corresponding distributions to still take the form of (3.5) and (3.6). Similarly, the voltages and currents along line 2 may be expressed by (3.1) and (3.2), where x takes values between x_1 and x_2. After applying the boundary conditions, matching the current and voltage at the $x = x_1$ boundary and with some manipulations, it is possible to arrive at the voltage and current distributions along the lines as (3.7) and (3.8) respectively.

$$V(x) = \begin{cases} 2V^+ \cos(\beta x), & x < x_1 \\ 2V^+ \dfrac{\cos(\beta x_1)\sin[\beta(x - x_2)]}{\sin[\beta(x_1 - x_2)]}, & x_1 \leq x \leq x_2 \end{cases} \tag{3.7}$$

$$I(x) = \begin{cases} -j\dfrac{2V^+}{Z_1}\sin(\beta x), & x < x_1 \\ j\dfrac{2V^+\cos(\beta x_1)}{Z_2\sin[\beta(x_1 - x_2)]}\cos[\beta(x - x_2)], & x_1 \leq x \leq x_2 \end{cases} \tag{3.8}$$

The condition for resonance in the even mode is a transcendental equation (3.9) which must be solved graphically or numerically to obtain the supported guided wavelengths for this mode.

$$\frac{Z_{2e}}{Z_1}\tan(\beta x_1)\tan[\beta(x_2 - x_1)] - 1 = \frac{Z_{2e}}{Z_1}\tan(\theta_1)\tan(\theta_2) - 1 = 0 \tag{3.9}$$

Fig. 3-5 plots the fundamental guided wavelength, computed from (3.9), normalized to the fundamental odd mode guided wavelength, against various impedance ratios Z_{2e}/Z_1 and line ratios expressed as a percentage of $(x_2 - x_1)/x_1$. It can be seen that as the impedance ratio tends towards unity and the length of line 2 approaches zero, the guided wavelength of the even mode tends towards that of the odd mode. In fact, the split in the resonant frequency between the even and odd mode is exclusively a consequence of the short circuited stub. Essentially, the resonant frequency split increases with stub length and characteristic impedance.

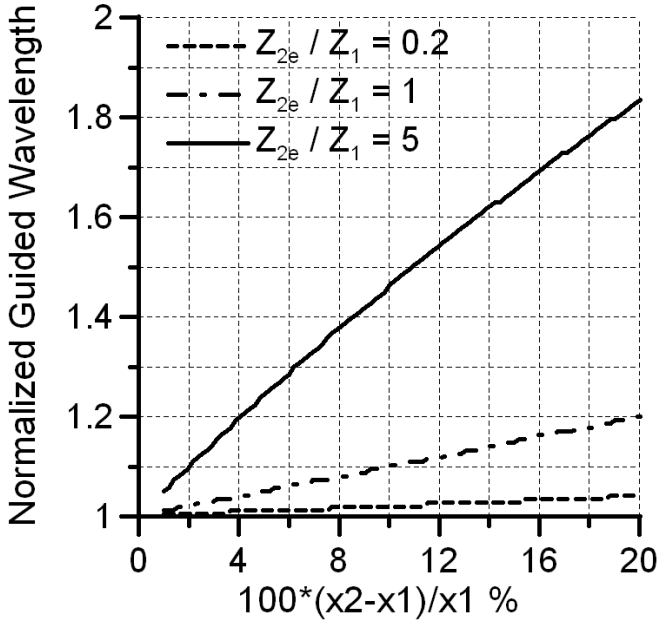

Fig. 3-5 Supported fundamental resonant guided wavelength of even mode, normalized to the first order odd mode guided wavelength, plotted against the length of line 2 expressed as a percentage of that of line 1 for various impedance ratios Z_{2e}/Z_1.

Fig. 3-6 (a) plots the magnitude of the voltage and current, for the even mode along the even mode resonator with normalized length, where $Z_1 = 1$ and $Z_{2e}/Z_1 = 2$. There is clearly a noticeable difference between the current and voltage on lines 1 and 2 due to the step change in characteristic impedance. This is the first order voltage and current standing wave pattern for the even mode, and from Fig. 3-5, it is evident that the even mode resonance is always at a lower frequency than that of the odd mode.

The voltage and current distributions along the dual-mode resonator for an even mode excitation can also be visualized through Fig. 3-6 (b), (c) and (d). It is immediately evident from the current distribution in the x direction, as illustrated in Fig. 3-6 (c), that there is a virtual open circuit along the symmetry plane of the resonator since there is no x-directed current in the center. The high current density present in both sides of the symmetry plane is in fact diverted to the short circuited stub as is illustrated by the y-directed current density in Fig. 3-6 (d). Similar to the odd mode the voltage standing wave reaches a maximum at both open ends as predicted.

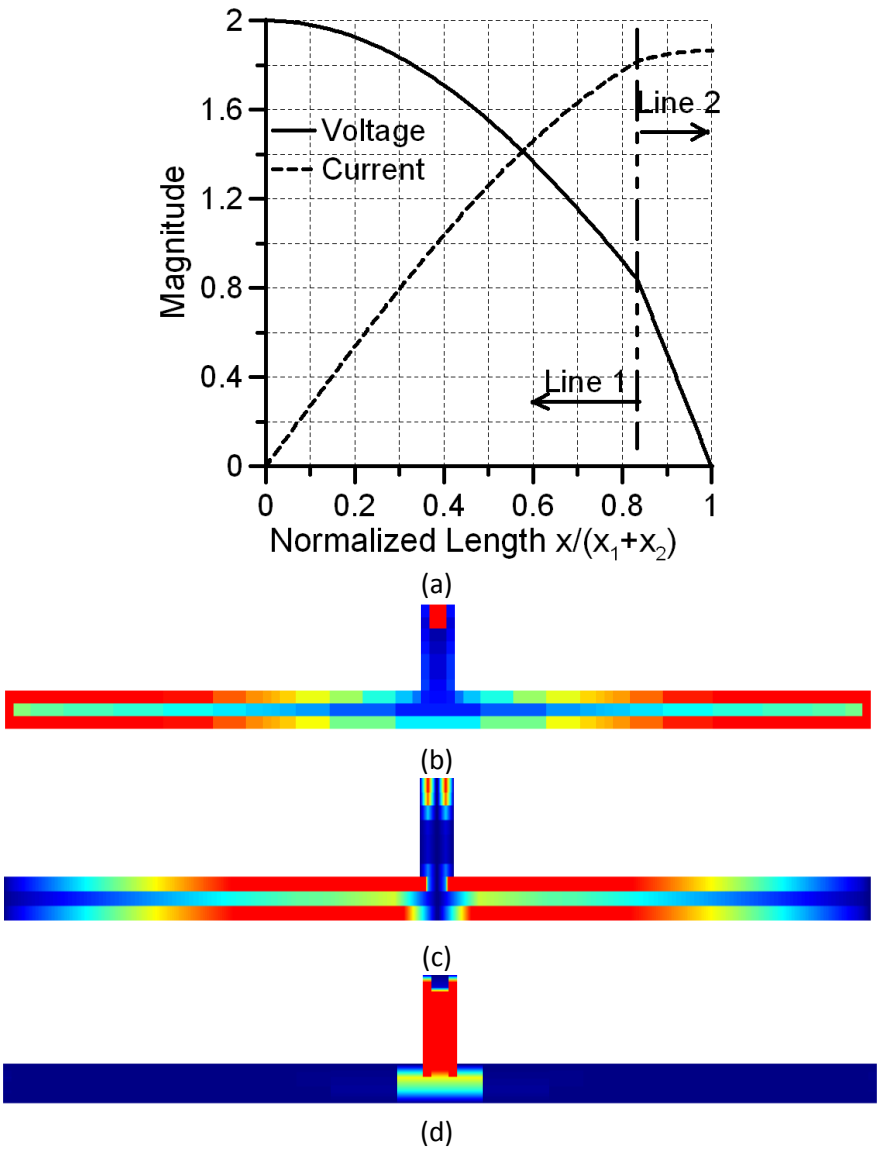

Fig. 3-6 (a) Voltage and current distribution along even mode resonator normalised to the resonator length (b) Full wave EM simulated charge distribution along dual-mode resonator (c) Full wave EM simulated current distribution in the x direction (d) Full wave EM simulated current distribution in the y direction.

3.1.3 Equivalent Electrical Model

The development of an equivalent circuit for the proposed compact dual-mode resonator is a critical step towards not only gaining insight into its electrical behaviour but also applying it in filter design. Although the fundamental even and odd mode resonant frequencies were determined from circuit analysis presented in the previous section, knowledge of the resonant frequencies alone is not sufficient for complete characterization. In addition, knowledge of the external quality factor as well as the inter-resonator coupling coefficients are also required. While these parameters are defined by the physical structure in the distributed dual-mode resonator, the equivalent lumped model, comprising of inductors, capacitors and inverters, will bear the same information within its element values.

Due to the presence of two resonant modes, it is assumed that the equivalent circuit would comprise of a pair of synchronously tuned resonators coupled via an immittance inverter. As such, there are two possible circuit implementations of the model as illustrated in Fig. 3-7 (a) and (b). For each model, the parameters, namely, the resonator inductance, capacitance, and inverter immitances must be extracted from the physical structure.

To determine the parameters of the first model, the distributed resonator circuit of Fig. 3-1 is redrawn as Fig. 3-7 (c), where the impedance looking into the short circuited stub is Z_{sc}. This configuration allows an impedance inverter of value $K = |Z_{sc}|$ to be extracted at the symmetry plane of the resonator and this is equated to K_2, as given by (3.10).

$$K_2 = Z_2 \tan(\theta_2) \tag{3.10}$$

The reactance, Z_{in1} given by (3.11), near resonance behaves as a series LC resonator. Applying $Z_{in1} = 0$ at resonance yields the resonance condition as (3.12) from which the angular resonant frequency, ω_0, may be determined.

$$Z_{in1} = [Z_2 \tan(\theta_2) - Z_1 \cot(\theta_1)] \tag{3.11}$$

$$\tan(\theta_1)\tan(\theta_2) = \frac{Z_1}{Z_2} \tag{3.12}$$

The reactance slope parameter, x_r, of the series distributed resonator may be derived from (3.11) and is found to be (3.13).

$$x_r = \frac{Z_1\theta_1 \operatorname{cosec}^2(\theta_1) + Z_2\theta_2 \sec^2(\theta_2)}{2} \tag{3.13}$$

The reactance slope parameter can be used to quantify the series inductance, L_s, as given by (3.14), from which the series capacitance C_s may be found from (3.15).

$$L_S = \frac{x_r}{\omega_0} \tag{3.14}$$

$$C_S = \frac{1}{\omega_0^2 L_S} \tag{3.15}$$

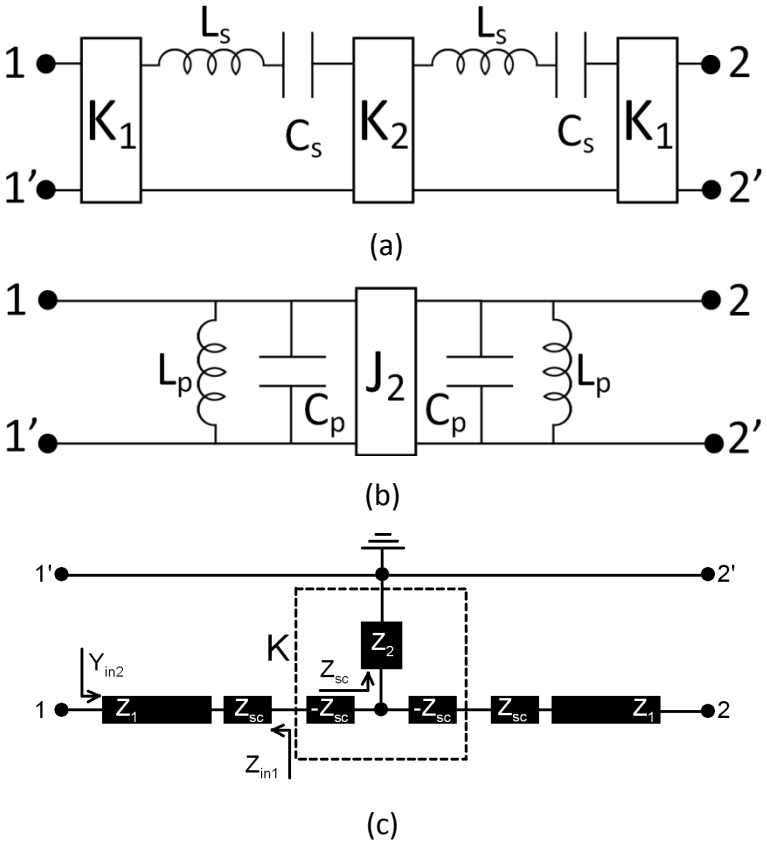

Fig. 3-7 (a) (b) Equivalent circuits of the dual-mode resonator (c) Dual-mode resonator with extracted impedance inverter

The parameters of the second model in Fig. 3-7 (b) may be obtained in a similar fashion by noting that the susceptance, Y_{in2} given by (3.16), behaves as that of a parallel LC resonant circuit near resonance.

$$Y_{in2} = \frac{1}{Z_1}\left(\frac{Z_2 \tan(\theta_1)\tan(\theta_2) - Z_1}{Z_1 \tan(\theta_1) + Z_2 \tan(\theta_2)}\right) \tag{3.16}$$

The resonant condition obtained by imposing Y_{in2} = 0 produces the same result given by (3.12) as expected. The susceptance slop parameter, x_s, can be derived from the susceptance as (3.17) from which the resonator capacitance, C_p, and inductance, L_p, may be determined from (3.18) and (3.19) respectively.

$$x_s = \frac{Z_2}{2Z_1}\left[\frac{\theta_1 \sec^2(\theta_1)\tan(\theta_2) + \theta_2 \sec^2(\theta_2)\tan(\theta_1)}{Z_1 \tan(\theta_1) + Z_2 \tan(\theta_2)}\right] \tag{3.17}$$

$$C_p = \frac{x_s}{\omega_0} \tag{3.18}$$

$$L_p = \frac{1}{\omega_0^2 C_p} \tag{3.19}$$

Due to the equivalence of the two models, it is now possible to determine the unknown parameter K_1 and J_2 from the expressions presented above. Since the reactance looking into port 1 of Fig. 3-7 (a) must match the susceptance looking into port 1 of Fig. 3-7 (b), K_1 must assume a value given by (3.20).

$$K_1 = \sqrt{\frac{x_r}{x_s}} \tag{3.20}$$

Imposing the condition that the split in the two resonant frequencies must be identical in the two models enables J_2 to be formulated as (3.21).

$$J_2 = \frac{x_r}{K_2 x_s} \tag{3.21}$$

In order to verify the models and the related expressions presented, the transmission response of the distributed resonator and the two models are compared in Fig. 3-8 (a), (b) and (c) , where $Z_1 = Z_2 = 50\ \Omega$, $\theta_1 = 85^0$ and $\theta_2 = 5^0$ at the center frequency with port terminating impedances of 5 kΩ.

A very good agreement between the model and resonator response is observed not only in the vicinity of the centre frequency but also for a wider frequency range. The harmonic resonances are illustrated in Fig. 3-8 (c), but are not modelled by the equivalent circuits.

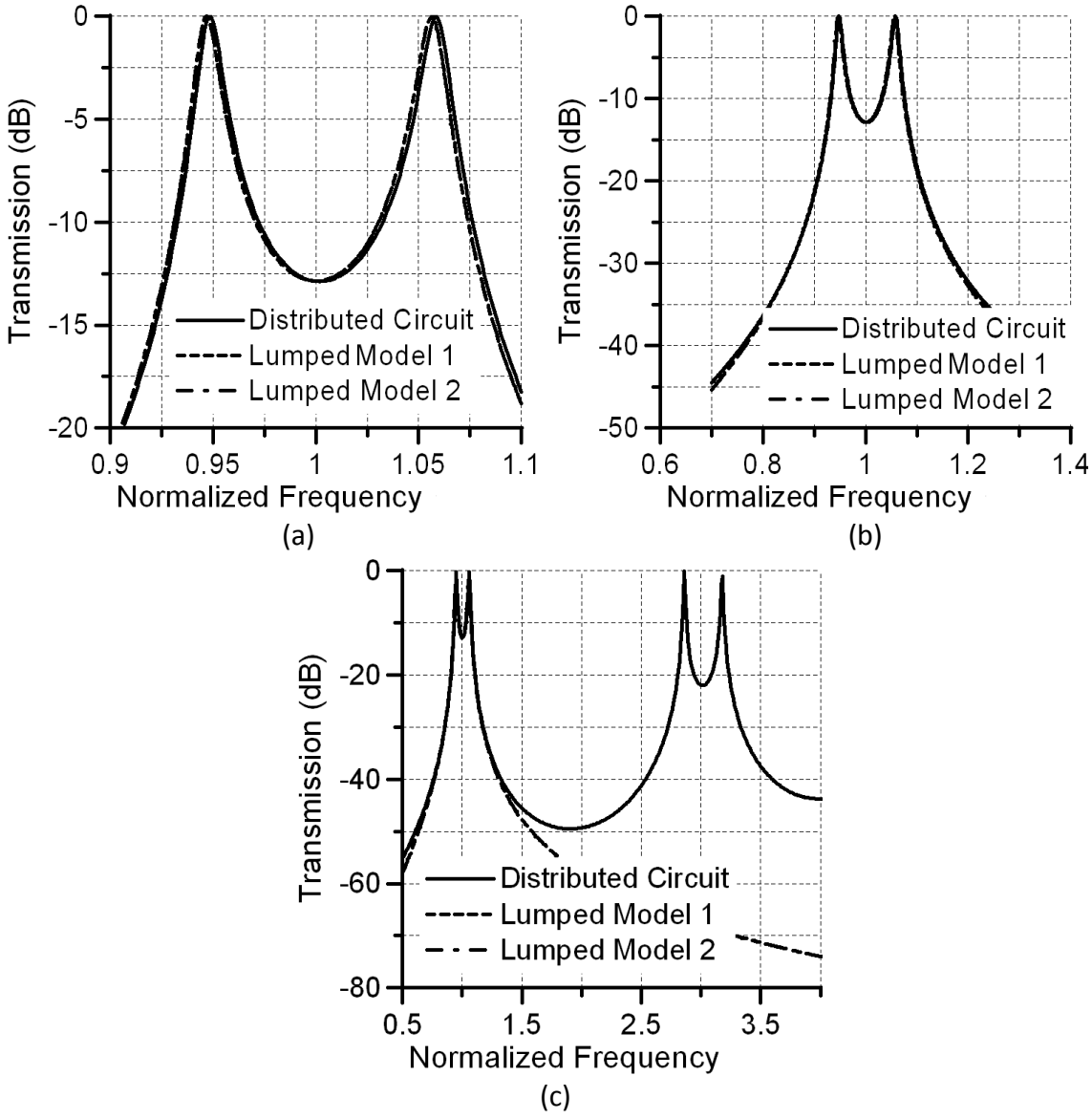

Fig. 3-8 Comparison of transmission response against normalized frequency between the two equivalent models and the distributed resonator. (a) Narrow band response (b) Fundamental band (c) Fundamental and first harmonic bands

3.1.4 Summary

A comprehensive analysis of the proposed dual-mode resonator was presented in this section as a base for later discussions. Mathematical expressions for the voltage and current standing waves naturally supported by the resonator are derived. In the absence of the short circuited stub, the odd and even modes resonate at the same frequency and the structure would therefore emulate a single-mode resonator. The second fundamental resonance is produced as a consequence of the short circuited stub, which lowers the even mode resonant frequency from that of the odd.

In particular, it was shown that these two resonances are indeed fundamental modes and are not harmonically related resonances. Also to be noted, from equation (3.6) and (3.9) is the fact that both the even and odd mode resonances generate second harmonics in the vicinity of $3f_0$ rather than $2f_0$. This is particularly desirable in microwave filter design especially in achieving a wider filter stopband.

Dual equivalent circuits have been presented and formulations for the related electrical parameters have been derived. The equivalent circuits were shown to accurately characterize the distributed dual-mode resonator in the vicinity of its fundamental resonances. The models however do not account for the characteristic spurious resonances of the distributed resonator.

3.2 Excitation of the Dual-Mode Resonator

The previous section detailed the theoretical resonant characteristics of the dual-mode resonator and presented equivalent circuit models for the resonator in an end-coupled configuration. In the majority of practical microstrip applications however, end-coupled feeding methods lack sufficient coupling strength in order to realize wideband filter networks. This section therefore gives an overview of two alternative, yet popular feeding methods that are easily adaptable and applicable to this resonator.

The first method is to directly connect the resonator via a transmission line to the input and output ports. This method is particularly suited for high fractional bandwidth filter design due to the relatively strong nature of coupling that may be achieved from a direct connection. However, sensitivity in the exact placement of the feed line towards the external quality factor for narrowband filters prevents this approach from being widely applied in most moderate to low fractional bandwidth applications. Furthermore, since the resonator is shorted to ground at the symmetry plane, it is critical that there is no D.C voltage on the input and output ports. Presence of any D.C voltage will cause a short circuit and may potentially damage the transmission line as well as any external drive circuitry.

The second approach is to employ parallel coupled line feeding. Although as high a coupling strength may not be achieved, this method is still highly suitable for narrowband filtering applications. The amount of coupling strength achievable with this method is highly dependent on the parameters of the particular microstrip employed such as substrate height and relative dielectric constant as well as process parameters such as minimum realizable gap size. Generally, substrates with lower dielectric constants and greater substrate heights permit stronger coupling to be achieved since this will enable a greater proportion of the electromagnetic field to extend from one line to the other. In contrast to the direct-coupled scheme, parallel coupled feeding methods cannot transmit direct current and therefore does not suffer from the presence of D.C voltages at the input and output ports.

3.2.1 Direct-Coupled Resonator Feeding

The dual-mode resonator may be directly coupled to the input and output ports via a section of transmission line, with characteristic impedance Z_0, as illustrated in Fig. 3-9 (a), where Z_0 is also the terminating port impedance and θ_B is the electrical length between the center of the feeding line to the symmetry plane of the resonator. With the direct coupled approach, the external quality factor, Q_e, may be adjusted simply by varying the placement of the feed line on the resonator.

The unique frequency behaviour of the direct-coupled resonator calls for a different equivalent circuit model from that of the end-coupled resonator. Firstly, the open circuit stubs on either end of the resonator with input impedance Z_{inOC} may be modelled with a shut series connected LC resonator. The equivalent circuit of the mid-section of the resonator is illustrated in Fig. 3-9 (b). The lumped element model in its final form may be drawn as illustrated in Fig. 3-9 (c).

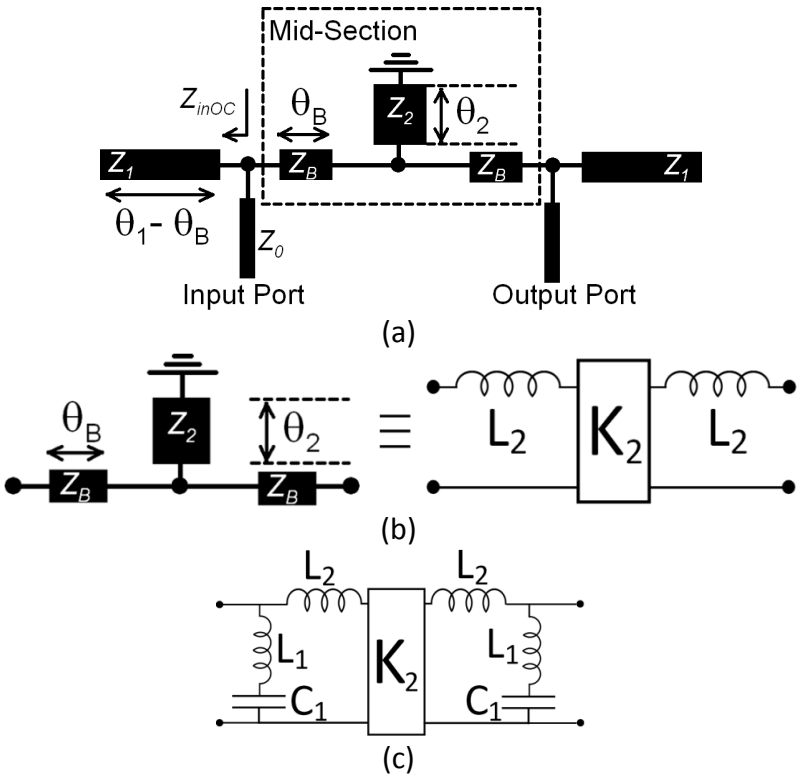

Fig. 3-9 (a) Directed-coupled dual-mode resonator configuration (b) Model of resonator mid-section (c) Equivalent lumped element circuit of direct-coupled dual-mode resonator

The ABCD parameters, given by (3.22), of the mid-section of the resonator, illustrated in Fig. 3-9 (b), may be equated to that of its lumped equivalent network from where it is possible to define the model parameters K_2 and L_2 as (3.23) and (3.24).

$$\begin{bmatrix} A & B \\ C & D \end{bmatrix} = \begin{bmatrix} \cos(\theta_B) & jZ_B\sin(\theta_B) \\ j\dfrac{\sin(\theta_B)}{Z_B} & \cos(\theta_B) \end{bmatrix} \begin{bmatrix} 1 & 0 \\ -\dfrac{j\cot(\theta_2)}{Z_2} & 1 \end{bmatrix} \begin{bmatrix} \cos(\theta_B) & jZ_B\sin(\theta_B) \\ j\dfrac{\sin(\theta_B)}{Z_B} & \cos(\theta_B) \end{bmatrix} \tag{3.22}$$

$$= \begin{bmatrix} \cos(2\theta_B) + \dfrac{Z_B}{2Z_2}\sin(2\theta_B)\cot(\theta_2) & j\left(Z_B\sin(2\theta_B) + \dfrac{[Z_B\sin(\theta_B)]^2}{Z_2}\cot(\theta_2)\right) \\ j\left(\dfrac{\sin(2\theta_B)}{Z_B} - \dfrac{\cos^2(\theta_B)\cot(\theta_2)}{Z_2}\right) & \cos(2\theta_B) + \dfrac{Z_B}{2Z_2}\sin(2\theta_B)\cot(\theta_2) \end{bmatrix}$$

$$K_2 = \frac{1}{jC} \tag{3.23}$$

$$L_2 = \frac{K_2 A}{\omega_0} \tag{3.24}$$

Since the model assumes frequency invariance of its parameters, an exact match may only be expected at the center frequency of the resonator. The impedance matrix parameters of the two circuits of Fig. 3-9 (b) may be compared to evaluate, verify and justify the use of this equivalent circuit. Fig. 10 plots the impedance parameters of the two circuits where $Z_B = Z_2 = 50\ \Omega$, $\theta_B = 20^0$, $\theta_2 = 2.5^0$. Corresponding model parameters were calculated to be $L_2 = 3.30$ nH and $K_2 = 2.55$ at the center frequency.

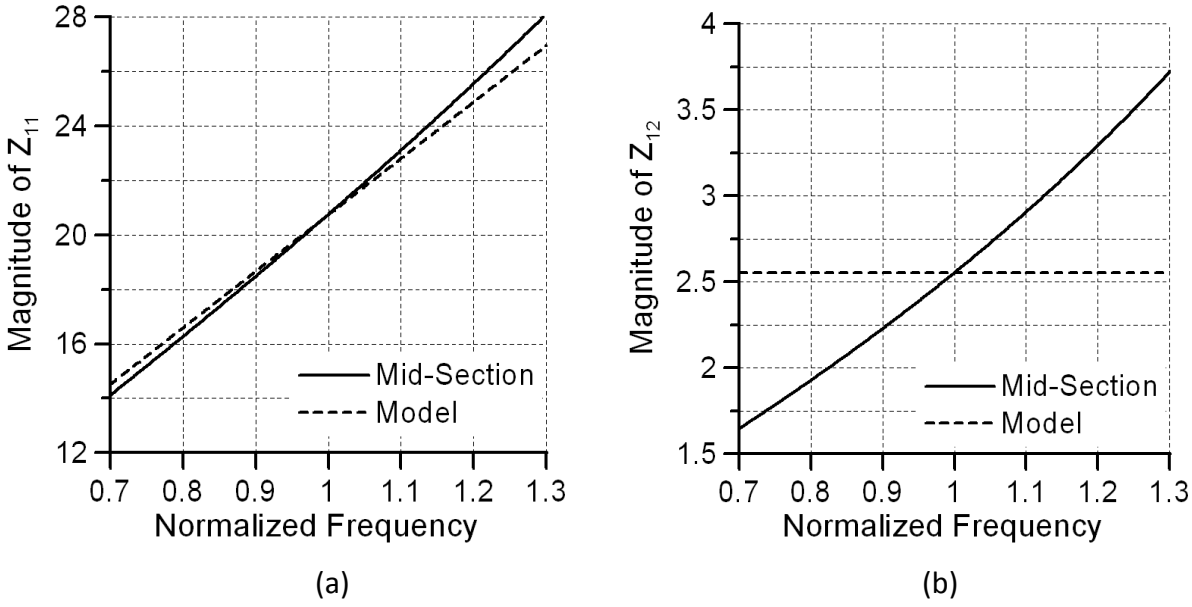

Fig. 3-10 Comparison of (a) driving point impedance (b) transfer impedance of direct coupled dual-mode resonator mid-section and that of equivalent circuit

There is a reasonably good agreement in the driving point impedances over a wide frequency range from which it may be deduced that the frequency dependence of L_2 is fairly small. The relatively strong frequency dependence of the transfer impedance, which is equivalent to the inverter impedance, K_2, is clearly evident. For narrow-band filter design (FBW ~ 10 %), this variation will not present any significant error. For a FBW of 10 %, the maximum error in K_2 within the passband is only 6.6 %. Since this error grows with FBW, it may be necessary to treat K_2 as a frequency dependent parameter for wide-band designs.

The impedance looking into the open ended line, Z_{inOC}, with electrical length $\theta_1 - \theta_B$, given by (3.25), behaves as shunt series connected LC network.

$$Z_{inOC}(\omega) = -jZ_1 \cot\left[\theta_1(\omega) - \theta_t(\omega)\right] \tag{3.25}$$

Due to the distributed nature of the line, the lumped element values are in fact frequency dependent. For a narrow frequency band however, a fixed inductance and capacitance model may still give a reasonably good agreement. It is possible to choose values of inductance L_1 and capacitance C_1, using curve fitting at two fixed frequency points, for an optimum match between Z_{inOC} and the model impedance. The results can be given as (3.26) and (3.27). Typically, in bandpass filter design, the two frequency points may be selected as the two band edge frequencies, ω_L and ω_H.

$$L_1 = \frac{\omega_H Z_{inOC}(\omega_H) - \omega_L Z_{inOC}(\omega_L)}{\omega_H^2 - \omega_L^2} \tag{3.26}$$

$$C_1 = \frac{1}{\omega_L^2 L_1 - \omega_L Z_{inOC}(\omega_L)} \tag{3.27}$$

Fig. 3-11 compares the impedance of the open circuited transmission line section and that of the LC shunt model, where Z_1 = 50 Ω, $\theta_1 - \theta_B = 67.5^0$. For purposes of illustration, the response of Fig. 3-11 (a) is where the two curve fitting frequency points are f_L = 0.9 and f_H = 1.1 (L_1 = 3.85 nH, C_1 = 3.55 pF) while that of Fig. 3-11 (b) is where these two points are f_L = 0.6 and f_H = 1.4 (L_1 = 4.04 nH, C_1 = 3.60 pF). When the two frequency points are closer, there is very high accuracy near the resonant frequency, but the position of the zero is relatively inaccurate. Conversely, if the two points were chosen further apart, the match between the two impedances agree better over a wider frequency range but at the cost of accuracy near the center frequency, which is somewhat compromised.

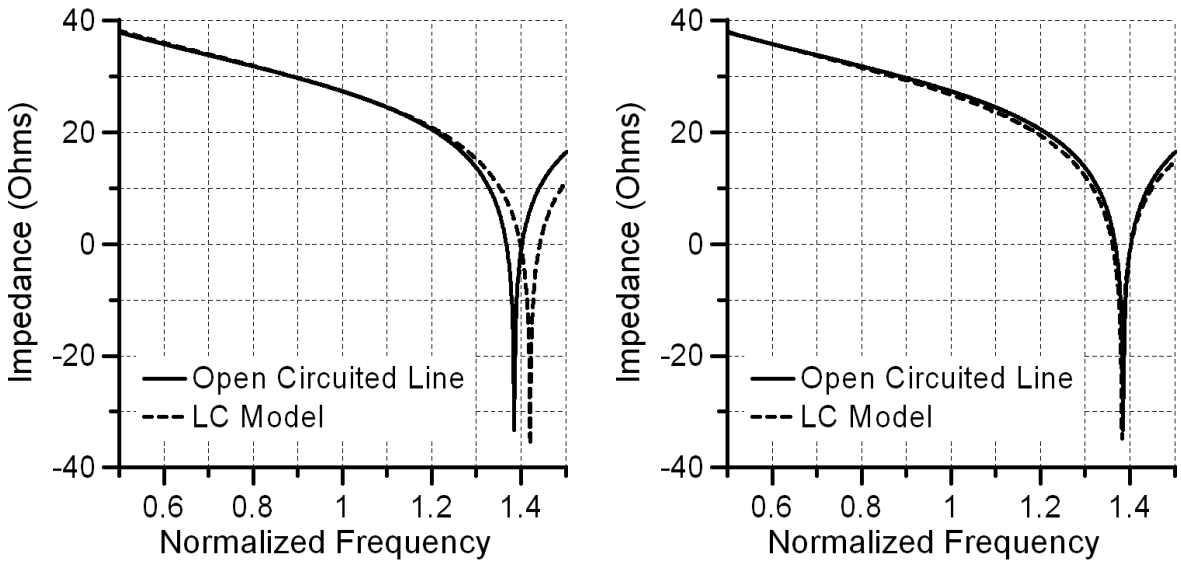

Fig. 3-11 Comparison of impedance against normalized frequency between open circuited stub and equivalent LC circuit for (a) f_L = 0.9, and f_H = 1.1 and (b) f_L = 0.6 and f_H = 1.4.

In order to obtain the external quality factor, it is convenient to model the entire distributed resonator as a parallel LC resonator near resonance, where the susceptance, *Y*, and the susceptance slope parameter, x_s, of the resonator in the odd mode are given by (3.28) and (3.29) respectively.

$$Y = \frac{1}{Z_1}[\tan(\theta_1 - \theta_B) - \cot(\theta_B)] \tag{3.28}$$

$$x_s = \frac{1}{2Z_1}\left[\frac{\theta_1 - \theta_B}{\cos^2(\theta_1 - \theta_B)} + \frac{\theta_B}{\sin^2(\theta_B)}\right] \tag{3.29}$$

The external quality factor, Q_e, of the direct-coupled resonator can then be defined in terms of the susceptance slope parameter and the port impedance Z_0 as given by (3.30), where it is assumed that $\theta_1 = \pi/2$ at resonance (for odd mode).

$$Q_e = Z_0 x_s = \frac{Z_0}{2Z_1}\left[\frac{\theta_1 - \theta_B}{\cos^2(\theta_1 - \theta_B)} + \frac{\theta_B}{\sin^2(\theta_B)}\right] = \frac{Z_0\pi}{4Z_1\sin^2(\theta_B)} \tag{3.30}$$

The direct-coupled dual-mode resonator produces a single transmission zero in the upper stopband. The transmission zero occurs at a frequency where the impedance Z_{inOC} becomes zero. This occurs when the open-circuited stub, illustrated in Fig. 3-9 (a) is exactly quarter wavelength long. The placement of the input feeding line determines the length of the open-circuited stub and therefore ultimately governs the position of this transmission zero.

Fig. 3-12 compares the frequency behaviour between the direct-coupled resonator and its equivalent model, where $Z_1 = Z_2 = 50\ \Omega$, $Z_0 = 5\ k\Omega$, $\theta_1 = 87.5^0$, $\theta_B = 20^0$, $\theta_2 = 2.5^0$ at the center frequency. From the equations above the model parameters were calculated to be $L_1 = 3.85$ nH, $L_2 = 3.29$ nH, $C = 3.55$ pF and $K_2 = 2.2$.

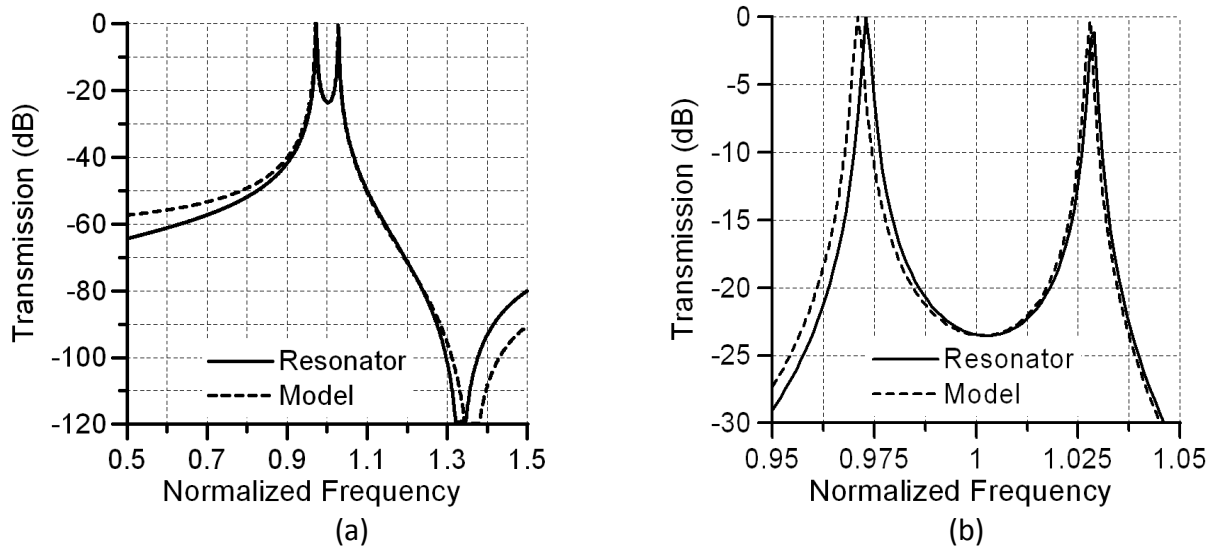

Fig. 3-12 Comparison of transmission response between direct-coupled distributed resonator and equivalent model. (a) Wideband response (b) Narrowband response.

The frequency offset of the transmission zero in the model is due to the shunt LC network being extracted at the two frequencies $0.9f_0$ and $1.1f_0$, which makes the model more precise in the vicinity of the center frequency, f_0, at the cost of accuracy at higher frequencies. The discrepancies near the center frequency, highlighted in Fig. 3-12 (b) are mainly due to the inverter impedance being a treated as a constant parameter in the model.

The direct-coupled approach allows relatively high coupling strengths, i.e. low Q_e, to be realised in microstrip technology relatively easily and is therefore particularly suited for high fractional bandwidth filter design. It may not be as suitable for narrowband filter design due to the increased sensitivity of the external quality factor to small variations in the electrical length, θ_t. Direct-coupled feeding is also seen to introduce a single transmission zero in the upper stopband of the filter whose location is determined purely from the placement of the feed connection. Filter design with this feeding approach is relatively complicated due to the non-standard form of the equivalent circuit.

3.2.2 Parallel-Coupled Resonator Feeding

The second method of exciting the resonator is via parallel coupled-lines of electrical length of around 60^0. Coupled-lines allow energy to be conveyed to and from the resonator through the mutual inductance and capacitance. Although the resonator mid-section is identical to the direct-coupled case, the open-ended arms either side of the mid-section are now coupled via parallel coupling. Fig. 3-13 illustrates this resonator configuration, where Z_e and Z_o are the even and odd mode impedances of the coupled-lines and θ_C is its electrical length at the centre frequency.

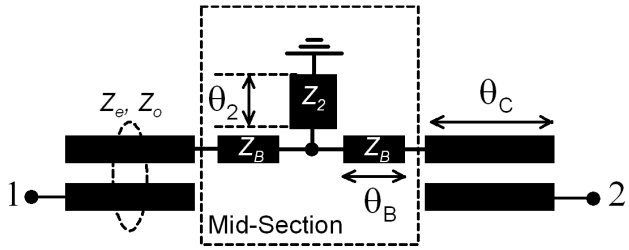

Fig. 3-13 Parallel-coupled dual-mode resonator configuration

The equivalent circuit of the resonator mid-section presented in the previous section may be employed here. Therefore, it is only required to find a lumped element equivalent network for the parallel-coupled lines. One particular approach is to use the impedance matrix and the corresponding T-equivalent circuit representation of the coupled lines as the starting point. The T-equivalent circuit as illustrated in Fig. 3.14 (a) may be redrawn as Fig. 3-14 (b) in order to extract an impedance inverter of value $|Z_{12}|$. Since the coupled line driving point impedance, Z_{11}, closely resembles that of a series LC circuit, the lumped element model may take the form of that illustrated in Fig. 3-14 (c).

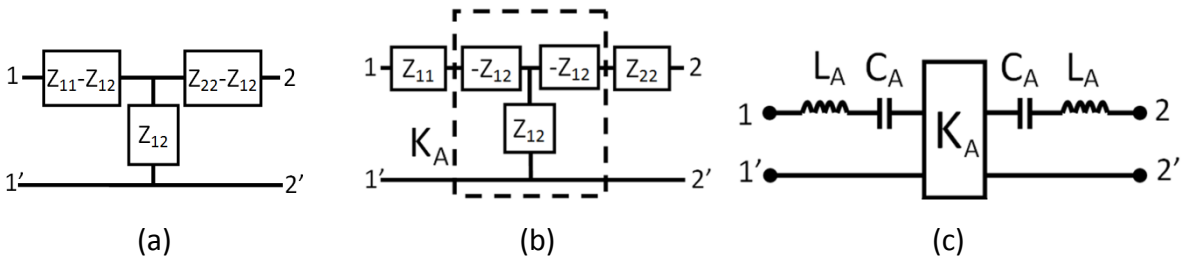

Fig. 3-14 (a) T-equivalent circuit with impedance matrix elements (b) T-equivalent circuit with extracted impedance inverter (c) Lumped coupled-line equivalent circuit.

The impedance matrix values of the coupled line are summarized by (3.31) and (3.32) [3-16], from which the inverter impedance is given by $|Z_{12}|$.

$$Z_{11} = Z_{22} = \frac{-j}{2}(Z_e + Z_o)\cot\theta_C \tag{3.31}$$

$$K_A = Z_{12} = Z_{21} = \frac{-j}{2}(Z_e - Z_o)\csc\theta_C \tag{3.32}$$

The series inductance, L_A, and capacitance, C_A, may be extracted from the impedance function (3.31) by curve fitting at two angular frequency points, ω_L and ω_H, either side of the angular resonant frequency of the resonator. These points may be chosen as the band-edge frequencies of a bandpass filter. To this end, the formulae (3.33) and (3.34) may be used.

$$L_A = \frac{\omega_H Z_{11}(\omega_H) - \omega_L Z_{11}(\omega_L)}{\omega_H^2 - \omega_L^2} \tag{3.33}$$

$$C_A = \frac{1}{\omega_L^2 L_A - \omega_L Z_{11}(\omega_L)} \tag{3.34}$$

For comparison and verification of the model, Fig. 3.15 (a) and (b) plot the driving point impedance, Z_{11}, of the coupled line and that of its model comprised of inductance L_A and capacitance C_A, where Z_e = 60 Ω, Z_o = 40 Ω and $\theta_C = 60^0$ at resonance. The corresponding model parameters were calculated to be L_A = 3.29 nH, C_A = 3.23 pF and K_A = 11.5. There is generally a very good agreement between the driving point impedance and its equivalent circuit. Fig. 3.15 (c) plots the transfer impedance, equivalent to the inverter impedance K_A, against normalized frequency. Although there is actually some frequency variation in K_A, this will not pose a significant error in moderate to low fractional bandwidth filters, since the variation of the inverter impedance is relatively small over a narrow frequency range.

Illustrated in Fig. 3-15 (d) is a comparison of the transmission response of the coupled line and its equivalent circuit. Since the model was only defined precisely at the center frequency, absolute agreement in the responses occurs only at this particular frequency. The error increases with deviating frequency primarily due to the variation in inverter impedance, which of course is not modelled. Nevertheless, the overall agreement in the transmission response is satisfactory.

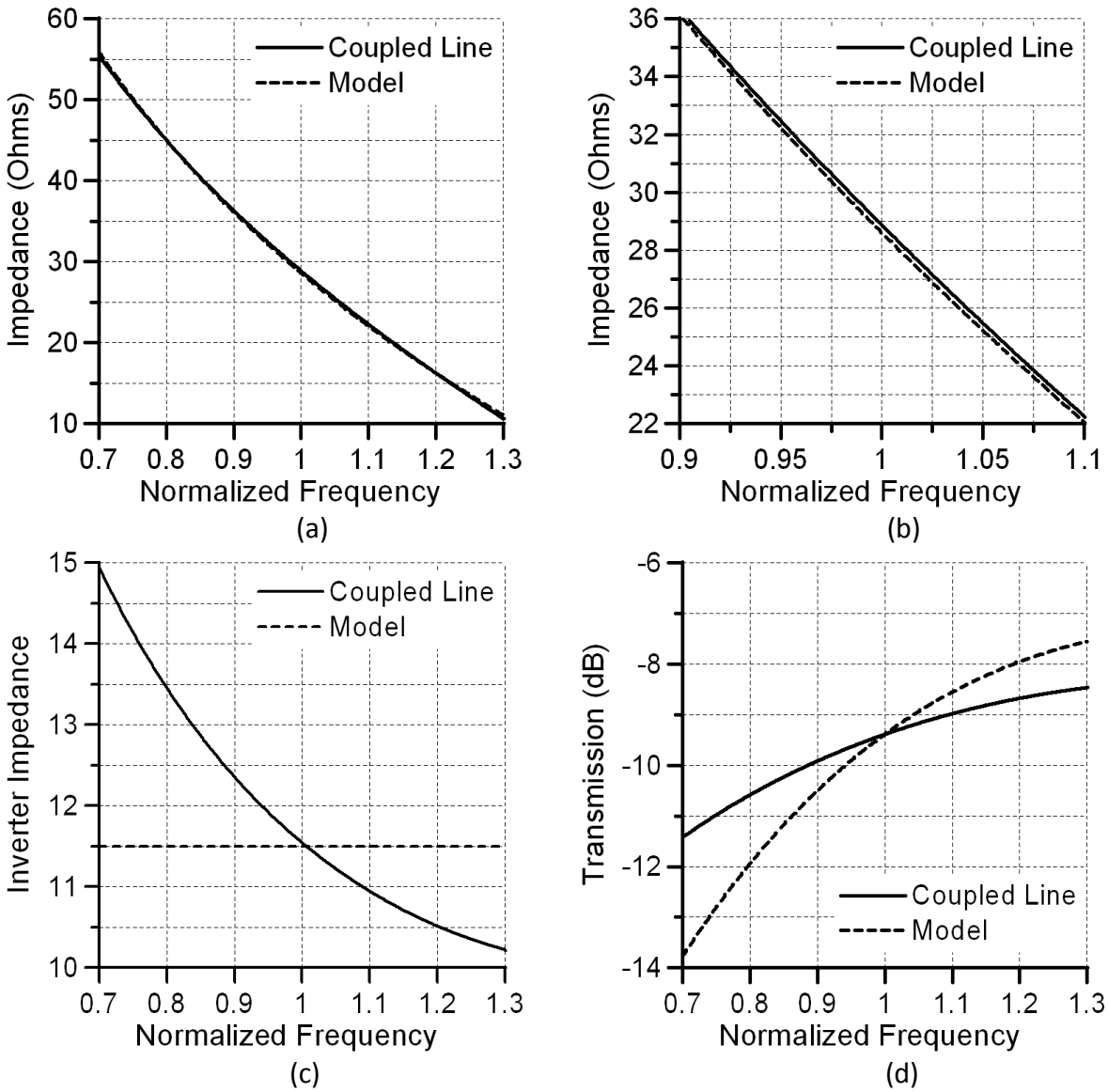

Fig. 3-15 Comparison of driving point impedance, Z_{11}, where (a) wide band plot (b) narrow band plot. (c) Comparison of inverter impedance and (d) transmission response of coupled-line and equivalent model.

The equivalent circuit of the resonator may be obtained by integrating the lumped models of the coupled lines and mid-section as illustrated in Fig. 3-16, which resembles an inverter coupled bandpass prototype network. The two synchronous resonators that comprise the dual-mode structure, the inter-resonator coupling coefficient as well as the input and output coupling coefficients are distinctly clear from this model, from which the angular resonant frequency of each resonator may be expressed by (3.35).

$$\omega_0 = \frac{1}{\sqrt{C_A(L_A + L_2)}} \tag{3.35}$$

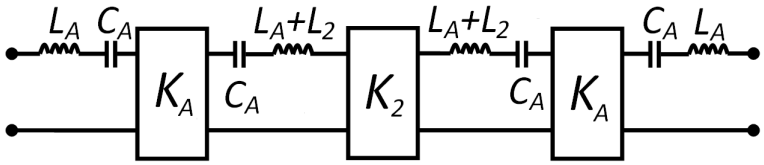

Fig. 3-16 Equivalent circuit of parallel-coupled dual-mode resonator in inverter coupled bandpass prototype form.

In contrast to an inverter coupled filter prototype however, the dual-mode resonator is seen to have an additional series connected LC resonator at each port end. This feature degrades the filtering response as this pair of resonators is detuned from the filter center frequency. However, a method of compensating for this effect, particularly effective for narrow band filters, is to insert an additional inductance to each port such that the total LC impedance at the ports is effectively zero at the center frequency and is relatively insignificant in its vicinity. This inductance may be realised as a section of high impedance microstrip line.

For evaluation of the resonator model and verification of the related equations, Fig. 3-17 plots the transmission response of the resonator and that of the model. The distributed resonator parameters were Z_B = 50 Ω, Z_e = 60 Ω, Z_o = 40 Ω, $\theta_C = 67.5^0$, $\theta_B = 20^0$, $\theta_2 = 2.5^0$, and the port impedance was 5 kΩ. The corresponding model parameters were calculated to be L_A = 3.89 nH, L_2 = 3.3 nH, C_A = 3.56 pF, K_A = 10.8 and K_2 = 2.55. There is good agreement between the resonator response and that of the model near the center frequency. The error in the model grows for frequencies deviating from the center due to the actual frequency dependent nature of the model parameters. Fortunately, for moderate to narrow fractional bandwidth filter design, these errors are negligible.

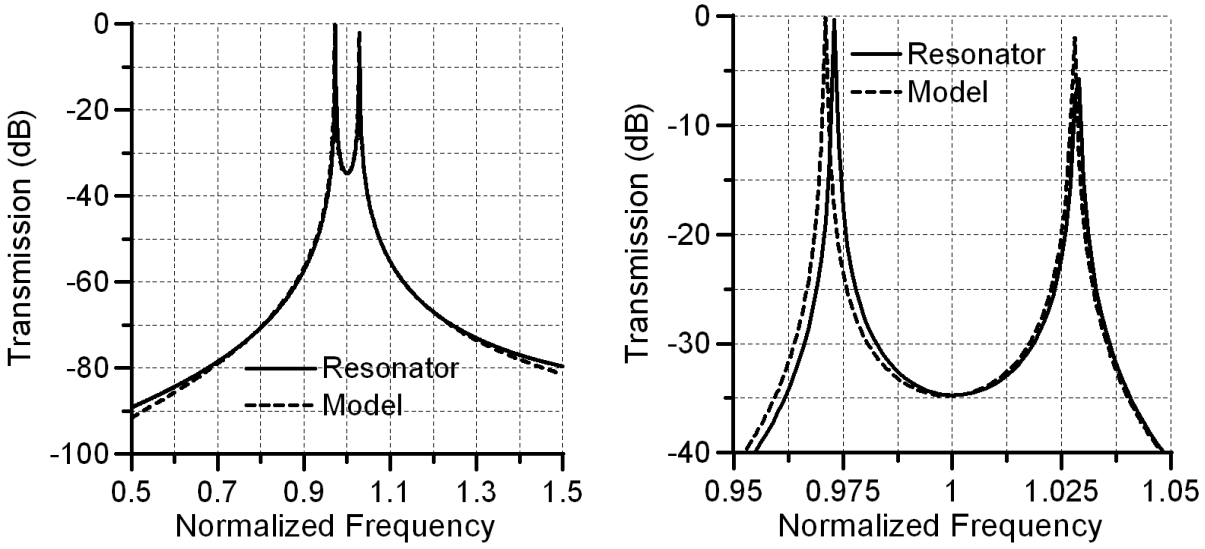

Fig. 3-17 Comparison of transmission response of parallel-coupled dual-mode resonator and that of the model where (a) wideband response (b) narrowband response.

This model is extremely useful in bandpass filter design as it allows physical transmission line parameters to be estimated relatively accurately from lumped element prototype networks. In contrast to the direct-coupled approach, the response obtained here has an all-pole type characteristic. Therefore, this method is particularly suited for Butterworth and Chebyshev Type 1 filter design. Nevertheless, there are methods of introducing transmission zeros to the stopband but these will be discussed at a later stage.

3.2.3 Summary

In order to realize purposeful filtering circuits, resonators must be coupled to the input and output ports of a network. Although in lumped element resonators and filters, there is limited choice in how the network may be excited, distributed structures may be fed in various different ways, where a choice is made depending on the strength of the coupling required.

Two feeding methods have been presented for the proposed dual-mode resonator. The direct-coupled method was shown to be highly suitable for wide fractional bandwidth filter applications while the parallel-coupled approach was appropriate for moderate to low fractional bandwidth designs. The development of equivalent circuits in both cases was described and the derivations of the related equations were presented. Each model was validated against the dual-mode resonator by comparison of their transmission responses. In both cases, there was very good agreement in the transmission response near the center frequency, which enables these models to be employed in filter design. Although the error grows at higher frequencies, this is negligible for moderate to low fractional bandwidth filter design.

The direct-coupled resonator exhibits a single transmission zero in the upper stopband and its position was shown to be purely dependent on the placement of the feed line. In order to reflect this feature, its equivalent circuit as a result is somewhat complex. In contrast, the parallel-coupled resonator exhibits an all-pole type response and the equivalent circuit resembles an inverter coupled bandpass prototype network. This enables the parallel coupled dual-mode resonator to be an ideal candidate for Butterworth and Chebyshev type I filter design.

The limitations of the proposed models arise mainly from the assumption that the impedance inverters are frequency independent. As a consequence, the accuracy of the equivalent model deteriorates gradually for filters with increasing fractional bandwidths.

3.3 Variants of the Dual-Mode Resonator

The previous sections have presented a detailed analysis of the basic dual-mode resonator. While these resonators may be employed as is in bandpass filter development, there may be more stringent specifications that may not be met with the basic resonator. The aim of this section is to address some of these issues by presenting various measures to enhance and adapt the performance of a single resonator unit to better match a given requirement may it be improving stopband performance, selectivity or achieving further compactness.

The first modification is to fold the resonator from a linear structure to a square form, which makes the resonator more compact by shortening its longest dimension. The resonator may be further miniaturized by extending the open ended sections inwards. For small extensions, the coupling between the arms of the resonator may be insignificant. However, for larger extensions, the capacitive type coupling will no longer be negligible and is seen to introduce a number of transmission zeros in the stopband of the resonator. Stepped impedances may also be applied in on these lines in addition to folding to greatly enhance the compactness of the structure.

The feeding methods discussed previously are still applicable to all the variants of the dual-mode resonator. In the discussions to follow however, little attention will be paid to direct-coupled resonator configurations since this approach does not find much use in regular filter design. Although this approach may be necessary in ultra-wideband filter design, this subject is outside the scope of this work.

3.3.1 Simple Folded Resonator

The open ended arms of the dual-mode resonator may be folded in order to reduce the overall length of the unit as illustrated in Fig. 3-18. Although structurally different from the linear resonator configuration, this resonator shares the same equivalent circuit of Fig. 3-16 as well as all its related equations. There are of course additional parasitic coupling which occur due to increased proximity of the various lines but these are relatively weak in order to produce any significant effects.

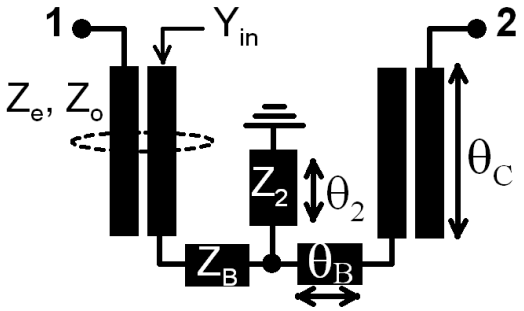

Fig. 3-18 Basic folded parallel-coupled dual-mode resonator

Typically, to achieve minimum footprint, the resonator is folded into a square topology, which may be achieved by setting $\theta_C = 2\theta_B$, at the center frequency of the resonator. The resonance condition for the parallel coupled resonator may be obtained by assuming that the characteristic impedance of the coupled line is $\sqrt{Z_e Z_o}$ [3-17], and solving for zero susceptance, Y_{in}, looking into the open ended arms of the resonator. The resonant frequency can therefore be determined by solving (3.36).

$$\frac{1}{Y_{in}} = \sqrt{Z_e Z_o} = Z_B \tan(\theta_C) \frac{Z_B \tan(\theta_B) + Z_2 \tan(\theta_2)}{Z_B - Z_B \tan(\theta_2) \tan(\theta_B)} \tag{3.36}$$

3.3.2 Compact Folded Resonator

In order to enhance the compactness of this structure, it is possible to extend the open ends with sections of microstrip line of electrical length θ_A as illustrated in Fig. 3-19. While the additional sections of microstrip line will not increase the footprint of the resonator, more compactness may be achieved by elongating the extensions.

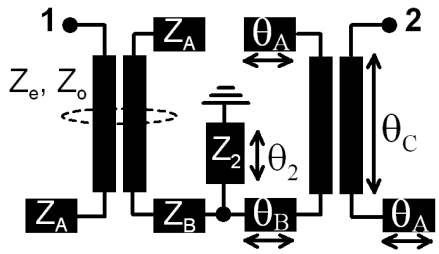

Fig. 3.19 Folded resonator with extensions to achieve compactness

The model of Fig. 3-16 still applies to this form of resonator. However, the resonator comprises of a modified coupled line section as illustrated in Fig. 3-20 and therefore new formulations must be used for extracting the coupled-line equivalent circuit parameters, L_A, C_A and K_A. The new driving point and transfer impedances of the modified coupled lines are found to be (3.37) and (3.38) respectively, where $D = -jZ_A \cot(\theta_A)$.

$$Z_{11N} = Z_{11} + \frac{(D + Z_{11})(Z_{12}^2 + Z_{14}^2) - 2Z_{12}Z_{13}Z_{14}}{Z_{13}^2 - (D + Z_{11})^2} \tag{3.37}$$

$$K_A = Z_{12N} = Z_{13} + \frac{2Z_{12}Z_{14}(D + Z_{11}) - Z_{13}(Z_{12}^2 + Z_{14}^2)}{Z_{13}^2 - (D + Z_{11})^2} \tag{3.38}$$

, where Z_{XX} are the impedance matrix elements of a regular coupled line given by [3-16]:

$$Z_{11} = -0.5j(Z_e + Z_o)\cot(\theta_C) \tag{3.39}$$

$$Z_{12} = -0.5j(Z_e - Z_o)\cot(\theta_C) \tag{3.40}$$

$$Z_{13} = -0.5j(Z_e - Z_o)\csc(\theta_C) \tag{3.41}$$

$$Z_{14} = -0.5j(Z_e + Z_o)\csc(\theta_C) \tag{3.42}$$

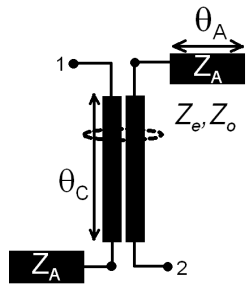

Fig. 3-20 Modified coupled lines

Similar to earlier discussions, a curve fitting approach can be used to extract a series inductance, L_A, and capacitance, C_A, in order to duplicate the driving point coupled line impedance, Z_{11N}. The resulting formulations for the inductance and capacitance are given by (3.43) and (3.44).

$$L_A = \frac{\omega_H Z_{11N}(\omega_H) - \omega_L Z_{11N}(\omega_L)}{\omega_H^2 - \omega_L^2} \qquad (3.43)$$

$$C_A = \frac{1}{\omega_L^2 L_A - \omega_L Z_{11N}(\omega_L)} \qquad (3.44)$$

To evaluate the modified coupled line model, Fig. 3-21 (a) compares the driving point impedances, where Z_e = 60 Ω, Z_o = 40 Ω, Z_A = 50 Ω, $\theta_A = 20^0$, $\theta_C = 47.4^0$, while Fig. 3-21 (b) compares the transfer impedances. Model parameters for the driving point impedance were extracted at of $0.8f_0$ and $1.2f_0$ (L_A = 3.85 nH, C_A = 3.58 nF, K_A = 8.62).

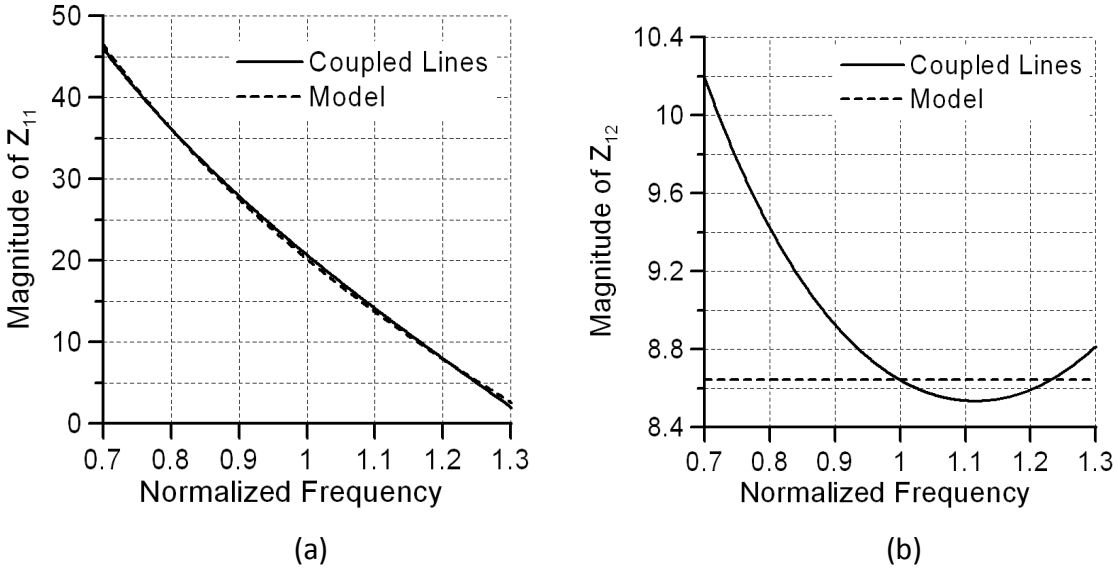

(a) (b)

Fig. 3-21 Comparison of (a) Driving point impedance (b) transfer impedance of modified coupled line and model.

Similar to the previous models, there is a good agreement in the driving point impedances while some frequency dependence is noticeable in the inverter impedance K_A. As with the previous cases, this variation is not very significant in narrowband filter design.

The lumped element circuit of Fig. 3-9 (b) may be used once again to model the mid-section of the resonator where K_2 and L_2 may be determined by (3.23) and (3.24) respectively. Once these parameters have been determined for a particular resonator structure, the equivalent circuit of Fig. 3-16 may be completed. In order to evaluate the model of the compact folded resonator, the transmission responses are compared between the resonator and its model in Fig. 22, where Z_e = 60 Ω, Z_o = 40 Ω, $Z_A = Z_B = Z_2$ = 50 Ω, $\theta_A = \theta_B = 20^0$, $\theta_C = 47.4^0$, $\theta_2 = 2.5^0$. The corresponding model parameters were calculated to be L_A = 3.81 nH, C_A = 3.57 nF, K_A = 8.62, L_2 = 3.3, K_2 = 2.55.

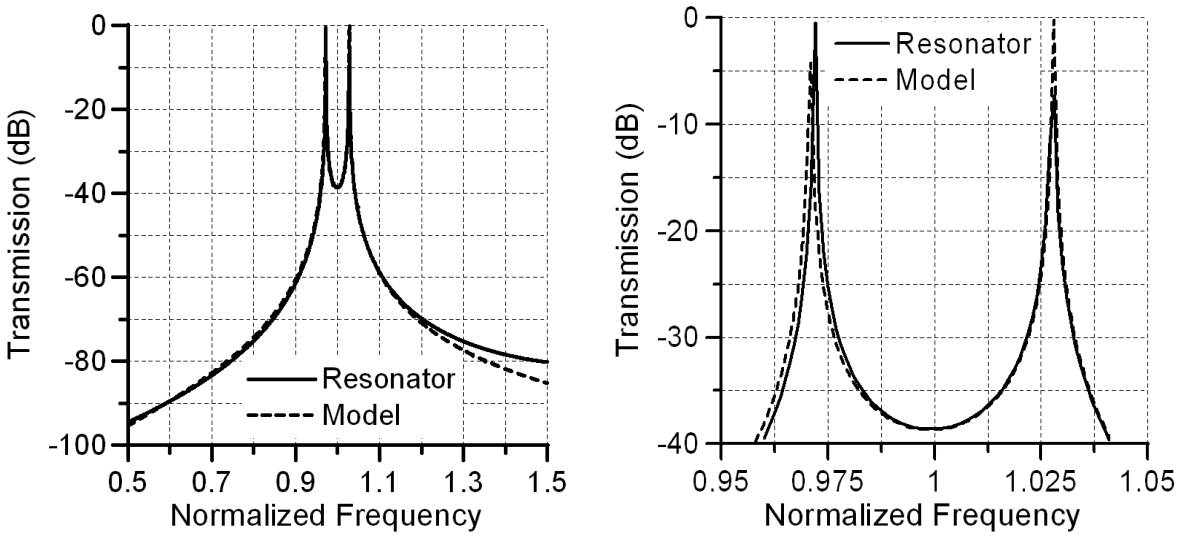

Fig. 3-22 Comparison of transmission response of compact parallel-coupled dual-mode resonator and that of the model where (a) wideband response (b) narrowband response.

A good agreement between the distributed resonator and that of the model is observed. The integrity of the model and the related equations are strong near the fundamental resonance of the resonator. Although the discrepancies are noticeable at frequencies beyond 1.3 GHz, these are insignificant with regard to moderate to low fractional bandwidth filter design.

3.3.3 Compact Folded Resonator with Capacitive Cross-Arm Coupling

If the extensions to the coupled line are sufficiently long, the parasitic capacitive coupling between the open ended sections of impedance Z_A will no longer be negligible. This parasitic capacitance, C_{INT}, vanishes in the even mode since there is no current flow across the symmetry plane of the resonator. Therefore, this coupling has no effect on the even mode resonant frequency. In the odd mode however, the capacitance doubles to $2C_{INT}$, and lowers the odd mode resonant frequency. In addition, this coupling introduces several transmission zeros into the resonator response, which may be useful for enhancing skirt selectivity of a filter. The resonator configuration and its equivalent circuit are presented in Fig. 3-23.

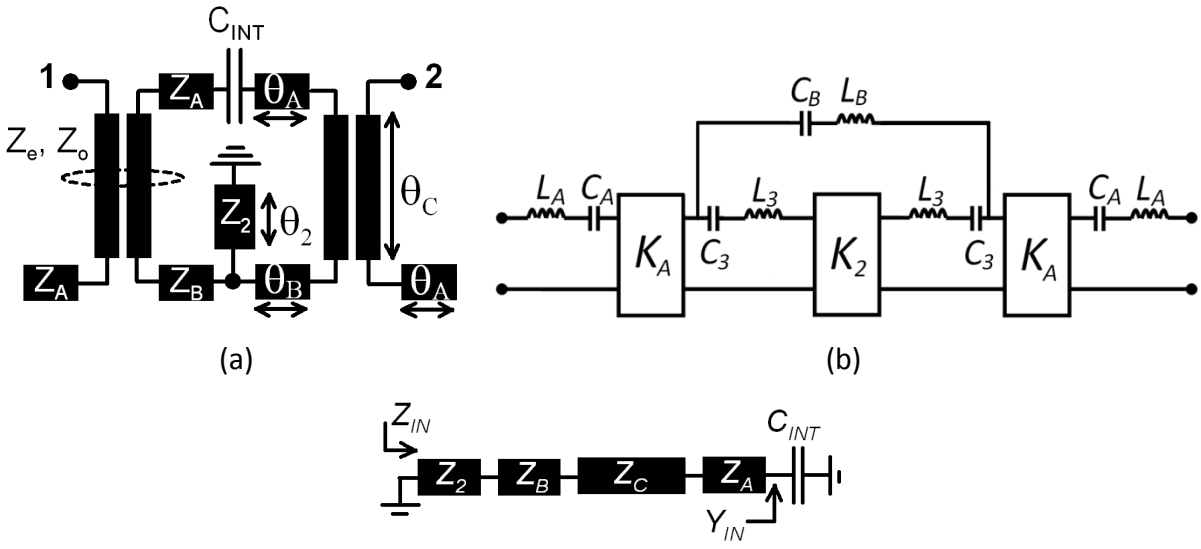

Fig. 3-23 (a) Dual-mode resonator with capacitive cross-arm coupling (b) Equivalent circuit (c) Equivalent transmission line resonator

This model bears resemblance to that of the folded resonator model, with the exception of the additional parameters L_B and C_B which account for the two transmission zeros that are produced in the lower and upper stopbands. The resonant frequency of the resonator may be determined from the input impedance, Z_{IN} given by (3.45) of the equivalent transmission line resonator illustrated in Fig. 3-23 (c), by applying the condition $Z_{IN} = 0$. This may be obtained by solving (3.46), where it is assumed that $Z_A = Z_B = Z_C = Z_0$.

$$Z_{IN} = j\left(Z_2 \tan(\theta_2) + Z_0\left[\frac{Z_0\omega C_{INT}\tan(\theta_A+\theta_B+\theta_C)-1}{Z_0\omega C_{INT}+\tan(\theta_A+\theta_B+\theta_C)}\right]\right) \quad (3.45)$$

$$\omega_0 = \frac{1}{Z_0 C_{INT}}\left[\frac{Z_0 - Z_2\tan(\theta_2)\tan(\theta_A+\theta_B+\theta_C)}{Z_2\tan(\theta_2)+Z_0\tan(\theta_A+\theta_B+\theta_C)}\right] \quad (3.46)$$

The inductance L_3 may be determined by the reactance slope parameter, x_r, evaluated at the angular center frequency ω_0 as given by (3.47).

$$L_3 = \frac{1}{2}\frac{dZ_{IN}}{d\omega}\bigg|_{\omega=\omega_0} = \frac{x_r}{\omega_0} \quad (3.47)$$

The susceptance slope parameter, x_s, of the resonator can be found from the derivative of Y_{IN} with respect to ω. In addition to the inductive impedance due to the short circuit stub Z_2, the inter-resonator inverter impedance K_2 is now also a function of the capacitance C_{INT}. The contributions of each toward K_2 are opposite in phase and thus result in a smaller overall inverter impedance, given by (3.48).

$$K_2 = Z_2\tan(\theta_2) - \frac{x_r\omega_0 C_{INT}}{x_s} \quad (3.48)$$

Transmission zeros occur under the condition that the even mode admittance of Y_{IN} is equal to that of the odd mode. Solving for this condition produces (3.49), which may be evaluated numerically to obtain the angular frequencies of the transmission zeros that occur either side of the center frequency.

$$2\omega C_{INT} - \frac{1}{Z_0 tan(\theta_A+\theta_B+\theta_C)} + \frac{1}{Z_0}\left(\frac{Z_0 - 2Z_2 tan(\theta_2)tan(\theta_A+\theta_B+\theta_C)}{2Z_2 tan(\theta_2)+Z_0 tan(\theta_A+\theta_B+\theta_C)}\right) = 0 \quad (3.49)$$

These two frequencies may be substituted into (3.50) to calculate L_B and ω_B, from which C_B may then be determined from (3.51).

$$L_B(\omega^2 + \omega_B^2) = \omega K_2 + \frac{(L_A + L_2 + L_3)^2}{\omega K_2}[\omega^4 - 2\omega_0^2\omega^2 + \omega_0^4] \tag{3.50}$$

$$C_B = \frac{-1}{L_B\omega_B^2} \tag{3.51}$$

Due to the complicated nature of the equations especially where the line impedances are non-uniform and when C_{INT} is unknown, an electromagnetic simulation based approach may be adopted to extract the inter-resonator coupling coefficient, M_2, defined by (3.52), where a full wave electromagnetic simulation must be performed to obtain the even and odd mode resonant frequencies, f_{even} and f_{odd} [3-1].

$$M_2 = \frac{K_2}{\omega_0 L_3} = \frac{{f_{odd}}^2 - {f_{even}}^2}{{f_{even}}^2 + {f_{odd}}^2} \tag{3.52}$$

The resonator center frequency f_0 can be defined as (3.53).

$$f_0 = \frac{1}{2\pi\sqrt{C_3 L_3}} = \sqrt{f_{even} f_{odd}} \tag{3.53}$$

These two parameters are sufficient for the purposes of bandpass filter design. In order to illustrate the response of this resonator, validate the model and the parameter extraction method, the transmission responses of the two circuits of Fig. 3-23 are compared in Fig. 3-24. The resonator parameters may be summarized as follows: $Z_A = Z_B = Z_2 = 50\ \Omega$, $Z_e = 60\ \Omega$, $Z_o = 41.67\ \Omega$, $\theta_A = 20^0$, $\theta_B = 20^0$, $\theta_C = 47.5^0$, $\theta_2 = 2.5^0$ and $C_{INT} = 0.5$ pF. The model parameters were determined by calculation to be $L_A = 3.81$ nH, $C_A = 3.57$ pF, $C_3 = 3.57$ pF, $L_3 = 8.56$ nH, $L_B = 25.3$ nH, $C_B = -0.234$ pF, $K_2 = 5.96$ and $K_A = 8.62$.

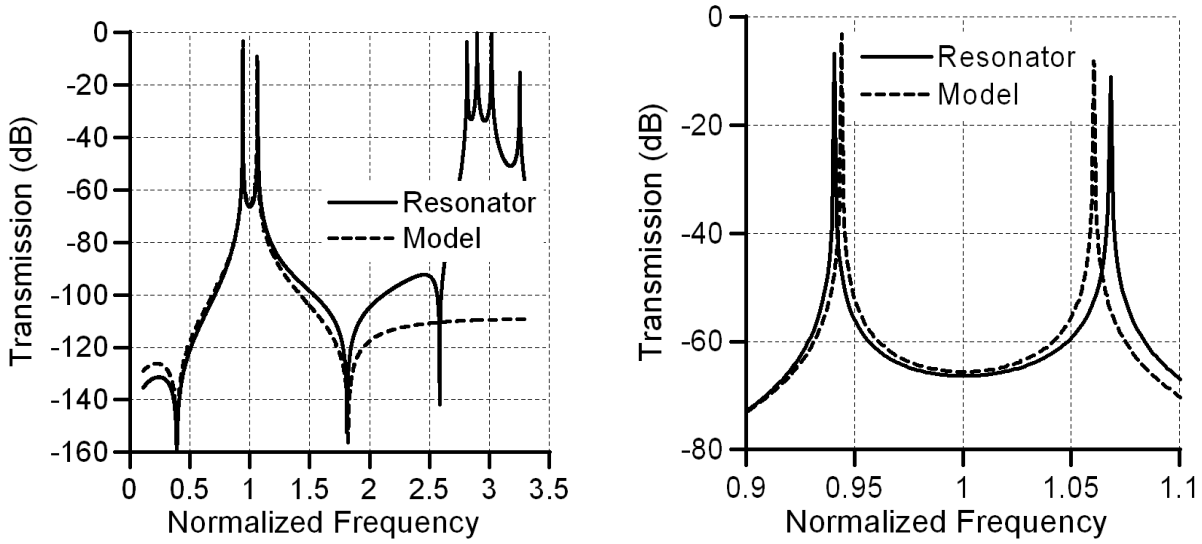

(a) (b)

Fig. 3-24 Transmission response of parallel-coupled dual-mode resonator with capacitive coupling and that of the model where (a) wideband response (b) narrowband response.

The figures above show a good agreement between the resonator and the model up to the second transmission zero frequency, beyond which the model response deviates significantly. This is acceptable for narrowband filter design, where any higher order harmonic resonances may be safely ignored. Although the third transmission zero in the stopband is not modelled, this may serve to improve the overall attenuation and enhance a filter's stopband rejection.

In addition to the transmission zeros, one of the interesting features of this resonator is that the inter-resonator impedance, K_2, can be either positive or negative depending on the resonator parameters and C_{INT} as given by (3.48). While the sign of coupling coefficients are not very important for direct-coupled filter design, the ability to realize both types of coupling is vital to the design of cross-coupled filters. This property of the resonator can be exploited in the design of cross-coupled bandpass filters.

3.3.3 Folded Resonators with Stepped Impedances

A widely used method of enhancing compactness in resonators is to use stepped impedance lines since this method is applicable to all one dimensional planar resonators consisting of transmission line segments. Another benefit gained from employing stepped impedances is the control of the second harmonic resonance frequency. Depending on the kind of stepped impedance ratio used, the harmonics may be shifted towards or away from the fundamental resonance frequency. For single passband filter design, this approach is commonly employed in shifting the second harmonic resonances outward so as to produce a wider stopband. On the other hand, control of the second resonance is exploited in dual-band filter design in order to produce two passbands at the desired frequencies.

Stepped impedances are employed in this work primarily for purposes of resonator size reduction rather than for dual-band filter design. For achieving size reduction, a stepped impedance transmission line of a particular length must in effect be electrically longer than its uniform impedance counterpart. Effectively, this allows a longer section of uniform impedance line to be replaced by a shorter segment of stepped impedance line, resulting in a more compact structure.

Since the dual-mode resonator behaves as a $\lambda_g/4$ short circuited resonator, it may be represented as Fig. 3-25, where two distinct line impedances, Z_1 and Z_2 are used. Resonance occurs at the frequency where the input admittance, Y_{in}, is zero and this condition may be written in terms of the resonator parameters as (3.54).

$$\tan(\theta_1)\tan(\theta_2) = \frac{Z_1}{Z_2} \tag{3.54}$$

In order to understand the effect of the ratio of the stepped impedance, $R_Z = Z_1/Z_2$, on the overall length of the resonator, the electrical lengths may be converted to physical lengths and normalized to the length of a uniform impedance resonator, for a fixed resonant frequency. The expression for the normalized resonator length, L_n, is then given by (3.55).

$$L_n = \frac{2}{\pi}\left[\theta_1 + \arctan\left(\frac{R_Z}{\tan(\theta_1)}\right)\right] \tag{3.55}$$

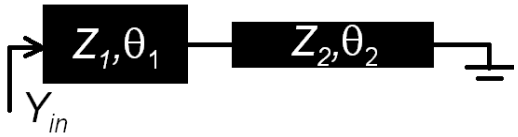

Fig. 3-25 Stepped impedance $\lambda_g/4$ transmission line resonator

Fig. 3-26 plots the normalized resonator length against θ_1 for various impedance ratios R_Z to visualize the effect of the stepped impedance on the length of the resonator and for the selection of the optimum θ_1 to maximize size reduction. The special case where R_Z = 1 is represents the uniform impedance resonator.

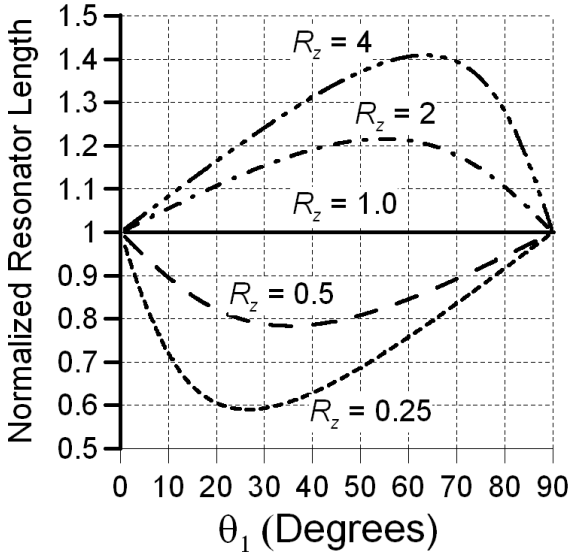

Fig. 3-26 Normalized length of resonator against θ_1 for various values of the stepped impedance ratio R_z

From the plot, it is evident that to achieve size reduction, the ratio R_Z must be less than unity. Therefore the aim is to have characteristic impedances such that $Z_2 > Z_1$, i.e. higher characteristic impedances towards the short circuited end. While theoretically, drastic size reductions may be achieved with an extremely small impedance ratio, a typical minimum practical impedance ratio realizable on microstrip technology would be around R_Z = 0.25. For this ratio, and for $\theta_1 \approx 25^0$, nearly 40% length reduction may be achieved as illustrated.

This method may be applied to all the variants of this resonator. For example, stepped impedance may be applied to the resonator of Fig. 3-19 by letting $Z_C > Z_A$, where $Z_c = (Z_e Z_o)^{0.5}$. The model parameters may still be determined with the same formulae presented in the earlier sections. In order to evaluate the performance of the model against the stepped impedance dual-mode resonator, Fig. 3-27 compares the transmission responses, where Z_e = 60 Ω, Z_o = 40 Ω, Z_A = 25 Ω, $Z_B = Z_2$ = 50 Ω, $\theta_A = \theta_B = 20^0$, $\theta_C = 30^0$, $\theta_2 = 2.5^0$. Model parameters were L_A = 3.56 nH, C_A = 4.03 nF, K_A = 6.4, L_2 = 3.3, K_2 = 2.55.

In addition to compactness, the first spurious resonance of a stepped impedance resonator is shifted further from the fundamental. This property can be seen in Fig. 3-27 (a), where the spurious response occurs around $3.5f_0$ rather than $3f_0$.

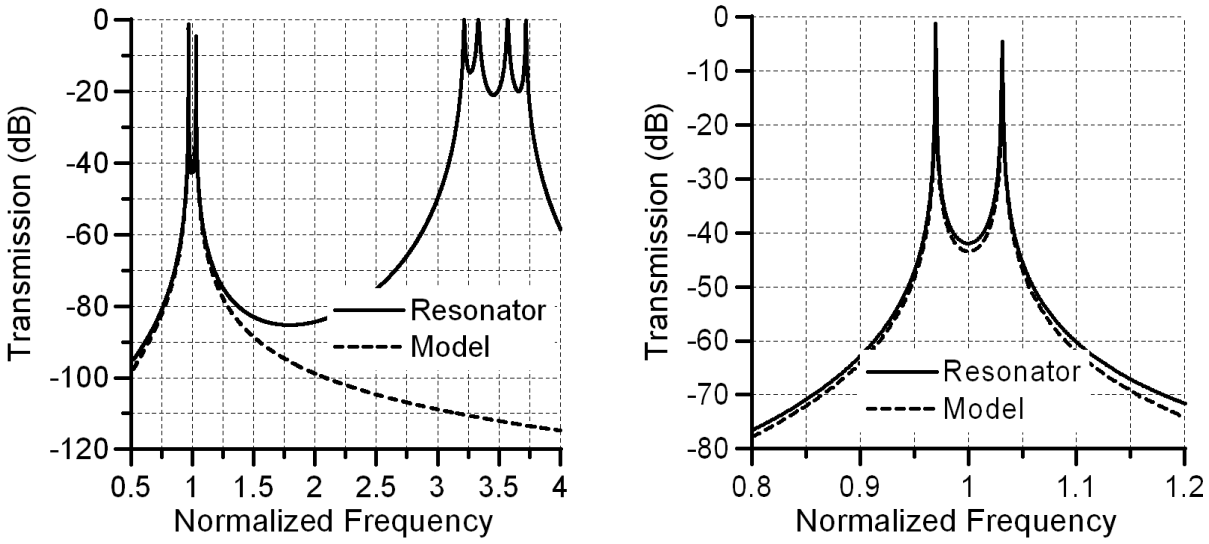

Fig. 3-27 Comparison of transmission response of compact stepped impedance parallel-coupled dual-mode resonator and that of the model where (a) wideband response (b) narrowband response

3.3.5 Summary

Four variants of the dual-mode resonator have been presented in this section. The unique properties of each resonator configuration, which may be particularly suited for different filtering applications, have been described. Equivalent lumped element models for each resonator together with the element value extraction formulae have been presented to facilitate filter design based on any resonator configuration.

The folded resonator topology is introduced as a means of reducing the overall dimensions of the resonator. Folding the resonator into a square form allows the largest overall dimension of the resonator to be reduced. It was shown that further compactness may be obtained by extending the folded arms of the resonator into the structure. In this case, although the inverter coupled filter model is still applicable, new formulae must be employed in order to account for the additional lengths of transmission line.

Finally, applying stepped impedances to the dual-mode resonator was discussed. Depending on the nature of the impedance ratio of a resonator, it was shown that the length of the resulting resonator may either be shortened or elongated. In order to achieve size reduction, it was necessary for the impedance ratio, R_z, to be less than unity. Although greater size reduction is theoretically possible with smaller impedance ratios, there is a limit to the minimum impedance ratio achievable in microstrip technology. Nevertheless, this technique is useful in producing highly compact dual-mode resonators.

The next two chapters describe the application of these resonators in the development of compact microstrip filters. While several compact filter examples are presented, the discussions are supplemented with simulated and experimental measurements for thorough evaluation. In addition, a filter design procedure is outlined to facilitate the design of Butterworth and Chebyshev all-pole filters employing these resonators. The possibility of applying these resonators in cross-coupled filter topologies is also investigated. Finally, constant bandwidth center frequency tunable bandpass filters using these resonators are presented.

3.4 References

[3-1] J.-S Hong and M. J. Lancaster, *Microstrip filters for RF/microwave applications*, New York: John Wiley & Sons, 2001.

[3-2] J.-S. Hong and M.J. Lancaster, “Theory and experiment of novel microstrip slow-wave open-loop resonator filters”, *IEEE Transactions on Microwave Theory and Techniques*, vol. 45, no. 12, pp. 2358-2365, Dec. 1997.

[3-3] P. Hoi-Kai, H. Ka-Meng, T. Kam-Weng, and R. P. Martins, "A compact microstrip g/4-SIR interdigital bandpass filter with extended stopband," *IEEE MTT-S, Int. Microwave Symp. Dig.*, pp. 1621- 1624, Jun. 2004.

[3.4] K. Chul-Soo, K. Duck-Hwan, S. In-Sang, K. M. K. H. Leong, T. Itoh, and A.Dal, "A design of a ring bandpass filters with wide rejection band using DGS and spur-line coupling structures," *IEEE MTT-S, Int. Microwave Symp. Dig.*, pp. 2183-2186, Jun. 2005.

[3.5] A. Griol, J. Marti, and L. Sempere, "Microstrip multistage coupled ring bandpass filters using spur-line filters for harmonic uppression," *Electronics Letters*, vol. 37, no. 9, pp. 572-573, Apr. 2001.

[3-6] P. Mondal and M. K. Mandal, “Design of dual-band bandpass filters using stub-loaded open-loop resonators”, *IEEE Transactions on Microwave Theory and Techniques*, vol. 56, no. 1, pp. 150-155, Jan. 2008.

[3-7] Y. Ping and M. Sun, “Dual-band microstrip bandpass filter using stepped-impedance resonators with new coupling schemes”, *IEEE Transactions on Microwave Theory and Techniques*, vol. 54, no. 10, pp. 3779-3785, Oct. 2006.

[3-8] J.-S. Hong, H. Shaman and Y.-H. Chun, “Dual-mode microstrip open-loop resonators and filters”, *IEEE Transactions on Microwave Theory and Techniques*, vol. 55, no. 8, pp. 1764-1770, Aug. 2007.

[3-9] A. C. Kundu and I. Awai, "Control of attenuation pole frequency of a dual-mode microstrip ring resonator bandpass filter", *IEEE Transactions on Microwave Theory and Techniques*, vol. 49, no. 6, pp. 1113-1117, Jun. 2001.

[3-10] J.-S. Hong and M.J. Lancaster, "Realisation of quasielliptic function filter using dual-mode microstrip square loop resonators", *Electronic Letters*, vol. 31, no. 24, pp. 2085-2086, Nov. 1995.

[3-11] J.-S. Hong and S. Li, "Theory and experiment of dual-mode microstrip triangular patch resonators and filters", *IEEE Transactions on Microwave Theory and Techniques*, vol. 52, no. 4, pp. 1237-1243, Apr. 2004.

[3-12] B. T. Tan, S. T. Chew, M. S. Leong and B. L. Ooi, "A modified microstrip circular patch resonator filter", *IEEE Microwave and Wireless Component Letters*, vol. 12, no. 7, pp. 252-254, Jul. 2002.

[3-13] W.-H. Tu and K. Chang, "Miniaturized dual-mode bandpass filter with harmonic control", *IEEE Microwave and Wireless Component Letters*, vol. 15, no. 12, pp. 838-840, Dec. 2005.

[3-14] L. Athukorala and D. Budimir, "Design of compact dual-mode microstrip filters", *IEEE Transactions on Microwave Theory and Techniques*, vol. 58, no. 11, pp. 2888-2895, Nov. 2010.

[3-15] J.-S. Hong and M.J. Lancaster, "Theory and experiment of novel microstrip slow-wave open-loop resonator filters", *IEEE Transactions on Microwave Theory and Techniques*, vol. 45, no. 12, pp. 2358-2365, Dec. 1997.

[3-16] D. M. Pozar, *Microwave engineering*, 3rd edition, New York: John Wiley & Sons, 2004.

[3-17] R. E. Collin, Foundations for microwave engineering, 2nd edition, New York: McGraw-Hill, 1992.

4.0 COMPACT MICROSTRIP BANDPASS FILTERS

Essentially, a bandpass filter may be constructed from a network of coupled resonators. Various unique filtering functions may be obtained depending on the particular frequency behaviour of the resonators and also on how they are coupled. While all-pole type bandpass filters may be designed from a simple cascade of LC type resonators [4-1], more complex filters with high skirt selectivity, such as the inverse Chebyshev or elliptic function filters require resonators which not only produce a transmission pole but also a zero [4-2]. Usually it is not practical to construct these complex resonators at microwave frequencies, especially with distributed resonators. However, it is still possible to obtain filtering functions with transmission zeros using only all-pole type resonators by employing unorthodox coupling mechanisms. The cross-coupled filter design is a popular approach especially at microwave filters in obtaining generalized Chebyshev type filtering characteristics [4-3]-[4-5].

This chapter focuses on the application of the dual-mode resonator, discussed in the previous sections, in bandpass filter design. Firstly, the development of all-pole Butterworth and Chebyshev bandpass filters comprising of the compact folded dual-mode resonator is discussed. A design method for obtaining the physical parameters of the resonator from the all-pole prototype networks values is outlined. The development of generalized Chebyshev bandpass filters with finite frequency transmission zeros is described next. It is shown that similar to single mode open loop resonators, the proposed dual-mode resonator may be readily used in cross-coupled resonator configurations to generate finite frequency zeros. Lastly, it is shown that the dual-mode resonators may also be configured in a concentric open-loop topology which will effectively allow filter size to be further cut in half.

4.1 All-Pole Bandpass Filter Design

Butterworth and Chebyshev bandpass filters, also known as all-pole filters, have transmission zeros that occur at infinity. Since all-pole filters may be constructed from cascading standard LC type resonators, which are characteristic of the majority of distributed resonators, these filters are widely used at RF and microwave frequencies. While Butterworth filters have a maximally flat passband, Chebyshev filters achieve significantly better skirt selectivity by having a certain degree of tolerable pass-band ripple. Although the insertion loss based design of lumped element all-pole filters had been well established with filter tables being widely available for their design [4-6], efficient realization of these circuits with transmission line distributed networks at microwave frequencies is still a subject of great research interest.

Dual-mode resonator based filters are naturally compact and generally offer the same fabrication simplicity as a regular microstrip single-mode filter. A number of highly compact dual-mode filters found in recent research include the open-loop [4-7], circular-ring [4-8] and square-loop [4-9] structures. There are only a few reports on the design of high order dual-mode filters in literature [4-10], especially using one dimensional resonators. A popular method of designing higher order filters is to couple dual-mode sections with non-resonating nodes [4-7]. However, this approach greatly compromises the compactness of the filter since the non-resonating node occupies a significant circuit area. Although single-mode filters such as the inter-digital and combline filters offer excellent size (area) reduction, they extend up to $\lambda/4$ in a single dimension and this may not always be acceptable for a given frequency and application.

This section presents an all-pole filter design technique based on the compact dual-mode resonator, described in section 3.3.2 [4-11]. While the dual resonance of each dual-mode resonator unit is ideal for the design of even order bandpass filters, odd order filters may also be constructed by having a mixture of single and dual-mode resonators. An effective method of realising inverter-coupled bandpass prototype filters using the dual-mode resonator without employing non-resonating nodes is described. This allows for the rapid design of compact, low loss and high performance filters.

Fig. 4-1 illustrates the inverter-coupled bandpass filter prototype network which is commonly used as a starting point for microwave filter design, where the resonator inductances, L_{resi}, and capacitances, C_{resi}, are to be determined from the physical structure of the particular distributed resonators to be employed in the filter [4-1]. Once determined, the inverter impedances are then found from (4.1) - (4.3), where g_i are the lowpass filter prototype element values, Z_S and Z_L are the source and load impedances respectively.

$$K_{01} = \sqrt{\frac{Z_S FBW\, \omega_0 L_{res1}}{g_0 g_1}} \tag{4.1}$$

$$K_{i,i+1} = FBW\, \omega_0 \sqrt{\frac{L_{res(i)} L_{res(i+1)}}{g_i g_{(i+1)}}}\Bigg|_{i=1\ to\ n-1} \tag{4.2}$$

$$K_{n,n+1} = \sqrt{\frac{Z_L FBW\, \omega_0 L_{resn}}{g_n g_{(n+1)}}} \tag{4.3}$$

It is common in microwave filters to employ identical resonators in filter design which effectively makes all the inductances and capacitances equal. In addition, the source and load terminations are typically 50 Ω.

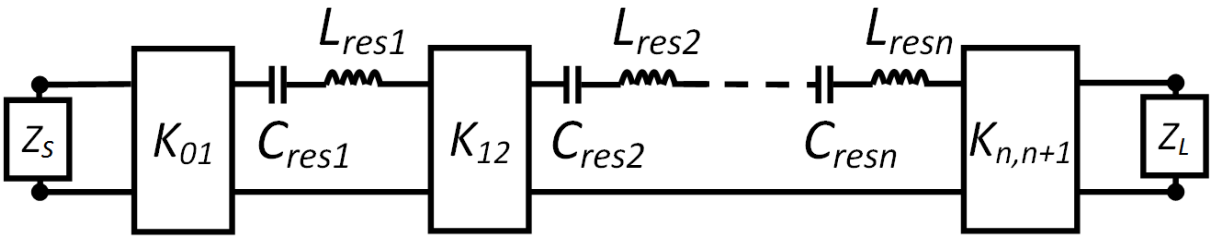

Fig. 4-1 Inverter coupled bandpass prototype network

The configuration of an even order filter constructed from the dual-mode resonator is shown in Fig. 4-2 (a), where n resonators are coupled through asymmetric parallel coupled-lines, with modal impedances given by Z_{ei} and Z_{oi}. The equivalent circuit of this filter configuration and the parameter values, as shown in Fig. 4-2 (b), may be obtained from the model of the resonator and the related equations presented in Chapter 3. The resonators are generally designed such that they are all synchronously tuned.

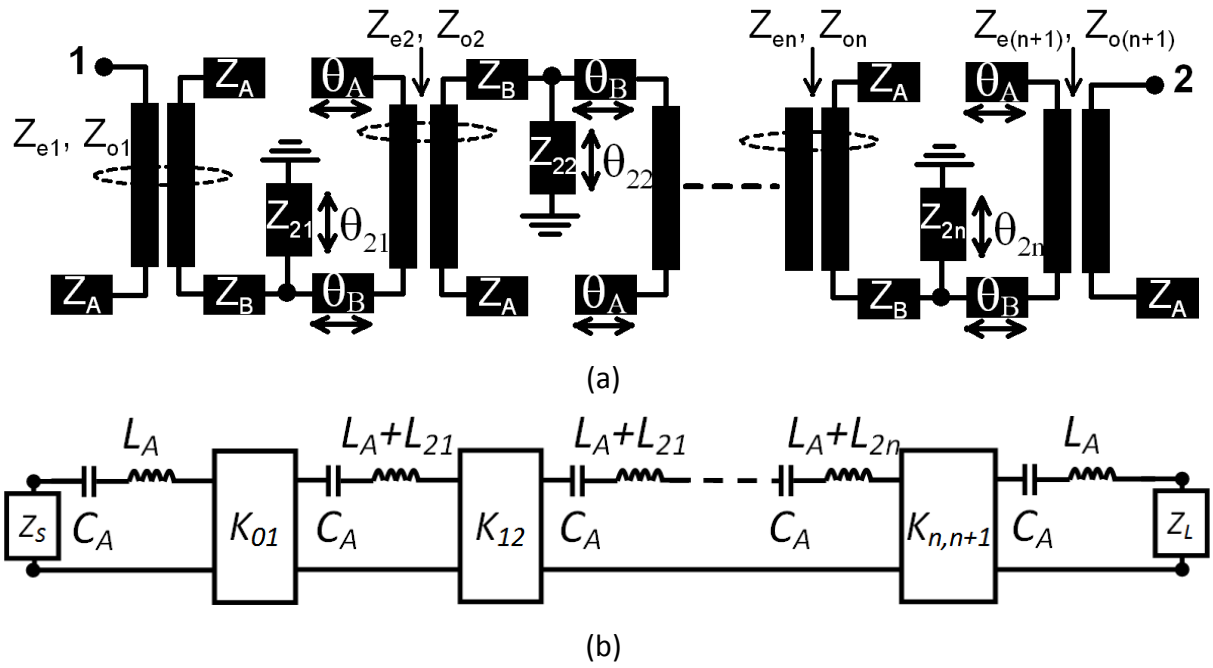

(a)

(b)

Fig. 4-2 (a) Configuration of an n[th] order all-pole bandpass filter based on the compact folded dual-mode resonator (b) Lumped element equivalent circuit of dual-mode filter

4.1.1 Second Order All-Pole Filters

This section presents the design of a simple second order Chebyshev bandpass filter, through which the filter design procedure is highlighted. The filter specifications are summarized in table 4-1 and the element values obtained from filter tables are g_0 = 1, g_1 = 0.4489, g_2 = 0.4078, g_3 = 1.1008.

Filter Specification	
Filter Order	2
Response Type	Chebyshev
Center Frequency	1.0 GHz
Fractional Bandwidth	10 %
Passband Ripple	0.01 dB
Source/Load Termination	50 Ω

Table 4-1: Filter specification of 2[nd] order Chebyshev filter

The first step in the design procedure is to select practical starting values for the resonator. The sum of the modal impedances of all the coupled lines, M, where $M = Z_{e1} + Z_{o1} = Z_{e2} + Z_{o2} = \ldots Z_{en} + Z_{on}$, is set according to the microstrip substrate parameters such that it is possible to readily realize all coupled line modal impedances in that particular substrate. In this particular example, M = 100 Ω. The other parameters to be initially assumed are suitable values for Z_A, θ_A, θ_B, θ_C and θ_2 where typically Z_A = 50 Ω and $\theta_A \approx 15^0$, $\theta_B \approx 22.5^0$, $\theta_C \approx 45^0$ and $\theta_2 \approx 10^0$ at the center frequency of the filter in order for the resonators to take a square like form. In this example, these typical values are assumed for the above parameters.

Once M and θ_C have been selected, it is possible to determine L_A and C_A for all the coupled lines from equations (3.43) and (3.44). Notice also that the inverter impedances of the coupled lines, K_A, may be set independently of L_A and C_A, since K_A only depends on the difference between the modal impedances. In this design example, L_A and C_A for all coupled lines were calculated to be 3.072 nH and 3.365 pF respectively. The total resonator inductance, $L_T = L_A + L_2$, can then be found from (4.4), which for this particular example was found to be 7.528 nH.

$$L_T = \frac{1}{\omega_0^2 C_A} \tag{4.4}$$

It is possible then to define $L_2 = L_T - L_A$ which is equal to 4.456 nH in this example. The next step is to use equations (4.1) – (4.3) to determine the inverter impedances using $L_T = L_{res}$. For this example, the inverter impedances were determined as $K_{01} = K_{23}$ = 23.3 and K_{12} = 11.4.

Subsequently, L_2 and K_{12} may be used in equation (3.23) and (3.24) to obtain the characteristic impedances Z_B and Z_2 which were calculated to be 40.7 Ω and 46.3 Ω respectively for this example.

Lastly, the modal impedances, Z_{ei} and Z_{oi}, of the coupled lines may be calculated using equation (3.38) and the calculated inverter impedances. For this example, these parameters were determined to be $Z_{e1} = Z_{e2}$ = 74.7 Ω and $Z_{o1} = Z_{o2}$ = 25.3 Ω.

The de-tuned resonators at the input and output ports of the filter as illustrated through the equivalent circuit in Fig. 4-2 (b) contribute to the distortion of the filter response. In order to minimize this effect, a simple solution is to add an inductive line at each port so as to tune these resonators to resonate at the filter center frequency. This inductance may be realised relatively accurately with a short segment of high impedance line with characteristic impedance Z_{ind} given by (4.5), where θ_{ind} is the electrical length at the center frequency. For this particular example, a characteristic impedance of 120 Ω was chosen where $\theta_{ind} = 7.9^0$.

$$Z_{ind} = \frac{Z_B tan(\theta_B)}{tan(\theta_{ind})} \tag{4.5}$$

Fig. 4-3 summarizes the results obtained from the filter design procedure in graphical form illustrating the element values for the lowpass filter prototype, bandpass filter prototype, filter model and finally, the parameters of the distributed filter, where $Z_S = Z_L = 50$ Ω.

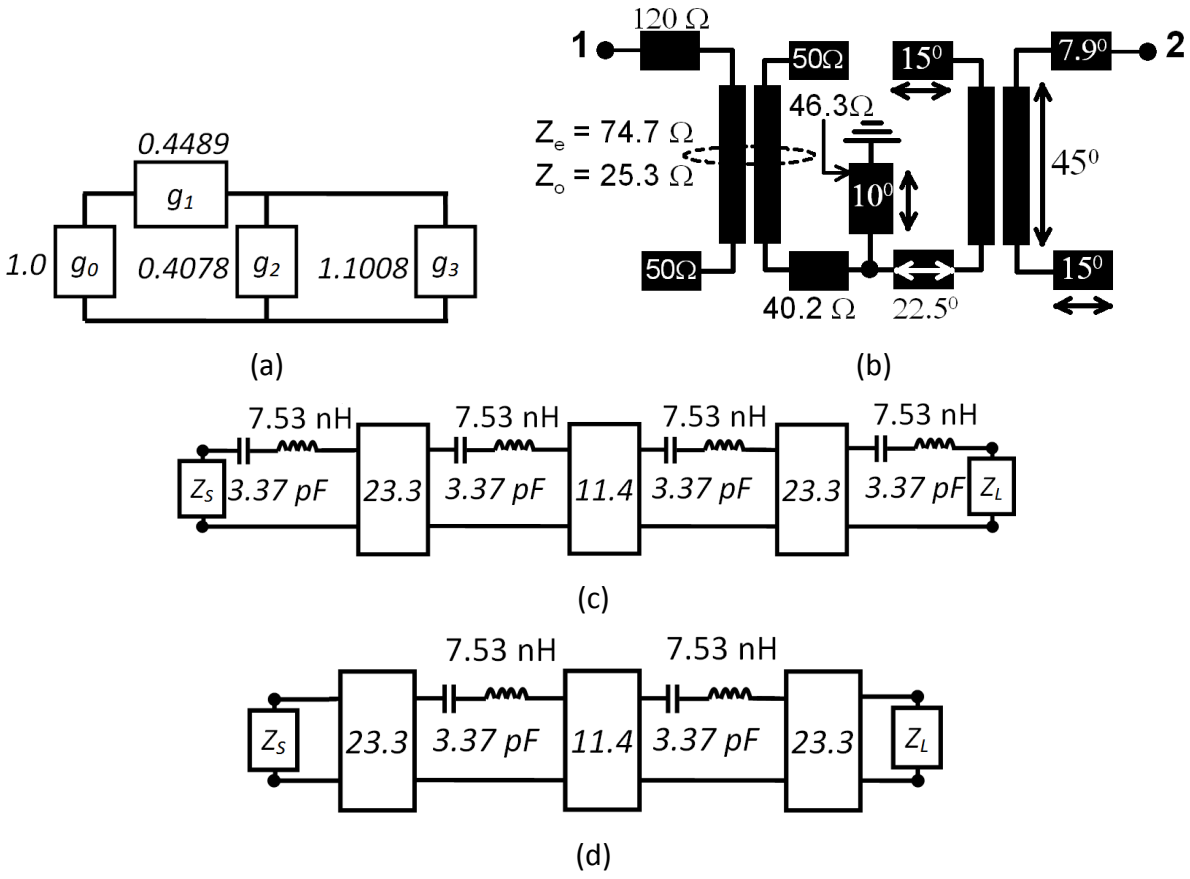

Fig. 4-3 Element values of (a) Lowpass prototype filter (b) dual-Mode transmission line filter (c) model of distributed filter (d) ideal inverter coupled bandpass prototype

Fig. 4-4 compares the transmission and the reflection coefficients of the ideal inverter coupled bandpass filter, the dual-mode filter and the filter model. All three circuits show a reasonably good agreement near the filter center frequency of 1.0 GHz, beyond which discrepancies become increasingly noticeable. In particular, although the ideal prototype response and the filter model do not produce a second harmonic passband, its presence, at around $3f_0$, in the actual filter response degrades the rejection of the filter considerably especially beyond 2 GHz. The reflection coefficients of the prototype and the actual filter appear to agree well at the center frequency while the model response is around 4 dB off.

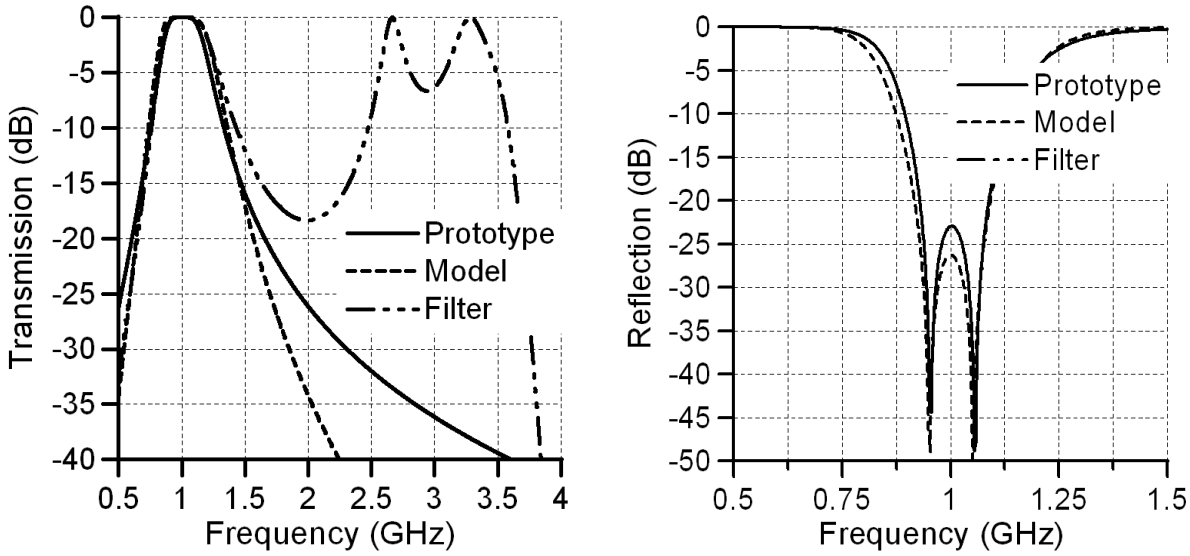

Fig. 4-4 Comparison of simulated (a) transmission (b) reflection of ideal lumped element bandpass filter prototype, distributed resonator filter and equivalent model

The overall dimensions of the second order filter stated in terms of electrical length are approximately 45^0 by 45^0. In comparison to compact filters such as open-loop single mode filters (electrical dimensions ~ 90^0 by 180^0) [4-12] – [4-14], the compact open-loop dual-mode filter (electrical dimensions ~ 80^0 by 80^0) [4-15] and patch based dual-mode filters (electrical dimensions ~ 180^0 by 180^0) [4-10], [4-16] and [4-17], filters based on the proposed dual-mode resonator achieve a considerable size reduction.

4.1.2 High Order All-Pole Filters

This section gives an overview of higher order filter development, from design to fabrication, with the proposed folded dual-mode resonator through a design example of a 4^{th} order Chebyshev bandpass filter. The filter specification is summarized in table 4-2. The element values obtained from filter tables are $g_0 = 1$, $g_1 = 0.7129$, $g_2 = 1.2004$, $g_3 = 1.3213$, $g_4 = 0.6476$ *and* $g_5 = 1.1008$.

Filter Specification	
Filter Order	4
Response Type	Chebyshev
Center Frequency	1.5 GHz
Fractional Bandwidth	25 %
Passband Ripple	0.01 dB
Source/Load Termination	50 Ω

Table 4-2: Filter specification of 4^{th} order Chebyshev filter

The selected value of M was 175 Ω for all coupled lines while $Z_A = 82$ Ω, $\theta_C = 45^0$ and $\theta_A = 15^0$ at 1.5 GHz. With these values, $L_A = 3.85$ nH, $C_A = 1.26$ pF and $L_T = 8.91$ nH. The impedance inverter parameters were then determined to be: $K_{01} = K_{45} = 31.4$, $K_{12} = K_{34} = 15.17$, $K_{23} = 11.14$.

L_2 was also calculated to be 5.06 nH. Setting $\theta_B = 20^0$ and $\theta_2 = 15^0$ at the centre frequency allows Z_B and Z_2 to be determined as 95 Ω and 56 Ω. The modal impedances of the input/output coupled-lines were determined from (3.38) to be $Z_e = 120$ Ω and $Z_o = 55$ Ω and those of the inter-resonator coupled lines were $Z_e = 100$ Ω and $Z_o = 75$ Ω.

Finally, the feed lines to the filter must have an inductance of 5.06 nH and this was realised by employing a 110 Ω line of electrical length 25^0. Fig. 4-5 (a) illustrates the initial and tuned response. Unlike the previous filter example, due to the relatively high filter FBW, the variation of impedance of the K_{12} and K_{34} inverters in the filter is responsible for the error in the initial response. Some tuning of the initial filter parameters was therefore required in order to compensate for these frequency effects. Tuning the design lead to following changes: $Z_B = 105$ Ω, $\theta_A = 11.9^0$ and the inductive feed line impedance was increased from 110 Ω to 125 Ω.

The filter was fabricated on 1.575 mm thick Rogers RT Duroid 5880 (ε_r = 2.2), with circuit board plotter LPKF C60E and measured with Agilent PNA (E8361A) network analyzer. A photograph of the fabricated filter, its layout and a comparison between the measured and full wave EM simulated results are illustrated in Fig. 4-5.

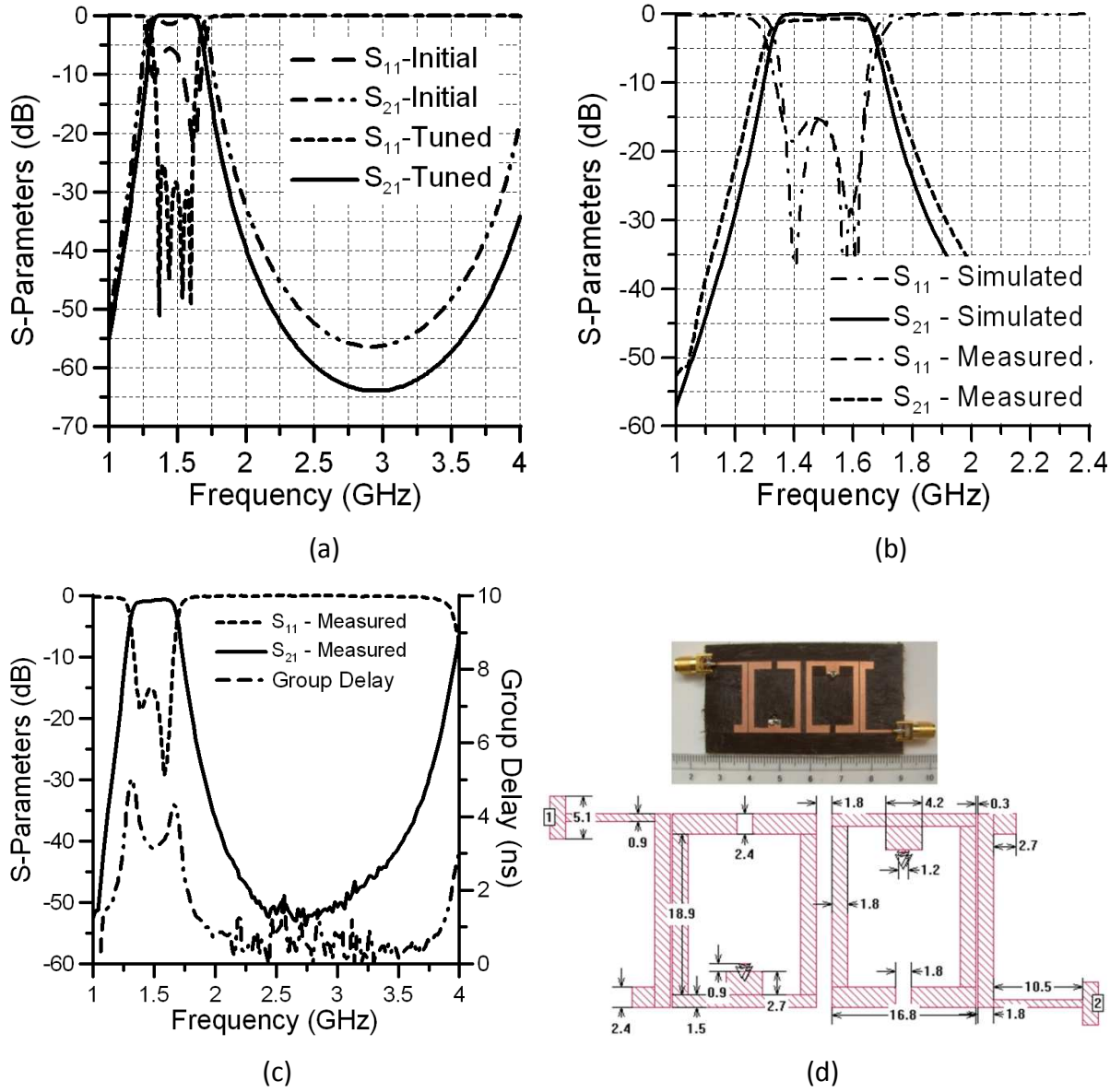

Fig. 4-5 (a) Circuit simulated S-parameters of 4th order filter before and after tuning (b) Comparison of EM simulated and measured filter S-parameters (c) Measured wideband S-parameters and group delay (d) Photograph of fabricated filter with layout, where dimensions are in millimetres.

The measured performance of the filter is in very good agreement with the simulated results. A pass-band insertion loss of around 0.66 dB was observed at the measured centre frequency of 1.50 GHz. This may be mainly attributed to conductor losses. The measured bandwidth was approximately 380 MHz (FBW = 25.33%) and this corresponds well with the specification of 25% FBW. The first harmonic response is roughly at 4.5 GHz ($3f_0$), which is another desirable characteristic of the filter. The measured return loss and group delay are approximately 15 dB and 3.2 ns at the filter center frequency.

This filter occupies an area of approximately 36 mm by 23 mm. In addition to having dual-mode behaviour, which effectively reduces filter area by half, each resonator corresponds to a $\lambda_g/8$ (electrical dimensions 45^0 by 45^0) type resonator, which makes this resonator a very favourable candidate for compact planar bandpass filter design.

4.1.3 Second Order Generalized Chebyshev Filters

This section describes a second order generalized Chebyshev bandpass filter based on the dual-mode resonator with capacitive cross-arm coupling. In Chapter 3, it was shown that this resonator is able to generate a number of finite frequency transmission zeros. These zeros may be used not only for enhancing skirt selectivity but also for suppressing spurious harmonics to some extent. The filter specification is outlined in Table 4-3 below.

Filter Specification	
Filter Order	2
Response Type	Gen. Chebyshev
Center Frequency	1.65 GHz
Fractional Bandwidth	6.5 %
Passband Ripple	0.1 dB
Source/Load Termination	50 Ω

Table 4-3: Filter specification of 2nd order generalized Chebyshev filter

For this design, simulation based parameter extraction was employed to obtain the dual-mode resonator parameters. The initial values for the electrical lengths of the resonator were chosen as $\theta_A = 35^0$, $\theta_B = 15^0$, $\theta_C = 40^0$ (90^0 in total at the center frequency). A uniform impedance of 120 Ω was assumed for the lines, except for Z_2 = 95 Ω. The final dimensions of the filter given in Fig. 4-7 (a) correspond to these values.

The lowpass prototype element values obtained from filter tables were g_0 = 1, g_1 = 0.8431, g_2 = 0.6220 and g_3 = 1.3554. The external quality factor and the inter resonator coupling coefficient, M_{12}, were calculated from (4.6) and (4.7) respectively as 13.0 and 0.89 [4-1].

$$Q_e = \frac{g_0 g_1}{FBW} \tag{4.6}$$

$$M_{i,i+1} = \frac{FBW}{\sqrt{g_i g_{i+1}}} \tag{4.7}$$

In order to physically realized M_{12}, simulations were used to iteratively extract the coupling coefficient from the structure of Fig. 4-7 (a) for various lengths L_1, using (3.52). The extracted coupling coefficient against L_1 is plotted in Fig. 4-6. From the plot, it can be seen that L_1 = 3 mm will produce the required coupling coefficient. A similar approach was used for realizing the external quality factor as outlined in [4-1], from which the required gap width of the input/output coupled lines were found to be 0.3 mm.

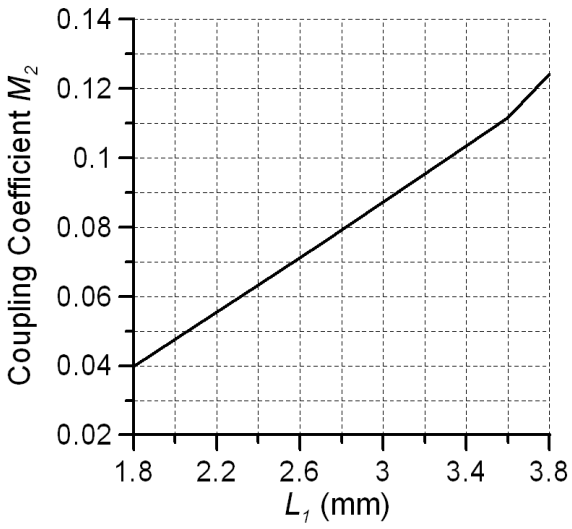

Fig. 4-6 Extracted coupling coefficient M_{12} plotted against length of short circuited stub

The dimensions together with a photograph of the fabricated filter are illustrated in Fig. 4-7, where L_1 = 3 mm. The filter was fabricated on 1.575 mm thick Rogers RT Duroid 5880 (ε_r = 2.2), with circuit board plotter LPKF C60E and measured with Agilent PNA (E8361A) network analyzer. The measured and full wave simulated results are illustrated in Fig. 4-8.

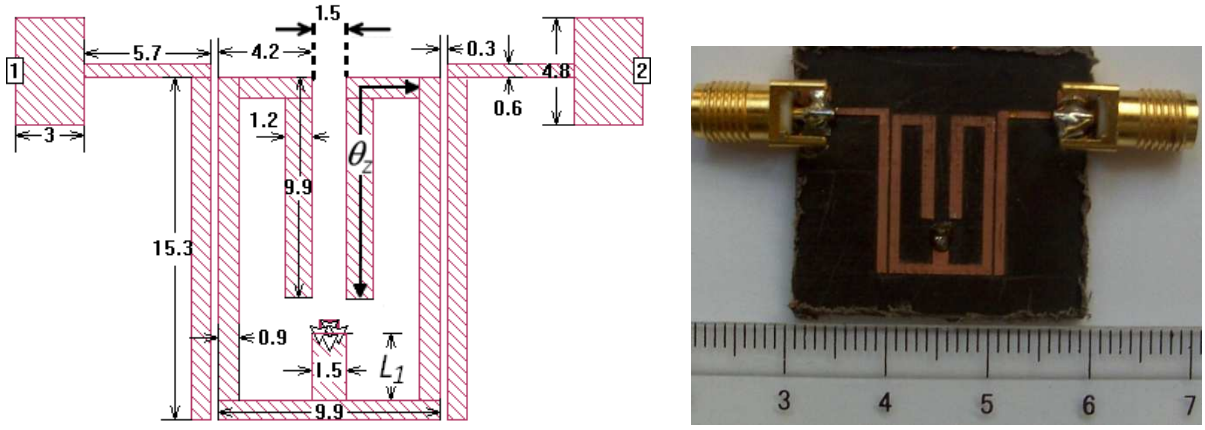

(a) (b)

Fig. 4-7 (a) Layout of 2nd order generalized Chebyshev filter with dimensions in millimetres. (b) Photograph of fabricated filter.

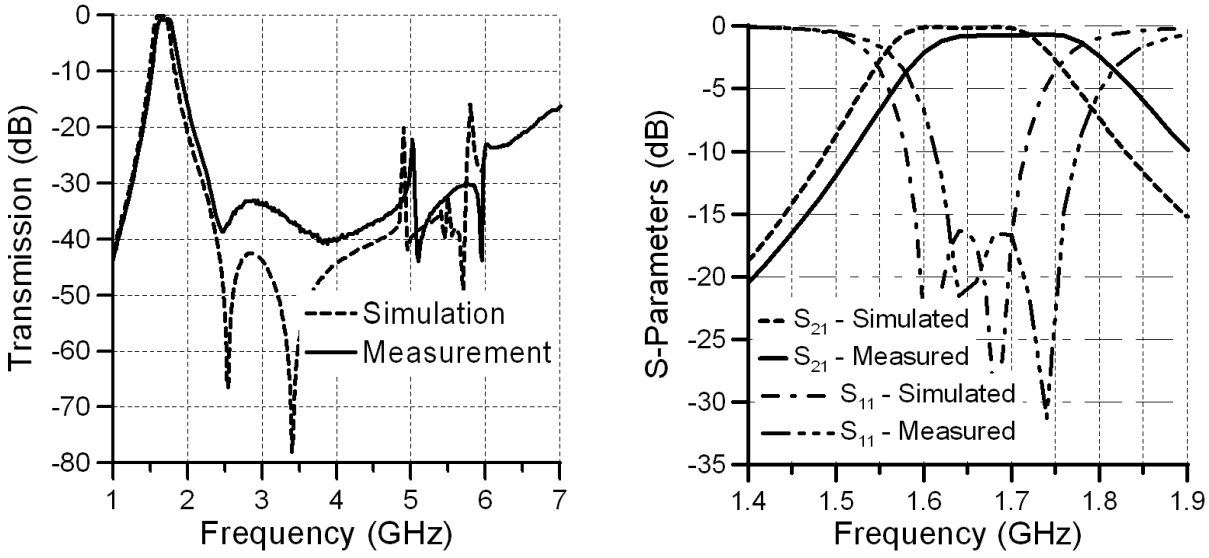

(a) (b)

Fig. 4-8 Comparison of simulated and measured (a) wide band transmission response and (b) narrow band S-parameter response.

The pass-band insertion loss of the fabricated filter was approximately 0.7 dB. The measured center frequency was found to be approximately 1.7 GHz, where a slight frequency shift of around 45 MHz was observed. This may have been due to the various tolerances involved. The two transmission zeros closest to the pass-band are produced as a result of coupling between the folded arms. The harmonics of these zeros that appear at around $3f_0$ can be seen to suppress the first spurious resonance of the filter. Consequently, the filter stopband is extended up to the second spurious response which occurs at around $5f_0$ ($\approx$ 8.25 GHz). The improvement to the filter stopband performance due to these transmission zeros is clear when comparing this response to that of Fig. 4-4. The dimensions of this filter are 15.3 mm by 9.9 mm. Equivalent to a $\lambda_g/10$ type filter, this achieves a significant size reduction over other dual-mode filters.

4.1.4 Dual-Mode Diplexers

A diplexer is a three port network which essentially consists of a pair of filters operating at two different center frequencies (usually at the transmission and reception frequencies of a transceiver) [4-19]. While diplexers are typically employed in connecting a single antenna with a transmitting and receiving end, the device must maintain high isolation between these ends. The design of a diplexer is generally a two step procedure. Firstly, it involves the separate design of the channel filters according to set specifications. Secondly, a suitable matching network at the source end must be designed such that the transmission characteristics of one filter are not affected by the other [4-20], [4-21].

The proposed dual-mode resonators may be readily employed in the development of diplexers. The filter design procedure outlined in the previous sections may be used to develop each channel filter accordingly. If the center frequencies of the two channel filters are relatively widely separated, then the requirements of the input matching network becomes less stringent and in some cases, the matching network may be avoided altogether. Since the design of matching networks is outside the scope of this work, this section presents a diplexer example where a matching network is not required.

This section presents a second-order diplexer based on the dual-mode resonator designed for WiMax frequency bands at 2.4 GHz and 3.4 GHz. Since the center frequencies are relatively distant, a matching network is not employed. In order to simultaneously excite both filters from a single source, a coupled line configuration consisting of three coupled lines may be employed as illustrated in Fig. 4-9 (c). The source is directly connected to the center line. The channel filters placed on either side are excited by this line. Although the center frequencies are approximately 1 GHz apart, this form of excitation will to some degree affect the performance of the individual filters but this may be rectified simply by optimization of the overall structure.

The filter was fabricated on 1.575 mm thick Rogers RT Duroid 5880 (ε_r = 2.2), with circuit board plotter LPKF C60E and measured with Agilent PNA (E8361A) network analyzer. The simulated and measured results are illustrated in Fig. 4-9 (a) and (b). The dimensions of the filter and its photograph are shown in Fig. 4-9 (c) and (d) respectively. There is very good agreement between the simulated and measured results. The measured passband insertion loss is better than 1 dB for both channels and the adjacent channel isolation is measured to be approximately 30 dB. The overall size of the diplexer is around 12 mm by 23 mm.

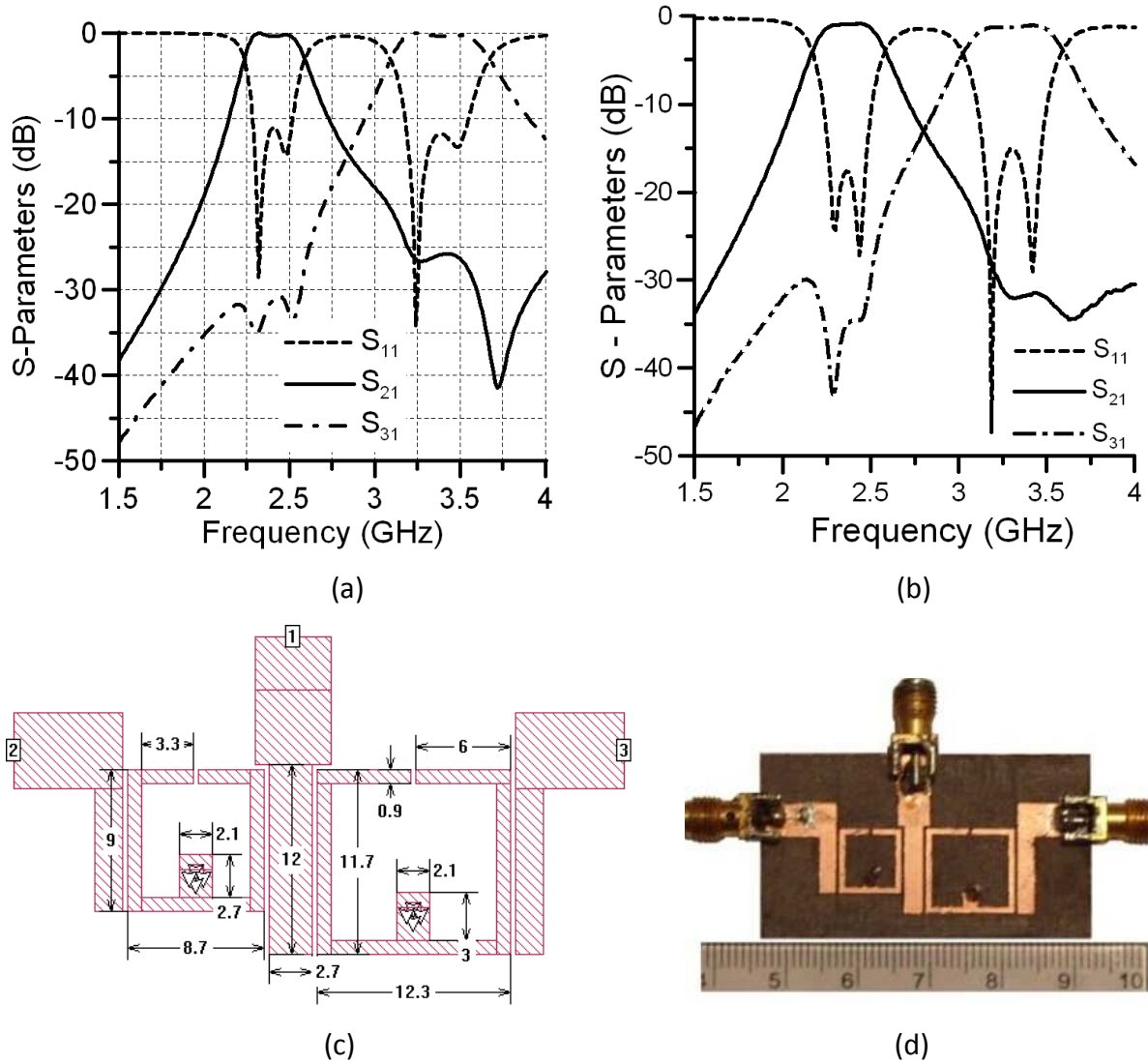

Fig. 4-9 (a) Simulated and (b) measured S-parameters. (c) Dimensions of the diplexer in millimetres and (d) photograph of fabricated filter.

4.1.5 Summary

This section has presented a filter design procedure for the development of all-pole bandpass filters from lowpass prototype networks. Given the lowpass prototype element values, the presented procedure allows the physical parameters of the resonators to be determined relatively quickly, with high accuracy especially for narrowband bandpass filter designs. It was shown that the equations still produce good approximations for the physical parameters for wideband filter designs, minimizing the required optimization/tuning effort.

In addition to greatly facilitating and expediting all-pole filter design, the proposed design procedure avoids the use of non-resonating nodes in coupling dual-mode resonators and enables considerable circuit space conservation especially for high order filters. Avoiding redundant elements such as non-resonating nodes also allows for filter loss minimization.

A simulation based design method for filters based on the dual-mode cross-arm coupled resonator was presented. This approach is adopted due to the difficulty in determining the cross-arm capacitance from the physical layout of the resonator. Simulation based extraction allows the required coupling coefficients and quality factors to be determined even for such a complicated structure relatively quickly and accurately thus greatly expediting the filter design process.

Several practical filter design examples were presented to supplement the discussions and also to verify the design procedures. The designed filters were fabricated and tested to evaluate and showcase their performance. All simulated results and filter measurements were in good agreement.

4.2 Cross-Coupled Filters

Although all-pole microwave filters may be conveniently realized in transmission line media, this type of filter generally does not offer the best skirt selectivity. In demanding applications where a sharp transition band is required, the only option available with all pole filters is to raise the filter order. Higher order filters occupy a larger circuit area. Moreover, the passband insertion loss of the microwave filter increases with filter order. These significant drawbacks associated with high order microwave filters have called for the development of alternative methods to achieve the required specifications with low order filters.

Despite the excellent skirt selectivity offered by Elliptic and inverse Chebyshev type filters, they are difficult to realize with distributed microwave elements. An alternative approach, although not as attractive performance wise as the latter filters, widely employed with distributed bandpass filters in achieving a sharp transition band is to use a cross-coupled resonator arrangement. The success of this method in microwave filter development arises from the ease of realization of this type of filter.

In addition to the direct coupling between adjacent resonators, cross-coupled filters employ non-zero couplings between non-adjacent resonators to produce a number of transmission zeros in the filter stopband. The non-zero coupling between non-adjacent resonators are able to produce multiple signal paths between the input and output ports. By assigning the coupling coefficients in an appropriate manner, it is possible to have the signals converging at the output port to interfere destructively resulting in complete signal cancellation at certain frequencies. While cross-coupled filters can generally be synthesised analytically based on low-pass prototype networks [4-1], a wider class of filtering functions may be realized through computer based optimization methods [4-18].

This section describes the use of the compact folded dual-mode resonator in the implementation of microwave cross-coupled filter networks. While coupling matrix optimization is used as the foundation for filter synthesis, the equivalent circuit of the dual-mode resonator and the related parameters facilitate the realization process.

4.2.1 Cross-Coupled Dual-Mode Resonator Configurations

This section describes several useful configurations for achieving cross-coupled filters with the proposed dual-mode resonator. Fig. 4-10 (a) and (b) illustrates two resonator configurations for achieving source-load coupled 4th order dual-mode filters, where the coupling scheme is summarized in Fig. 4-10 (c), and the resonators are numbered 1 to 4. Asymmetric resonators are employed to reduce the strength of the K_{14} coupling, in which case this coupling may be negligible. Symmetric resonators may be used but the K_{14} coupling must be considered when performing optimisation.

The sign of the cross-coupling is important in order to realise finite zeros. With reference to Fig. 4-10, it is important to note that coupling generated from the parallel coupled line sections of line, K_{S1} and K_{4L}, introduce a -90^0 phase shift while coupling generated from the short-circuited stub, K_{12} and K_{34} introduce a +90^0 phase shift. In both configurations K_{SL} generates a -90^0 phase shift. Since K_{23} and K_{14} have the same sign in each structure, the K_{14} cross coupling is not able to produce finite transmission zeros. In contrast, the K_{SL} and K_{23} coupling is oppositely signed in each case and produce finite zeros. Structure 4-9 (a) generates a single pair of zeros at finite frequencies while structure 4-9 (b) generates two pairs. Source-load coupled filters are explored in more detail in [4-5].

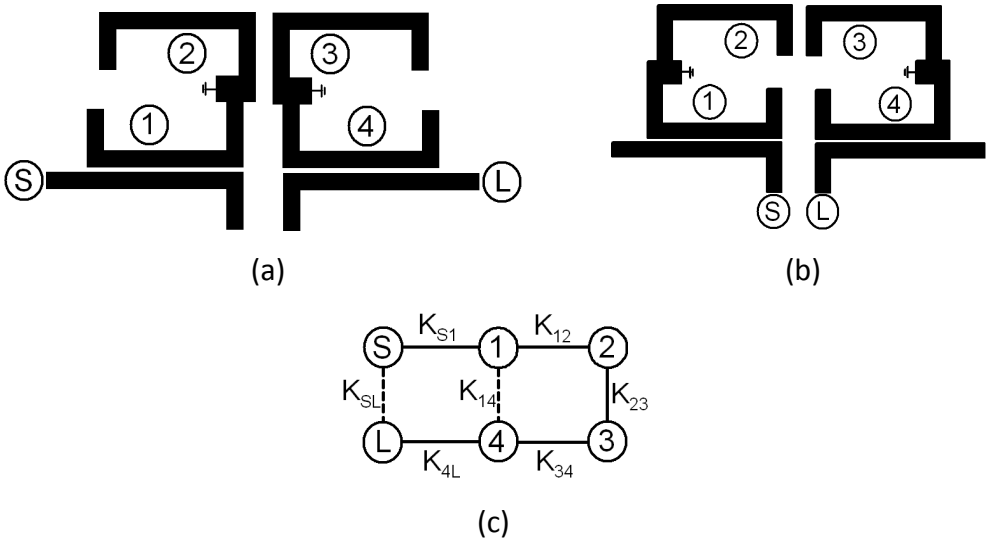

Fig. 4-10 (a) and (b) Fourth order cross coupled filter configurations (c) Coupling scheme.

Fig. 4-11 presents two highly compact filter configurations for developing microstrip trisection and quadruplet filters. These filter configurations can be readily employed in the modular design of high order, low loss and compact cross-coupled bandpass filters. While both structures are based on the dual-mode resonator, the proposed configurations allow the filter size to be further reduced as much as by 50%. Compactness is achieved by inserting a second resonator unit within the loop of the first, allowing a pair of units to occupy the area of just one.

The trisection filter of Fig. 4-11 (a) consists of three coupled resonators. Resonators 1 and 3 are a product of the dual-mode resonator, while the central resonator is of single-mode open loop type. The cross-coupling of the filter (M_{13}) occurs between the first and the third resonator and is the sum of M_{13P} and M_{13N}, with phases of $+90^0$ and -90^0 respectively. Therefore, both a positive or negative cross-coupling coefficient may be realized when $|M_{13P}| > |M_{13N}|$ and vice versa.

The generic fourth order quadruplet filter section illustrated in Fig. 4-11 (b) consists of a pair of coupled dual-mode resonators. In contrast to the configurations of Fig. 4-10, this configuration permits both positive and negative cross coupling to be established between resonators 1 and 4 relatively easily by appropriately setting the positive and negative type coupling M_{14P} and M_{14N} respectively.

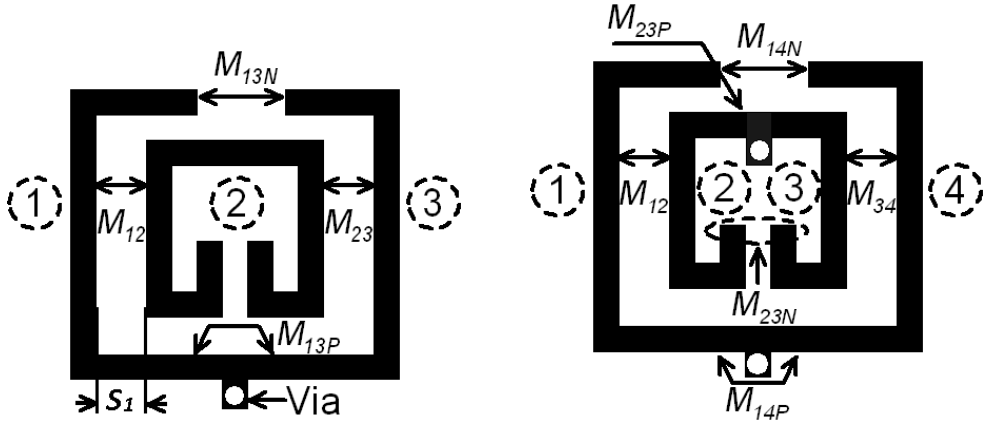

(a) (b)

Fig. 4-11 Cross-coupled (a) tri-section filter configuration and (b) quadruplet filter configuration

The design of such cross-coupled filters may be performed by adopting the approach described in [4-18]. Only a brief description of the method is described here. The coupling coefficients are first determined either through optimization or through an equivalent prototype circuit. Coupling coefficients are then extracted from full-wave EM simulations for various physical parameters of the resonators. Finally, the desired filter coupling coefficients are realised by setting appropriate values for the physical parameters of the resonators, such as gap widths or stub lengths. It is also possible to realize some coupling, such as those produced by the parallel coupled lines, with the aid of equations presented in Chapter 3.

4.2.2 Trisection Filters

This section presents a third order trisection bandpass filter example, employing the configuration of Fig. 4-11 (a), in order to produce a generalized Chebyshev type response with a single transmission zero. The filter specification is outlined in Table 4-4. The normalized coupling coefficients of the filter were optimized with the aid of a computer and were finalized as (4.8), where the diagonal entries denote the normalized resonator de-tuning parameters b_i for the i^{th} resonator, where the cross-coupling coefficient between resonator 1 and 3 was determined to be 0.3.

$$[m] = \begin{bmatrix} 0 & 1.23 & 0 & 0 & 0 \\ 1.23 & -0.15 & 1.21 & 0.3 & 0 \\ 0 & 1.21 & .2 & 1.21 & 0 \\ 0 & 0.3 & 1.21 & -0.15 & 1.23 \\ 0 & 0 & 0 & 1.23 & 0 \end{bmatrix} \tag{4.8}$$

Filter Specification	
Filter Order	3
Response Type	Gen. Chebyshev
Center Frequency	1.0 GHz
Fractional Bandwidth	10 %
Passband Ripple	0.01 dB
Source/Load Termination	50 Ω
Transmission Zero	0.8 GHz

Table 4-4: Third order trisection bandpass filter specification

Once the normalized coupling matrix is determined, the angular resonant frequencies, ω_i, of the resonators may be computed from (4.9), where ω_0 is the filter mid-band angular frequency and FBW is the filter fractional bandwidth, which may be used to independently set the natural frequencies of the three resonators [4-1].

$$\omega_i = \omega_0 \frac{-FBWb_i + \sqrt{(FBWb_i)^2 + 4}}{2} \tag{4.9}$$

From the given specifications and the optimized coupling coefficients, the resonant frequencies of the three resonators were determined to be 1.0075 GHz, 0.99 GHz and 1.0075 GHz respectively. After designing the individual resonators, full wave electromagnetic simulations may be performed on the entire structure in order to determine the filter pole and zero frequencies. These frequencies may be compared to that of the trisection lowpass prototype in order to extract the coupling coefficients M_{12} and M_{13}.

A trisection lowpass prototype filter is illustrated in Fig. 4-12. The input even and odd mode admittance, y_{ine} and y_{ino}, are given by (4.10) and (4.11) respectively.

$$y_{ine} = \frac{M_{01}^2}{j\left(\omega + b_1 - M_{13} - \frac{2M_{12}^2}{\omega + b_2}\right)} \tag{4.10}$$

$$y_{ino} = \frac{M_{01}^2}{j(\omega + b_1 + M_{13})} \tag{4.11}$$

Applying the transmission zero frequency condition ($y_{ine} = y_{ino}$) leads to the lowpass transmission zero angular frequency, ω_{LPz} , as given by (4.12).

$$\omega_{LPz} = -\left(b_2 + \frac{M_{12}^2}{M_{13}}\right) \tag{4.12}$$

The transmission pole condition of the filter is $y_{ine}\, y_{ino} = 1$. Solving for this condition under the assumption that M_{01} is negligible (weak coupling at the input and output ports) allows the coupling coefficient M_{12} to be extracted from (4.13), where ω_{LPp} is the lowpass left most frequency pole.

$$M_{12} = \sqrt{\frac{\omega_{LPp}^2 + (b_1 + b_2)\omega_{LPp} + b_1 b_2}{2 - \frac{\omega_{LPp} + b_2}{\omega_{LPz} + b_2}}} \tag{4.13}$$

Substitution of M_{12} in (4.12) enables M_{13} to be extracted. When using these formulae in extracting the coupling coefficients, the simulated pole and zero frequencies must be first converted into the corresponding lowpass frequencies by using the bandpass transformation given by (4.14).

$$\omega_{LP} = \frac{1}{FBW}\left[\frac{\omega_{BP}}{\omega_0} - \frac{\omega_0}{\omega_{BP}}\right] \tag{4.14}$$

The formulae can be employed to extract the coupling coefficients M_{12} and M_{13} against the various physical parameters of the structure affecting these couplings (such as gap width or stub length) with the aid of an electromagnetic simulation package. For example, the M_{12} coupling is inversely proportional to the spacing between the parallel coupled lines, S_1, of resonator 1 and 2 of Fig. 4-11 (a).

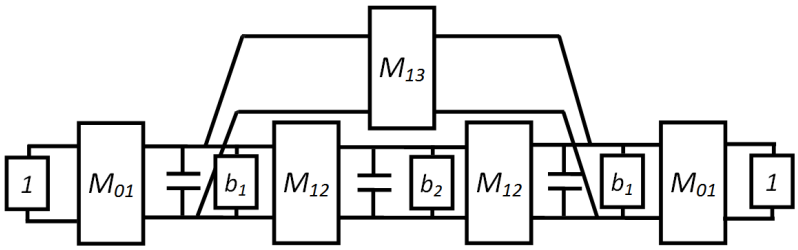

Fig. 4-12 Trisection lowpass prototype filter where all capacitances = 1 F.

The transmission response for a parallel coupled line spacing of 1.1 mm is illustrated in Fig. 4-13 (a), as an example for extraction of the corresponding coupling coefficient. The measured pole and zero frequencies of 0.92 GHz and 0.77 GHz respectively are firstly converted to the lowpass frequencies via (4.14). M_{12} may then be determined by employing (4.13), and in this example was found to be 1.25. Similarly the coupling coefficient M_{12} may be found for other values of S_1 as plotted in Fig. 4-13 (b), from which a coupling coefficient of M_{12} = 1.21 is realized with a line spacing of S_1 = 1.1 mm for this particular design.

The sign of M_{13} determines the position of the transmission zero. This sign may be selected by opting for the dominant cross coupling to be either capacitive via M_{13N} or inductive coupling via M_{13P}. The length of the short circuited stub or the gap width between the open circuited arms of resonators 1 and 3 may be used to tune M_{13}. Therefore, the value of coupling coefficient extracted can be plotted against one of these two physical parameters in order to determine an appropriate value.

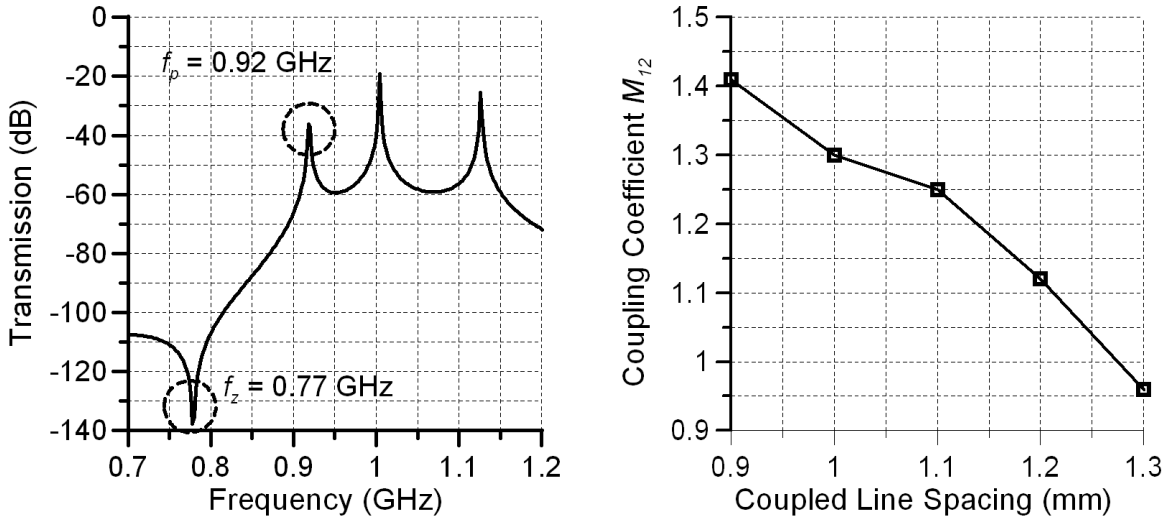

Fig. 4-13 (a) Transmission response of weakly coupled trisection filter whose dimensions are given in Fig. 4-14 (c). (b) Extracted coupling coefficient M_{12} against spacing between parallel coupled lines, S_1, of resonators 1 and 2 of Fig. 4-11 (a).

The designed filter was fabricated on 1.27 mm thick Rogers RT Duroid 6010LM (ε_r = 10.2), with circuit board plotter LPKF C60E and measured with Agilent PNA (E8361A) network analyzer. A photograph of the fabricated filter, its layout and a comparison of the measured and full wave EM simulated results are illustrated in Fig. 4-14.

There is good overall agreement between simulation and measurement. The measured mid-band insertion loss of the filter, mainly due to conductor loss, was only 0.83 dB. The low insertion loss is attributed to the compactness of the filter configuration, which minimizes the impact of the transmission line losses. The measured filter bandwidth is approximately equal to the specification. The fabricated compact third order trisection bandpass filter occupies an area of around 18 mm by 18 mm, which is almost the same as the compact second order filter reported in [4-15].

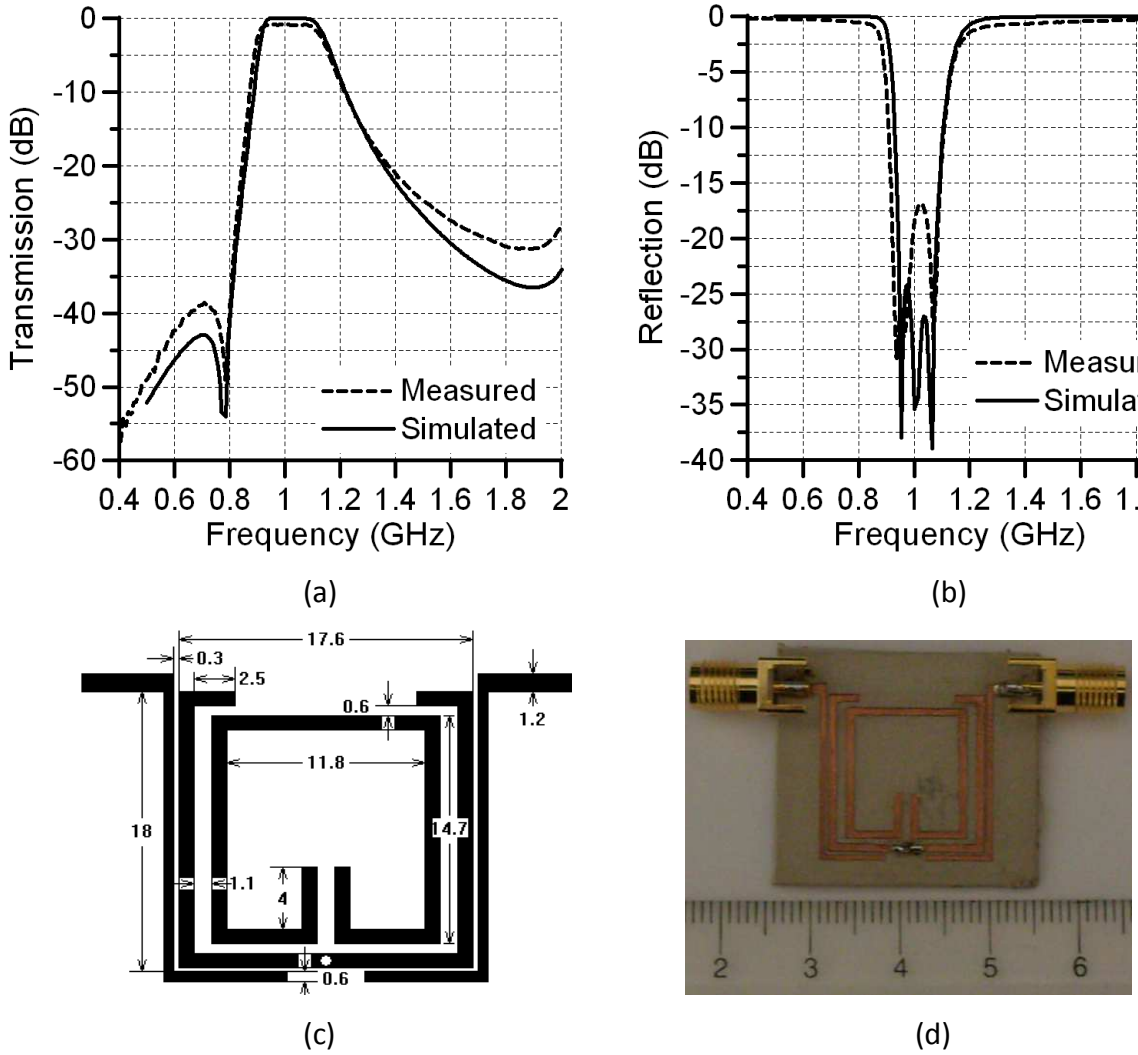

Fig. 4-14 Measured and simulated (a) transmission and (b) reflection of third order trisection filter. (c) Layout with dimensions in millimetres and (d) photograph of fabricated filter

4.2.3 Quadruplet Filters

This section presents a fourth order source-load coupled quadruplet bandpass filter example, employing the configuration of Fig. 4-11 (b), in order to produce a generalized Chebyshev type response with a pair of transmission zeros. The filter specification is outlined in Table 4-5. The normalized coupling coefficients of the filter were optimized with the aid of a computer and were finalized as (4.15).

$$[m] = \begin{bmatrix} 0 & 1.1844 & 0 & 0 & 0 & -0.00015 \\ 1.1844 & 0 & 1.081 & 0 & 0 & 0 \\ 0 & 1.081 & 0 & 0.794 & 0 & 0 \\ 0 & 0 & 0.794 & 0 & 1.081 & 0 \\ 0 & 0 & 0 & 1.081 & 0 & 1.184 \\ -0.00015 & 0 & 0 & 0 & 1.184 & 0 \end{bmatrix} \tag{4.15}$$

Filter Specification	
Filter Order	4
Response Type	Gen. Chebyshev
Center Frequency	1.0 GHz
Fractional Bandwidth	10 %
Passband Ripple	0.01 dB
Source/Load Termination	50 Ω
Upper Transmission Zero	1.60 GHz

Table 4-5: Fourth order quadruplet section bandpass filter specification

All resonators in the quadruplet configuration are synchronous and have a center frequency of 1.0 GHz. The coupling coefficients above were realised in a similar fashion to the previous examples using simulation based extraction. The filter was fabricated on 1.27 mm thick Rogers RT Duroid 6010LM (ε_r = 10.2), with circuit board plotter LPKF C60E and measured with Agilent PNA (E8361A) network analyzer. A photograph of the fabricated filter, its layout and a comparison of the measured and full wave EM simulated results are illustrated in Fig. 4-15. There is good overall agreement between simulation and measurement. The measured mid-band insertion loss of the filter, mainly due to conductor loss, was around 1.2 dB. The fabricated compact quadruplet bandpass filter occupies an area of around 18 mm by 18 mm, which is highly compact since this is almost the same as the compact second order filter reported in [4-15].

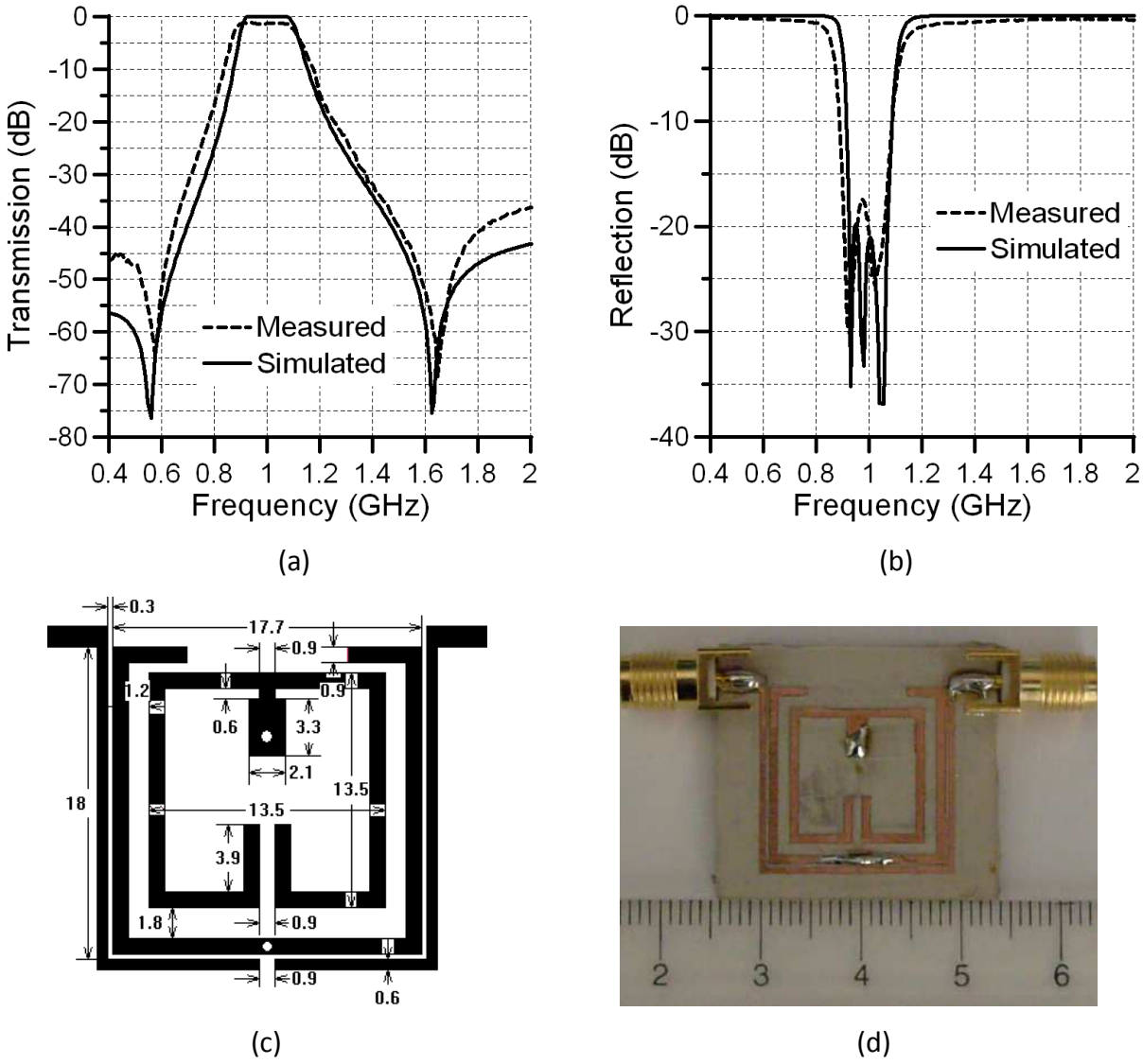

Fig. 4-15 Measured and simulated (a) transmission and (b) reflection of quadruplet filter. (c) Layout with dimensions in millimetres and (d) photograph of fabricated filter

4.2.4 Fourth Order Cross-Coupled Filters with Asymmetric Structure

A fourth order filter example, whose specifications are outlined in Table 4-6, based on the source-load coupled filter of Fig. 4-9 (a) is presented to demonstrate yet another compact cross-coupled filter configuration with the dual-mode resonator. The optimized coupling coefficient matrix for the design is given by (4.16).

$$[m] = \begin{bmatrix} 0 & 1.184 & 0 & 0 & 0 & -0.01 \\ 1.184 & 0 & 1.076 & 0 & 0 & 0 \\ 0 & 1.076 & 0 & 0.794 & 0 & 0 \\ 0 & 0 & 0.794 & 0 & 1.076 & 0 \\ 0 & 0 & 0 & 1.076 & 0 & 1.184 \\ -0.01 & 0 & 0 & 0 & 1.184 & 0 \end{bmatrix} \tag{4.16}$$

Filter Specification	
Filter Order	4
Response Type	Gen. Chebyshev
Center Frequency	2.5 GHz
Fractional Bandwidth	10 %
Passband Ripple	0.01 dB
Source/Load Termination	50 Ω
Upper Transmission Zero	3.0 GHz

Table 4-6: Fourth order asymmetric cross-coupled bandpass filter specification

Similar to the previous designs, simulation based coupling coefficient extraction was employed in realizing the calculated coupling coefficients. The filter was fabricated on Rogers RT Duroid 5880 substrate with a relative dielectric constant of 2.2 and substrate thickness of 1.575 mm.

The transmission and reflection parameters of the simulated and measured filter are compared in Fig. 4-16 (a) and (b). The mid-band insertion loss of the filter, mainly due to conductor loss, was around 1.0 dB. A shift of around 50 MHz is observed in the measured passband center frequency and this may be attributed to fabrication tolerances. This filter occupied an area of approximately 27 mm by 17 mm.

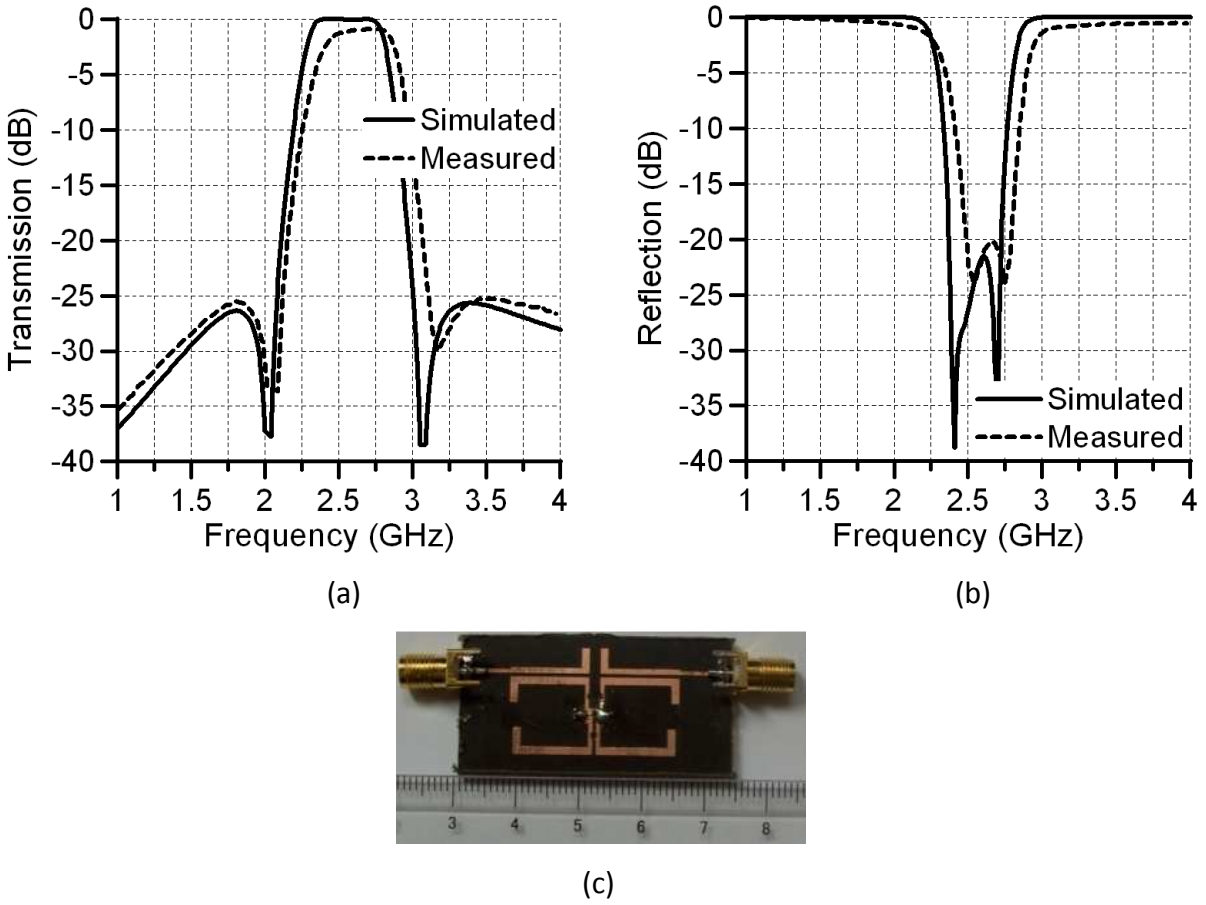

Fig. 4-16 Measured and simulated (a) transmission and (b) reflection of quadruplet filter. (c) photograph of fabricated filter

4.2.5 Dual-Band Filter Example

The most widely recognized approach to dual-band filter synthesis is to employ dual-band resonators. However, distributed dual-band resonators are difficult to tune and filter optimization is usually very time consuming. Consequently, as detailed in Chapter one, various other innovative methods have been developed.

Theoretically, the design of such filters may be greatly simplified if single-band resonators may somehow be employed instead. Adopting this perspective, this section presents the design of dual-passband filters utilizing only single-band resonators. Dual-band performance is obtained by simultaneously employing cross-coupled resonator configurations together with asynchronous resonators.

Given a specification, the prototype parameters such as the coupling coefficients as well as the frequency detuning parameters may be found through computer based optimization. Generally, direct optimization could possibly lead to a large number of non-zero cross-coupling within a filter some of which may be non-realizable. Therefore, physically simpler cross-coupled structures such as the quadruplet filter section of Fig. 4-10 (b) may be employed. In contrast to single-passband quadruplet filters presented earlier, dual-passband filters rely on relatively strong cross-coupling as wells as the use of detuned resonators.

In order to illustrate a typical dual-passband filter realization, a second-order dual-band filter, whose specifications are outlined in Table 4-7 is designed. The filter is realized with the dual-mode quadruplet resonator configuration of Fig. 4-10 (b). The optimized coupling coefficient matrix for the design is given by (4.17).

$$[m] = \begin{bmatrix} 0 & 0.7344 & 0 & 0 & 0 & 0 \\ 0.7344 & 0 & 2.081 & 0 & 0.78 & 0 \\ 0 & 2.081 & 0 & -0.180 & 0 & 0 \\ 0 & 0 & -0.180 & 0 & 2.081 & 0 \\ 0 & 0.78 & 0 & 2.081 & 0 & 0.7344 \\ 0 & 0 & 0 & 0 & 0.7344 & 0 \end{bmatrix} \tag{4.17}$$

Dual-passband Filter Specification	
Filter Order	2
Center Frequency and FBW	1.19 GHz at 2% FBW
Center Frequency and FBW	1.47 GHz at 2% FBW
Passband Ripple	0.05 dB
Source/Load Termination	50 Ω

Table 4-7: Dual-passband filter specification

The coupling matrix is physically realized through optimization of the quadruplet configuration with the aid of an electromagnetic simulator. In this particular example, it was possible to achieve the desired response exclusively with fully synchronous resonators. Therefore the resonator detuning parameters corresponding to the diagonal entries of the matrix are all zero. A negative coupling coefficient of -0.180 between the second and third resonator was realized by the capacitive cross-arm coupling between these resonators as illustrated in Fig. 4-10 (b). In addition, the positive cross-coupling between resonators 1 and 4 was realized by employing an appropriate length of short circuited stub.

After optimization, the designed filter was fabricated on Rogers RT Duroid 6010 substrate with a relative dielectric constant of 10.2 and substrate thickness of 1.27 mm. Fig. 4-17 (a) and (b) shows a comparison between the theoretical, simulated and measured filter s-parameters. The layout and a photograph of the fabricated filter are illustrated in Fig. 4-16 (c) and (d) respectively. There is excellent agreement between the theoretical and simulations responses. Despite the losses of around 1.8 dB in both passbands, the measured filter response is also seen to correspond very well, especially with regard to center frequencies and the locations of the transmission zeros. The measured loss is mainly attributed to conductor and dielectric losses and is seen to adversely affect the mid-band insertion loss and passband edge selectivity.

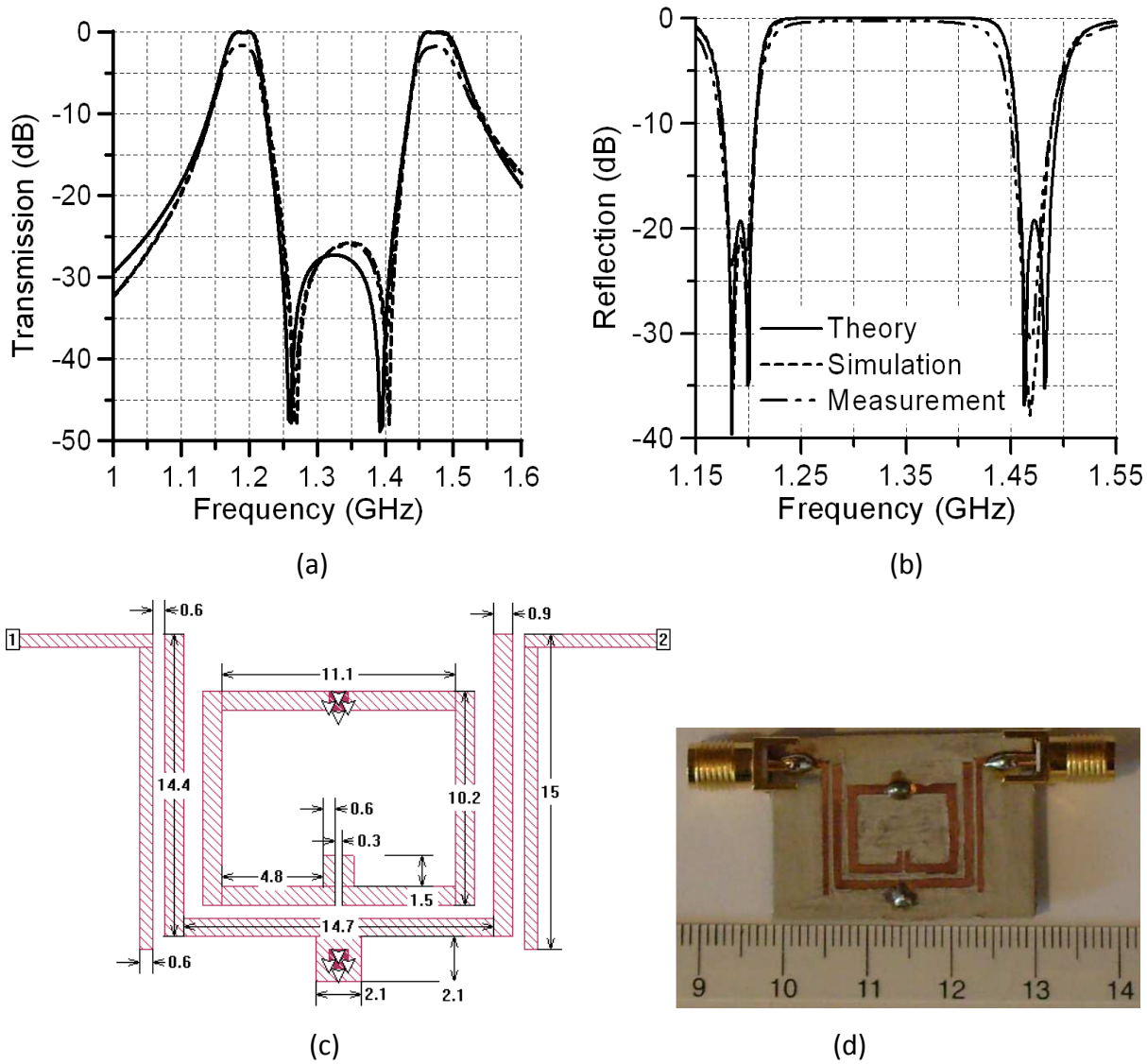

Fig. 4-17 Measured and simulated (a) transmission and (b) reflection of dual-passband filter. (c) Dimensions of filter in millimetres (d) photograph of fabricated filter.

Despite the simplicity, there are limitations of this approach in designing dual-band filters. Firstly, the coupling coefficients increase for wider passband separations. Narrower gap widths are required to realize larger coupling coefficients which may not always be possible due to fabrication limitations. Secondly, this approach is only suitable for designing dual-band filters with the same fractional bandwidth for the upper and lower passbands.

4.2.6 Summary

This section presented several highly compact cross-coupled filter configurations comprising the dual-mode resonator for the development of advanced single and dual-band bandpass filters. While the trisection configuration comprises of a single-mode resonator embedded within the dual-mode resonator, the quadruplet filter configuration consists of two concentrically placed dual-mode resonators. These configurations are not only useful in the development of highly compact third and fourth order filters but are also solutions for the modular design of higher order cross-coupled filters [4-1]. Furthermore, the quadruplet configuration may also be employed in the design of dual-passband filters.

The design of single and dual passband cross-coupled filters in this section was performed through computer based coupling matrix optimization. The design examples were supplemented with simulated and experimental measurements to demonstrate not only the theoretical but also the practical performance of such filters and also to highlight the compactness achieved with these configurations especially in comparison to other research work. The key aspects of the design process were also highlighted in the examples. Experimental results were in very good agreement to both design specification and simulated results. Furthermore, owing to the nature of the dual-mode resonator, the first spurious response of these filters occurs at $3f_0$ rather than $2f_0$. They are also relatively simple and inexpensive to fabricate compared to other popular approaches such as multilayer filters.

4.3 References

[4-1] J.-S Hong and M. J. Lancaster, *Microstrip filters for RF/microwave applications*, New York: John Wiley & Sons, 2001.

[4-2] I. C. Hunter, *Theory and design of microwave filters*, London: Institution of Electrical Engineers, 2001.

[4-3] R.J. Cameron and J.D Rhodes, "Asymmetric realizations for dual-mode bandpass filters", *IEEE Transactions on Microwave Theory and Techniques*, Vol. 29, No. 1, pp. 51 – 58, Jan. 1981.

[4-4] R.J. Cameron, "General coupling matrix synthesis methods for Chebyshev filtering functions", *IEEE Transactions on Microwave Theory and Techniques*, Vol. 51, No. 1, pp. 1 – 10, Jan. 2003.

[4-5] R.J. Cameron, "Advanced coupling matrix synthesis techniques for microwave filters", *IEEE Transactions on Microwave Theory and Techniques*, Vol. 51, No. 1, pp. 1 – 10, Jan. 2003.

[4-6] G.L. Matthaei, L. Young and E.M.T. Jones, *Microwave filters, impedance matching networks, and coupling structures*, Dedham, MA: Arthec House 1964.

[4-7] J.S. Hong, H. Shaman and Y.H. Chun, "Dual-mode microstrip open-loop resonators and filters", *IEEE Transactions on Microwave Theory and Techniques*, Vol. 55, No. 8, pp. 1764 – 1770, Aug. 2007.

[4-8] U. Karacaoglu, I.D. Robertson and M. Guglielmi, "An improved dual-mode microstrip ring resonator filter with simple geometry", Proc. European Microwave Conference, pp 472-477, 1994.

[4-9] L.-H. Hsieh and K. Chang, "Compact, Low Insertion-Loss, Sharp-Rejection, and Wide-Band Microstrip Bandpass Filters", *IEEE Transactions on Microwave Theory and Techniques*, Vol. 51, No. 4, pp. 1241 – 1246, Apr. 2003.

[4-10] J.S. Hong and S. Li, "Theory and experiment of dual-mode microstrip triangular patch resonators and filters", *IEEE Transactions on Microwave Theory and Techniques*, Vol. 45, No. 12, pp. 1237 – 1243, Apr. 2004.

[4-11] L. Athukorala and D. Budimir, "Design of compact dual-mode microstrip filters", *IEEE Transactions on Microwave Theory and Techniques*, vol. 58, no. 11, pp. 2888-2895, Nov. 2010.

[4-12] J.S. Hong and M.J Lancaster, "Theory and experiment of novel microstrip slow-wave open-loop resonator filters", *IEEE Transactions on Microwave Theory and Techniques*, Vol. 45, No. 12, pp. 2358 – 2365, Dec. 1997.

[4-13] J.S. Hong and M.J Lancaster, "Aperture-Coupled Microstrip Open-Loop Resonators and Their Applications to the Design of Novel Microstrip Bandpass Filters", *IEEE Transactions on Microwave Theory and Techniques*, Vol. 47, No. 9, pp. 1848 – 1855, Sep. 1999.

[4-14] S.-M. Wang, C.-H. Chi, M.-Y. Hsieh, and C.-Y. Chang, "Miniaturized Spurious Passband Suppression Microstrip Filter Using Meandered Parallel Coupled Lines", *IEEE Transactions on Microwave Theory and Techniques*, Vol. 53, No. 2, pp. 747 – 753, Feb. 2005

[4-15] J.S. Hong, H. Shaman and Y.H. Chun, "Dual-mode microstrip open-loop resonators and filters", ", *IEEE Transactions on Microwave Theory and Techniques*, Vol. 55, No. 8, pp. 1764 – 1770, Aug. 2007.

[4-16] U. Karacaoglu, I.D. Robertson and M. Guglielmi, " An improved dual-mode microstrip ring resonator filter with simple geometry", Proc. European Microwave Conference, pp 472-477, 1994.

[4-17] B. T. Tan, S. T. Chew, M. S. Leong and B. L. Ooi, “A modified microstrip circular patch resonator filter”, *IEEE Microwave and Wireless Component Letters*, vol. 12, no. 7, pp. 252-254, Jul. 2002.

[4-18] J.S. Hong and M.J Lancaster, “Design of highly selective microstrip bandpass filters with a single pair of attenuation poles at finite frequencies”, *IEEE Transactions on Microwave Theory and Techniques*, Vol. 48, pp. 1098 – 1107, Jul. 2000.

5.0 CONSTANT BANDWIDTH CENTER FREQUENCY TUNABLE BANDPASS FILTERS

Exponential growth in the applications for tunable bandpass filters over the past few years has been fuelled not only by the increasing number of wireless services but also as a result of the desire to access multiple services through a single technology. Typical applications of such filters are in multi-band communication systems, where a single transceiver may operate on multiple frequency bands. The channel bandwidth may generally differ for each channel, but may be identical in some applications.

Compactness, tuning range and linearity are key performance measures of tunable filters. Miniaturised filters are always more practical in modern communication systems where circuit space is costly [5-1]. Filter tuning range directly impacts on the range of services the system is able to offer [5-2]. Low distortion is a feature that is vital in filters with high input powers [5-3].

The most prevalent commercial filter tuning element is the varactor diode. Commercial viability of this device stems from the well established, highly precise manufacturing process yielding extremely low cost high quality units. Moreover, its performance attributes such as high reliability, extremely fast switching speeds, high power efficiency and great versatility in circuit implementations make the varactor diode the device of choice in most planar tunable filter applications [5-4].

However, one of the most significant drawbacks of varactor diodes is signal distortion. Since the capacitance of a varactor diode is voltage controlled, the state of the diode is always vulnerable to any RF signal superimposed on the D.C biasing. Consequently, all tunable filters employing such a device will inherently possess low linearity. This is exacerbated further at lower bias voltages where the R.F signal is comparable to the D.C biasing resulting in very severe signal distortion.

Academic research on the subject of tunable planar microwave filters has seen a sharp rise especially over the past decade and includes [5-5]-[5-24], where various degrees of tunability have been quoted for various structures. A tunable filter with 45% tuning range is presented in [5-6] but it occupies a relatively large circuit area. A tunable open-loop filter with constant bandwidth is presented in [5-9] where a piezoelectric transducer (PET) was used for tuning. The PET had little effect on filter bandwidth and facilitated the design of the fixed-bandwidth tunable filter. However, only 10% tunability was achieved due to limitations of the PET. Tunable comb-line filters were first presented in [5-11], where 53% tunability had been achieved but with wide variation (12%) in absolute bandwidth and high loss (6 dB).

In [5-17], a tunable filter is presented where an optimization method was used to design coupling structures. However, this approach cannot be adopted to design filters with prescribed filtering functions. Tang *et al*. [5-19] have recently developed a new constant bandwidth tunable dual-mode bandpass filter with an excellent tuning range. The proposed filter also produces a single transmission zero enhancing the skirt selectivity of the filter, but it requires three identical varactors.

More recently, tunable filter linearity has also become a growing concern. Peng *et al.* [5-7] have proposed a novel constant bandwidth pin diode based reconfigurable filter with improved linearity, where the filter tuning range was quoted to be 35 % and a measured IIP3 > 32 dBm. Although the losses are low (1.7 dB), the filter consumes a relatively large circuit area (150 mm by 150 mm) and does not allow continuous center frequency tuning.

A varactor diode based tunable second-order filter has been presented in [5-20] with a tuning range of 35%, but with a bandwidth variation of around 15 % and measured IIP3 between 22 - 42 dBm. This kind of IIP3 variation is very typical of varactor tuned circuits where the varactor linearity deteriorates heavily at low reverse voltages.

This chapter presents a novel highly linear second-order varactor-tuned filter, based on the dual-mode resonator, with constant 3 dB bandwidth. Filter equivalent circuits are re-evaluated to describe the variation and control of coupling coefficients and quality factor. A resonator configuration that provides an improvement in linearity is described clearly. It is shown that varactor based tunable filters employing such resonators do not suffer from high distortion typically experienced at low bias voltages. Furthermore, it is shown that there is considerable linearity improvement even for higher bias voltages. These filters have the advantage of simultaneously achieving a high tuning range (30%), very low bandwidth variation (less than 4.6%) , excellent skirt selectivity, high linearity (IIP3 > 43 dBm) in addition to a highly compact design (30 mm by 10 mm). The proposed filters only require two varactor diodes with common bias voltage and do not require additional tuning elements for control of coupling coefficients or the input/output quality factor. As a result, these filters are simple to design and exhibit relatively low-loss.

5.1 Varactor Tuned Dual-Mode Filters

Illustrated in Fig. 5-1 is the layout of the proposed second order dual-mode tunable filter excited through 50 Ω ports labelled 1 and 2. The filter is composed of a pair of coupled lines with even and odd mode impedances Z_e and Z_o respectively and electrical length θ_C. These are connected to the ports via inductive lines with impedance Z_{IND}. The end of each coupled line is extended to produce capacitive coupling between the source and load, where C_{SL} is the corresponding capacitance. A second resonance arises due to the short circuited stub with characteristic impedance Z_D [5-26]. Two identical varactor diodes, supplied with a common reverse voltage, are required for tuning and the simple biasing circuit shown is adequate for achieving sufficient isolation.

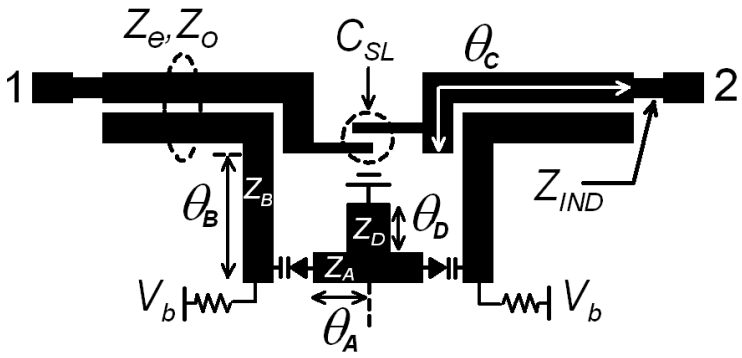

Fig. 5-1 Layout of dual-more varactor tuned filter

When designing the filter, the varactor capacitance is assumed to be at maximum. In this state, the filter will operate at the lowest frequency band. Reducing the varactor capacitance causes the center frequency of the filter to increase. However, all electrical lengths in the following analysis would be referenced to the lowest operational center frequency f_L for consistency. At f_L, the electrical lengths of the lines are approximately: $\theta_C \approx 60^0$ and $\theta_A + \theta_B \approx 30^0$. The tuning range of the filter is such that the highest passband center frequency is around 1.5 f_L.

For relatively weak source-load coupling, C_{SL} has a negligible impact on the filter pass-band performance, and therefore, the analysis of transmission zeros will be deferred to a later section.

Firstly, the coupled lines may be treated as an impedance inverter with series reactance functions as in Fig. 2, where Z_{11} is the driving point impedance of the coupled lines [5-26]. For a fixed narrow-band filter, the inverter may be regarded as a frequency independent element, as was assumed in the previous chapters. In contrast, although a tunable filter may have a narrow pass-band, it shifts across a relatively wide frequency range and it is therefore necessary to consider the frequency dependence of the inverter. The frequency dependence of the coupled line can be incorporated into the model by employing (5.1) and (5.2).

$$Z_{11} = \frac{Z_e + Z_o}{j2\tan(\theta_C)} \tag{5.1}$$

$$K_C = \frac{Z_e - Z_o}{2\sin(\theta_C)} \tag{5.2}$$

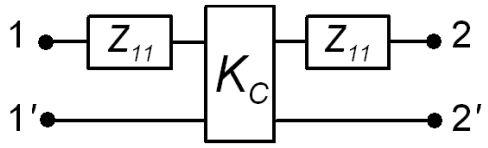

Fig. 5-2 Frequency dependent coupled line model.

The remaining elements of the filter consisting of transmission lines with characteristic impedance Z_A, Z_B and Z_D and varactor capacitance C_0 can be redrawn as Fig. 5-3 (a). If short circuited stub Z_D is now used to realise an impedance inverter, the equivalent circuit may be drawn as Fig. 5-3(b), where the inverter impedance K_L is given by (5.3).

$$K_L = Z_D \tan(\theta_D) \tag{5.3}$$

Fig. 5-3(c) illustrates the effective resonator employed in the filter. Near the resonant frequency, this structure can be shown to behave as a series resonator with effective inductance L_{eff} and capacitance C_{eff}. Although the values of these elements vary with filter mid-band frequency, they may be assumed constant within the pass-band of a narrow-band filter. The varactor capacitance only modifies the effective capacitance and therefore allows the resonators to be tuned synchronously.

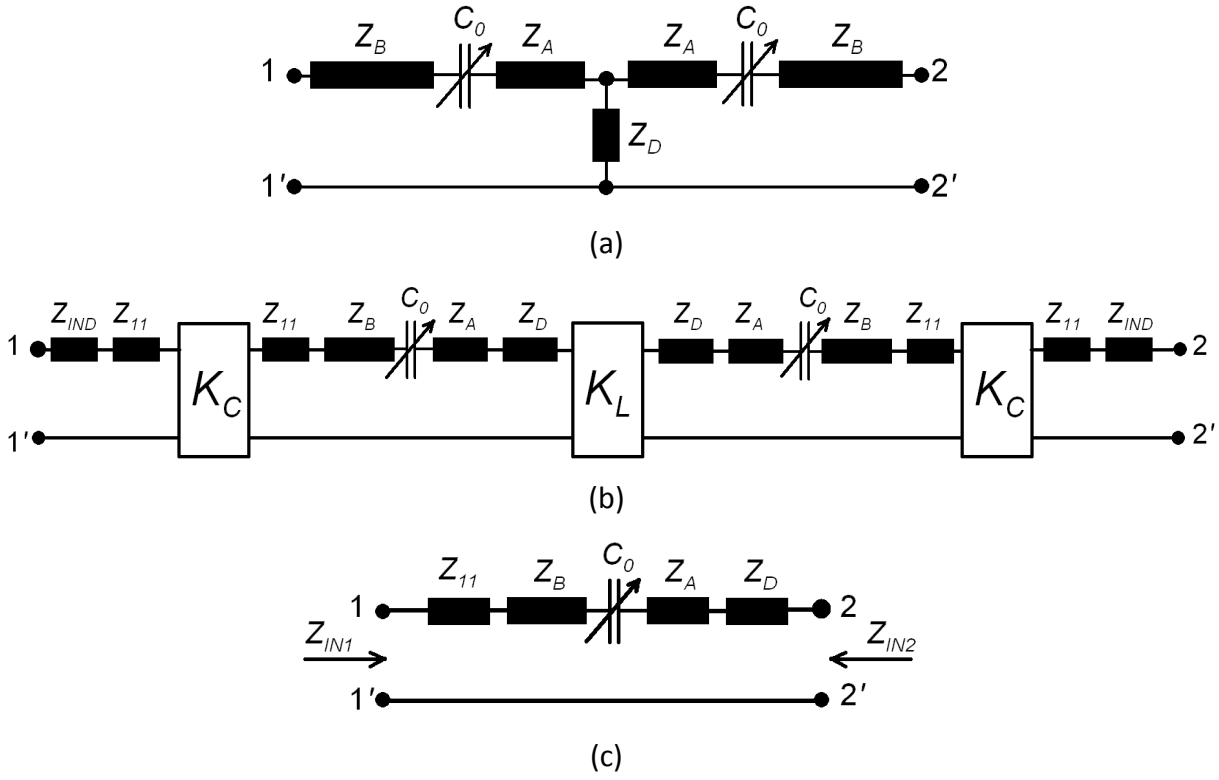

Fig. 5-3 (a) Filter equivalent circuit (coupled line model omitted) (b) Filter circuit with extracted impedance inverter (c) Effective resonator employed in the filter.

Constant bandwidth tunability demands firstly that the input/output quality factor *Q* be linear with frequency at least within the filter tuning range. Expressed mathematically, this may be written as (5.4), where *k* is a constant and ω_0 is the angular mid-band frequency.

$$Q = k\omega_0 \tag{5.4}$$

Secondly, the pole separation, Δf, must be constant, again at least throughout the tuning range. For narrow-band two-pole filters, it may be shown that the pole separation is expressed by (5.5), where f_H and f_L are the upper and lower pole angular frequencies respectively. For constant pole separation, this ratio must be fixed.

$$\Delta f = f_H - f_L = \frac{K_L}{2\pi L_{eff}} \tag{5.5}$$

The effective resonator inductance, L_{eff}, is a key design parameter in that it not only is related to the *Q* factor but also determines the pole separation. This inductance may be found from (5.6), where $Z_{IN1}(\omega_x)$ is the input impedance of the resonator of Fig. 5-3 (c) at angular frequency ω_x with port 2 grounded.

$$L_{eff} = \frac{\omega_H Z_{IN1}(\omega_H) - \omega_L Z_{IN1}(\omega_L)}{\omega_H^2 - \omega_L^2} \tag{5.6}$$

The circuit in Fig. 5-4, obtained through narrowband approximation, may be used to determine the input/output *Q* factor of the filter. It is possible to show that the *Q* factor may be described by (5.4), where *k* is given by (5.7).

$$k = \frac{(R_s^2 + |Z_{11} + j\omega_0 L_{IND}|^2)}{R_s} \times \frac{L_{eff}}{K_c^2} \tag{5.7}$$

Notice that the *Q* factor is not a function of the varactor capacitance since the inverter K_C has transformed this into a shunt inductance. However, due to the frequency dependent feeding of the resonant tank and due to the frequency dependent nature of the effective resonator inductance L_{eff}, the *Q* factor is generally nonlinear. To improve linearity, it is necessary to restrict the frequency variation of *k*, which can be achieved by selecting an appropriate value for L_{IND}. Fig. 5-5(a) plots *k* against resonant frequency for various values of L_{IND} to illustrate the relationship graphically. The center frequency is raised by lowering the varactor capacitance from around 20 pF to 2 pF.

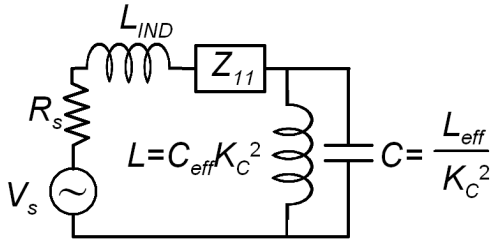

Fig. 5-4 Equivalent circuit for extracting input/output quality factor

With an almost linear *Q* factor, the second necessary condition for ensuring constant bandwidth tuning is constant pole separation. As indicated by (5.5), the pole separation is a function of the effective resonator inductance as well as the inverter impedance K_L. Due to the distributed nature of the resonators, the effective inductance seen by the inverter K_L is slightly different to that defined by (5.6). It can be shown that the effective inductance seen by K_L is given by (5.8), where Z_{IN2} is used instead and port 1 is grounded.

$$L_{eff} = \frac{\omega_H Z_{IN2}(\omega_H) - \omega_L Z_{IN2}(\omega_L)}{\omega_H^2 - \omega_L^2} \tag{5.8}$$

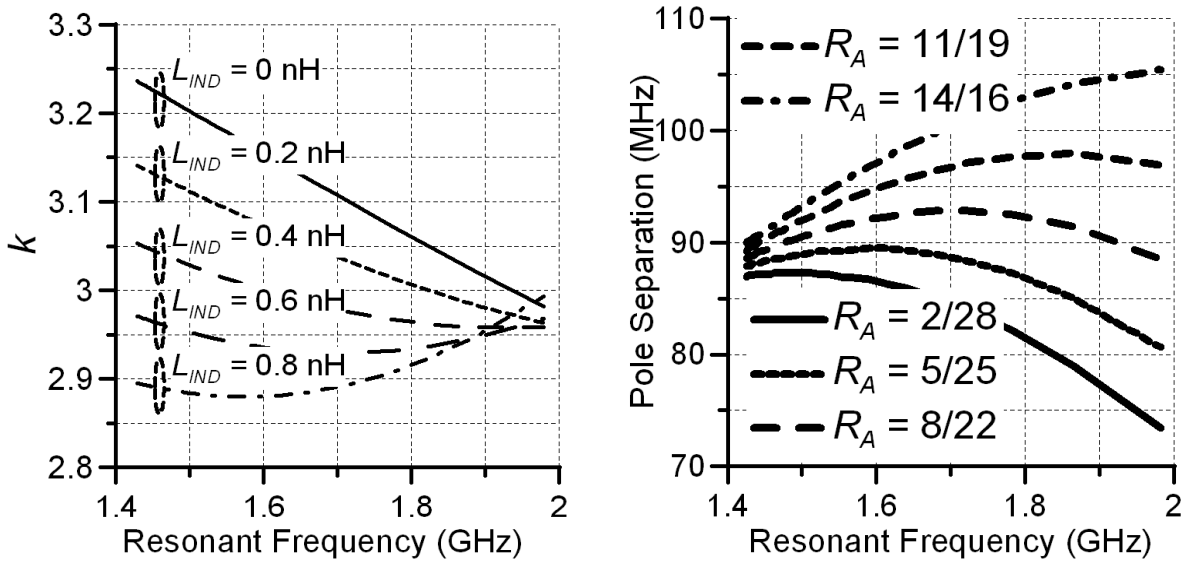

(a) (b)

Fig. 5-5(a) Variation of *k* with frequency for various inductances L_{IND}, where $Z_e + Z_o = 100\ \Omega$, $\theta_B = 22^0$, $\theta_A = 8^0$, $\theta_C = 60^0$, $\theta_D = 5.5^0$, $Z_A = Z_B = 50\ \Omega$, $Z_D = 28\ \Omega$ where all electrical lengths are referenced to 1.4 GHz. (b) Variation of pole separation against frequency for various ratios R_A, where $\theta_A + \theta_B = 30^0$.

It can be shown that selecting an appropriate ratio, R_A, of θ_A to θ_B can be employed to control L_{eff} in such a way as to compensate for the frequency deviation of K_L hence enforcing the ratio in (5.5) to be near constant. Fig. 5-5(b) plots the pole separation against resonant frequency for various values of ratio R_A. Although a perfectly constant pole separation is not achieved, its variation can be restricted considerably.

The selectivity of the proposed filter is greatly enhanced by the pair of transmission zeros generated by the capacitive source-load coupling C_{SL} illustrated in Fig. 5-1. It is possible to place the transmission zeros almost independently of the passband response for weak source-load coupling. The zero conditions may be expressed approximately as the first two roots of (5.9) where $Z_{sum} = Z_e + Z_o$ and $Z_{diff} = Z_e - Z_o$.

$$\frac{j}{(Z_{IN1} + jK_L)\omega C_{SL}} \cong \frac{Z_{sum}\cot(\theta_C)}{K_L} + \frac{{Z_{sum}}^2(Z_{IN1} - jK_L)}{jK_L{Z_{diff}}^2} \tag{5.9}$$

This section has presented an accurate filter model, which was analysed to identify the key parameters that affected tunability and bandwidth of the proposed dual-mode tunable filter. Methods of correcting the *Q* factor and fixing the pole separation have been described. Finally, a formula to determine the transmission zero frequencies has been presented.

5.2 Filter Distortion Analysis

The varactor depletion capacitance, C_0', is a function of the applied reverse bias voltage, V_{bias}, as well as the RF signal, V_{RF}, as defined by (5.10), where V_j is the junction potential, m is the junction grading coefficient and C_{j0} is the zero bias capacitance.

$$C_0' = \frac{C_{j0}}{\left(1 + \frac{V_{bias} + V_{RF}}{V_j}\right)^m} \tag{5.10}$$

The modulation of the depletion capacitance from the RF signal introduces distortion [5-27]. The most detrimental distortion products are caused by third order inter-modulation and will appear within the filter passband.

Fundamentally, for a given input power, the amount of distortion generated from a varactor diode is proportional to the RF signal voltage across it. The proposed filter is able to achieve higher linearity than most varactor tuned filters, especially for low bias voltages, since the RF voltage across the varactor diode is lower for a given input power.

A simple first order filter is analysed to illustrate the improvement in linearity. Fig. 5-6 compares the proposed resonator to a typical varactor tuned series transmission line resonator, where C_0 refers to the linear capacitance of the varactor. The capacitance of a typical tunable transmission line resonator arises from the varactor capacitance alone. In contrast, the proposed resonator has a fixed capacitance, C_A, given by (5.11), arising from Z_{11}, which is in series with the varactor capacitance C_0' [5-26].

$$C_A = \frac{5\sqrt{3}}{9\pi f_L (Z_e + Z_o)} \tag{5.11}$$

This series connection of the two capacitances effectively acts as a capacitive potential divider. The reduced overall RF voltage across the varactor diode thus gives better linearity for the same input power.

Generally, varactor diodes are mostly nonlinear under low bias voltages due to the RF modulation of the bias voltage being more significant and also due to the more sensitive nature of the capacitance at lower bias voltages. The advantage gained with the proposed resonator is that the action of the potential divider is most effective in suppressing distortion for lower bias voltages, where the distortion is normally higher.

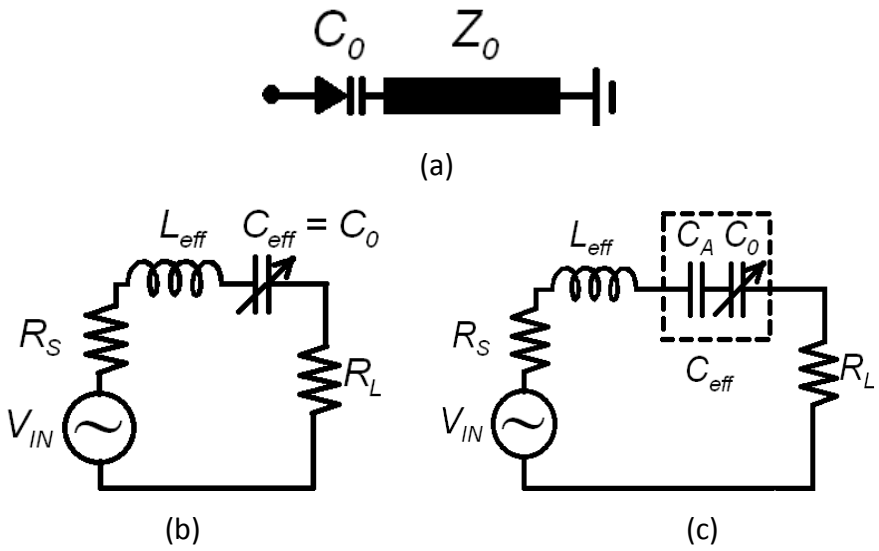

Fig. 5-6(a) Regular series transmission line tunable resonator, Model of 1st order filter with (b) regular tunable resonator (c) proposed tunable resonator.

For a given filter specification, L_{eff} and C_{eff} must be identical for the filters in Fig. 5-6 (b) and Fig. 5-6(c). Therefore, the effect of the potential divider on third order inter-modulation products is analysed using the Volterra series. The first, second and third order Volterra kernels describing the signals across the varactor of Fig. 5-6(c) are given by (5.12), (5.13) and (5.14) respectively , where A and B are given by (5.15) and (5.16) while $\omega_s = \omega_1 + \omega_2 + \omega_3$.

$$H_1(\omega) = \frac{C_A}{C_A + C_0 - \omega^2 L C_0 C_A + j2\omega R_S C_0 C_A} \tag{5.12}$$

$$H_2(\omega_1, \omega_2) = \frac{[C_1 - LC_1C_A(\omega_1 + \omega_2)^2 + j2RC_1C_A(\omega_1 + \omega_2)]H_1(\omega_1)H_1(\omega_2)}{LC_0C_A(\omega_1 + \omega_2)^2 - (C_0 + C_A) - j2RC_0C_A(\omega_1 + \omega_2)} \tag{5.13}$$

$$H_3(\omega_1, \omega_2, \omega_3) = \frac{[C_1A + C_2B][1 - LC_A\omega_s^2 + j2RC_A\omega_s]}{6[LC_0C_A\omega_s^2 - (C_0 + C_A) - j2RC_0C_A\omega_s]} \tag{5.14}$$

$$A = 4\{H_2(\omega_1, \omega_2)H_1(\omega_3) + H_2(\omega_1, \omega_3)H_1(\omega_2) + H_2(\omega_2, \omega_3)H_1(\omega_1)\} \quad (5.15)$$

$$B = 6H_1(\omega_1)H_1(\omega_2)H_1(\omega_3) \quad (5.16)$$

The varactor capacitance coefficients C_n given by (5.17), where $V_T = V_{bias} + V_{RF,}$ are such that the RF charge, q, stored in the varactor can be described by (5.18).

$$C_n = \frac{1}{(n+1)n!}\frac{d^n C_0'(V_T)}{dV_t^n}\bigg|_{V_T=V_{bias}} \quad (5.17)$$

$$q = C_0 V_{RF} + C_1 V_{RF}^2 + C_2 V_{RF}^3 \quad (5.18)$$

Fig. 5-7 (a) plots the calculated third order inter-modulation product power for a given C_{eff} and L_{eff}, for a range of potential divider factors, β, where $\beta = 1 + C_0/C_A$. The circuit of Fig. 5-6(b) corresponds to β = 1 where $C_A = \infty$ and β >1 corresponds to the circuit of Fig. 5-6(c) under a range of combinations of C_A and C_0 resulting in the same C_{eff}, so as to maintain the same resonant frequency. Improvement to linearity is proportional to β.

Improvement to linearity however comes at a price. The series connected capacitance C_A effectively restricts the range of effective capacitance values that may be realised with the tunable varactor. This directly translates to the restriction of the filter tuning range to that mentioned in the previous section. Fig. 5-7 (b) plots the trade off between linearity and tuning range for the filter, where 100% tuning range corresponds to the case with no fixed capacitance (i.e. $C_A = \infty$). These results were obtained with the varactor diode model BB179 from NXP, with a capacitance tuning range from 20 pF to 2 pF for bias voltages from 0 to 30 V. Key varactor parameters such as V_j, C_{j0} and m were found to be 1.38 V, 27.7 pF and 0.7 respectively from the spice model for the varactor obtained from [5-28].

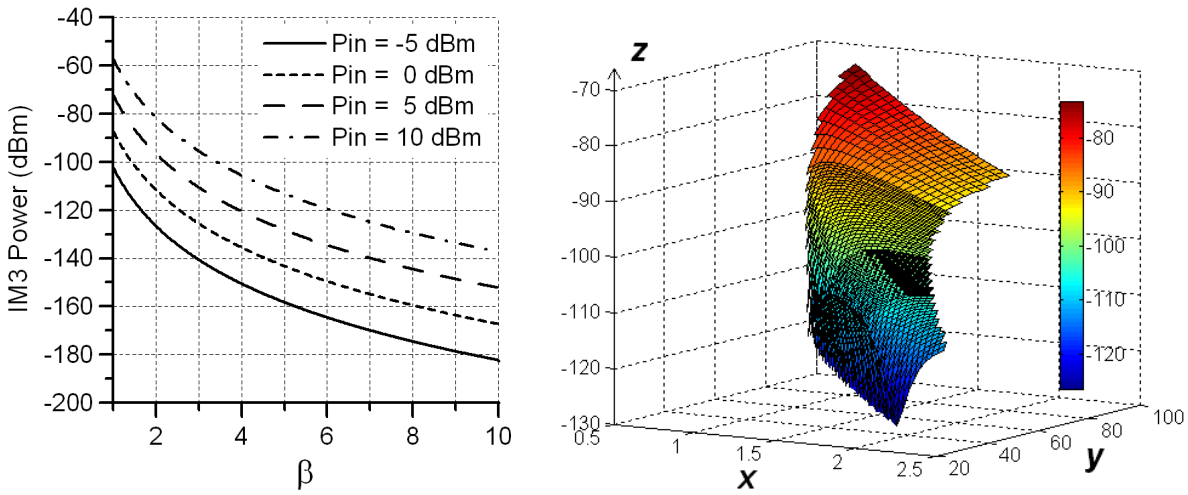

(a) (b)

Fig. 5-7 (a) Calculated third order intermodulation powers against potential divider factor for various input powers, where tone spacing is 100kHz, filter center frequency is 1.5 GHz, L_{eff} = 2.5 nH, C_{eff} = 4.5 pF, C_1 = 100 fF, C_2 = 50 fF. (b) Trade off between linearity and filter tuning range, where the *x*-axis is the filter center frequency in GHz, y-axis is the available tuning range as a percentage, z-axis is IM3 power in dBm and L_{eff} = 2.5 nH. 100% tuning range corresponds to $C_A = \infty$.

It may be necessary to better visualize the effectiveness of this technique in practical filters, where C_A would be fixed. The linearity and β will then directly depend on the varactor biasing voltage and hence the resonant frequency. As an illustrative example, the third order intermodulation response of circuits in Fig. 5-6 are compared against resonant frequency in Fig. 5-8 for the following component values; L_{eff} = 2.5 nH, C_A = 8 pF, where the BB179 varactor diode is employed as the tuning element.

It is very clear from Fig. 5-8 that a typical varactor based tunable filter would suffer from nonlinearity effects mostly for low bias voltages, which correspond to operation at lower resonant frequencies. With increasing bias voltage, as expected, the third order inter-modulation distortion product power diminishes. In contrast, under the proposed configuration, the inter-modulation distortion product power is smallest for lower bias voltages, where β is higher and gradually increases with resonant frequency as β falls. Overall, third order inter-modulation power has been suppressed by at least 25 dB for lower resonant frequencies and around 8 dB for higher frequencies.

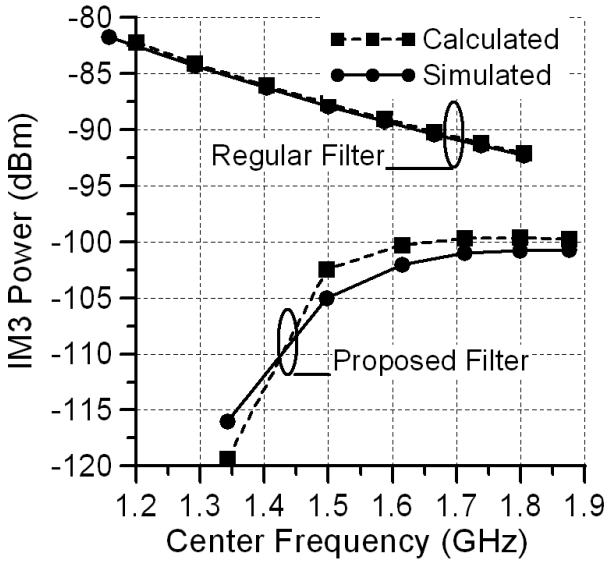

Fig. 5-8 Comparison of calculated and simulated third order intermodulation power against filter resonant frequency for a tone spacing of 100 kHz and Pin = 10 dBm (for varactor diode model BB179 from NXP).

5.3 Experiment and Verification

To demonstrate the performance of the proposed compact tunable highly linear bandpass filter, a microstrip prototype filter was designed and fabricated to operate between frequencies from 1.5 GHz to 2.0 GHz with a bandwidth of 220 MHz. The circuit was constructed on Rogers 6010(LM) substrate with a relative dielectric constant of 10.2 and a substrate thickness of 1.27 mm.

Very good agreement is observed between the measured and simulated S-parameters of the filter, which are illustrated in Fig. 5-9. Simulations assumed a constant varactor resistance of 0.6 Ω to model the losses [5-28]. The filter insertion loss varied from around 2.4 dB to around 1.6 dB. The measured tuning range was 1.45 GHz – 1.96 GHz and the 3-dB bandwidth was found to increase from approximately 210 MHz at 1.45 GHz to 220 MHz at 1.96 GHz as illustrated in Fig. 5-9 (c). A photograph of the filter is shown in Fig. 5-9 (e), where filter circuit size was 29 mm x 9.8 mm.

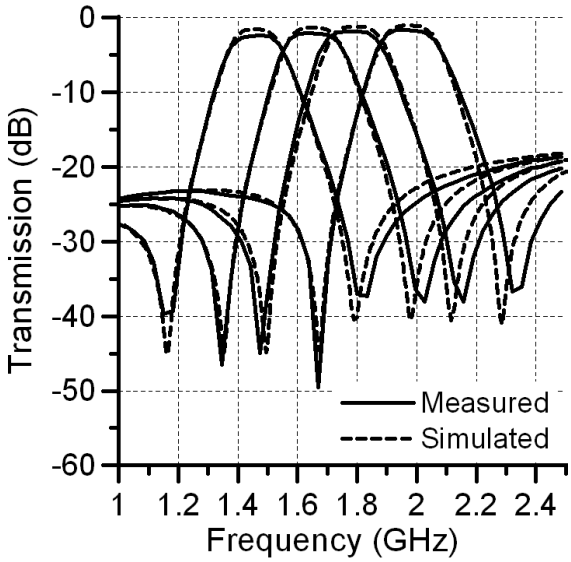

(a)

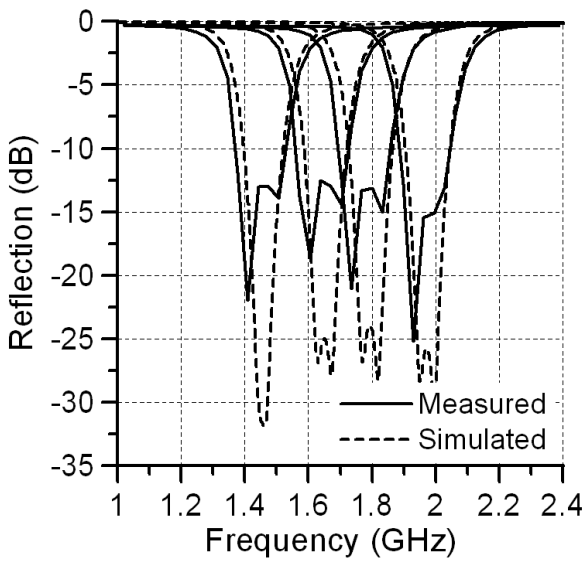

(b)

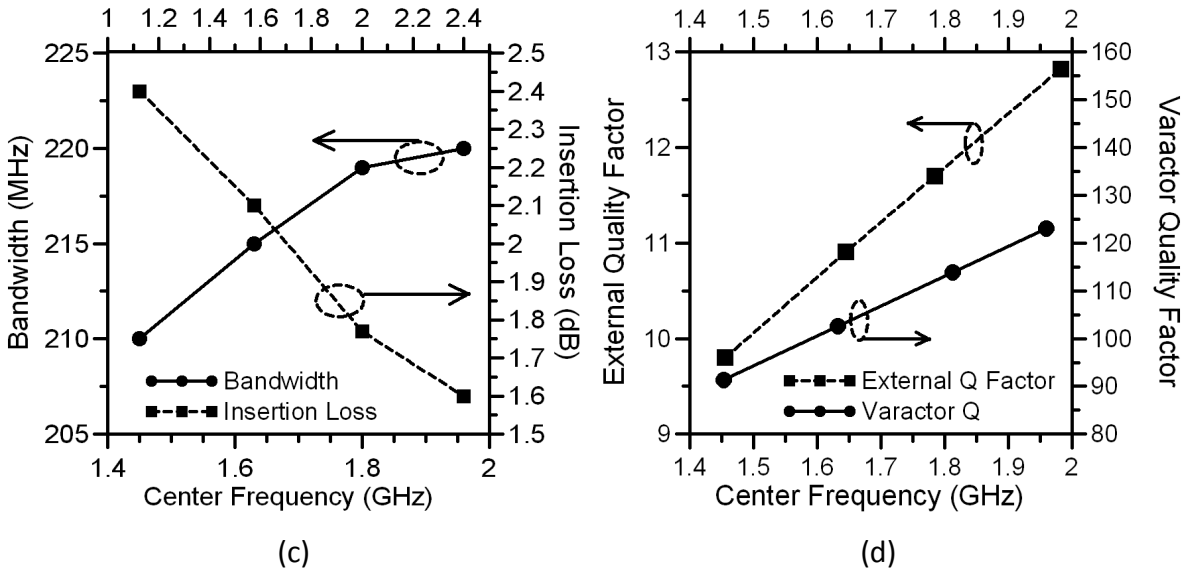

(c) (d)

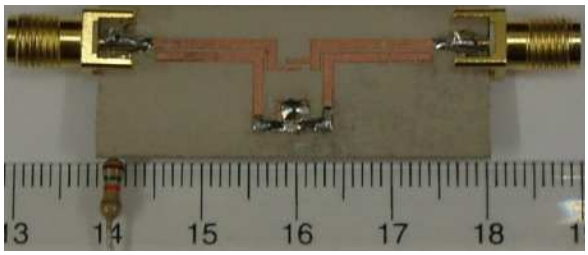

(e)

Fig. 5-9 (a) and (b) Simulated and measured s-parameters of second order highly linear tunable filter for bias voltages of: 1V, 7V, 15V, 30V from left to right. (c) Measured filter bandwidth and insertion loss across tuning range. (d) External Q factor of filter and varactor *Q* against center frequency (e) Photograph of fabricated filter.

Fig. 5-10 (a) plots the input power against the output power for the filter with a bias voltage of 1V and a tone spacing of 100 kHz. The measured third order input and output referred intercept points are as high as 43 dBm and 40 dBm respectively even under this low bias voltage. Fig. 5-10 (b) plots the measured input referred intercept point against the filter center frequency. It can be observed that linearity is best at around 1.7 GHz. Overall, the filter has excellent linearity.

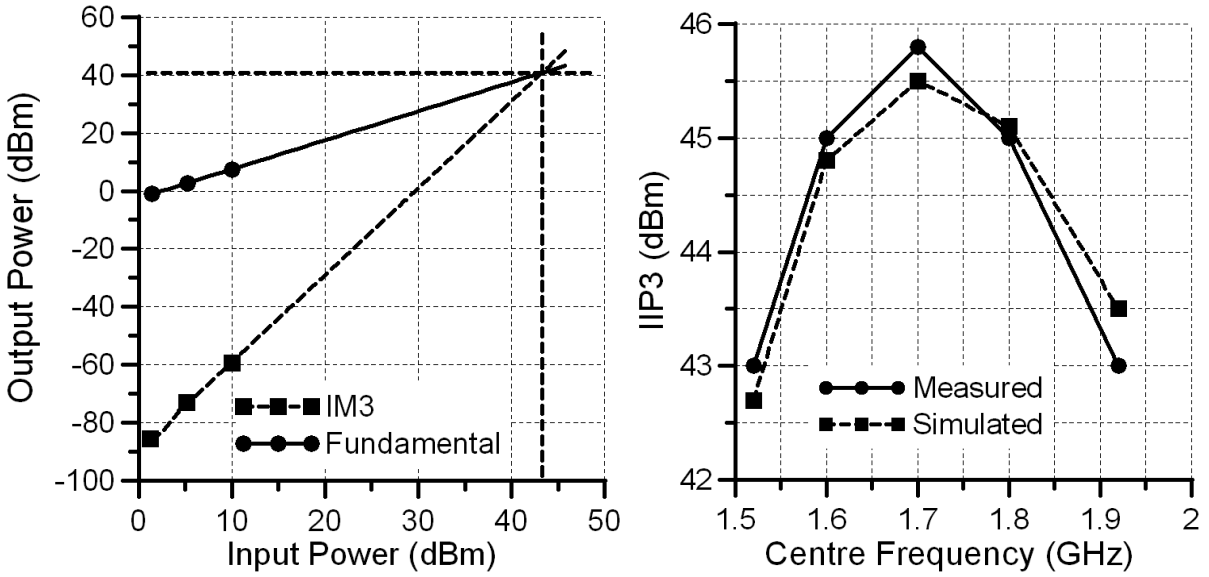

Fig. 5-10 (a) Output power of fundamental tones and IM3 product against input power under a bias voltage of 1V and tone separation of 100 kHz. (b) Measured and simulated IIP3 against filter center frequency for tone separation of 100 kHz.

5.3.1 Summary

This section presented a compact highly linear fixed bandwidth tunable filter for modern communications systems. Methods to obtain a near linear *Q* factor and to achieve near constant pole separation have been described. A pair of transmission zeros generated from the source load coupling greatly enhances the skirt selectivity of the filter. The resonator configuration employed is shown to improve filter linearity drastically especially for low bias voltages, where distortion is normally strongest. A filter was fabricated for demonstration and verification. The filter tuning range was observed to be from 1.45 – 1.96 GHz (30%), with a 3 dB bandwidth variation from 210 MHz at 1.45 GHz to 220 MHz at 1.96 GHz corresponding to only 4.6% total bandwidth deviation. Additionally, it is shown that the filter exhibits an IIP3 of better than 43 dBm throughout the entire filter tuning range. The proposed dual-mode filters also have their first spurious response at $3f_0$ rather than at $2f_0$ so they suffer less from adjacent channel interference when being tuned especially towards higher frequency bands [5-26]. Moreover, they are also relatively simple and inexpensive to fabricate.

5.4 References

[5-1] Y.-C. Chiou and Gabriel M. Rebeiz, “A tunable three-pole 1.5–2.2-GHz bandpass filter with bandwidth and transmission zero control”, *IEEE Transactions on Microwave Theory and Techniques*, vol. 59, no. 11, pp. 2872-2878, Nov. 2011.

[5-2] J. S. Sun, N. Kaneda, Y. Baeyens, T. Itoh and Y.-K. Chen, “Multilayer planar tunable filter with very wide tuning bandwidth”, *IEEE Transactions on Microwave Theory and Techniques*, vol. 59, no. 11, pp. 2864-2871, Nov. 2011.

[5-3] I. C. Hunter, *Theory and design of microwave filters*, London: Institute of Electrical Engineers, 2001.

[5-4] C. Huang, K. Buisman, M. Marchetti, L. K. Nanver,M. Popadic, T. L Scholtes, H. Schellevis, L. E. Larson,and L. C. Vreede, “Ultra linear low-loss varactor diode configurations for adaptive RF systems”, *IEEE Transactions on Microwave Theory and Techniques*, vol. 57, no. 1, pp. 205-215, Jan. 2009.

[5-5] Y.H Chun,J.S Hong, “Electronically reconfigurable dual-mode microstrip open-loop resonator filter”, *IEEE Microwave and Wireless Component Letters*, Vol. 18, No. 7, pp. 449-451, July. 2008.

[5-6] P.W. Wong, I.C. Hunter, “Electronically Reconfigurable Microwave Bandpass Filter”, *IEEE Transactions on Microwave Theory and Techniques*, vol. 57, no. 12, pp.3070-3079, Dec. 2009.

[5-7] P.W. Wong, I.C. Hunter, “A new class of low-loss high-linearity electronically reconfigurable microwave filter”, *IEEE Transactions on Microwave Theory and Techniques*, vol. 56, no. 8, pp.1945-1953, Aug. 2008.

[5-8] Y.M. Chen, S.F. Chang, C.Y Chou and K.H Liu., "A reconfigurable bandpass-bandstop filter based on varactor-loaded closed-ring resonators" Microwave Magazine, IEEE, Vol. 10, Issue 1, Feb. 2009, pp. 138-140.

[5-9] L.-H. Hsieh and K. Chang, "Tunable microstrip bandpass filters with two transmission zeros", *IEEE Transactions on Microwave Theory and Techniques*, vol. 51, no. 2, pp. 520–525, Feb. 2003.

[5-10] M. Makimoto and M. Sagawa, "Varactor tuned bandpass filters using microstrip-line ring resonators", *IEEE MTT-S Int. Microwave Symposium Digest*, Jun. 1986, pp. 411–414.

[5-11] I.C. Hunter and J.D Rhodes, "Electronically tunable microwave bandpass filters", *IEEE Transactions on Microwave Theory and Techniques*, vol. 30, no. 9, pp. 1354-1360, Sept. 1982.

[5-12] B.-W. Kim and S.-W. Yun, "Varactor-tuned combline bandpass filter using step-impedance microstrip lines," *IEEE Transactions on Microwave Theory and Techniques*, vol. 52, no. 4, pp. 1279–1283, Apr. 2004.

[5-13] B.E.C Smith, P.A Warr, M.A Beach, "Wide Tuning Range Planar Filters Using Lumped-Distributed Coupled Resonators", *IEEE Transactions on Microwave Theory and Techniques*, vol. 53, no. 2, pp. 777–785, Feb. 2005.

[5-14] L.Athukorala, D.Budimir, "Frequency Tunable Microstrip Resonators and Filters", *Proceedings of European Microwave Conference*, 2009, pp. 1239-1242, Oct. 2009.

[5-15] W.M. Fathelbab and M.B.Steer, "A reconfigurable bandpass filter for RF/microwave multifunctional systems", *IEEE Transactions on Microwave Theory and Techniques*, vol. 53, no. 3, pp. 1111-1116, Mar. 2005.

[5-16] H.Joshi, H.H.Sigmarsson, S.Moon, D Peroulis and W.J Chappell, "High Q fully reconfigurable tunable bandpass filters", *IEEE Transactions on Microwave Theory and Techniques*, vol. 57, no. 12, pp. 3525-3533, Dec. 2009.

[5-17] B. Kapilevich, “A varactor-tunable filter with constant bandwidth and loss compensation,” *Microwave Journal*, vol. 50, no. 4, pp. 106–114, Apr. 2007.

[5-18] S.J Park and G.M. Rebeiz, “Low-loss two-pole tunable filters with three different predefined bandwidth characteristics”, *IEEE Transactions on Microwave Theory and Techniques*, vol. 56, no. 5, pp. 1137-1148, May 2008.

[5-19] W. Tang and J.S. Hong, “Varactor-tuned dual-mode bandpass filters”, *IEEE Transactions on Microwave Theory and Techniques*, vol. 58, no. 8, pp. 2213-2219, Aug. 2010.

[5-20] M. Tanani and G.M. Rebeiz, “A two-pole two-zero tunable filter with improved linearity”, *IEEE Transactions on Microwave Theory and Techniques*, vol. 57, no. 4, pp. 830-839, April 2009.

[5-21] E. E. Hoppenjans and W. J. Chappell, "A vertically integrated tunable UHF filter," *IEEE MTT-S International Microwave Symposium Digest*, May 2010, pp. 1380-1383.

[5-22] A. R. Brown and G. M. Rebeiz, "A varactor-tuned RF filter," *IEEE Transactions on Microwave Theory and Techniques*, vol. 48, no. 7, pp. 1157-1160, Aug. 2002.

[5-23] M. A. El-Tanani and G. M. Rebeiz, “High Performance 1.5-2.5 GHz RF MEMS Tunable Filters for Wireless Applications,” *IEEE Transactions on Microwave Theory and Techniques*, Vol. 58, No. 6, pp. 1629-1637, June 2010.

[5-24] L. Athukorala and D. Budimir, “Compact high linearity tunable dual-mode microstrip filters”, *European Microwave Conference*, pp.834 – 837,2010.

[5-25] L. Athukorala and D. Budimir, “Compact dual-mode open-loop microstrip resonators and filters”, *IEEE Microwave and Wireless Component Letters*, Vol. 19, No. 11, pp. 698-700, July. 2009.

[5-26] L. Athukorala and D. Budimir, “Design of compact dual-mode microstrip filters”, *IEEE Transactions on Microwave Theory and Techniques*, vol. 58, no. 11, pp. 2888-2895, Nov. 2010.

[5-27] B.E. Carey-Smith and P.A Warr, “Distortion mechanisms in varactor diode-tuned microwave filters”, *IEEE Transactions on Microwave Theory and Techniques*, vol. 54, no. 9, pp. 3492-3500, Sept. 2006.

[5-28] NXP, BB179 Varactor Diode Spice Model, NXP, [Online], Available: http://www.nxp.com/models/spicespar/data/BB179.html

6.0 CONCLUSION AND FUTURE WORK

The central aim of this research effort is the development of enhanced planar RF and microwave bandpass filters for wireless communications. In particular, the investigation addressed some of the key challenges surrounding RF and microwave bandpass filters such as compactness, harmonic suppression and tunability with the proposal of a novel compact planar dual-mode resonator configuration.

This dissertation has proposed a novel compact planar dual-mode resonator configuration for bandpass filter applications in RF and microwave communications systems. A rigorous analysis of the proposed transmission line dual-mode resonator was presented in order to prove the existence of two unique modes of resonance. An equivalent electrical model for the resonator was subsequently proposed in order to gather deeper insight into the relationship between the physical and electrical parameters. In addition to the fundamental resonator configuration, several variants, each with unique properties, were also presented as candidates for filter design applications.

Application of the proposed resonators in filter design was tackled in two stages. The first aim was the development of all-pole Butterworth and Chebyshev filters. The form of the resonator was shown to be readily extendable to all-pole filter design. The development of a complete filter design procedure for all-pole filters, starting from lowpass prototype networks to the realization of distributed filter parameters, was also described. Discussions were supplemented with several filter design examples to highlight the key stages of the

design process. The effectiveness of the design method is reflected in the experimental results, which were observed to be in very close agreement to theory and simulations.

Secondly, the application of these resonators in generalized Chebyshev bandpass filters was investigated. The cross-coupled filter approach was adopted for the modular design of high order generalized Chebyshev bandpass filters. Several highly compact cross-coupled filter topologies were proposed including trisection and quadruplet filter units. Source-load coupled fourth order filtering units were also described. The design of such filters adopted a simulation based parameter extraction method in order to realize the desired coupling coefficients. Coupling matrices may be optimized with the aid of a computer. Several cross coupled filter design examples were presented for each filter configuration to showcase their performance. The calculated filter responses were found to be in very close agreement to the experimentally measured results.

Finally, the application of these resonators in the development of tunable filters was investigated, with a particular focus on highly linear constant bandwidth, center frequency tunable filters. Measures to control the filter external quality and coupling coefficients were described in order to considerably restrict the variation of filter bandwidth with center frequency. The varactor diode was employed as the tuning element due to its numerous benefits over other devices such as superior tuning speed, extremely low power consumption, high reliability, wide tuning range and versatility in planar circuit implementation. In addition to compactness, the proposed tunable dual-mode resonator was shown to exhibit a unique highly linear circuit configuration. Significant improvements to filter linearity were proved both analytically and experimentally. The theoretical results were in excellent agreement with experimental results.

6.1 Contributions of the Thesis

The contributions of the research are recaptured in the following summary:

1. A novel highly compact dual-mode resonator is presented for RF and microwave bandpass filter applications. The proposed resonator is rigorously analyzed and fully characterized to prove the existence of two unique modes of resonance. Several variants with unique properties were also proposed. Electrical equivalent circuits for each configuration were also established in order to fully comprehend the relationship between distributed and electrical parameters.

2. A comprehensive filter design procedure is presented for all-pole bandpass filters to expedite the development process. This allows the design process to effectively commence from the given specification and terminate with the evaluation of the distributed filter parameters. Since the proposed design procedure borrows heavily from the established equivalent circuits of the resonators, the filter design equations are based on these models.

3. Application of dual-mode resonators in cross-coupled filter design in order to obtain filters with enhanced skirt selectivity is described. To this end, several highly compact filter configurations were proposed. In particular, trisection and quadruplet filter configurations with the dual-mode resonator were presented for application in high order modular cross coupled single and dual passband filter design.

4. Application of dual-mode resonators in varactor tunable filter design was investigated. The research focused exclusively on the application of the dual-mode resonator in the development of fixed bandwidth, center frequency tenable bandpass filters. Measures of constraining the variation of filter bandwidth were described and supported analytically. While these filters have a high tuning range, and near constant bandwidth, proposed filters were shown to exhibit significantly low signal distortion even under low reverse bias voltages.

6.2 Future Work

This dissertation presented a novel highly compact dual-mode resonator for application in RF and microwave fixed and tunable filters. Although as many aspects of this resonator were investigated within the allotted time, there still remains several interesting lines of investigation which may possibly enable the employment of these resonators in addressing a broader range of filter applications.

Firstly, the thesis focused on the development of bandpass filters where the input and output couplings where exclusively achieved through parallel coupled lines. As described earlier, this approach is excellent for narrow to medium fractional bandwidth filters. However, investigations on direct tapped coupling of the resonator may be performed to assess the feasibility of employing these resonators in wide or ultra-wideband filter design. Since the integrity of the proposed equivalent circuits is only strong under narrowband approximations, new equivalent circuits, possibly based on simplified transmission line structures must instead be employed.

Secondly, the modification of the dual-mode resonator in obtaining a dual-band response is worthy of further investigation. This may be achieved by the addition of a pair of symmetrically placed open circuited-stubs either side of the short circuit plane of the resonator. The new dual-mode dual-band resonator must be fully characterized with its own equivalent circuit and filter design procedure. There may however be limitations to the kind of achievable transmission response at least in terms of the degree of freedom in the placement of the two passbands and independent control of their bandwidths. These must of course be fully examined.

Significantly more compactness may be achieved especially for higher order filters if the proposed resonators were configured on multi-layer printed circuit boards. Since the resonator coupling mechanisms will be greatly different to that of single layer filters, these effects must be understood and quantified prior to dealing with multi layer filter applications.

RELEVANT PUBLICATIONS

Open-Loop Tunable Resonators and Filters with Constant Bandwidth

L. Athukorala[1] and D.Budimir[2]

Wireless Communications Research Group, School of Electronics and Computer Science,

University of Westminster, 115 New Cavendish Street, London, W1W 6UW, UK

lakshman.athukorala@westminster.ac.uk[1]

d.budimir@westminster.ac.uk[2]

Abstract—This paper presents a compact novel design for achieving constant bandwidth tunable filters with wide tuning range. A method for linearizing the Q factor against frequency is proposed. A modified coupling structure is introduced to compensate for variations in filtering characteristic across the theoretical 50% tuning range of the filter. Filter design equations are provided for designing Butterworth or Chebyshev filters. An experimental second order filter is demonstrated with 22.5% pass-band shift with only 3% bandwidth variation and insertion loss better than 3 dB. Furthermore, a third order tunable bandpass filter with tuning range of 45% and less than 5% bandwidth variation is illustrated through simulation and modelling to show feasibility with higher filter orders. There is very good agreement between theoretical and experimental results.

Index Terms— Tunable filter, tunable resonator, open-loop resonator, constant bandwidth

1.0 INTRODUCTION

Tunable microstrip bandpass filters find numerous potential applications in current and emerging technologies. In particular, it may be necessary for modern wireless systems to communicate via a range of channels with identical bandwidths and the need for constant bandwidth tunable filters becomes apparent here.

Recent research on tunable or reconfigurable microstrip resonators and filters include work presented in [1]-[14], where various degrees of tunability have been quoted for various structures. A tunable filter with 45% tuning range is presented in [2] but it consumes a relatively large amount of circuit area. A tunable open-loop filter with constant bandwidth is presented in [5] where a piezoelectric transducer (PET) was used for tuning. Apparently, the PET had

little effect on the filter bandwidth which facilitated the design of the fixed-bandwidth tunable filter. However, only 10% tunability was achieved due to limitations of the PET. Tunable comb-line filters were first presented in [7] where 53% tunability had been achieved but with wide variation (12%) in absolute bandwidth and high loss (6 dB). Improvements to this have been suggested in [8], but constant bandwidth was achieved for only 12.5% tuning range. In [13], a tunable filter is presented where an optimization method was used to design coupling structures. However, this approach cannot be adopted to design filters with prescribed filtering functions.

This paper presents a compact novel design for obtaining constant bandwidth varactor tuned filters based on the asymmetrically coupled open-loop resonator. Not only do these filters have a wide tuning range (50%) but much better control of bandwidth (less than 5%) and insertion-loss may be attained compared to previous work. Additionally, a design method is outlined to facilitate the design of Butterworth and Chebyshev filters. Resonators which comprise the filter may be tuned with a single voltage. Additionally, it was found that the proposed method eliminates the need for tuning elements to control coupling coefficients which greatly simplifies the layout.

The proposed filters are relatively compact and offer a good tuning range and allow an improved regulation of bandwidth in comparison to [2], [5], [7] and [13].

2.0 PROPOSED TUNABLE RESONATOR

The varactor-tuned, open-loop resonator is illustrated in Fig. 1. It consists of two sections of equal-length transmission lines with impedance Z_2 and a pair of asymmetrically driven coupled lines with even mode impedance Z_e and odd mode impedance Z_o. The input and output feed lines with characteristic impedance Z_0, are 50 Ω.

The varactor diode consists of series resistance, inductance and the depletion capacitance C_0. In practice, the series resistance of the varactor diode limits the quality factor of the resonator and introduces losses. This resistance is inversely proportional to the applied reverse voltage and, as a consequence, the diode loss will be greatest for low reverse voltages. The modulation of the depletion capacitance from the AC signal also introduces distortion [15]. For simplicity, only the depletion capacitance and series resistance are modelled; all higher order effects are not considered in this paper.

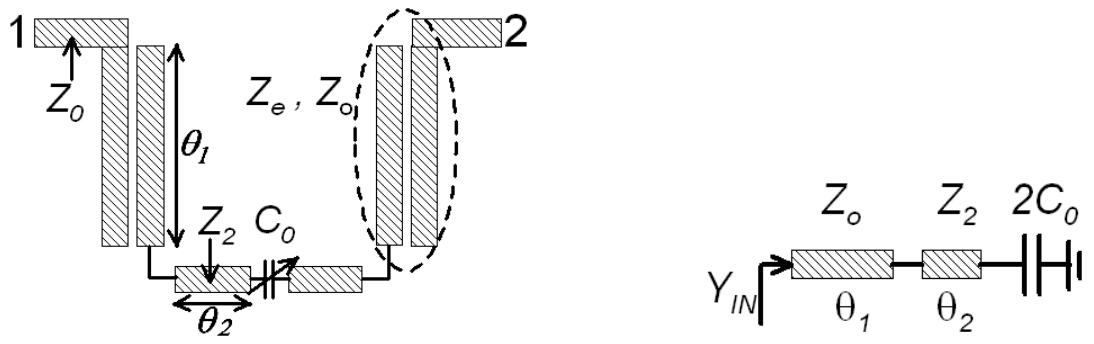

(a) (b)

Fig. 1 (a) Layout of tunable resonator (b) Transmission line equivalent circuit of resonator

A detailed study on fixed frequency open loop resonators may be found in [16]. However, the considerable effect of the inserted varactor capacitance on the open loop resonator is presented here. Illustrated in Fig. 1 (b) is the odd mode transmission line equivalent circuit of the resonator, whose resonant condition is found to be Y_{IN} = 0 S and it may be shown that the input admittance Y_{IN} of the resonator is given by equation (1), where Z_o is the odd mode impedance of the coupled lines.

$$Y_{IN} = \frac{Z_O[2\omega C_0 Z_2 + \tan(\theta_2)] - Z_2\tan(\theta_C)[2Z_2\omega C_0\tan(\theta_2) - 1]}{jZ_O[Z_2(2Z_2\omega C_0\tan(\theta_2) - 1) + Z_O\tan(\theta_C)(2\omega C_0 Z_2 + \tan(\theta_2))]} \qquad (1)$$

Varying the reverse bias applied across the varactor changes the depletion capacitance and, as a result, causes the shifting of the resonant frequency of the structure, since the input admittance is a function of C_0. Fig. 2 plots the resonant frequency of the resonator against the varactor capacitance, where a 50% frequency shift may be observed starting from a lower resonant frequency of 2 GHz up to around 3 GHz, provided that the varactor is able to offer a sufficient capacitance ratio.

The proposed resonator is designed such that electrical length $\theta_1 = 60^0$ at the lowest resonant frequency of the tuning range. The resonator may be tuned up to a frequency at which $\theta_1 = 90^0$. Therefore, the frequency range for which $60^0 < \theta_1 < 90^0$ defines the tuning range of the resonator. The transmission line with electrical length θ_2, usually smaller than 30^0 at the lowest resonant frequency, is primarily employed as an inductance.

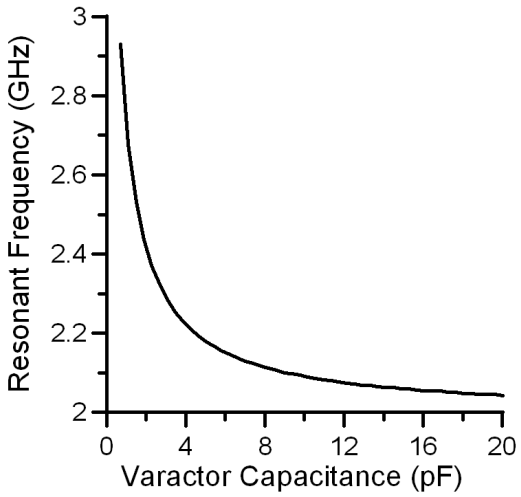

Fig. 2 Relationship between the resonant frequency of the tunable resonator and the varactor capacitance

If the higher order effects of the varactor diode are ignored, the resonator may be modelled within the tuning frequency range fairly accurately using only linear lumped elements and inverters. Additionally, a linear model would facilitate constant bandwidth filter design since it allows the direct application of circuit theory. To this end, it is important to ensure that the model is accurate across the full tuning range of the filter. The remainder of this section details the derivation of a lumped element resonator model and addresses the validity of the model across the full tuning range. Finally, a method of linearising the input/output quality factor is described.

The coupled lines comprising the filter has the T-equivalent circuit of Fig. 3 (a), which may be transformed into the circuit of Fig. 3(b) by extracting an impedance inverter and describing the driving point impedance with the inductance L_A and the capacitance C_A. The equivalent model parameters may be defined by (2) – (4) where f_L is the lowest resonant frequency of the tunable resonator. Although the inverter impedance varies with frequency in the model, it may be assumed constant at the test resonant frequency for narrow band applications. Fig. 3 (c) compares simulated and the lumped element model response of the coupled line. The slight discrepancy in responses between the model and the simulated response is due to the actual frequency dependence of the parameters C_A and L_A.

The transmission line of characteristic impedance Z_2 may be modelled relatively accurately as an inductance L_B and it will be shown that it is desirable to have a short high impedance line. The inductance may be determined from (5), where θ_{2L} is the electrical length of the line at the lowest resonant frequency of the tunable resonator.

$$C_A = \frac{5\sqrt{3}}{9\pi f_L (Z_e + Z_o)} \quad (2)$$

$$L_A = \frac{(Z_e + Z_o)}{5\sqrt{3}\pi f_L} \quad (3)$$

$$K = \frac{(Z_e - Z_o)}{2\sin(\theta_1)} \quad (4)$$

$$L_B = \frac{Z_2 \sin(\theta_{2L})}{2\pi f_L} \quad (5)$$

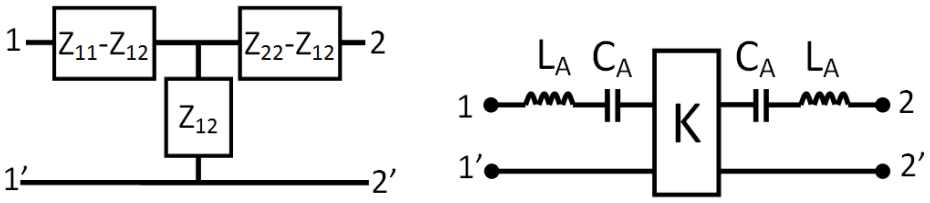

(a) (b)

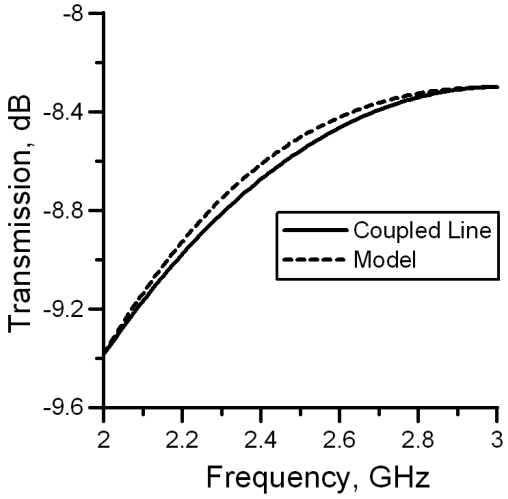

(c)

Fig. 3. Coupled line models (a) Z-parameter model (b) Lumped equivalent circuit with extracted inverter (c) Comparison of simulated and theoretical model response of coupled ($\theta_1 = 60^0$ at 2 GHz, $Z_e = 60\ \Omega$ and $Z_o = 40\ \Omega$)

The complete resonator model and the related parameters are obtained after assembling the equivalent circuits accordingly. The model depicted in Fig. 4 and summarised by equations (4), (6) and (7). The series resonator formed by L_1 and C_1, under the action of the inverters, will behave as a parallel resonant tank. The angular resonant frequency, ω_{res}, can be directly determined from L_1 and C_1. The quality factor, Q, of the circuit may be determined from (9), where R is the source/load impedance.

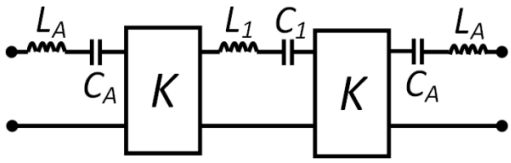

Fig. 4. Resonator equivalent circuit

$$C_1 = \frac{C_A C_0}{2C_0 + C_A} \tag{6}$$

$$L_1 = 2L_A + 2L_B \tag{7}$$

$$\omega_{res} = \frac{1}{\sqrt{L_1 C_1}} \tag{8}$$

$$Q = \omega_{res}\left(\frac{L_1}{|K|^2}\right)\frac{(R^2 + |Z_{11}(\omega_{res})|^2)}{2R} \tag{9}$$

The Q factor of a tunable resonator must increase in direct proportion with the resonant frequency in order to maintain bandwidth of the resonant peak. Usually, this requires that the input and output coupling to the resonator is tuned in addition to tuning the resonator itself. This approach is relatively cumbersome. Certain properties of the proposed resonator may be exploited to inherently maintain an approximately constant bandwidth characteristic, thus eliminating the need for extra tuning elements as well as the adverse side effects they introduce.

Equation (9) can be re-arranged to form an expression for the bandwidth of the resonator, as given by (10). It can be assumed that the $R/(\pi L_1)$ and $(Z_e - Z_o)$ terms are frequency independent. Under condition (11), the coefficients of

the sine and the cosine term in the denominator will be equal and will allow the use of the identity ($sin^2x + cos^2x = 1$) to simplify the above expression into one that is frequency independent. This permits constant bandwidth characteristic across a frequency shift.

$$\Delta f = \left(\frac{R}{\pi L_1}\right)\frac{|K|^2}{(R^2 + |Z_{11}(\omega_{res})|^2)} = \left(\frac{R}{\pi L_1}\right)\frac{(Z_e - Z_o)^2}{4R^2 sin^2\theta_1 + (Z_e + Z_o)^2 cos^2\theta_1} \quad (10)$$

$$(Z_e + Z_o) = 2R \rightarrow \text{constant bandwidth} \quad (11)$$

Under this condition, a linearly varying Q factor may be achieved across the entire frequency tuning range. Condition (11) is easily achieved and will guarantee constant bandwidth as long as inductance L_1 is frequency independent. L_1, however, is composed of L_A and L_B. It was shown earlier that the frequency dependence of L_A is negligible. Variation in L_B can be tightly controlled by increasing line impedance, Z_2, and reducing electrical length, θ_2. This effectively allows the line to more accurately resemble a lumped inductance and with this measure, it is possible to significantly restrict the change in bandwidth.

Finally, it should be noted that the lowest resonant frequency attainable is limited by the two capacitances of value C_A, which appear in series with C_0 to give C_1. Therefore, the minimum angular resonant frequency of the resonator will be limited to $\omega_{min} = \left(\sqrt{0.5L_1C_A}\right)^{-1}$. The maximum attainable resonant frequency is $2\omega_{min}$. Constant bandwidth tuning is possible up to $1.6\omega_{min}$ as the model parameters no longer are linear beyond this frequency.

To illustrate the validity of the complete resonator model, Fig. 5(a) compares the simulated transmission response to the response of the proposed lumped model. The resonator parameters are as follows: Z_e = 65 Ω, Z_o= 35 Ω, Z_2 = 66 Ω, where θ_1 is 60^0 and θ_2 is 22^0 at 2 GHz. The simulated bandwidth varied from 193.5 MHz at 2.05 GHz to 195.5 MHz at 2.93 GHz, which is roughly 1% change in bandwidth. The model bandwidth varied from 196 MHz at 2.06 GHz to 194 MHz at 3.0 GHz. Generally, a good agreement is observed.

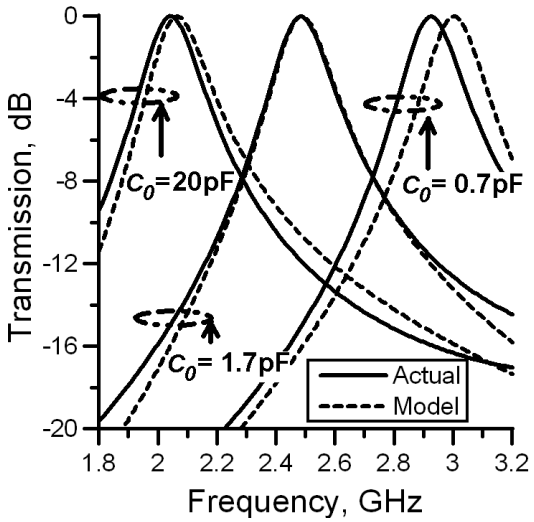

Fig. 5 (a). Comparison of simulation and theoretical model response of the resonator

3.0 TUNABLE FILTERS

Tunable filters may be implemented by cascading the proposed resonator. In this section, a simple second order tunable filter is analyzed to gain insight into the affect of tuning on filter bandwidth. Key filter parameters that affect the pole separation are identified and a method is proposed in order to control these as required.

When tuning a generic filter, it is necessary not only to tune each resonator but also the inter-resonator coupling to regulate a fixed bandwidth. Failure to do so will cause the filter bandwidth to vary and the pass-band ripple to suffer. To this effect, extra-tuning elements, in addition to those present in each resonator, are necessary to tune the inter-resonator coupling appropriately.

In contrast, the proposed filter can be designed to control the coupling coefficients such that the need for additional inter-resonator tuning elements is eliminated. This characteristic of the proposed tunable filter greatly simplifies the tuning process and, therefore, effectively allows an N^{th} order constant bandwidth filter to be tuned with only N identical tuning capacitors. If varactor diodes are used to realize this variable capacitance, for example, then all N varactors may be tuned with a common bias voltage. This property enables tuning to be a relatively simple procedure, which greatly improves the feasibility of the solution.

The second order tunable filter structure and its model are illustrated in Fig. 6. The input and output are coupled with regular asymmetrically driven coupled lines, while the coupling between adjacent resonators employs a modified coupling structure presented in Fig. 7. The impedance inverter, K_{12}, couples the resonant tanks each composed of inductance L and capacitance C, which may be determined from (6) and (7).

The impedance inverters labelled K_{01} (equal to K_{23}), together with L, L_A and C_A, affects the input/output Q factor of the filter and (10) may be employed to fix a desired bandwidth. Near-constant bandwidth may be achieved across the tuning range if condition (11) is adhered to while employing high line impedance for Z_2. The pass-band may be tuned by varying the common DC bias voltage to the two varactor diodes.

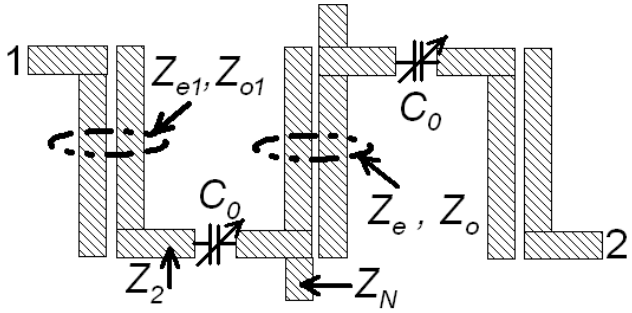

(a)

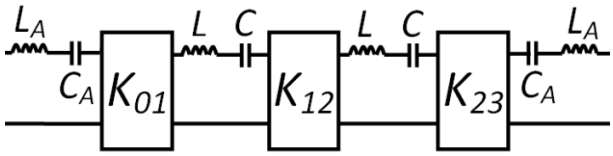

(b)

Fig. 6. (a) Layout of second order tunable filter (b) Equivalent circuit of filter

The filter may be analyzed in terms of ABCD parameters of the equivalent circuit to extract a relationship for the pole separation. L_A and C_A will have no affect on the pole separation, so their effects are not considered in the derivation. The ABCD parameters of the equivalent circuit, given in (12), where$Z = sL + 1/sC$, may be used to evaluate the impedance matrix parameter Z_{21}, whose poles are also the poles of the filter. Solving for this leads to the split angular resonant frequencies as given by (14). This result may be extended to show that the separation of the two resonant frequencies is given by (15).

$$\begin{pmatrix} \boldsymbol{A} & \boldsymbol{B} \\ \boldsymbol{C} & \boldsymbol{D} \end{pmatrix} = \begin{pmatrix} -\frac{\boldsymbol{jZ}}{\boldsymbol{K_{12}}} & -\frac{\boldsymbol{jK_{01}^2}}{\boldsymbol{K_{12}}} \\ -\frac{\boldsymbol{j\left(\frac{K_{12}}{K_{01}}+\frac{Z^2}{K_{12}K_{12}}\right)}}{\boldsymbol{K_{01}}} & -\frac{\boldsymbol{jZ}}{\boldsymbol{K_{12}}} \end{pmatrix} \tag{12}$$

$$Z_{21} = \frac{1}{C} = \frac{-j\omega^2 C^2 K_{01}^2 K_{12}}{\omega^4 L^2 C^2 - \omega^2 (2LC + K_{12}^2 C^2) + 1} \tag{13}$$

$$\omega_p = \frac{1}{\sqrt{LC}} \left(1 \pm \frac{K_{12}}{2} \sqrt{\frac{C}{L}} \right) \tag{14}$$

$$\omega_1 - \omega_2 = \frac{1}{\sqrt{LC}} \left(K_{12} \sqrt{\frac{C}{L}} \right) = \frac{K_{12}}{L} \tag{15}$$

The pole separation is, indeed, independent of the capacitance, *C*, and is fixed to a simple ratio. Since the filter tuning mechanism is based on capacitive tuning, it is evident that the pole separation will be constant over the tuning range as long as the ratio K_{12}/L is constant. It is reasonable to assume that the resonator inductance is constant from previous discussions. The K_{12} inverter impedance is however subject to a significant frequency deviation if regular coupled lines were employed for inter-resonator coupling (about 15% across the tuning range), which degrades the bandwidth regulation of the filter. A modified inter-resonator coupling structure is thus employed, as depicted in Fig. 6 (a), to mitigate this frequency variation to around 5 % so to improve the filter performance.

The proposed coupling structure depicted in Fig. 7 may also be modelled with the circuit in Fig. 3(b), except that the value of *K*, L_A and C_A are now described by equations (16)-(18), where $Z_{11NEW}(f_L)$ is the value of the driving point impedance of at the lowest resonant frequency. An optimum line impedance for Z_N, which yields the lowest possible variation in *K*, is given by equation (21), where θ_{NL} corresponds to the electrical length of the stub at the lowest resonant frequency used in the filter. The proposed modification effectively lowers the frequency at which the inverter impedance attains a minimum to the centre of the frequency tuning range. Since the inverter impedance function happens to be symmetrical about the minimum, the overall variation in the inverter impedance is better constrained.

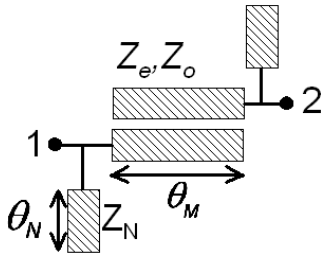

Fig. 7. Proposed inter-resonator coupling structure

$$C_A = \frac{5}{18\pi f_L Z_{11NEW}(f_L)} \tag{16}$$

$$L_A = \frac{4}{18\pi^2 f_L C_A} \tag{17}$$

$$K = \frac{Z_{12}Z_s^2}{(Z_{11} + Z_s + Z_{12})(Z_{11} + Z_s - Z_{12})} \tag{18}$$

$$Z_{11NEW} = \frac{Z_s({Z_{11}}^2 + Z_s Z_1 - {Z_{12}}^2)}{(Z_{11} + Z_s + Z_{12})(Z_{11} + Z_s - Z_{12})} \tag{19}$$

$$Z_s = -jZ_N \cot(\theta_N) \tag{20}$$

$$Z_{Nopt} = \frac{(Z_e + Z_o)}{(2 - \sqrt{3})\cot(\theta_{NL})} \tag{21}$$

It is generally desirable to limit the electrical lengths of the added stubs below 15^0 to conserve circuit space. Fig. 8 compares the variation in inverter impedance of a regular coupled line to that of the modified coupled line and illustrates the effectiveness of the proposed technique, where $\theta_1 = 60^0$ at 2 GHz, $Z_e = 60\ \Omega$ and $Z_o = 40\ \Omega$.

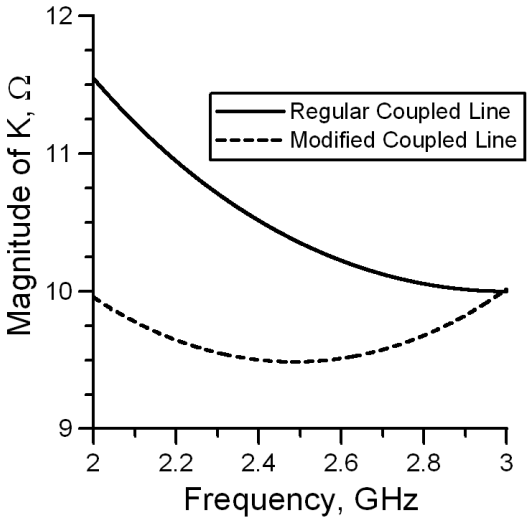

Fig. 8. Inverter impedance of regular and modified coupled lines

As an illustration of the effectiveness of the modification, taking Z_{e1} = 51 Ω, Z_{o1} = 49 Ω, Z_e = 53 Ω, Z_o = 48 Ω, Z_2 = 75 Ω, and $\theta_1 = 60^0$ and $\theta_2 = 20^0$ at 2 GHz and varying C_0 from 0.75 pF to 8 pF, it may be seen that there is only a 3.9 % deviation in pole separation in the whole tuning range from 2.15 GHz to 2.85, GHz as plotted in Fig. 9, for a weakly coupled second order tunable filter. As the deviation is quite small, it is not necessary to include additional tuning elements between the resonators for the adjustment of the inter-resonator coupling. Finally, it should be noted that, the filter model and the related approximations are valid only for narrowband filters.

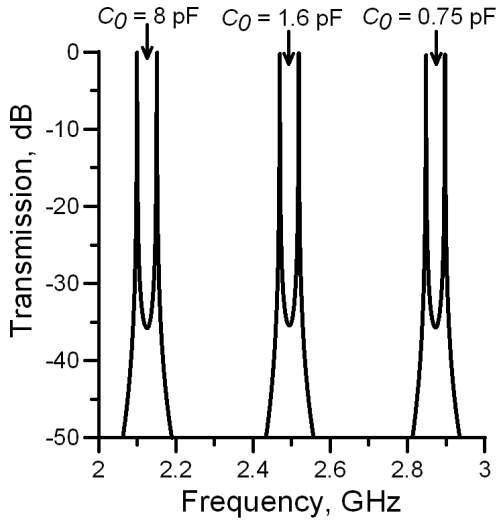

Fig. 9. Simulated deviation in pole separation with centre frequency of 2nd order tunable filter

Before demonstrating a few examples, design equations (22) and (23) are provided to facilitate filter design, where Z_0 is the source/load impedance, L is the series resonator inductance as illustrated in Fig. 6 (b) which may be determined from (7) and B is the fractional bandwidth at the highest mid-band angular frequency of the tunable filter ω_H [17].

$$K_{01} = K_{n,n+1} = \sqrt{\frac{L\omega_H Z_0 B}{g_0 g_1}} \tag{22}$$

$$K_{i,i+1} = L\omega_H B \sqrt{\frac{1}{g_i g_{i+1}}}\Bigg|_{i=1\ to\ n-1} \tag{23}$$

Due to various inter-coupling within the open loop structure, as well as the reactance due to L_A and C_A at the source and load ends of the filter, these equations will not lead to a perfect initial response. The design equations must only be used to obtain a good first approximation to the desired specification. These values for the inverter impedances, in conjunction with condition (11), may be used to set the modal impedances of the coupled lines. With knowledge of the coupled line parameters, L_A and C_A may be determined and, from this, it is possible to determine $L_B = 0.5(L-2L_A)$. This value of L_B can then be used to obtain values for Z_2 and θ_2 using equation (5).

4.0 TUNABLE FILTER APPLICATIONS

This section will describe two filter design examples where the proposed tunable resonator is employed. The first example details the design of a second order tunable bandpass filter, where the modelled results are compared against simulations and experimental measurements for assessment of the model as well as filter performance. The second example demonstrates a third order tunable filter design where simulated results are compared against theoretical results to support the discussion.

4.1 Example A: 2nd Order Chebyshev Tunable Bandpass Filter

A second-order tunable bandpass filter is designed and demonstrated. The filter was designed on a substrate of relative dielectric constant 2.2 and a thickness of 1.575 mm. The assumed specification required a 3-dB bandwidth of 160 MHz and tuning range from 2.0 GHz to 2.5 GHz. The dimensions of the filter are outlined in Fig. 10.

Transmission and reflection parameters of the filter obtained from the theoretical model, simulations and experimental measurements under four different tuning capacitance values (2 pF, 4 pF, 10 pF and 20pF) are illustrated in Fig. 11. The varactor resistance was assumed to be 1 Ω for the purposes of simulations and filter modeling in order to obtain more realistic results. A photograph of the fabricated filter is illustrated in Fig. 11 (c). Low insertion loss (3 dB maximum) and high return loss (15 dB minimum) are observed across the tuning range. There is good agreement between the modeled, simulated and measured results.

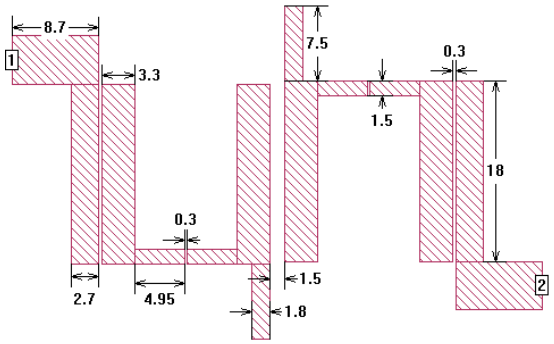

Fig. 10. Dimensions in millimeters of tunable filter

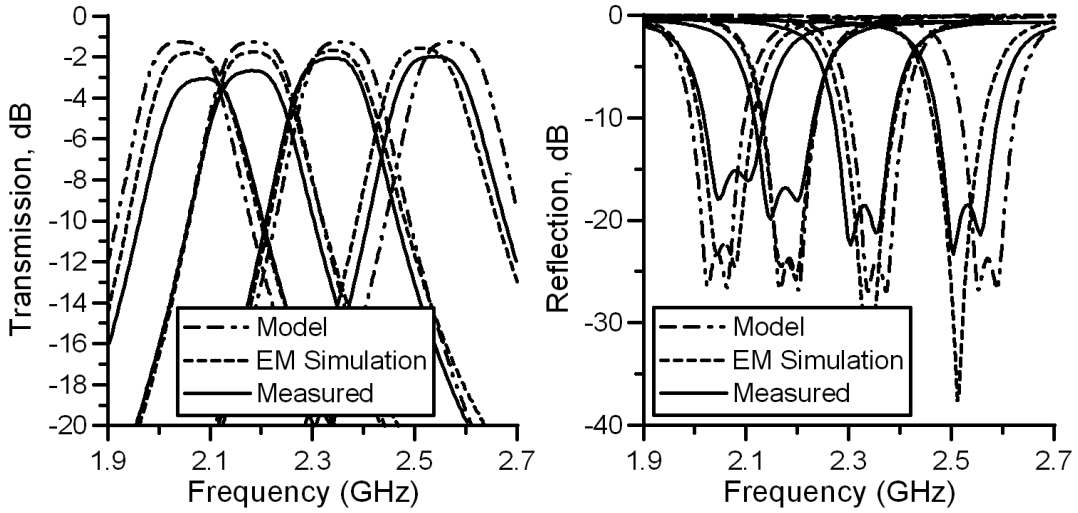

(a) (b)

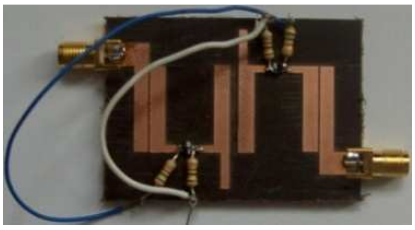

(c)

Fig. 11. Modeled, simulated and experimentally measured (a) Transmission parameters (b) Reflection parameters (c) Photograph of filter

The 3-dB bandwidth of the measured filter response was 160 MHz at 2.1 GHz and 165 MHz at 2.55 GHz corresponding to 3% change in bandwidth. The simulated response was nearly identical, showing a 3-dB bandwidth of 160 MHz at 2.05 GHz and 164 MHz at 2.5 GHz. The filtering characteristic is relatively unaltered across the tuning. A pass-band shift of 450 MHz is achieved experimentally and this amounts to a 22.5% overall shift.

In this design, two varactor diodes (model number BB833E6327) in a parallel configuration were used to implement each tuning capacitance, primarily to reduce the losses. As a consequence, the lowest possible capacitance attainable from the pair was limited to around 2 pF. It is possible to achieve a higher percentage shift of up to 50% with a tuning capacitance which can be tuned a lower capacitance. This is possible if a single diode is used, but the resulting design may exhibit extra loss especially at lower frequencies, since the series resistance of the varactor diode varies inversely with the varactor bias voltage. The effect of this variation is observed in the transmission response of the filter, with the insertion loss improving at higher passband frequencies. There are of course other higher order effects due to varactor diodes on tunable filter performance and a comprehensive coverage of these may be found in [15].

4.2 Example B: Third Order Tunable Bandpass Filter

This section demonstrates a third order tunable constant bandwidth filter. Substrate parameters are the same as those in example A. The design specification is a third order tunable Chebyshev filter with 3-dB bandwidth of 110 MHz, a tunable range from 2 GHz to 3 GHz and a pass-band ripple of 0.043 dB. Using (22) and (23), the

corresponding modal impedances of the coupled lines were found to be $Z_{e01} = Z_{e34} = 65.24\ \Omega$, $Z_{e12} = Z_{e23} = 54.08\ \Omega$, $Z_{o01} = Z_{o34} = 34.76\ \Omega$ and $Z_{o12} = Z_{o23} = 45.92\ \Omega$. The other parameters were $Z_2 = 100\ \Omega$, $Z_N = 65.8\ \Omega$, $\theta_2 = 16^0$ and $\theta_N = 10^0$ both at 2 GHz. These parameters were translated to microstrip line parameters using Agilent ADS. Simulation results are compared to theoretical results obtained from the model and are illustrated in Fig. 12, where the series varactor loss is assumed to be 1 Ω. The 3-dB bandwidth varied from around 107 MHz at 2.05 GHz to 112 MHz at 2.9 GHz, corresponding to a 4.5% deviation in bandwidth across a frequency shift of 42%.

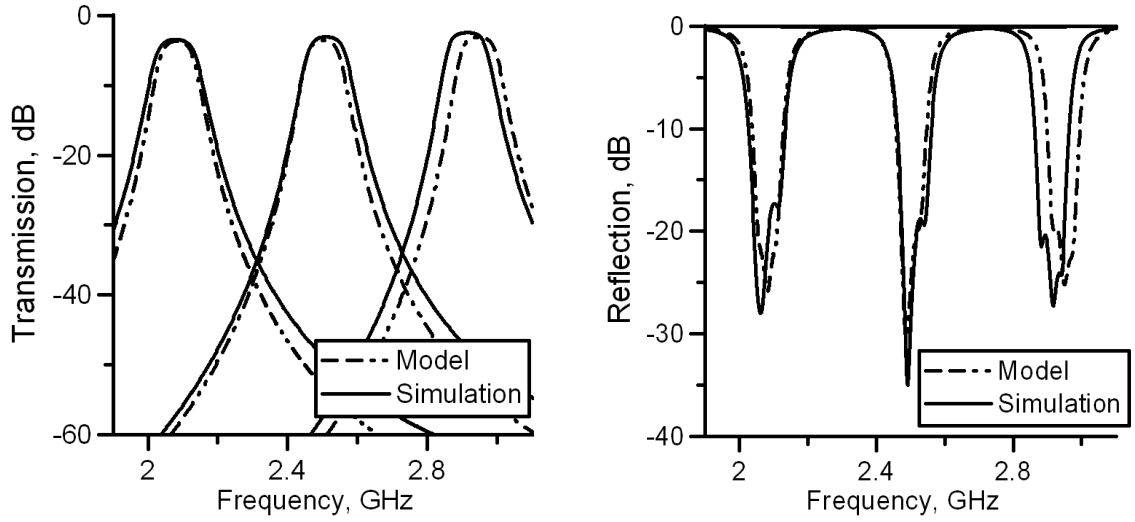

(a) (b)

Fig. 12. Comparison of simulated results against results from the filter model of third order bandpass filter, where $C_0 = 0.7$ pF for higher pass-band, $C_0 = 1.5$ pF for middle pass-band, $C_0 = 10$ pF for lower pass-band.

5.0 CONCLUSIONS

Compact tunable constant bandwidth filters, with a wide tuning range, based on asymmetrically coupled open-loop resonators, were presented. It is shown that up to 50% tuning range is available for constant bandwidth tuning, where variation in bandwidth can be limited to below 5%. Presented experimental results are in excellent agreement to theory, where the minimum return loss was better than 15 dB, maximum insertion loss was better than 3 dB for a 22.5% tuning range. The full 50% tuning range would be possible with a high capacitance ratio varactor diode.

Since varactors are situated across the virtual earth of the structure, sufficient RF isolation was achieved by employing resistors to avoid cumbersome DC bias circuitry. Compensation for correcting variations in coupling coefficient and *Q* factor is proposed so that these need not be tuned. An N^{th} order filter will therefore require only N tuning varactors simply to change the natural resonant frequencies. A design method is provided so that Butterworth and Chebyshev filters may be fabricated relatively quickly. Finally, higher order filters are demonstrated through simulation with 50% pass-band shift with around 4.5% variation in 3-dB bandwidth. The relative compactness, high consistent return-loss, low consistent insertion-loss, wide tuning range and excellent control of bandwidth makes this candidate a very practical solution.

REFERENCES

[1] Y.H Chun and J.S Hong.: 'Electronically reconfigurable dual-mode microstrip open-loop resonator filter' *IEEE Microw. And Wireless Comp. Lett.*, 2008, Vol. 18, No. 7, pp. 449-451.

[2] P.W. Wong, I.C. Hunter.: 'Electronically Reconfigurable Microwave Bandpass Filter', *IEEE Microw. Theory and Trans*., 2009, Vol. 57, No. 12, pp. 3070-3079.

[3] P.W. Wong, I.C. Hunter.: 'A new class of low-loss high-linearity electronically reconfigurable microwave filter', *IEEE Microw. Theory and Trans*., 2008, Vol. 56, No. 8, pp.1945-1953.

[4] Y.M. Chen, S.F. Chang et al.: 'A reconfigurable bandpass-bandstop filter based on varactor-loaded closed-ring resonators', *Microwave Magazine, IEEE*, 2009, Vol. 10, Issue 1, pp. 138-140.

[5] L.-H. Hsieh and K. Chang.: 'Tunable microstrip bandpass filters with two transmission zeros' *IEEE Trans. Microw. Theory Tech.*, 2003, Vol. 51, No. 2, pp. 520–525.

[6] M. Makimoto and M. Sagawa.: 'Varactor tuned bandpass filters using microstrip-line ring resonators' *IEEE MTT-S Int. Microw. Symp. Dig.*, 1986, pp. 411–414.

[7] I.C. Hunter and J.D Rhodes.: 'Electronically tunable microwave bandpass filters', *IEEE Trans. Microw. Theory Tech.*, 1982, Vol. 30, No. 9, pp. 1354-1360

[8] B.-W. Kim and S.-W. Yun.: 'Varactor-tuned combline bandpass filter using step-impedance microstrip lines', *IEEE Trans. Microw. Theory Tech.*, 2004, Vol. 52, No. 4, pp. 1279–1283

[9] B.E.C Smith,P.A Warr, M.A Beach.: 'Wide Tuning Range Planar Filters Using Lumped-Distributed Coupled Resonators', *IEEE Trans. Microw. Theory Tech.*, 2005, Vol. 53, No. 2, pp. 777–785

[10] L.Athukorala, D.Budimir.: 'Frequency Tunable Microstrip Resonators and Filters', *Proc. EuMC'09*, 2009, pp. 1239-1242

[11] W.M. Fathelbab and M.B.Steer.: 'A reconfigurable bandpass filter for RF/microwave multifunctional systems', *IEEE Trans. Microw. Theory Tech.*, 2005, Vol. 53, No. 3, pp. 1111-1116

[12] H.Joshi, H.H.Sigmarsson, S.Moon, D Peroulis and W.J Chappell.: 'High Q fully reconfigurable tunable bandpass filters', *IEEE Trans. Microw. Theory Tech.*, 2009, Vol. 57, No. 12, pp. 3525-3533

[13] B. Kapilevich.: 'A varactor-tunable filter with constant bandwidth and loss compensation', *Microw. J.*, 2007, Vol. 50, No. 4, pp. 106–114

[14] S.J Park and G.M. Rebeiz.: 'Low-loss two-pole tunable filters with three different predefined bandwidth characteristics', *IEEE Trans. Microw. Theory Tech.*, 2008, Vol. 56, No. 5, pp. 1137-1148

[15] B.E.C Smith and P.A Warr.: 'Distortion mechanisms in varactor diode –tuned microwave filters', *IEEE Trans. Microw. Theory Tech.*, 2006, Vol. 54, No. 9, pp. 777–785

[16] J.S Hong and M.J. Lancaster.: 'Couplings of microstrip square open-loop resonators for cross-coupled planar microwave filters', *IEEE Microw. Theory and Trans.*, 1996, Vol. 44, No. 11, pp. 2099-2109.

[17] J.S Hong and M.J. Lancaster.: 'Microstrip filters for RF/microwave applications', (Wiley, New York, 2001)

Compact Filter Configurations Using Concentric Microstrip Open-Loop Resonators

L.Athukorala, *Student Member, IEEE* and D.Budimir, *Senior Member, IEEE*,

***Abstract*—This paper presents two highly compact filter configurations using concentric open-loop resonators. A description of each filter configuration is presented, where a linkage between structural features and coupling coefficients is outlined. A third order trisection and a fourth order source-load coupled filter were designed and fabricated at 1.0 GHz, and each filter was shown to occupy an area of just 18 mm by 18 mm. The measured insertion loss of the third and fourth order filters was 0.83 dB and 1.20 dB respectively. Moreover, these structures may also be cascaded to produce higher order compact filters.**

***Index Terms*—compact filter, microstrip filter, bandpass filter**

I. Introduction

MICROSTRIP bandpass filters find extensive applications in low to medium power RF and microwave technology due to size, cost, weight, and fabrication advantages.

Filter miniaturisation can not only be used for realising compact filters. Various approaches to microstrip filter miniaturisation may be found in recent research work. Some distinctly miniature filters reported in literature include the use of dual-mode resonators [1]-[5], slow-wave resonators [6], multilayer filters [7], meandering [8], high dielectric constant substrates [9] and lumped element filters [9]. Slow-wave designs are not so practical for high fractional bandwidths although they offer excellent wideband response. Multilayer structures introduce complexity and additional tolerances to the fabrication process while realising lumped-elements may not always be practical. The idea of concentric resonators has been recently explored in multiband filter design [12].

Dual-mode resonator based filters are naturally compact and generally offer the same fabrication simplicity as a regular microstrip filter. A number of highly compact dual-mode filters found in recent research include the open-loop [2], circular-ring [3], square [4] and triangular [5] structures.

This paper presents two highly compact filter configurations for developing microstrip trisection and quadruplet filters. Both structures are based on the dual-mode resonator, reported in [1]. With the proposed configurations, however, the filter size is effectively halved. Compactness was achieved by inserting concentric resonators within the loop of the dual-mode resonator. Moreover, these filter configurations can be readily employed in designing high order, low loss, super compact microstrip filters.

The authors are with the Department of Electronic, Communication and Software Engineering, University of Westminster, 115 New Cavendish Street, London, W1W 6UW, United Kingdom, E-mail: d.budimir@wmin.ac.uk

II. Trisection Filter Configuration

A trisection filter consists of three coupled resonators which may be realised with the filter section illustrated in Fig. 1 (a). Resonators 1 and 3 are a product of the dual-mode resonator presented in [1], while the central resonator is a single-mode open loop structure. Although a comprehensive design procedure for trisection filters may be found in [9], a simple electromagnetic simulation based design process is outlined.

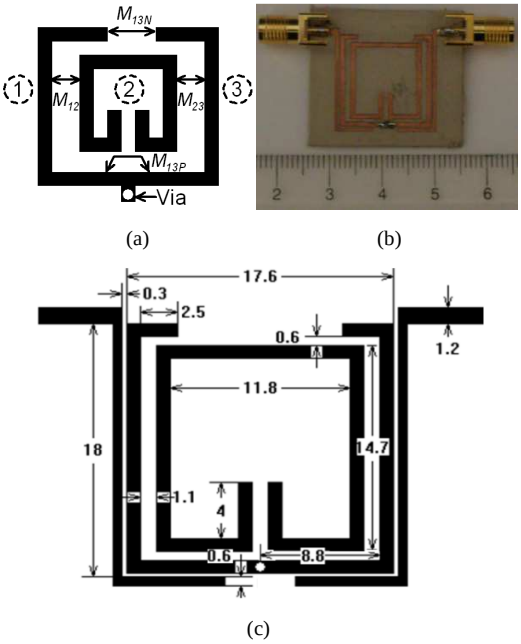

Fig. 1. (a) Resonator arrangement and coupling mechanism of trisection filter (b) Photograph of fabricated filter (c) Layout of fabricated parallel coupled trisection filter with dimensions in mm (via diameter = 0.6 mm).

The coupling mechanism of the filter is illustrated in Fig. 1 (a), where M_{13P} and M_{13N} are couplings with $+90^0$ and -90^0 phase respectively. When designing third order filters, the identical M_{12} and M_{23} coupling coefficients result in equal spacing of asymmetrically driven coupled lines on either side of the central resonator preserving physical symmetry. M_{S1} and M_{3L} coupling coefficient is adjusted by varying the gap of the input output coupled lines.

The assumed filter specification for the trisection filter is as follows: 1 GHz center frequency, 0.01 dB ripple, 10% fractional bandwidth, transmission zero located at 0.8 GHz. The specification may be used to compute the normalized lowpass prototype coupling matrix, $m_{,}$ from optimization, as given by (1), where the diagonal entries denote the normalized resonator de-tuning parameters b_i for the i^{th} resonator.

$$m = \begin{bmatrix} 0 & 1.20 & 0 & 0 & 0 \\ 1.20 & -0.15 & 1.15 & 0.3 & 0 \\ 0 & 1.15 & 0.2 & 1.15 & 0 \\ 0 & 0.3 & 1.15 & -0.15 & 1.20 \\ 0 & 0 & 0 & 1.20 & 0 \end{bmatrix} \quad (1)$$

Once the coupling matrix is obtained, the angular resonant frequencies, ω_i, of the resonators may be computed from (2), where ω_0 is the filter mid-band radian frequency and F is the filter fractional bandwidth. The coupling coefficients M_{12} and M_{13} may be extracted with the aid of an electromagnetic simulation package together with (3) and (4), where ω_P is either the upper or lower radian pole frequency and ω_Z is the transmission zero frequency of the weakly excited filter. M_{12} is inversely proportional to the coupled line spacing between resonators 1 and 2. The sign of M_{13} determines the position of the transmission zero. The sign may be selected by opting for the dominant cross coupling to be either capacitive coupling via M_{13N} or inductive coupling via M_{13P}. To this end, the length of the short circuited stub or the gap width between the open circuited arms may be used to adjust M_{13} precisely.

$$\omega_i = \omega_0 \frac{-Fb_i + \sqrt{(Fb_i)^2 + 4}}{2} \quad (2)$$

$$M_{12} = M_{23} = \sqrt{\frac{\omega_{pN}^2 + (b_1 + b_2)\omega_{pN} + b_1 b_2}{2 - \dfrac{\omega_{pN} + b_2}{\omega_{zN} + b_2}}} \quad (3)$$

$$M_{13} = \frac{-M_{12}^2}{b_2 + \omega_{zN}} \quad (4)$$

, where

$$\omega_{(p/z)N} = \frac{1}{F}\left[\frac{\omega_{(P/Z)}}{\omega_0} - \frac{\omega_0}{\omega_{(P/Z)}}\right] \quad (5)$$

The filter was designed and fabricated on Rogers 6010 LM substrate with a relative dielectric constant of 10.2 and substrate thickness of 1.27 mm. The layout of the filter is detailed in Fig. 1 (c). The transmission and reflection parameters of the theoretical, simulated and measured filter response are compared in Fig. 2. There is good overall agreement between simulation and measurement. The measured mid-band insertion loss of the filter, mainly due to conductor loss, was 0.83 dB. The fabricated bandpass filter is seen to occupy an area of around 18 mm by 18 mm.

III. Quadruplet Filter Configuration

The generic fourth order filter section illustrated in Fig. 3 (a) consists of a pair of coupled dual-mode resonators proposed in [1]. The proposed configuration, however, provides significantly better size reduction and also may be conveniently employed in the development of high order cascaded quadruplet filters such as [9], since the structure permits both positive and negative cross coupling to be established between resonators 1 and 4 rather easily. Comprehensive analysis of the dual-mode resonator is presented in [1] and is therefore is not repeated here.

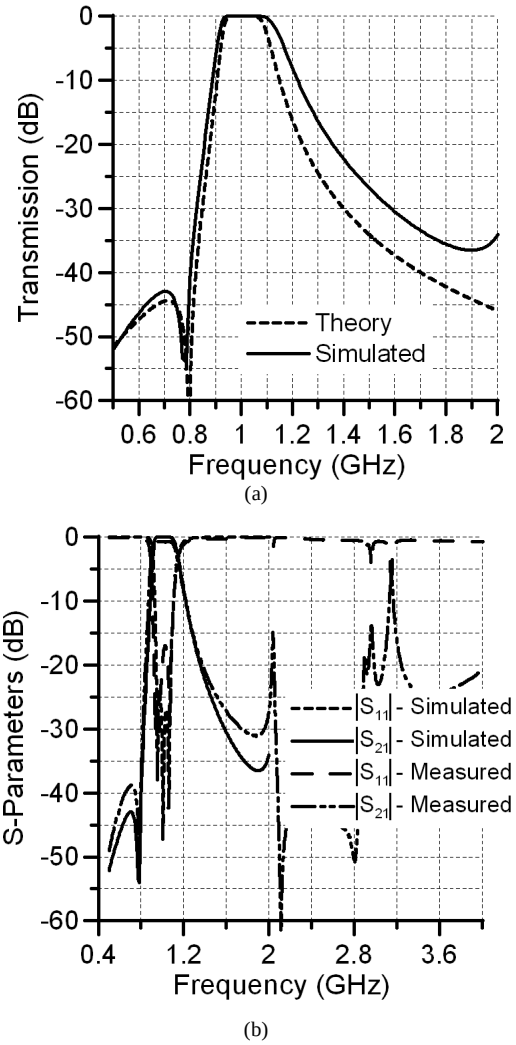

Fig. 2 (a) Comparison of (a) theoretical and simulated (b) simulated and measured response of microstrip trisection bandpass filter.

The unit is physically symmetric for fourth order designs due to the equivalence of M_{12} and M_{34}. As illustrated in Fig. 3 (a), the M_{14P} and M_{23P} introduce positive coupling while M_{14N} and M_{23N} generate negative coupling. These may be readily adjusted to obtain the required coupling sign and magnitude. Higher filter orders, such as 8 or 12 may be realised simply by cascading two or three such units respectively.

A fourth order filter example is presented to demonstrate the compact filter configuration. The filter designed at a center frequency of 1.0 GHz, 0.01 dB ripple, and 10% fractional bandwidth employs source load coupling to generate a pair of transmission zeros which improves skirt selectivity. The filter was designed, optimized and fabricated on Rogers 6010 LM substrate with a relative dielectric constant of 10.2 and substrate thickness of 1.27 mm, where the final coupling coefficients are given by (6). The layout of the filter is illustrated in Fig. 3 (c). The S-parameters of the simulated and measured filter response are compared in Fig. 4. The measured mid-band insertion loss of the filter was around 1.20 dB.

$$[m] = \begin{bmatrix} 0 & 1.184 & 0 & 0 & 0 & -0.00015 \\ 1.184 & 0 & 1.081 & 0 & 0 & 0 \\ 0 & 1.081 & 0 & 0.794 & 0 & 0 \\ 0 & 0 & 0.794 & 0 & 1.081 & 0 \\ 0 & 0 & 0 & 1.081 & 0 & 1.184 \\ -0.00015 & 0 & 0 & 0 & 1.184 & 0 \end{bmatrix} \quad (6)$$

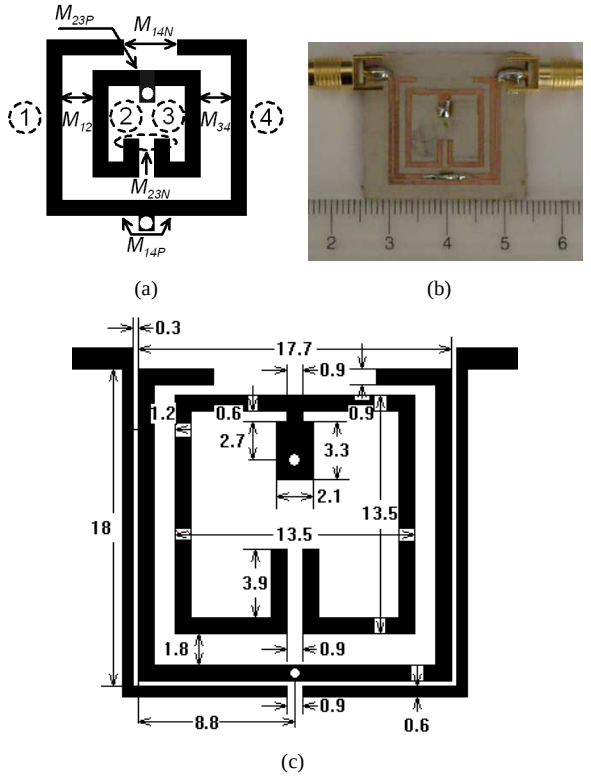

Fig. 3 (a) Resonator arrangement and coupling mechanism of quadruplet filter section (b) Photograph of fabricated filter (c) Layout of fabricated parallel coupled quadruplet filter with dimensions in mm (via diameter = 0.6 mm).

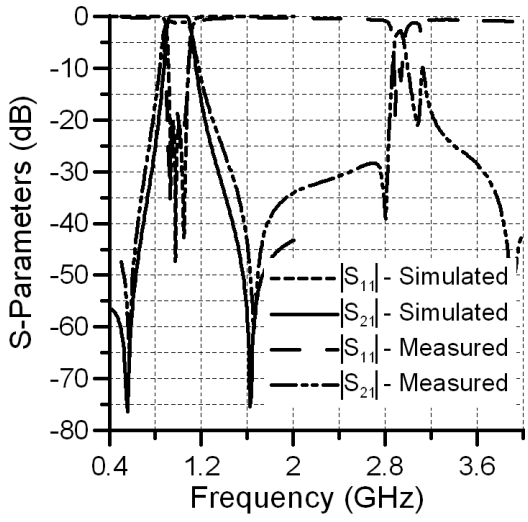

Fig. 4 Comparison of simulated and measured response of microstrip fourth order source-load coupled bandpass filter.

IV. Conclusion

This paper has presented two highly compact filter configurations with concentric open-loop resonators. A description of the filter configurations was supported with filter examples for illustration and verification. The trisection filter and the fourth order filter were designed and fabricated at a centre frequency of 1.0 GHz with a measured passband insertion loss of 0.83 dB and 1.20 dB respectively. Each filter occupied an area of just 18 mm by 18 mm. Moreover, these filter sections may be readily cascaded to produce compact high order filters with low loss.

The trisection filter occupies approximately a third of the circuit area relative to a regular single mode open-loop configuration [6]. The third order filter proposed in [10] occupies roughly the same area as the trisection filters proposed here. However, the filters proposed in this paper achieve a much wider stop-band. Relative to the triple order bandpass filter [11], this configuration is 66 % more compact due to the utilization of the concentric resonator. The quadruplet filter configuration occupies roughly 50% of the area relative to filters described in [1] and [2].

References

[1] L. Athukorala and D. Budimir, "Design of compact dual-mode microstrip filters", *IEEE Trans. Microw. Theory Tech.*, vol. 58, no. 11, pp. 2888-2895, Nov. 2010.

[2] J.S. Hong, H. Shaman and Y.H. Chun, "Dual-mode microstrip open-loop resonators and filters", *IEEE Trans. Microwave Theory and Tech.*, Vol. 55, No. 8, pp. 1764 – 1770, Aug. 2007.

[3] U. Karacaoglu, I.D. Robertson and M. Guglielmi, " An improved dual-mode microstrip ring resonator filter with simple geometry", *Proc. European Microwave Conference*, pp 472-477, 1994.

[4] L.-H. Hsieh and K. Chang, "Compact, Low Insertion-Loss, Sharp-Rejection, and Wide-Band Microstrip Bandpass Filters", *IEEE Trans. Microw. Theory and Tech.*, Vol. 51, No. 4, pp. 1241 – 1246, Apr. 2003.

[5] J.S. Hong and S. Li, "Theory and Experiment of Dual-Mode Microstrip Triangular Patch Resonators and Filters", *IEEE Trans. Microwave Theory and Tech.*, Vol. 52, No. 4, pp. 1237 – 1243, Apr. 2004.

[6] J.S. Hong and M.J Lancaster, "Theory and experiment of novel microstrip slow-wave open-loop resonator filters", *IEEE Trans. Microw. Theory and Tech.*, Vol. 45, No. 12, pp. 2358 – 2365, Dec. 1997.

[7] J.S. Hong and M.J Lancaster, "Aperture-Coupled Microstrip Open-Loop Resonators and Their Applications to the Design of Novel Microstrip Bandpass Filters", *IEEE Trans. Microwave Theory and Tech.*, Vol. 47, No. 9, pp. 1848 – 1855, Sep. 1999.

[8] S.-M. Wang, C.-H. Chi, M.-Y. Hsieh, and C.-Y. Chang, "Miniaturized Spurious Passband Suppression Microstrip Filter Using Meandered Parallel Coupled Lines", *IEEE Trans. Microwave Theory and Tech.*, Vol. 53, No. 2, pp. 747 – 753, Feb. 2005.

[9] J.S Hong., M.J Lancaster, *Microstrip filters for RF/Microwave applications*, *John Wiley*, Chapter 10, pp. 315 – 377, 2001.

[10] M. Zhou, X. Tang, and F. Xiao, "Compact Transversal Bandpass Filter Incorporating Microstrip Dual-Mode Open-Loop Resonator and Slot Line Resonator with Source-Load Coupling,' *Microwave and Optical Tech. Lett.*, Vol. 51, No. 12, pp. 2927-2929, Dec. 2009.

[11] F. Xiao, M. Norgren and S. He, "Compact third-order microstrip bandpass filter using hybrid resonators," *Progress in Electromagnetics Research C*, Vol. 19, 93-106, 2011.

[12] RH Geschke, B Jokanovic, P Meyer, 'Filter Parameter Extraction for Triple-Band Composite Split-Ring Resonators and Filters', IEEE Transactions on Microwave Theory and Techniques, vol. 59, no. 6, June 2011, pp 1500-1508.

Compact Second-Order Highly Linear Varactor-Tuned Dual-Mode Filters With Constant Bandwidth

Lakshman Athukorala, *Student Member, IEEE*, and Djuradj Budimir, *Senior Member, IEEE*

***Abstract*—This paper presents a compact highly linear tunable second-order quasi-elliptic filter with constant 3-dB bandwidth. The proposed filter is thoroughly analyzed to clearly describe the filter equivalent circuit and the tuning mechanism involved. In addition, the tunable resonator configuration employed is shown to improve filter linearity, especially for low bias voltages where distortion is normally stronger. A quasi-elliptic tunable filter was designed, built, and tested for illustration and verification. With a 3-dB bandwidth variation of only 4.6%, the filter had a frequency coverage from 1.45 to 1.96 GHz, an insertion loss better than 2.5 dB, and measured IIP3 $>$ 43 dBm throughout. The experimental results are in excellent agreement to theory and simulations.**

***Index Terms*—Constant bandwidth, distortion, dual mode, microstrip filter, tunable filter, varactor.**

I. Introduction

TUNABLE bandpass filters are in increasing demand in current and emerging multifunctional RF and microwave wireless systems. Typical applications of such filters include multiband communication systems, where a single transceiver may operate on multiple bands. Generally the channel bandwidth may differ for each channel, but in some applications, it may be identical.

Compactness, tuning range, and linearity are key performance measures of tunable filters. Miniaturized filters are always more practical in modern communication systems where circuit space is very costly. Filter tuning range has a direct impact on the range of services the system is able to offer. Low signal distortion is a feature that is vital in filters operating with high input powers.

Research into tunable RF filters is growing sharply and includes work presented in [1]–[20], where various degrees of tunability have been quoted for various structures. A tunable filter with 45% tuning range is presented in [2], but it consumes a relatively large amount of circuit area. A tunable open-loop filter with constant bandwidth is presented in [5] where a piezoelectric transducer (PET) was used for tuning. Apparently, the PET had little effect on the filter bandwidth that facilitated the design of the fixed-bandwidth tunable filter. However, only 10% tunability was achieved due to limitations of the PET. Tunable comb-line filters were first presented in [7], where 53% tunability had been achieved, but with wide variation (12%) in absolute bandwidth and high loss (6 dB).

In [13], a tunable filter is presented where an optimization method was used to design coupling structures. However, this approach cannot be adopted to design filters with prescribed filtering functions. Tang *et al.* [15] have recently developed a new constant bandwidth tunable dual-mode bandpass filter with an excellent tuning range. The proposed filter also produces a single transmission zero enhancing the skirt selectivity of the filter, but it requires three identical varactors.

More recently, tunable filter linearity has also become a point of interest. Peng *et al.* [3] have proposed a novel constant bandwidth p-i-n diode based reconfigurable filter with improved linearity, where the filter tuning range was quoted to be 35% and a measured IIP3 $>$ 32 dBm. Although the losses are low (1.7 dB), the filter consumes a relatively large circuit area and does not allow continuous center frequency tuning. A varactor diode based tunable second-order filter has been presented in [16] with a tuning range of 35%, but with a bandwidth variation of around 15% and measured third-order intermodulation intercept point (IIP3) between 22–42 dBm. This kind of IIP3 variation is very typical of varactor tuned circuits where the varactor linearity improves with increasing reverse voltage.

This paper presents a novel highly linear second-order varactor-tuned filter with constant 3-dB bandwidth. Filter equivalent circuits are presented and thoroughly analyzed to describe the variation and control of coupling coefficients and quality factor. A resonator configuration that provides an improvement in linearity is described clearly. It is shown that varactor based tunable filters employing such resonators do not suffer from high distortion normally experienced at low bias voltages. Furthermore, it is shown that there is considerable linearity improvement even for higher bias voltages. These filters have the advantage of simultaneously achieving a high tuning range (30%), very low bandwidth variation (less than 4.6%), excellent skirt selectivity, high linearity (IIP3 $>$ 43 dBm), and a highly compact design. The proposed filters only require two varactor diodes with common bias voltage and do not require additional tuning elements for control of coupling coefficients or the input/output quality factor. As a result, these filters are simple to design and exhibit relatively low loss.

Manuscript received February 03, 2011; revised May 10, 2011; accepted May 27, 2011. Date of publication July 22, 2011; date of current version September 14, 2011.

The authors are with the Wireless Communications Research Group, University of Westminster, London W1W 6UW, U.K., (e-mail: d.budimir@wmin.ac.uk).

Color versions of one or more of the figures in this paper are available online at http://ieeexplore.ieee.org.

Digital Object Identifier 10.1109/TMTT.2011.2160279

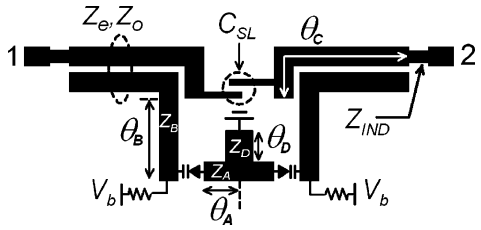

Fig. 1. Layout of dual-mode second-order tunable filter.

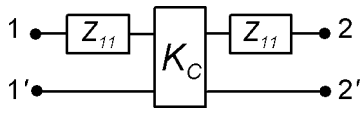

Fig. 2. Equivalent frequency-dependent coupled line model.

II. Analysis of Proposed Filter

Illustrated in Fig. 1 is the layout of the proposed second-order dual-mode tunable filter excited through 50-Ω ports labeled 1 and 2. The filter is composed of a pair of coupled lines with even- and odd-mode impedances Z_e and Z_o, respectively, and electrical length θ_C. These are connected to the ports via inductive lines with impedance $Z_{\rm IND}$. The end of each coupled line is extended to produce capacitive coupling between the source and load, where $C_{\rm SL}$ is the corresponding capacitance. A second resonance arises due to the short-circuited stub with characteristic impedance Z_D [22]. Two identical varactor diodes are required for tuning and the simple biasing circuit shown is adequate for achieving sufficient isolation.

When designing the filter, the varactor capacitance is assumed to be a maximum. In this state, the filter will operate at the lowest frequency band. Reducing the varactor capacitance causes the center frequency of the filter to increase. However, all electrical lengths in the following analysis would be referenced to the lowest operational center frequency f_L for consistency. At f_L, the electrical lengths of the lines are approximately $\theta_C \approx 60^\circ$ and $\theta_A + \theta_B \approx 30^\circ$. The tuning range of the filter is such that the highest passband center frequency is around 1.5 f_L.

Sections of the proposed tunable dual-mode filter will be described and analyzed in this section. For relatively weak source–load coupling, $C_{\rm SL}$ has a negligible impact on the filter passband performance, and therefore, the analysis of transmission zeros will be deferred to a later section.

Firstly, the coupled lines may be treated as an impedance inverter with series reactance functions, as in Fig. 2, where Z_{11} is the driving point impedance of the coupled lines [22]. For a fixed narrowband filter, the inverter may be regarded as a frequency-independent element. In contrast, although a tunable filter may have a narrow passband, it shifts across a relatively wide frequency range and it is, therefore, necessary to consider the frequency dependence of the inverter. The frequency dependence of the coupled line can be incorporated into the model by employing (1) and (2).

The remaining elements of the filter consisting of transmission lines with characteristic impedance Z_A, Z_B, and Z_D and varactor capacitance C_0 can be redrawn as Fig. 3(a). If short-circuited stub Z_D is now used to realize an impedance inverter, the equivalent circuit may be drawn as Fig. 3(b), where the inverter impedance K_L is given by (3). Fig. 3(c) illustrates the effective resonator employed in the filter. Near the resonant frequency, this structure can be shown to behave as a series resonator with effective inductance $L_{\rm eff}$ and capacitance $C_{\rm eff}$. Although these elements vary with filter midband frequency, they may be assumed constant within the passband of a narrowband filter. The varactor capacitance only alters the effective capacitance, and therefore, allows the resonators to be tuned

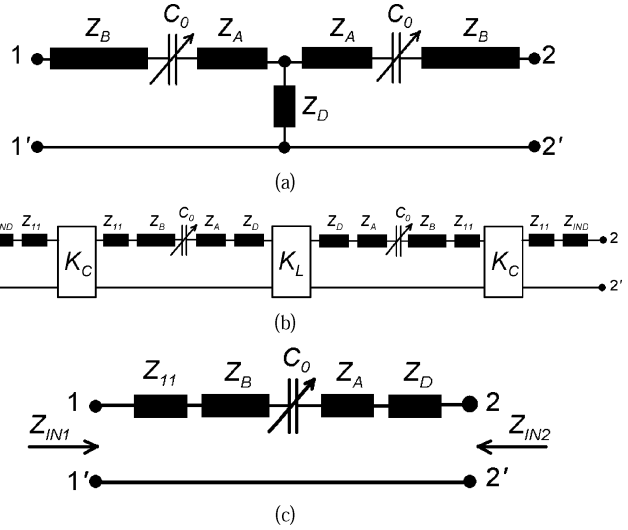

Fig. 3. (a) Filter equivalent circuit without coupled lines. (b) Filter circuit with extracted impedance inverter. (c) Effective resonator employed in the filter.

$$Z_{11} = \frac{Z_e + Z_o}{j2\tan(\theta_C)} \tag{1}$$

$$K_C = \frac{Z_e - Z_o}{2\sin(\theta_C)} \tag{2}$$

$$K_L = Z_D \tan(\theta_D). \tag{3}$$

Constant bandwidth tunability demands firstly that the input/output quality factor Q be linear with frequency at least within the filter tuning range. Expressed mathematically, this may be written as (4), where k is a constant and ω_0 is the angular midband frequency. Secondly, the pole separation, Δf, must be constant, again at least throughout the tuning range. For narrowband two-pole filters, it may be shown that the pole separation is expressed by (5), where f_H and f_L are the upper and lower pole angular frequencies, respectively. For constant pole separation, this ratio must be fixed.

The effective resonator inductance, $L_{\rm eff}$, is a key design parameter in that it not only is related to the Q factor, but also determines the pole separation. This inductance may be found from (6), where $Z_{\rm IN1}(\omega_x)$ is the input impedance of the resonator of Fig. 3(c) at angular frequency ω_x with port 2 grounded

$$Q = k\omega_0 \tag{4}$$

$$\Delta f = f_H - F_L = \frac{K_L}{2\pi L_{\rm eff}} \tag{5}$$

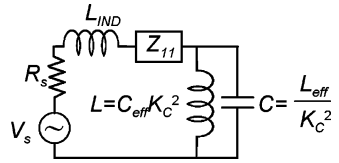

Fig. 4. Equivalent circuit for extracting input/output quality factor.

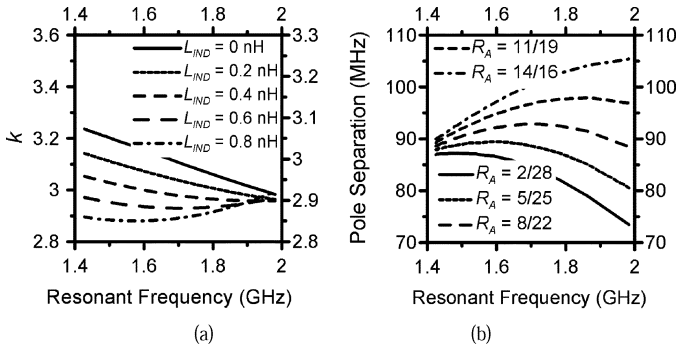

Fig. 5. (a) Variation of k against frequency for various inductances $L_{\rm IND}$, where $Z_e + Z_o = 100, \theta_B = 22°, \theta_A = 8°, \theta_C = 60°, \theta_D = 5.5°, Z_A = Z_B = 50\,\Omega, Z_D = 28\,\Omega$ where all electrical lengths are referenced to 1.4 GHz. (b) Variation of pole separation against frequency for various ratios R_A, where $\theta_A + \theta_B = 30°$.

$$L_{\rm eff} = \frac{\omega_H Z_{\rm IN1}(\omega_H) - \omega_L Z_{\rm IN1}(\omega_L)}{\omega_H^2 - \omega_L^2} \tag{6}$$

$$k = \frac{\left(R_S^2 + |Z_{11} + j\omega_0 L_{\rm IND}|^2\right)}{R_S} \times \frac{L_{\rm eff}}{K_C^2}. \tag{7}$$

The circuit in Fig. 4, obtained through narrowband approximation, may be used to determine the input/output Q factor of the filter. It is possible to show that the Q factor may be described by (4), where k is given by (7). Notice that the Q factor is not a function of the varactor capacitance since the inverter K_C has transformed this into a shunt inductance. However, due to the frequency-dependent feeding of the resonant tank and due to the frequency-dependent nature of the effective resonator inductance $L_{\rm eff}$, the Q factor is generally nonlinear. To improve linearity, it is necessary to restrict the frequency variation of k, which can be achieved by selecting an appropriate value for $L_{\rm IND}$. Fig. 5(a) plots k against resonant frequency for various values of $L_{\rm IND}$ to illustrate the relationship graphically. The center frequency is increased by lowering the varactor capacitance from around 20 to 2 pF.

With an almost linear Q factor, the second necessary condition for ensuring constant bandwidth tuning is constant pole separation. As indicated by (5), the pole separation is a function of the effective resonator inductance, as well as the inverter impedance K_L. Due to the distributed nature of the resonators, the effective inductance seen by the inverter K_L is slightly different to that defined by (6). It can be shown that the effective inductance seen by K_L is given by (8) as follows, where $Z_{\rm IN2}$ is used instead and port 1 is grounded:

$$L_{\rm eff} = \frac{\omega_H Z_{\rm IN2}(\omega_H) - \omega_L Z_{\rm IN2}(\omega_L)}{\omega_H^2 - \omega_L^2}. \tag{8}$$

It can be shown that selecting an appropriate ratio R_A of θ_A to θ_B can be employed to control $L_{\rm eff}$ in such a way as to compensate for the frequency deviation of K_L, hence enforcing the ratio in (5) to be near constant. Fig. 5(b) plots the pole separation against resonant frequency for various values of ratio R_A. Although a perfectly constant pole separation is not achieved, its variation can be restricted considerably.

The selectivity of the proposed filter is greatly enhanced by the pair of transmission zeros generated by the capacitive source–load coupling $C_{\rm SL}$ illustrated in Fig. 1. The zero conditions may be expressed approximately as the first two roots of (9) where $Z_{\rm sum} = Z_e + Z_o$ and $Z_{\rm diff} = Z_e - Z_o$. It is possible to place the transmission zeros almost independently of the passband response for weak source–load coupling.

This section has presented an accurate filter model, which was analyzed to identify the key parameters that affected tunability and bandwidth of the proposed dual-mode tunable filter. Methods of correcting the Q factor and fixing the pole separation have been described. Finally, a formula to obtain the transmission zero frequencies has been presented.

The methods proposed in this section were employed in designing the filter presented in Section IV. For brevity, the final filter parameters are given as $L_{\rm eff} \approx 8.2$ nH and $R_A \approx 8:22$

$$\frac{j}{(Z_{\rm IN1} + jK_L)\omega C_{\rm SL}} \cong \frac{Z_{\rm sum}\cot(\theta_C)}{K_L} + \frac{Z_{\rm sum}^2(Z_{\rm IN1} - jK_L)}{jK_L Z_{\rm diff}^2}. \tag{9}$$

III. Filter Distortion Analysis

The varactor depletion capacitance, C_0', is a function of the applied reverse bias voltage, $V_{\rm bias}$, as well as the RF signal, $V_{\rm RF}$, as defined by (10), where V_j is the junction potential, m is the junction grading coefficient, and C_{j0} is the zero bias capacitance. The modulation of the depletion capacitance from the RF signal introduces distortion [23]. The most detrimental distortion products are caused by third-order intermodulation (IM3) and will appear within the filter passband.

Fundamentally, for a given input power, the amount of distortion generated from a varactor diode is proportional to the RF signal voltage across it. The proposed filter is able to achieve higher linearity than most varactor tuned filters, especially for low bias voltages since the RF voltage across the varactor diode is lower for a given input power.

A simple first-order filter is analyzed to illustrate the improvement in linearity. Fig. 6 compares the proposed resonator to a typical varactor tuned series transmission line resonator, where C_0 refers to the linear capacitance of the varactor. The capacitance of a typical tunable transmission line resonator arises from the varactor capacitance alone. In contrast, the proposed resonator has a fixed capacitance, C_A, arising from Z_{11}, which is in series with the varactor capacitance C_0' [22]. This series connection of the two capacitances effectively acts as a capacitive potential divider. The reduced overall RF voltage across the varactor diode thus gives better linearity for the same input power.

Generally, varactor diodes are mostly nonlinear under low bias voltages due to the RF modulation of the bias voltage being

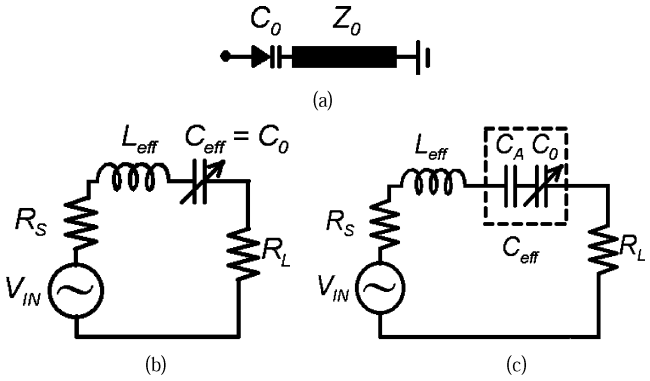

Fig. 6. (a) Regular series transmission line tunable resonator. Model of first-order filter with: (b) regular tunable resonator and (c) proposed tunable resonator.

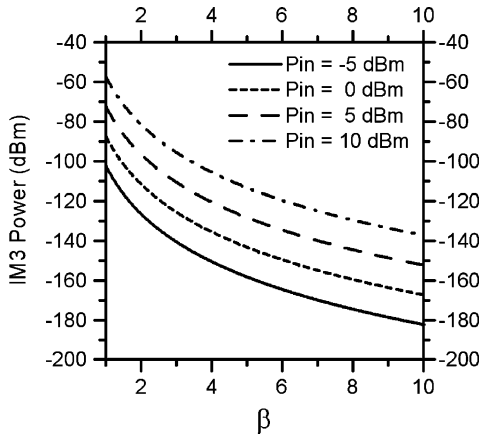

Fig. 7. Calculated IM3 powers against potential divider factor for various input powers, where tone spacing is 100 kHz, filter center frequency is 1.5 GHz, $L_{\text{eff}} = 2.5$ nH, $C_{\text{eff}} = 4.5$ pF, $C_1 = 100$ fF, and $C_2 = 50$ fF.

more significant and also due to the more sensitive nature of the capacitance at lower bias voltages. The advantage gained with the proposed resonator is that the action of the potential divider is most effective in suppressing distortion for lower bias voltages, where the distortion is normally higher

$$C_0' = \frac{C_{j0}}{\left(1 + \dfrac{V_{\text{bias}} + V_{\text{RF}}}{V_j}\right)^m} \tag{10}$$

$$C_A = \frac{5\sqrt{3}}{9\pi f_L (Z_e + Z_o)}. \tag{11}$$

For a given filter specification, L_{eff} and C_{eff} must be identical for the filters in Fig. 6(b) and (c). Therefore, the effect of the potential divider on IM3 products is analyzed using the Volterra series. The first-, second-, and third-order Volterra kernels describing the signals across the varactor of Fig. 6(c), given by (12)–(14), respectively, are shown at the bottom of this page. The varactor capacitance coefficients C_n is given by (15) as follows:

$$C_n = \frac{1}{(n+1)n!} \left. \frac{d^n C_0'(V_T)}{dV_t^n} \right|_{V_T = V_{\text{bias}}} \tag{15}$$

where $V_T = V_{\text{bias}} + V_{\text{RF}}$, are such that the RF charge, q, stored in the varactor can be described by (18), where

$$A = 4\{H_2(\omega_1, \omega_2)H_1(\omega_3) + H_2(\omega_1, \omega_3)H_1(\omega_2) + H_2(\omega_2, \omega_3)H_1(\omega_1)\} \tag{16}$$

$$B = 6H_1(\omega_1)H_1(\omega_2)H_1(\omega_3) \tag{17}$$

$$q = C_0 V_{\text{RF}} + C_1 V_{\text{RF}}^2 + C_2 V_{\text{RF}}^3 \tag{18}$$

and $\omega_s = \omega_1 + \omega_2 + \omega_3$. Fig. 7 plots the calculated IM3 product power for a given C_{eff} and L_{eff} for a range of potential divider factors β, where $\beta = 1 + C_0/C_A$. The circuit of Fig. 6(b) corresponds to $\beta = 1$, where $C_A = \infty$ and $\beta > 1$ corresponds to the circuit of Fig. 6(c) under a range of combinations of C_A and C_0, resulting in the same C_{eff}, so as to maintain the same resonant frequency. Improvement to linearity is proportional to β.

Improvement to linearity, however, comes at a price. The series connected capacitance C_A effectively restricts the range of effective capacitance values that may be realized with the tunable varactor. This directly translates to the restriction of the filter tuning range to that mentioned in Section II. Fig. 8 plots the tradeoff between the linearity and tuning range for the filter, where 100% tuning range corresponds to the case with no fixed capacitance (i.e., $C_A = \infty$). These results were obtained with the varactor diode model BB179 from NXP, with a capacitance tuning range from 20 to 2 pF for bias voltages from 0 to 30 V. Key varactor parameters such as V_j, C_{j0}, and m were found to be 1.38 V, 27.7 pF, and 0.7, respectively, from the spice model for the varactor obtained from NXP.[1]

It may be necessary to better visualize the effectiveness of this technique in practical filters, where C_A would be fixed. The linearity and β will then directly depend on the varactor biasing voltage, and hence, the resonant frequency. As an illustrative example, the IM3 response of circuits in Fig. 6 are compared

[1]NXP, USA, BB179 Varactor Diode SPICE Model, 2011. [Online]. Available: http://www.nxp.com/models/spicespar/data/BB179.html

$$H_1(\omega) = \frac{C_A}{C_A + C_0 - \omega^2 L C_0 C_A + j2\omega R_S C_0 C_A} \tag{12}$$

$$H_2(\omega_1, \omega_2) = \frac{\left[C_1 - LC_1C_A(\omega_1+\omega_2)^2 + j2RC_1C_A(\omega_1+\omega_2)\right] H_1(\omega_1)H_1(\omega_2)}{LC_0C_A(\omega_1+\omega_2)^2 - (C_0+C_A) - j2RC_0C_A(\omega_1+\omega_2)} \tag{13}$$

$$H_3(\omega_1, \omega_2, \omega_3) = \frac{[C_1A + C_2B]\left[1 - LC_A\omega_S^2 + j2RC_A\omega_S\right]}{6\left[LC_0C_A\omega_S^2 - (C_0+C_A) - j2RC_0C_A\omega_S\right]} \tag{14}$$

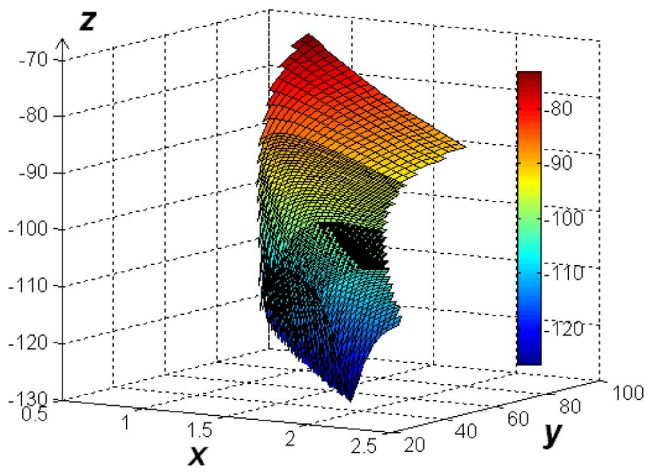

Fig. 8. Tradeoff between linearity and filter tuning range, where the x-axis is the filter center frequency in gigahertz, the y-axis is the available tuning range as a percentage, and the z-axis is IM3 power in dBm and $L_{\text{eff}} = 2.5$ nH. 100% tuning range corresponds to $C_A = \infty$.

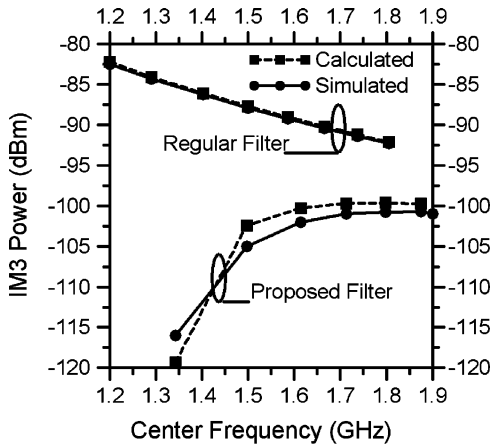

Fig. 9. Comparison of calculated and simulated IM3 power against filter resonant frequency for a tone spacing of 100 kHz and $P\text{in} = 10$ dBm (for varactor diode model BB179 from NXP).

against resonant frequency in Fig. 9 for the following component values: $L_{\text{eff}} = 2.5$ nH and $C_A = 8$ pF, where the BB179 varactor diode is employed as the tuning element.

It is very clear from Fig. 9 that a typical varactor based tunable filter would suffer from nonlinearity effects mostly for low bias voltages, which correspond to operation at lower resonant frequencies. With increasing bias voltage, as expected, the IM3 distortion product power diminishes. In contrast, under the proposed configuration, the intermodulation distortion product power is smallest for lower bias voltages, where β is higher and gradually increases with resonant frequency as β falls. Overall, IM3 power has been suppressed by at least 25 dB for lower resonant frequencies and around 8 dB for higher frequencies.

IV. Experiment and Verification

To demonstrate the performance of the proposed compact tunable highly linear bandpass filter, a microstrip prototype filter

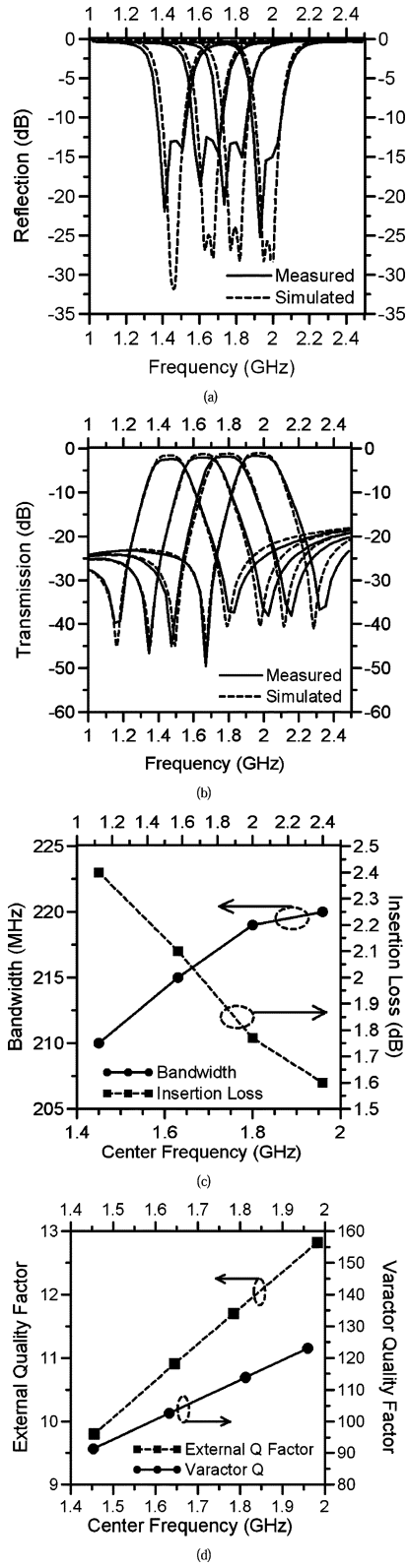

Fig. 10. (a) and (b) Simulated and measured s-parameters of second-order highly linear tunable filter for bias voltages of: 1, 7, 15, 30 V (from left to right). (c) Measured filter bandwidth and insertion loss across tuning range. (d) External Q factor of filter and varactor Q against center frequency.

was designed and fabricated to operate between frequencies from 1.5 to 2.0 GHz with a bandwidth of 220 MHz. The circuit was constructed on a Rogers 6010(LM) substrate with a relative dielectric constant of 10.2 and a substrate thickness of

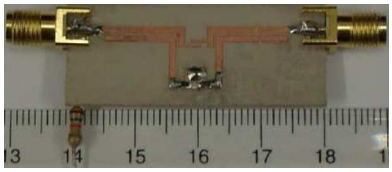

Fig. 11. Photograph of fabricated filter (metric ruler). Reference planes are located at the SMA tips.

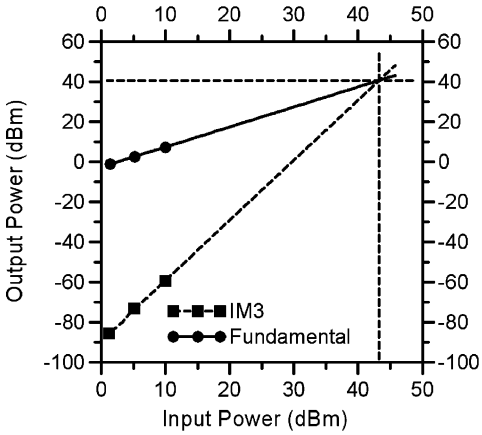

Fig. 12. Output power of fundamental tones and IM3 product against input power under a bias voltage of 1 V and tone separation of 100 kHz.

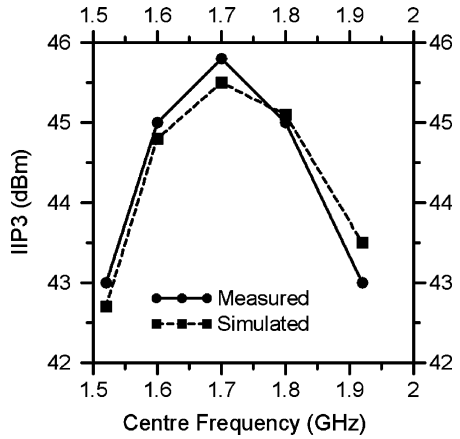

Fig. 13. Measured and simulated IIP3 against filter center frequency for tone separation of 100 kHz.

1.27 mm. Very good agreement is observed between the measured and simulated S-parameters of the filter, which are illustrated in Fig. 10. Simulations assumed a constant varactor resistance of 0.6 Ω to model the losses. The filter insertion loss varied from around 2.4 dB to around 1.6 dB. The measured tuning range was 1.45–1.96 GHz and the 3-dB bandwidth was found to increase from approximately 210 MHz at 1.45 GHz to 220 MHz at 1.96 GHz, as illustrated in Fig. 10(c). A photograph of the filter is shown in Fig. 11, where the filter circuit size was 29 mm × 9.8 mm.

Fig. 12 plots the input power against the output power for the filter with a bias voltage of 1 V and a tone spacing of 100 kHz. The measured third-order input and output referred intercept points are as high as 43 and 40 dBm, respectively, even under this low bias voltage. Fig. 13 plots the measured input referred intercept point against the filter center frequency. It can be observed that linearity is best at around 1.7 GHz. Overall, the filter has excellent linearity.

V. Conclusion

This paper has presented a compact highly linear fixed bandwidth tunable filter for modern communications systems. Methods to obtain a near linear Q factor and to achieve near-constant pole separation have been described. A pair of transmission zeros generated from the source–load coupling greatly enhances the skirt selectivity of the filter. The resonator configuration employed is shown to improve filter linearity drastically, especially for low bias voltages, where distortion is normally strongest. A filter was fabricated for demonstration and verification. The filter tuning range was observed to be from 1.45 to 1.96 GHz (30%) with a 3-dB bandwidth variation from 210 MHz at 1.45 GHz to 220 MHz at 1.96 GHz corresponding to only 4.6% total bandwidth deviation. Additionally, it is shown that the filter exhibits an IIP3 of better than 43 dBm throughout the entire filter tuning range. The proposed dual-mode filters also have their first spurious response at $3f_0$ rather than at $2f_0$ so they suffer less from adjacent channel interference when being tuned, especially toward higher frequency bands [22]. Moreover, they are also relatively simple and inexpensive to fabricate.

References

[1] Y. H. Chun and J. S. Hong, "Electronically reconfigurable dual-mode microstrip open-loop resonator filter," *IEEE Microw. Wireless Compon. Lett.*, vol. 18, no. 7, pp. 449–451, Jul. 2008.

[2] P. W. Wong and I. C. Hunter, "Electronically reconfigurable microwave bandpass filter," *IEEE Trans. Microw. Theory Tech.*, vol. 57, no. 12, pp. 3070–3079, Dec. 2009.

[3] P. W. Wong and I. C. Hunter, "A new class of low-loss high-linearity electronically reconfigurable microwave filter," *IEEE Trans. Microw. Theory Tech.*, vol. 56, no. 8, pp. 1945–1953, Aug. 2008.

[4] Y. M. Chen, S. F. Chang, C. Y. Chou, and K. H. Liu, "A reconfigurable bandpass–bandstop filter based on varactor-loaded closed-ring resonators," *IEEE Microw. Mag.*, vol. 10, no. 1, pp. 138–140, Feb. 2009.

[5] L.-H. Hsieh and K. Chang, "Tunable microstrip bandpass filters with two transmission zeros," *IEEE Trans. Microw. Theory Tech.*, vol. 51, no. 2, pp. 520–525, Feb. 2003.

[6] M. Makimoto and M. Sagawa, "Varactor tuned bandpass filters using microstrip-line ring resonators," in *IEEE MTT-S Int. Microw. Symp. Dig.*, Jun. 1986, pp. 411–414.

[7] I. C. Hunter and J. D. Rhodes, "Electronically tunable microwave bandpass filters," *IEEE Trans. Microw. Theory Tech.*, vol. MTT-30, no. 9, pp. 1354–1360, Sep. 1982.

[8] B.-W. Kim and S.-W. Yun, "Varactor-tuned combline bandpass filter using step-impedance microstrip lines," *IEEE Trans. Microw. Theory Tech.*, vol. 52, no. 4, pp. 1279–1283, Apr. 2004.

[9] B. E. C. Smith, P. A. Warr, and M. A. Beach, "Wide tuning range planar filters using lumped-distributed coupled resonators," *IEEE Trans. Microw. Theory Tech.*, vol. 53, no. 2, pp. 777–785, Feb. 2005.

[10] L. Athukorala and D. Budimir, "Frequency tunable microstrip resonators and filters," in *Proc. Eur. Microw. Conf.*, Oct. 2009, pp. 1239–1242, 2009.

[11] W. M. Fathelbab and M. B. Steer, "A reconfigurable bandpass filter for RF/microwave multifunctional systems," *IEEE Trans. Microw. Theory Tech.*, vol. 53, no. 3, pp. 1111–1116, Mar. 2005.

[12] H. Joshi, H. H. Sigmarsson, S. Moon, D. Peroulis, and W. J. Chappell, "High Q fully reconfigurable tunable bandpass filters," *IEEE Trans. Microw. Theory Tech.*, vol. 57, no. 12, pp. 3525–3533, Dec. 2009.

[13] B. Kapilevich, "A varactor-tunable filter with constant bandwidth and loss compensation," *Microw. J.*, vol. 50, no. 4, pp. 106–114, Apr. 2007.
[14] S. J. Park and G. M. Rebeiz, "Low-loss two-pole tunable filters with three different predefined bandwidth characteristics," *IEEE Trans. Microw. Theory Tech.*, vol. 56, no. 5, pp. 1137–1148, May 2008.
[15] W. Tang and J. S. Hong, "Varactor-tuned dual-mode bandpass filters," *IEEE Trans. Microw. Theory Tech.*, vol. 58, no. 8, pp. 2213–2219, Aug. 2010.
[16] M. Tanani and G. M. Rebeiz, "A two-pole two-zero tunable filter with improved linearity," *IEEE Trans. Microw. Theory Tech.*, vol. 57, no. 4, pp. 830–839, Apr. 2009.
[17] E. E. Hoppenjans and W. J. Chappell, "A vertically integrated tunable UHF filter," in *IEEE MTT-S Int. Microw. Symp. Dig.*, May 2010, pp. 1380–1383.
[18] A. R. Brown and G. M. Rebeiz, "A varactor-tuned RF filter," *IEEE Trans. Microw. Theory Tech.*, vol. 48, no. 7, pp. 1157–1160, Aug. 2002.
[19] M. A. El-Tanani and G. M. Rebeiz, "High performance 1.5–2.5 GHz RF MEMS tunable filters for wireless applications," *IEEE Trans. Microw. Theory Tech.*, vol. 58, no. 6, pp. 1629–1637, Jun. 2010.
[20] L. Athukorala and D. Budimir, "Compact high linearity tunable dual-mode microstrip filters," in *Eur. Microw. Conf.*, 2010, pp. 834–837.
[21] L. Athukorala and D. Budimir, "Compact dual-mode open-loop microstrip resonators and filters," *IEEE Microw. Wireless Compon. Lett.*, vol. 19, no. 11, pp. 698–700, Jul. 2009.
[22] L. Athukorala and D. Budimir, "Design of compact dual-mode microstrip filters," *IEEE Trans. Microw. Theory Tech.*, vol. 58, no. 11, pp. 2888–2895, Nov. 2010.
[23] B. E. Carey-Smith and P. A. Warr, "Distortion mechanisms in varactor diode-tuned microwave filters," *IEEE Trans. Microw. Theory Tech.*, vol. 54, no. 9, pp. 3492–3500, Sep. 2006.

Lakshman Athukorala (S'09) received the B.Eng. degree in electronic engineering from the University of Westminster, London, U.K., in 2008, and is currently working toward the engineering Ph.D. degree at the University of Westminster.

His research interests are in the area of compact and tunable microwave filters.

Djuradj Budimir (M'93–SM'02) received the Dipl.Ing. and M.Sc. degrees in electronic engineering from the University of Belgrade, Belgrade, Serbia, in 1981 and 1985, respectively, and the Ph.D. degree in electronic and electrical engineering from The University of Leeds, Leeds, U.K., in 1995.

In March 1994, he joined the Department of Electronic and Electrical Engineering, Kings College London, University of London. Since January 1997, he has been with the School of Electronics and Computer Science, University of Westminster, London, U.K., where is currently a Reader of wireless communications and leads the Wireless Communications Research Group. He has authored or coauthored over 240 journal and conference papers in the field of RF, microwave, and millimeter-wave wireless systems and technologies. He authored *Generalized Filter Design by Computer Optimization* (Artech House, 1998), *EPFIL-Waveguide E-Plane Filter Design* (Artech House, 2000), and a chapter in *Encyclopaedia of RF and Microwave Engineering* (Wiley, 2005). He is a regular reviewer for *IET Electronic Letters*, *IET Microwaves, Antennas, and Propagation*, and the *International Journal of RF and Microwave Computer-Aided Engineering*. His research interests include analysis and design of hybrid and monolithic microwave integrated circuits, the design of amplifiers, filters, and multiplexing networks for RF, microwave and millimeter-wave applications, and RF and microwave wireless system design.

Dr. Budimir is a Charter Engineer in the U.K. He is a member of the EPSRC Peer Review College. He is a regular reviewer for the IEEE MICROWAVE AND WIRELESS COMPONENTS LETTERS, IEEE TRANSACTIONS ON MICROWAVE THEORY AND TECHNIQUES, and PROCEEDINGS OF THE IEEE.

Design of Compact Dual-Mode Microstrip Filters

Lakshman Athukorala, *Student Member, IEEE*, and Djuradj Budimir, *Senior Member, IEEE*

***Abstract*—This paper presents a novel filter design technique for the compact microstrip dual-mode filters. An equivalent circuit for the single dual-mode filter section is derived to show that a single unit behaves as a pair of coupled synchronously tuned single-mode resonators. The equivalent circuit was linked to the inverter-coupled bandpass prototype network to allow higher order filters to be realized. A complete design example (from design to realization) of a fourth-order Chebyshev bandpass filter is presented. It is shown that the dual-mode resonator may be employed to design cross-coupled filters with finite frequency zeros. Two filters are designed using optimized coupling matrix method, fabricated and tested. Experimental and simulation results are presented to validate the argument. Finally, it is shown that more compactness may be achieved with narrowband filters by employing folded resonators.**

***Index Terms*—Compact filters, dual-mode filters, microstrip filters, microstrip resonators.**

I. Introduction

MICROSTRIP bandpass filters have gained popularity due to size, cost, weight, and fabrication advantages and find extensive applications in low-power to medium-power RF transceivers. High-performance bandpass filters having a low insertion loss, compact size, wide stopband, and high selectivity are essential for modern communication systems.

Various approaches to microstrip filter miniaturization are available through recent research. Some popular miniaturization methods reported in literature include the use of slow-wave resonators [1], multilayer filters [2], meandering [3], high-dielectric-constant substrates [4], lumped-element filters [4], and dual-mode resonators [5]–[9]. Slow-wave designs are not so practical for high fractional bandwidths although they offer excellent wideband response. Multilayer structures introduce complexity to the fabrication process while realizing that lumped elements may not always be practical.

Dual-mode resonator-based filters are naturally compact and generally offer the same fabrication simplicity as a regular microstrip filter. A number of highly compact dual-mode filters found in recent research include the open-loop [5], circular-ring [6], and square-loop [7] structures.

There are only a few reports on the design of high-order dual-mode filters in literature [8], especially using 1-D resonators.

Manuscript received June 03, 2010; revised July 28, 2010; accepted August 11, 2010. Date of publication October 18, 2010; date of current version November 12, 2010.

The authors are with the Department of Electronic, Communication and Software Engineering, University of Westminster, London W1W 6UW, U.K. (e-mail: d.budimir@wmin.ac.uk).

Color versions of one or more of the figures in this paper are available online at http://ieeexplore.ieee.org.

Digital Object Identifier 10.1109/TMTT.2010.2079110

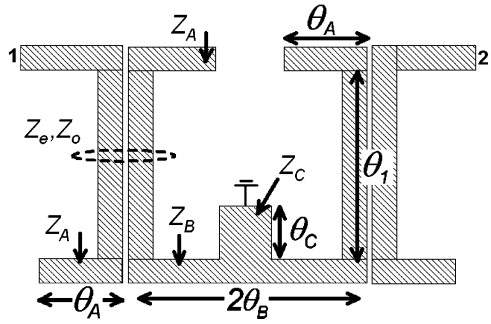

Fig. 1. Layout of a dual-mode filter.

A popular method of designing higher order filters is to couple dual-mode sections with nonresonating nodes between resonators [5]. However, this approach greatly compromises the compactness of the filter.

Single-mode filters such as the interdigital filter and combline filters offer excellent size (area) reduction as they employ quarter-wavelength resonators. However, they extend up to $\lambda/4$ in a single dimension, and this may not always be acceptable for a given frequency and application.

This paper presents a novel filter design technique for dual-mode filters based on the compact open-loop dual-mode resonator [9]. An equivalent lumped circuit model is presented. An effective method of realizing inverter-coupled bandpass prototype filters using the dual-mode resonator without employing nonresonating nodes is described. This allows for compact, low-loss, and high-performance filters to be designed rapidly. Selective filters with finite frequency zeros are proposed next. Two different configurations are presented as examples that produce two and four transmission zeros. Finally, highly compact second-order filters with improved stop-band are presented for applications where space is at a premium.

II. Dual-Mode Filter Model

The dual-mode filter shown in Fig. 1 is excited via parallel coupling and will produce a second-order response. The feeding to the coupled lines are usually 50-Ω lines in the case of simple second-order filters, but higher order filters may need additional inductances prior to the input and output coupled lines for there to be a good match at the center frequency. The general layout is similar to a regular open-loop filter except for the presence of the short-circuited stub in the symmetry plane of the structure. This additional element is responsible for producing dual-mode behavior.

We present here the derivation of an equivalent model for the above structure in order to facilitate filter design. A pair of coupled lines may be described with their impedance matrix

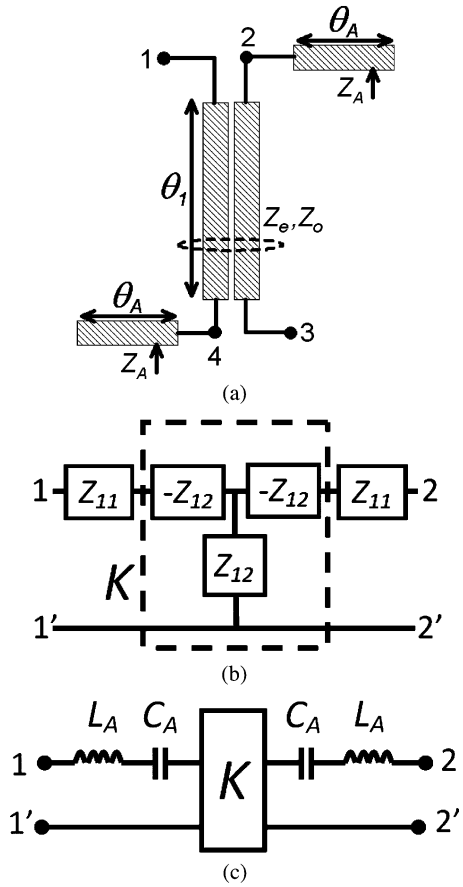

Fig. 2. (a) Coupled lines with stubs loading ports 2 and 4, (b) T-equivalent circuit. (c) Proposed equivalent model.

elements given by

$$Z_{11C}=Z_{22C}=Z_{33C}=Z_{44C}=-0.5j(Z_e+Z_o)\cot(\theta_1) \quad (1)$$
$$Z_{12C}=Z_{21C}=Z_{34C}=Z_{43C}=-0.5j(Z_e-Z_o)\cot(\theta_1) \quad (2)$$
$$Z_{13C}=Z_{31C}=Z_{24C}=Z_{42C}=-0.5j(Z_e-Z_o)\csc(\theta_1) \quad (3)$$
$$Z_{14C}=Z_{41C}=Z_{23C}=Z_{32C}=-0.5j(Z_e+Z_o)\csc(\theta_1) \quad (4)$$

where Z_e and Z_o denote the modal impedances [15].

The loading stub of impedance Z_A not only allows for a better match of the filter at resonance but also allows higher order filters to have better symmetry and, thus, simplifies filter design.

The impedance matrix for the coupled lines loaded asymmetrically with open-circuited stubs of length θ_A, as shown in Fig. 2(a), may be summarized as

$$Z_{11}=Z_{11C}+\frac{(D+Z_{11C})\left(Z_{12C}^2+Z_{14C}^2\right)-2Z_{12C}Z_{13C}Z_{14C}}{Z_{13C}^2-(D+Z_{11C})^2} \quad (5)$$
$$Z_{12}=Z_{13C}+\frac{2Z_{12C}Z_{14C}(D+Z_{11C})-Z_{13C}\left(Z_{12C}^2+Z_{14C}^2\right)}{Z_{13C}^2-(D+Z_{11C})^2} \quad (6)$$
$$D=-jZ_A\cot(\theta_A). \quad (7)$$

Its T-equivalent circuit is shown in Fig. 2(b).

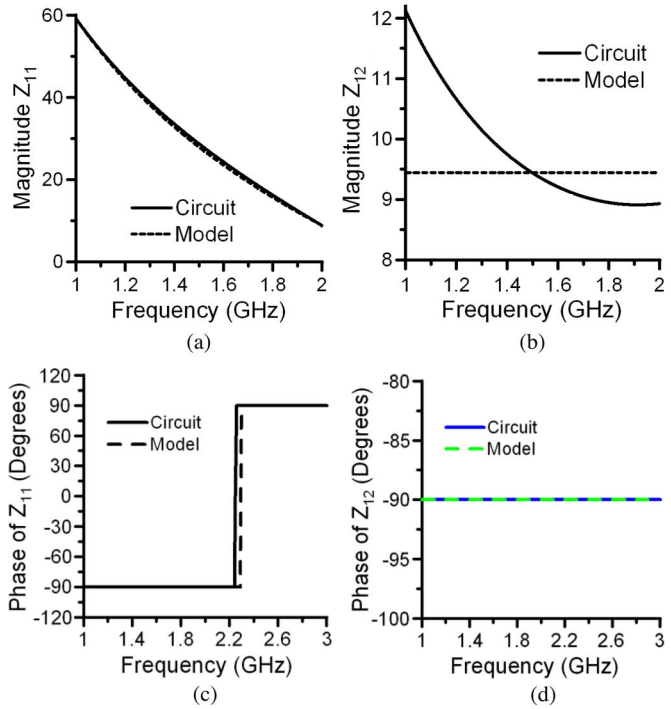

Fig. 3. Driving-point and transfer impedances of stub-loaded coupled lines and proposed model and their phase information.

Extraction of an impedance inverter from Fig. 2(b) leads to the representation in Fig. 2(c), where Z_{11} is modeled with inductance L_A and capacitance C_A. When θ_A is zero, the circuit corresponds to a parallel coupled filter section, in which case a transmission-line model instead of a circuit model could have been used.

It is possible to determine L_A and C_A, respectively, from

$$L_A=\frac{\omega_2 Z_{11}(\omega_2)-\omega_1 Z_{11}(\omega_1)}{\omega_2^2-\omega_1^2} \quad (8)$$
$$C_A=\frac{1}{\omega_1^2 L_A-\omega_1 Z_{11}(\omega_1)} \quad (9)$$

where $Z_{11}(\omega_x)$ is the driving-point impedance at angular frequency ω_x. These elements will accurately describe the driving-point impedance between the two chosen angular frequencies ω_1 and ω_2. These angular frequencies should therefore be chosen such that ω_1 is less than the lower passband edge frequency and ω_2 is higher than the upper passband edge frequency to ensure the validity of the model. The impedance of the inverter may be determined by evaluating (6) at the midband frequency of the filter.

The impedance matrix elements of the circuit and model are compared in Fig. 3, where $Z_e = 60\,\Omega$, $Z_o = 40\,\Omega$, $Z_A = 50\,\Omega$, $\theta_A = 15°$, and $\theta_1 = 45°$, at 1.5 GHz. The model parameters were evaluated at frequencies 1 and 2 GHz. There is excellent agreement between the circuit and model for Z_{11}. The frequency dependence of Z_{12} is not modeled and causes the discrepancy in Fig. 3(b). However, the variation in Z_{12} is small ($<10\%$) over the passband of filters with fractional bandwidths less than 25% and does not cause a significant error.

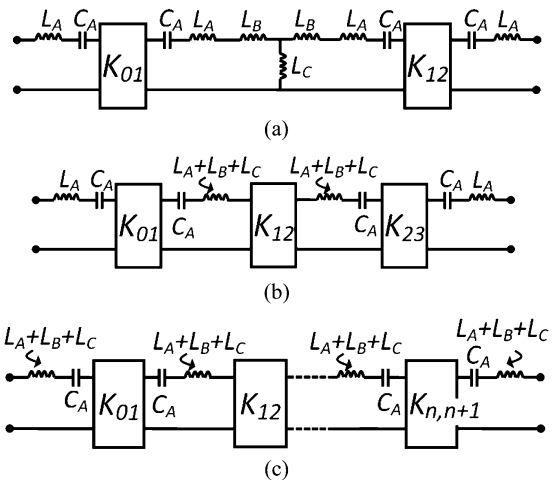

Fig. 4. Equivalent circuit for: (a) single dual-mode filter, (b) single dual-mode filter section with extracted inverter, and (c) for asymmetrically coupled dual-mode filter sections.

The lines with characteristic impedance Z_B and Z_C in Fig. 1 mainly serve as inductances, and these corresponding inductances L_B and L_C may be determined from

$$L_B = \frac{Z_B \sin(\theta_B)}{\omega_0} \tag{10}$$

$$L_C = \frac{Z_C \tan(\theta_C)}{\omega_0} \tag{11}$$

where ω_0 is the midband frequency of the filter.

The complete equivalent circuit for the filter in Fig. 1 may now be as depicted shown in Fig. 4(a), where $K_{01} = K_{12}$. It is possible to further extract an impedance inverter from this circuit, which ultimately yields the model in Fig. 4(b), where $K_{01} = K_{23}$ [determined from (6)] and K_{12} is given by

$$\omega_0 = \frac{1}{\sqrt{C_A(L_A + L_B + L_C)}} \tag{12}$$

$$K_{12} = \omega_0 L_C. \tag{13}$$

Since L_A and C_A do not resonate, Fig. 4(b) corresponds to a filter comprised of a pair of coupled identical single-order resonators, each resonating at a natural angular frequency given by (12). From Fig. 4(c), it may be seen that an asymmetrically coupled cascade of such dual-mode filter sections resembles an inverter-coupled bandpass prototype network.

A filter design method is outlined in Fig. 5. A suitable value for M is selected initially. Fixing a value for M effectively sets an identical capacitance C_A for all resonators and thus allows the total inductance L_T ($L_T = L_A + L_B + L_C$) to be determined. Parameter M must be identical for all coupled lines used in the filter to allow all resonators to be synchronously tuned. The value of M should be chosen to allow the coupled lines to be most conveniently realized in a given substrate. Z_A can be selected independently of M. It is also convenient to set θ_1 to around 45° and θ_A to about 15°. Although L_A and C_A depend also on the relative difference in the modal impedances of the coupled lines (i.e., $Z_e - Z_o$), this dependency is quite small and can be neglected for narrowband filters.

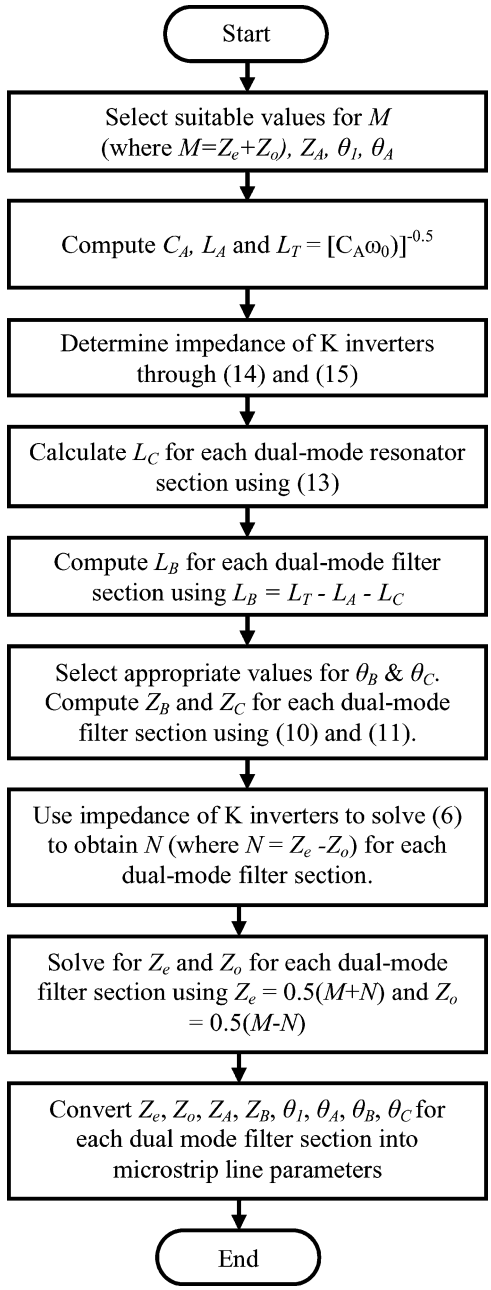

Fig. 5. Direct-coupled filter design flowchart.

Impedance inverter parameters can be evaluated from

$$K_{01} = K_{n,n+1} = \sqrt{\frac{L_T \omega_0 Z_0 B}{g_0 g_1}} \tag{14}$$

$$K_{i,i+1} = L_T \omega_0 B \left. \sqrt{\frac{1}{g_i g_{i+1}}} \right|_{i=1 \text{ to } n-1} \tag{15}$$

where B is the fractional bandwidth of the filter and Z_0 is the source/load impedance. The element values g_n may be from a Butterworth or Chebyshev prototype circuit.

The input and output of the filter are coupled through elements L_A and C_A as in Fig. 4(b), which degrades the coupling. To minimize degradation, the total series inductance is increased to generate a transmission pole at the filter midband frequency.

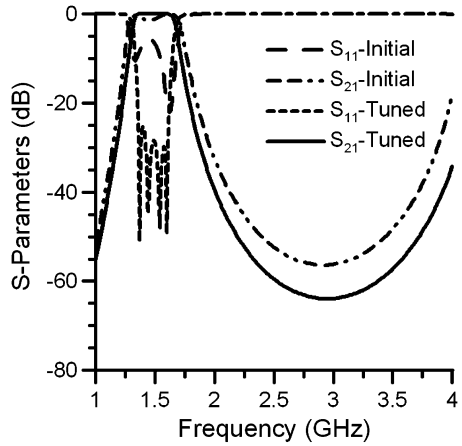

Fig. 6. Circuit simulation results for designed filter before and after tuning.

This is achieved by having inductive feed lines of inductance equal to $L_B + L_C$, as depicted in Fig. 4(c).

The limitation of the proposed model arises from the assumption that the impedance inverters are frequency-independent. Therefore, the accuracy of the equivalent model deteriorates gradually for filters with increasing fractional bandwidths (FBWs). For nonnarrowband filters (i.e., $\mathrm{FBW} > 10\%$), some tuning may be necessary to refine the response.

The design procedure is greatly facilitated with the aid of a computer. The filters presented in this paper were designed by employing a MATLAB program, which allowed all of the filter parameters to be determined relatively quickly given the prototype element values. In Section III, we will demonstrate the filter design procedure by presenting a full design example from prototype to realization.

III. Direct-Coupled Filter Design Example

Here, we demonstrates a fourth-order Chebyshev filter designed with two direct-coupled dual-mode resonators. The filter must have a passband at 1.5 GHz with passband ripple of 0.01 dB. An FBW of 25% was required. The prototype element values were: $g_0 = 1$, $g_1 = 0.7129$, $g_2 = 1.2004$, $g_3 = 1.3213$, $g_4 = 0.6476$, and $g_5 = 1.1008$.

The selected value of M was 175 Ω for all coupled lines while $Z_A = 82\ \Omega$, $\theta_1 = 45°$, and $\theta_A = 15°$ at 1.5 GHz. With these values, $L_A = 3.85$ nH, $C_A = 1.26pF$ and $L_T = 8.91$ nH. The impedance inverter parameters were then determined to be: $K_{01} = K_{45} = 31.4$, $K_{12} = K_{34} = 15.17$, and $K_{23} = 11.14$.

L_C was also calculated from the K_{12} and K_{34} impedance inverter value to be 1.61 nH, and L_B, therefore, is 3.45 nH. Setting $\theta_B = 20°$ and $\theta_C = 15°$ at the center frequency allows Z_B and Z_C to be determined as 95 and 56 Ω. The modal impedances of the input/output coupled lines were determined from (6) to be $Z_e = 120\ \Omega$ and $Z_o = 55\ \Omega$ and those of the inter-resonator coupled lines were $Z_e = 100\ \Omega$ and $Z_o = 75\ \Omega$.

Finally, the feed lines to the filter must have an inductance of 5.06 nH $(L_B + L_C)$; as mentioned earlier, this was realized by employing a 110-Ω line of electrical length 25°. Fig. 6 illustrates the initial and tuned response. Fine tuning the design lead to following changes: $Z_B = 105\ \Omega$, $\theta_C = 11.9°$, and the inductive feed line impedance was increased to 125 Ω.

The variation of impedance of the K_{12} and K_{34} inverters in the filter (modeled by the T-connected inductors L_C and $-L_C$) is responsible for the error in the initial response. K_{12} varied by around 25% across the passband, while $K_{01} = K_{23}$ (impedance inverters due to coupled lines) varied only by 10%. Therefore, L_B had to be increased while decreasing L_C in order to optimize K_{12} without altering the center frequency of the filter.

The filter was fabricated on RT Duroid 5880 with $\varepsilon_r = 2.2$ and $h = 1.575$ mm. A photograph of the fabricated filter, its layout, and a comparison between the measured and full-wave EM simulated results are illustrated in Fig. 7.

The measured performance of the filter is in very good agreement with the simulated results. A passband insertion loss of around 0.66 dB was observed at the center frequency of the filter. This may be mainly attributed to ohmic loss. The measured 3-dB bandwidth was approximately 380 MHz, which corresponds to an FBW of 25.33%. The first harmonic response is roughly at $3f_0$, which is another desirable characteristic of the filter. Due to fabrication errors, the return loss is only 15 dB.

This compact filter occupies an area of approximately 36 mm $\times$ 23 mm. As well as having dual-mode behavior, each resonator corresponds to a $\lambda_g/8$-type resonator, and these features make this resonator a very suitable candidate for compact filter designs.

IV. Filters With Finite Zeros

More selective filter configurations may be developed with the proposed dual-mode filter with the introduction of cross coupling. Asymmetric resonators are employed to reduce the strength of the K_{14} coupling, in which case this coupling may be negligible. Symmetric resonators may be used but the K_{14} coupling must be considered when performing optimization.

The sign of the cross coupling is important in order to realize finite zeros. With reference to Fig. 4(b), it is important to note that coupling generated from asymmetrically coupled sections of line K_{01} and K_{23} introduce a $-90°$ phase shift, while coupling generated from the short-circuited stub K_{12} introduce a $+90°$ phase shift.

Fig. 8 illustrates two configurations for the design of fourth-order cross-coupled filters. The coupling scheme in Fig. 8(c) applies to both structures, where the solid lines denote direct coupling and the dotted lines denote cross coupling. In both configurations, K_{S1} and K_{SL} generate a $-90°$ phase shift while K_{12} and K_{34} generate a $+90°$ shift. K_{23} and K_{14} have the same sign in each structure so the K_{14} cross coupling does not generate finite transmission zeros. In contrast, the K_{SL} and K_{23} coupling is oppositely signed in each case and produce finite zeros. The structure in Fig. 8(a) generates a single pair of zeros at finite frequencies while the structure in Fig. 8(b) generates two pairs. Source-load coupled filters are explored in more detail in [10].

The design of such cross-coupled filters may be performed by adopting the approach described in [11]. Only a brief description of the method is described here. The coupling coefficients are first determined either through optimization or through an equivalent prototype circuit. Coupling coefficients are then extracted from full-wave EM simulations for various gaps between resonators. Finally, the desired filter coupling coefficients are realized by setting the corresponding gaps between the resonators.

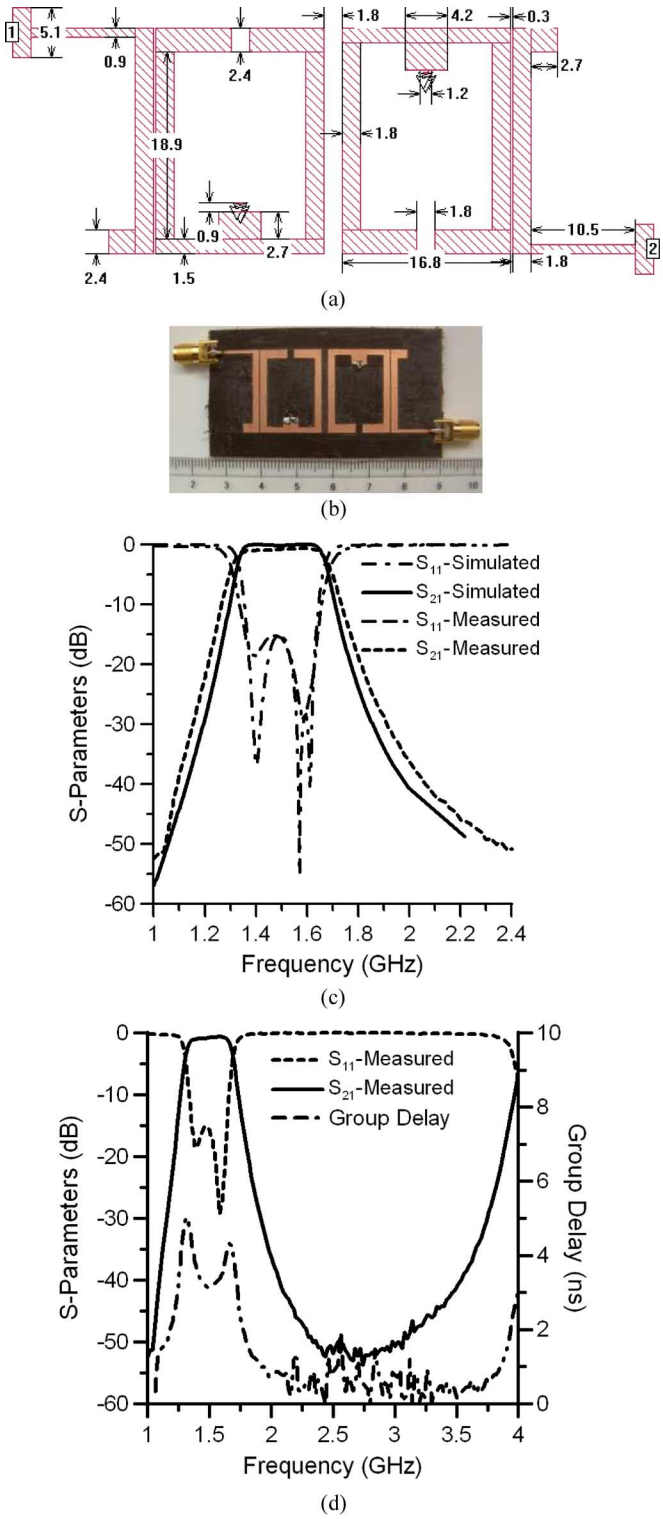

Fig. 7. (a) Layout of filter with dimensions in mm. (b) Photograph of filter. (c) Comparison of full-wave EM simulated and measured responses. (d) Measured wideband response and group delay of filter.

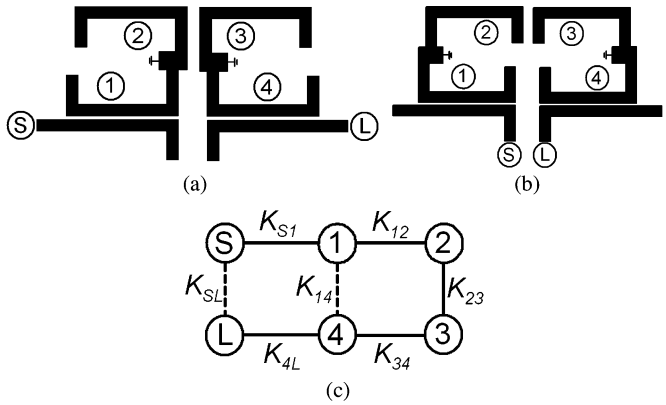

Fig. 8. (a) Magnetically coupled fourth-order filter. (b) Electrically coupled fourth-order filter. (c) Coupling scheme.

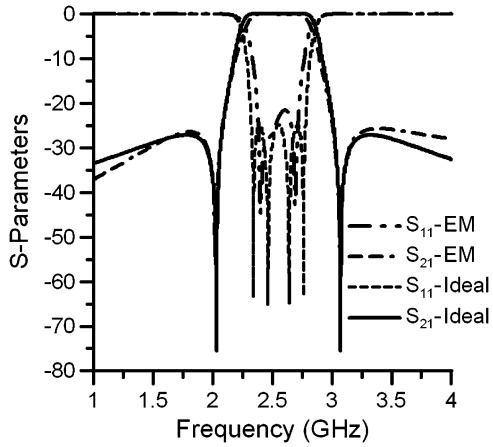

Fig. 9. Comparison of ideal response with EM simulation for cross-coupled filter of the structure in Fig. 8(a).

However, with dual-mode resonators, some coupling such as K_{12} and K_{34} in Fig. 8 can actually be realized with the aid of (13).

A selective filter based on the configuration in Fig. 8(a) was designed and fabricated. The optimized normalized coupling coefficients are as follows: $m_{S1} = m_{4L} = -0.297$, $m_{12} = m_{21} = m_{34} = m_{43} = 0.124$, $m_{23} = m_{32} = 0.107$, and $m_{SL} = -0.02$. The Q factor was 1.59.

The design method mentioned earlier was employed together with these optimized values to design the filter at 2.5 GHz. Fig. 9 is a comparison of the full-wave EM simulated results with the ideal response obtained from the coupling matrix. The filter was fabricated on RT Duroid 5880 substrate with $\varepsilon_r = 2.2$ and $h = 1.575$ mm. Fig. 10(a) compares the simulated results with measurements. A passband insertion loss of between 0.8–1 dB was observed in the measurements while the slight frequency shift may be attributed to various tolerances. Generally, there is very good agreement between the ideal, simulated, and measured results. The overall size of the filter was 27 mm $\times$ 17 mm.

The structure in Fig. 8(b) produces two pairs of transmission zeros due to a more complex source-load coupling mechanism as illustrated in Fig. 11, where the filter block is comprised of the circuit in Fig. 4(c). Although the coupling K_{SL1} is present in both structures depicted in Fig. 8, the coupling K_{SL2} is only present in the second structure.

A fourth-order filter based on Fig. 8(b) was designed at 2.8 GHz with the following inverter impedances: $K_{S1} = -27$, $K_{12} = K_{34} = 14.5$, $K_{23} = -13$, $K_{SL1} = 0.54$, and $K_{SL2} = 16000$. Fig. 12(b) compares the ideal response obtained from the coupling matrix with the full-wave simulated

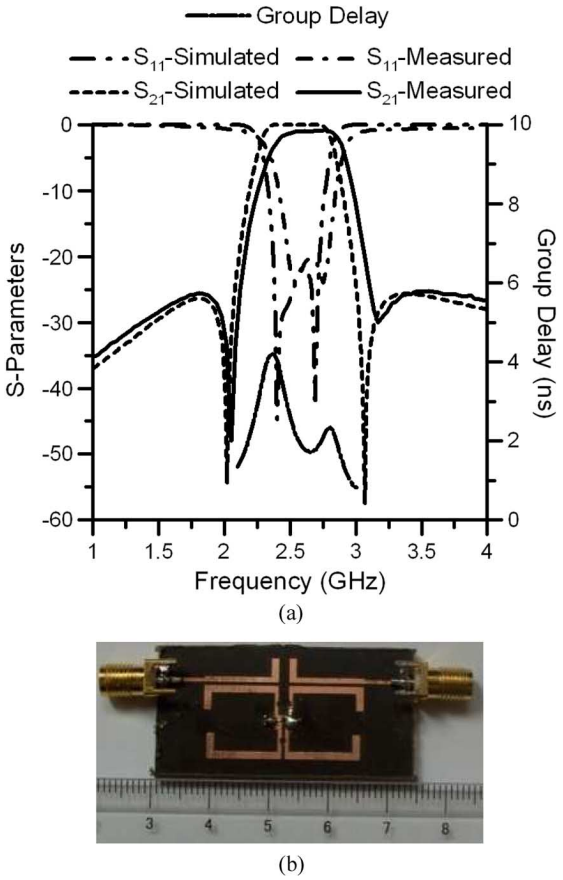

(a)

(b)

Fig. 10. (a) Comparison of EM simulated and measured response of filter. (b) Photograph of the fabricated filter.

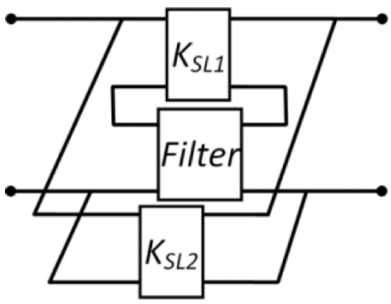

Fig. 11. Source-load coupling for the structure in Fig. 8(b).

response. There is good agreement. Discrepancies are mainly due to parasitic coupling.

Although only fourth-order cross-coupled filters are presented here, higher order cross-coupled filters may be realized with dual-mode resonators to satisfy more stringent specifications. Moreover, higher order cross-coupled filters may be realized with a mixture of single- and dual-mode resonators to improve practicality and achieve compactness.

V. Narrowband Filters

The bandwidth of these filters depends mainly on the gap between the I/O coupled lines and the length of these lines. For a narrowband filter, the I/O coupling strength need not be as large and therefore allows the reduction of either the I/O coupling gap

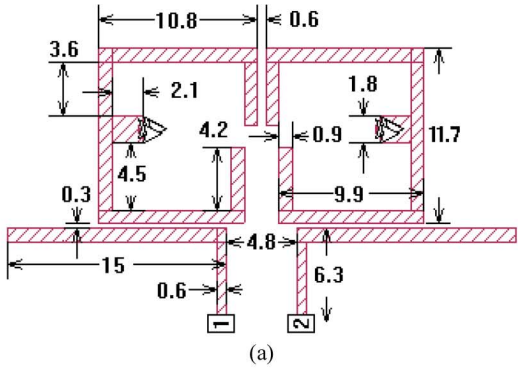

(a)

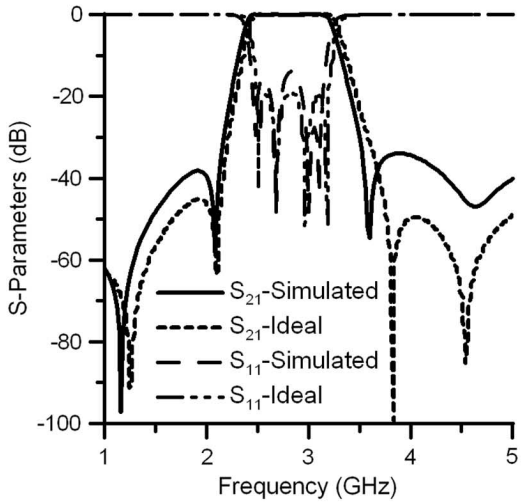

(b)

Fig. 12. (a) Layout of the filter with dimensions in mm. (b) Comparison of ideal and EM simulated responses of the filter.

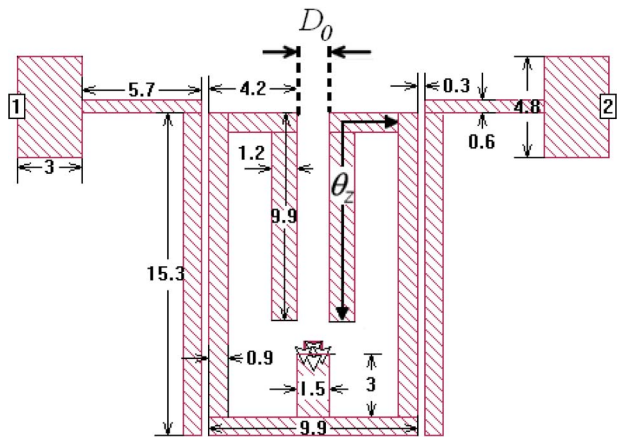

Fig. 13. Layout of narrowband dual-mode filter with dimensions in mm.

or the length of the I/O coupled lines. By performing the latter, filter size can be reduced, but the reduction in length here must be compensated by elongating the rest of the resonator (to maintain the same center frequency). To avoid an increase in size, the extensions are folded into the resonator, as illustrated in Fig. 13. The coupling between the folded open lines has little influence on the bandwidth.

The modeling method illustrated earlier may be applied to the narrowband filter above to extract the corresponding equivalent circuit parameters. It is then possible, as before, to obtain filter

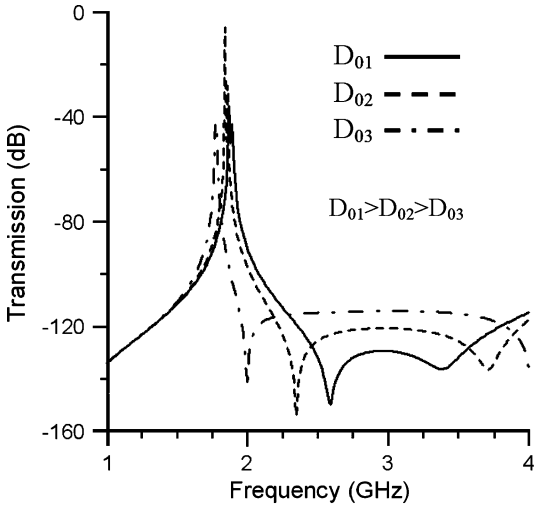

Fig. 14. Splitting of transmission zeros for various widths D_0.

design equations, which will facilitate higher order filter design problems. Here, however, we will pay attention to second-order filters and present a filter example that demonstrates performance and compactness.

An interesting characteristic of this second-order filter is that it may be designed to have transmission zeros at finite frequencies. The lines folded into the filter form a set of coupled lines. Assuming that there is no coupling between these lines, there will be exactly one useful transmission zero generated in the upper stopband (TEM approximation). This occurs when θ_Z is 90°. When there is coupling between the lines, the transmission zero splits into two. The split widens with increased coupling strength, and Fig. 14 illustrates the split between the two zeros for different gap widths.

This coupling, however, also affects the odd-mode resonance and, therefore, does not allow the zeros to be set independently. Nevertheless, these zeros will significantly improve the performance of the second-order compact filter, making it a suitable candidate where space is at a premium.

A narrowband second bandpass filter with a center frequency of 1.65 GHz and a fractional bandwidth of 13% was designed and fabricated to illustrate compactness and performance. The filter was fabricated on RT Duroid 5880 with $\varepsilon_r = 2.2$ and $h = 1.575$ mm. Fig. 13 shows the filter dimensions in millimeters, while Fig. 15 illustrates the simulated and measured results.

The passband insertion loss of the fabricated filter was approximately 0.7 dB. A slight frequency shift was observed in the measured passband, and this may be due to the various tolerances involved. The two transmission zeros closest to the passband are produced as a result of coupling between the folded arms. As a result, the first spurious response of the filter occurs roughly at $4f_0$.

The dimensions of this filter are 15.3 mm × 9.9 mm. This is equivalent to a $\lambda_g/10$-type resonator and is 64% more compact compared with a regular open-loop filter, which is around 37% more compact than the filters proposed in [5] and [12]. More miniaturization may be achieved for filters with lower fractional bandwidths since the required input and output coupling strength is even lower.

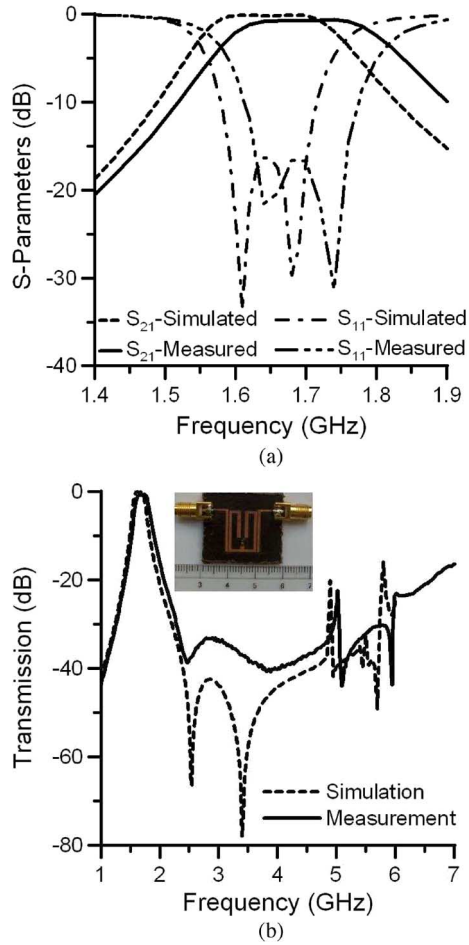

Fig. 15. Comparison of simulated and measured results for: (a) filter passband and (b) filter stopband.

VI. Conclusion

This paper presented several filter implementation techniques for the compact dual-mode open-loop resonator. First, an accurate equivalent model for a single dual-mode section was presented to illustrate the relationship between the two degenerate modes within a single unit. This was then extended to illustrate how an all-pole filter may be constructed from asymmetrically coupled dual-mode resonators without a need for nonresonating nodes. A clear link to the inverter coupled bandpass filter prototype was provided so as to allow prototype filters to be realized with ease. An example was provided to demonstrate the design process. Experimental results were in very good agreement with both design specification and simulated results. Cross-coupled filters were then discussed, and focus was given to fourth-order structures that produced two and four transmission zeros. A design procedure based on coupling coefficient extraction was outlined, and two cross-coupled filter examples were presented to support the discussion. Finally, narrowband second-order filters based on the dual-mode resonator were shown to be highly compact while producing high stopband attenuation. Furthermore, the first spurious response of these filters occurs at $3f_0$ rather than $2f_0$. They are also relatively simple and inexpensive to fabricate.

REFERENCES

[1] J. S. Hong and M. J. Lancaster, "Theory and experiment of novel microstrip slow-wave open-loop resonator filters," *IEEE Trans. Microw. Theory Tech.*, vol. 45, no. 12, pp. 2358–2365, Dec. 1997.

[2] J. S. Hong and M. J. Lancaster, "Aperture-coupled microstrip open-loop resonators and their applications to the design of novel microstrip bandpass filters," *IEEE Trans. Microw. Theory Tech.*, vol. 47, no. 9, pp. 1848–1855, Sep. 1999.

[3] S.-M. Wang, C.-H. Chi, M.-Y. Hsieh, and C.-Y. Chang, "Miniaturized spurious passband suppression microstrip filter using meandered parallel coupled lines," *IEEE Trans. Microw. Theory Tech.*, vol. 53, no. 2, pp. 747–753, Feb. 2005.

[4] J. S. Hong and M. J. Lancaster, *Microstrip Filters for RF/Microwave Applications*. New York: Wiley, 2001.

[5] J. S. Hong, H. Shaman, and Y. H. Chun, "Dual-mode microstrip open-loop resonators and filters," *IEEE Trans. Microw. Theory Tech.*, vol. 55, no. 8, pp. 1764–1770, Aug. 2007.

[6] U. Karacaoglu, I. D. Robertson, and M. Guglielmi, "An improved dual-mode microstrip ring resonator filter with simple geometry," in *Proc. Eur. Microw. Conf.*, 1994, pp. 472–477.

[7] L.-H. Hsieh and K. Chang, "compact, low insertion-loss, sharp-rejection, and wideband microstrip bandpass filters," *IEEE Trans. Microw. Theory Tech.*, vol. 51, no. 4, pp. 1241–1246, Apr. 2003.

[8] J. S. Hong and S. Li, "Theory and experiment of dual-mode microstrip triangular patch resonators and filters," *IEEE Trans. Microw. Theory Tech.*, vol. 45, no. 12, pp. 1237–1243, Apr. 2004.

[9] L. Athukorala and D. Budimir, "Compact dual-mode open loop microstrip resonators and filters," *IEEE Microw. Wireless Compon. Lett.*, vol. 19, no. 11, pp. 698–700, Sep. 2009.

[10] R. J. Cameronc, "Advanced coupling matrix synthesis techniques for microwave filters," *IEEE Trans. Microw. Theory Tech.*, vol. 51, no. 1, pp. 1–10, Jan. 2003.

[11] J. S. Hong and M. J. Lancaster, "Design of highly selective microstrip bandpass filters with a single pair of attenuation poles at finite frequencies," *IEEE Trans. Microw. Theory Tech.*, vol. 48, pp. 1098–1107, Jul. 2000.

[12] A. Görür, C. Karpuz, and M. Akpinar, "A reduced-size dual-mode bandpass filter with capacitively loaded open-loop arms," *IEEE Microw. Wireless Compon. Lett.*, vol. 13, no. 9, pp. 385–387, Sep. 2003.

[13] S. C. Lin, Y.-S. Lin, and C. H. Chen, "Extended-stopband bandpass filter using both half- and quarter-wavelength resonators," *IEEE Microw. Wireless Compon. Lett.*, vol. 16, no. 1, pp. 43–45, Jan. 2006.

[14] Q. X. Chu and H. Wang, "A compact open-loop filter with mixed electric and magnetic coupling," *IEEE Trans. Microw. Theory Tech.*, vol. 56, no. 2, pp. 431–439, Feb. 2008.

[15] D. M. Pozar, *Microwave Engineering*, 2nd ed. New York: Wiley, 1998.

Lakshman Athukorala (S'09) received the B.Eng. degree in electronic engineering from the University of Westminster, London, U.K., in 2008, where he is currently working toward the Ph.D. degree in engineering.

His research interests are in the area of miniature tunable microwave filters.

Djuradj Budimir (M'93–SM'02) received the Dipl. Ing. and M.Sc. degrees in electronic engineering from the University of Belgrade, Belgrade, Serbia, and the Ph.D. degree in electronic and electrical engineering from the University of Leeds, Leeds, U.K.

In March 1994, he joined the Department of Electronic and Electrical Engineering, Kings College London, University of London, London, U.K. Since January 1997, he has been with the Department of Electronic, Communication and Software Engineering, University of Westminster, London, where he is now a Reader of wireless communications. He has authored or coauthored over 210 papers in major journal and conference proceedings in the field of RF, microwave, and millimeter-wave (mm-wave) wireless systems and technologies. He is the author of the books *Generalized Filter Design by Computer Optimization* (Artech House, 1998) and *Software and Users Manual EPFIL-Waveguide E-plane Filter Design* (Artech House, 2000) and a chapter in the book *Encyclopaedia of RF and Microwave Engineering* (Wiley, 2005). He is a Member of the EPSRC Peer Review College. He is also a regular reviewer for *Electronic Letters* and *IET Proceedings Microwaves, Antennas, and Propagation*. His research interests include analysis and design of hybrid and monolithic microwave integrated circuits, the design of amplifiers, filters, and multiplexing networks for RF, microwave, and mm-wave applications, and RF and microwave wireless system design.

Dr. Budimir is a reviewer for the IEEE MICROWAVE AND WIRELESS COMPONENTS LETTERS, the IEEE TRANSACTIONS ON MICROWAVE THEORY AND TECHNIQUES, and the IEEE TRANSACTIONS ON CIRCUITS AND SYSTEMS.

Compact Dual-Mode Open Loop Microstrip Resonators and Filters

L. Athukorala, *Student Member, IEEE*, and D. Budimir, *Senior Member, IEEE*

***Abstract*—A novel compact microstrip dual-mode resonator and filter are proposed. The characteristics of the dual mode resonator are investigated. It is found that the filter response exhibits a desirable stopband response where the first spurious passband naturally occurs at $3f_0$. Finally, methods of miniaturizing such resonators and filters are discussed. The proposed structure was able to achieve 60% size reduction.**

***Index Terms*—Compact resonators, dual-mode filters, dual-mode resonators, microstrip filters, microstrip resonators.**

I. Introduction

MICROSTRIP dual-mode bandpass filters (BPFs) and diplexers are generally preferred and are used extensively in low to medium power RF transceivers due to the relative size reductions that can be obtained.

This letter presents a novel microstrip dual-mode open loop resonator and filter. The proposed resonator may be designed as necessary to yield $\lambda_g/4$ to $\lambda_g/12$ type resonators, where λ_g is the guided wavelength. A filter example is provided for demonstration. This resonator/filter is more compact than the recent dual-mode open loop resonator [1] and [10], circular ring [2], square patch [3], square loop dual-mode resonators [4], [5] and [9] and stepped impedance type resonators such as in [6] and [8] and the filter proposed in [11].

The characteristics of the proposed resonator are presented in Section II. Section III demonstrates an application. Conclusions will be presented in Section IV.

II. Proposed Dual-Mode Resonator

The proposed dual mode resonator shown in Fig. 1 is excited via capacitive couplings by ports 1 and 2. The input feed lines are kept at 50 Ω. A single connection to ground is applied at the symmetry plane of the resonator as shown to achieve dual mode performance.

The line lengths L_1, L_2, L_3 and widths W_1, W_2 and W_3 determine the even and odd mode resonant frequencies. Modal decomposition provides a deeper insight to the operation of the resonator. Illustrated in Fig. 2 are the corresponding even and odd mode resonators assuming for now that $W_2 = 2W_1$.

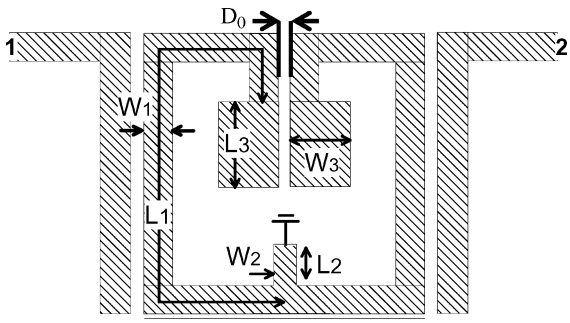

Fig. 1. Layout of proposed dual mode resonator.

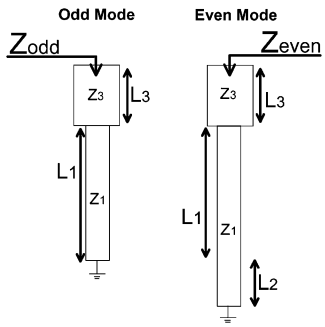

Fig. 2. Equivalent odd and even mode resonators.

The odd mode resonator is identical to that for the single mode open-loop resonator since a virtual ground exists in the symmetry plane. Therefore, the perturbation element has no effect on the odd mode. For the even mode resonance, the virtual ground is replaced by a virtual open circuit. The perturbation element is dissected and the width W_2 is split in half.

Both resonators here are of the type $\lambda_g/4$, where λ_g is the guided wavelength. Dual modes result from the difference in operating lengths of each resonator. The simplest case is when both the equivalent resonators are of the uniform impedance (UI) type where $W_2 = 2W_1$ and $W_1 = W_3$. In this case, when $L_2 = 0$, the unit behaves as the conventional single mode open loop resonator. However, when L_2 is non-zero, dual mode performance can be observed. In the UI case, the respective resonant frequencies can be calculated relatively simply with good accuracy.

For the purpose of analysis, such a resonator was simulated on a substrate of relative dielectric constant of 2.2 and thickness 0.51 mm. $W_1 = W_3 = 1$ mm and $W_2 = 2$ mm to maintain UIRs for both modes. Length of L_1 was 21 mm and the length

Manuscript received May 23, 2009; revised August 04, 2009. First published October 20, 2009; current version published November 06, 2009.

The authors are with the Department of Electronic, Communication and Software Engineering, University of Westminster, London, W1W 6UW, U.K. (e-mail: d.budimir@wmin.ac.uk).

Color versions of one or more of the figures in this letter are available online at http://ieeexplore.ieee.org.

Digital Object Identifier 10.1109/LMWC.2009.2032003

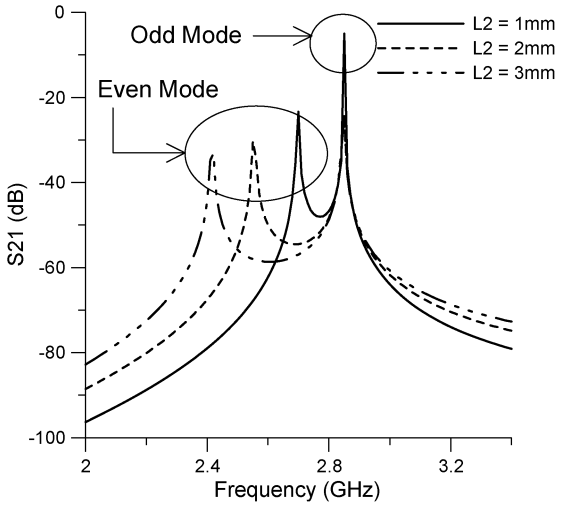

Fig. 3. Variation of modal resonant characteristics on L_2 while $\mathrm{L}_1 = 21\,\mathrm{mm}$.

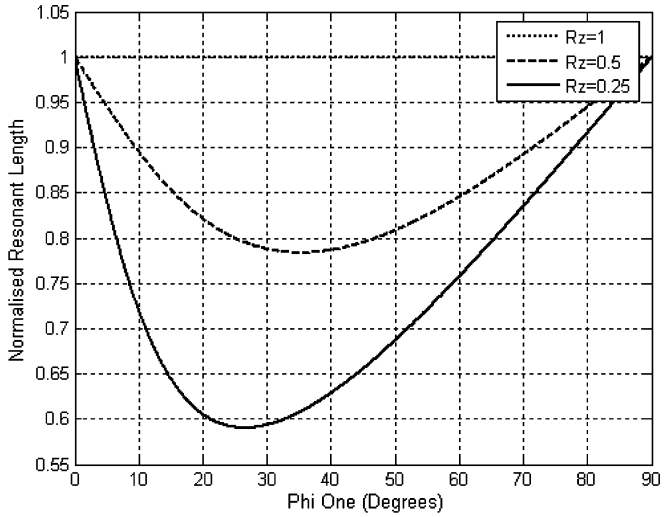

Fig. 4. Resonator length with φ_1 for various values of Rz.

of the perturbation element L_2 was varied to demonstrate the variation in even mode resonance. Fig. 3 illustrates the results.

The odd mode remains unaffected due to the virtual ground that forms in the symmetry plane while the even mode is directly dependant on L_2.

There are several methods that may be employed to miniaturise the proposed resonator such as elongating the length of L_1 and to use stepped impedance affects for miniaturisation.

Odd and even mode decomposition shows respective resonators to be of the form shown in Fig. 2 (assuming that the width $\mathrm{W}_2 = 2\mathrm{W}_1$). At their resonance, $\mathrm{Yodd} = 0$ and $\mathrm{Yeven} = 0$ give rise to these conditions for the odd mode resonator [7]:

$$\frac{Z_3}{Z_1} = \tan(\varphi_1) + \tan(\varphi_3) \tag{1}$$

and similarly for the even mode resonator

$$\frac{Z_3}{Z_1} = \tan(\varphi_1 + \varphi_2) + \tan(\varphi_3) \tag{2}$$

where φ_1, φ_2 and φ_3 refer to the electrical lengths of the sections of lengths L_1, L_2 and L_3 respectively. Z_1 and Z_3 are the characteristic impedances of the ordinary resonator section and the added stepped impedance respectively. The lengths of the odd and even mode resonators $\mathrm{L}_{\mathrm{odd}}$ and $\mathrm{L}_{\mathrm{even}}$ are found to be the following [7]:

$$Lodd = \varphi_1 + \arctan\left(\frac{Rz}{\tan(\varphi_1)}\right) \tag{3}$$

$$Leven = \varphi_1 + \arctan\left(\frac{Rz}{\tan(\varphi_1 + \varphi_2)}\right) \tag{4}$$

where Rz is the impedance ratio $\mathrm{Z}_3/\mathrm{Z}_1$. Both of the modes will be affected in an identical manner when the impedance ratio Rz is varied. Fig. 4 illustrates the variation of resonator length for various impedance ratios to illustrate size reduction.

The amount of size reduction that can be achieved is inversely proportional to the impedance ratio Rz and is a function of φ_1. Compact units may be obtained by having small impedance ratios and having an appropriate φ_1.

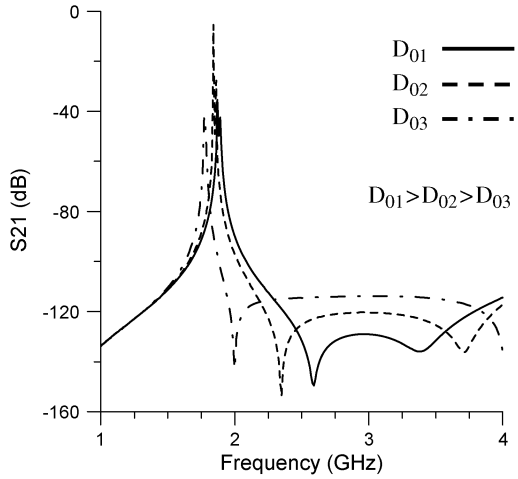

Fig. 5. Splitting of tx. zeros with inter-arm gap D_0.

The resonator has two transmission zeros in the upper stopband which are illustrated in Fig. 5. The zeros are attributed to the folded arms of the resonator, which generate a virtual earth at the input/output coupling points. Tighter inter-arm coupling widens the split between the zeros as shown.

III. Dual Mode Compact Bandpass Filters

A 2nd order BPF at 1.35 GHz was designed and fabricated. Stepped impedance and folding had been employed to achieve compactness and the overall filter size amounted to 15.8 mm $\times$ 16.5 mm. This was equivalent to a $\lambda_{\mathrm{g}}/10$ type resonator and achieves relative size reduction of 64% compared with an open loop filter. This filter is also 37% more compact compared to that proposed in [1] and [9] and 85% more compact than the filters in [11]. The filter was designed on a substrate with relative dielectric constant 2.2 and thickness 0.508 mm. The layout, response and photograph of the filter are depicted in Fig. 6 and Fig. 7. The FBW of this filter is approximately 5%. The wideband response of the fabricated filter is illustrated in Fig. 8. The first spurious response is at 4 GHz, which is at $3\mathrm{f}_0$ as expected. Simulations and measurements are in good agreement. The higher insertion

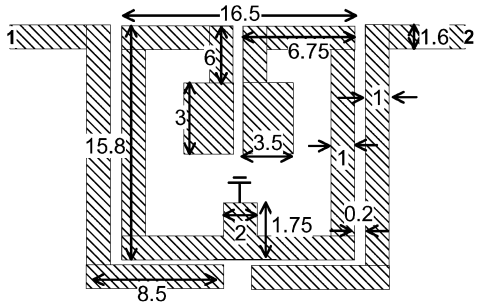

Fig. 6. Layout of Filter (all dimension in mm).

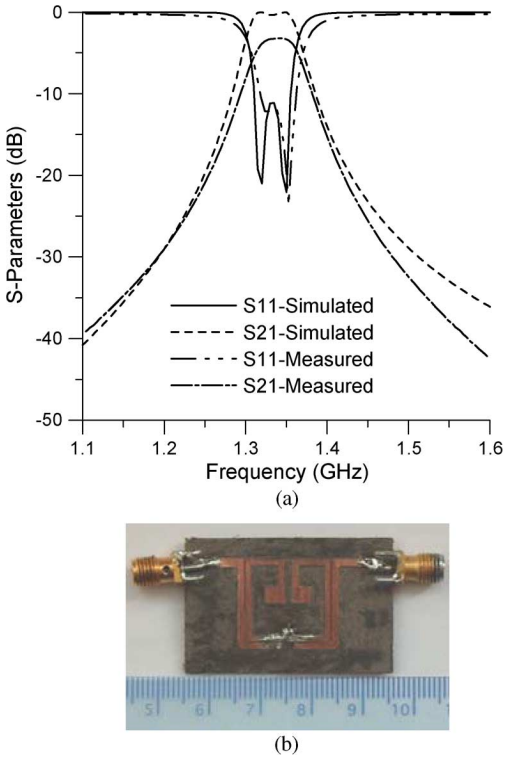

Fig. 7. (a) Measured and Simulated Response; (b) photograph of fabricated filter.

loss observed in the measurement is due to tolerances involved in the fabrication process which may be minimised with better fabrication tools or by meticulous use of available tools.

IV. Conclusion

A compact dual mode open-loop resonator has been proposed for filter applications. Operation of the dual mode resonator has been investigated with an analysis of the even and odd mode resonances. The resonator was shown to have two controllable transmission zeros on the upper stop-band. It was shown that the filters derived from the proposed resonator are capable of achieving significant size reduction.

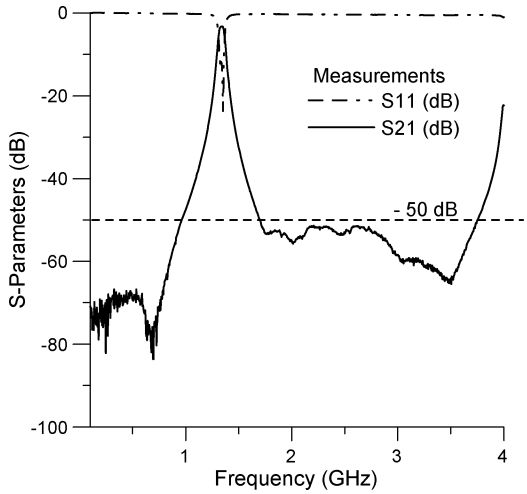

Fig. 8. Wideband response of filter.

References

[1] J.-S. Hong, H. Shaman, and Y.-H. Chun, "Dual-mode microstrip open-loop resonators and filters," *IEEE Trans. Microw. Theory Tech.*, vol. 55, no. 8, pp. 1764–1770, Aug. 2007.

[2] I. Wolfe, "Microstrip bandpass filter using degenerate modes of a microstrip ring resonator," *Electron. Lett.*, vol. 8, no. 12, pp. 302–303, Jun. 15, 1972.

[3] J. A. Curitis and S. J. Fiedziuszko, "Miniature dual mode microstrip filters," in *IEEE MTT-S Int. Dig.*, Jun. 1991, pp. 443–446.

[4] J.-S. Hong and M. J. Lancaster, "Bandpass characteristics of new dual-mode microstrip square loop resonators," *Electron. Lett.*, vol. 31, no. 11, pp. 891–892, 1995.

[5] S. W. Fok, P. Cheong, K. W. Tam, and R. P. Martins, "A novel microstrip square-loop dual-mode bandpass filter with simultaneous size reduction and spurious response suppression," *IEEE Trans. Microw. Theory Tech.*, vol. 4, no. 5, pp. 2033–2041, May 2006.

[6] D. Budimir and L. Athukorala, "Miniaturised microstrip dipexers for WiMAX applications," in *Proc. IEEE AP-S.*, Jul. 5–11, 2008, pp. 1–4.

[7] M. Makimoto and S. Yamashita, "Bandpass filters using parallel coupled stripline stepped impedance resonators," *IEEE Trans. Microw. Theory Tech.*, vol. MTT-28, no. 12, pp. 1413–1417, Dec. 1980.

[8] K. U-yen, W. J. Wollack, T. Doiron, J. Papapolymerou, and J. Laskar, "The design of a compact, wide spurious-free bandwidth bandpass filter using stepped impedance resonators," in *Proc. 35th Eur. Microw. Conf.*, Paris, France, Oct. 2005, pp. 925–928.

[9] A. Görür, C. Karpuz, and M. Akpinar, "A reduced-size dual-mode bandpass filter with capacitively loaded open-loop arms," *IEEE Microw. Wireless Compon. Lett.*, vol. 13, no. 9, pp. 385–387, Sep. 2003.

[10] X.-C. Zhang, Z.-Y. Yu, and J. Xu, "Design of microstrip dual-mode filters based on source-load coupling," *IEEE Microw. Wireless Compon. Lett.*, vol. 18, no. 10, pp. 677–679, Oct. 2008.

[11] S.-C. Lin, Y.-S. Lin, and C. H. Chen, "Extended-stopband bandpass filter using both half- and quarter-wavelength resonators," *IEEE Microw. Wireless Compon. Lett.*, vol. 16, no. 1, pp. 43–45, Jan. 2006.